Investigating the intrinsic photophysical properties and potential anticancer activity of compound DHF from *Alpinia nigra*

A Thesis submitted in Partial Fulfilment of the Requirements for the Degree of

Doctor of Philosophy

By

Heeramoni Boro

Roll no.166106029

Department of Biosciences and Bioengineering,

Indian Institute of Technology Guwahati

Guwahati-781039, Assam, India

November 2023

INDIAN INSTITUTE OF TECHNOLOGY

GUWAHATI, Assam, India

Department of Biosciences and Bioengineering

STATEMENT

I do hereby declare that the matter embodied in this thesis is the result of investigations carried out by me in the Department of Biosciences and Bioengineering, Indian Institute of Technology Guwahati, India, under the guidance of Prof. Latha Rangan and Prof. Rajaram Swaminathan.

In keeping with the general practice of reporting scientific observations, due acknowledgements have been made wherever the work described is based on the findings of other investigators.

Heeramoni Boro
3/11/2023

Heeramoni Boro

Department of BSBE

IIT Guwahati

Guwahati 781039, Assam India

November, 2023

INDIAN INSTITUTE OF TECHNOLOGY

GUWAHATI, Assam, India

Department of Biosciences and Bioengineering

CERTIFICATE

It is certified that the work described in this thesis, entitled "**Investigating the intrinsic photophysical properties and potential anticancer activity of compound DHF from *Alpinia nigra* "**, done by Heeramoni Boro for the award of the degree of Doctor of Philosophy is an authentic record of the results obtained from the research work carried out under my supervision in the Department of Biosciences and Bioengineering, Indian Institute of Technology Guwahati, India, and this work has not been submitted elsewhere for a degree.

Prof. Latha Rangan
Department of BSBE
IIT Guwahati

3rd November, 2023

Prof. Rajaram Swaminathan
Department of BSBE
IIT Guwahati

TO

MY BELOVED FAMILY

ACKNOWLEGEMENTS

I am profoundly grateful for the chance to extend my sincere thanks and gratitude to everyone who has helped and guided me along this great journey of earning my Ph.D. Their unwavering support, experience, and assistance have been invaluable in influencing my research and academic development.

First and foremost, I extend my deepest gratitude to my supervisors, Prof. Latha Rangan and Prof. Rajaram Swaminathan, for their exceptional mentorship and guidance. Timely constructive criticism, feedbacks with brilliant insights and tireless dedication to my research have been pivotal in shaping the direction and quality of this work. I am truly fortunate to have had the privilege of working under their supervision.

Also, I am indebted to the members of my Doctoral Committee members, Prof. Aiyagari Ramesh, Dr. Priyadarshi Satpati and Dr. Akshai Kumar A.S, for their constructive feedback, timely evaluation and thought-provoking discussions that have elevated in shaping the direction of this research.

I am thankful to IIT Guwahati for the facilities and the Ministry of Human Resource Development (MHRD) for providing me financial support. I also extend my sincere thanks to Department of Biosciences and Bioengineering, Central Instrumental Facilities (CIF), North East Centre for Biological Sciences and Healthcare Engineering (NECBH) for the facilities which enabled me to carry out this research effectively. I would like to thank all the BSBE department staff members for being highly cooperative.

I would like to express my deep gratitude to Prof. Ajaikumar B Kunnumakkara for guiding me throughout the cancer research objective and providing the facility to conduct the experiments. Also, I would like to thank Dr. Mangala Hegde for assisting me and help me in conducting cancer research experiments.

Next, I wish to express my heartfelt appreciation to all the current and former members of the Lab of Applied Biodiversity and Protein Biophysics, including Dr. Anuma Singh, Dr. Reshmi Das, Dr. Ishani Chakrabartty, Dr. Shrutidhara Biswas, Dr. Mohd. Ziauddin Ansari, Dr. Amrendra Kumar, Dr. Shah Ekramul Alom, Dr. Dileep Ahari, Dr. Anurag Priyardarshi, Dr. S. Sanjana, Dr. Manish Kumar Gupta, Dr. Jobina Rajkumari, Bimal Kumar Chetri, Gaurav Bhatt, Alok Senapati, Nuzelu, Alka Singh, Rashmi Singh, Rubeca, and Anamika. Their continuous

motivation and exchange of ideas have greatly enhanced the quality of my research study. I deeply appreciate their contributions.

I would like to express my heartfelt thanks to my friends Ekramul, Swati, Srirupa, Anjali, Alka, Sanjana, Gaurav, Nuzelu, Alok, Manish, Mrigyanka, Bandita, Areef whose unwavering support and camaraderie have been a constant source of inspiration throughout my PhD journey. Your friendship has been an integral part of my growth as a researcher and as an individual. Thank you for standing by me every step of the way.

I would like to express my deepest gratitude to my parents for their unconditional love and support, my husband and my in-laws for their constant love and moral support. I would like to thank my little brother Bhrigu who has been my constant support. Thank you for being the incredible brother that you are.

Lastly, this thesis is a monument to the joint efforts, wisdom, and support of several individuals who have shaped my academic and personal progress. While words will never adequately explain how grateful I am, I hope that this acknowledgement serves as a little measure of my thanks for everything they have done.

ABBREVIATIONS

DHF	3,5-dihydroxy-7,4'- dimethoxyflavone
UV-Vis	Ultraviolet-Visible
ESIPT	Excited-state intramolecular proton-transfer
SDS	Sodium Dodecyl Sulphate
CTAB	Cetyltrimethylammomium Bromide
T20	Tween20
TLC	Thin layer Chromatography
RP-HPLC	Reverse Phase-High Performance Liquid Chromatography
HR-MS	High Resolution Mass Spectrometry
NMR	Nuclear Magnetic Resonance
HEWL	Hen Egg-White Lysozyme
ThT	Thioflavin T
ANS	1-anilino-8-naphthalene sulphonate
MTT	3-(4,5-dimethylthiazol-2-yl)-2,5-diphenyl tetrazolium bromide
PI	Propidium Iodide
PS	Phosphatidylserine
HOMO	Highest Occupied Molecular Orbital
LUMO	Lowest Unoccupied Molecular Orbital
CMC	Critical micelle concentration
HaCaT	Human keratinocyte cells

Thesis Abstract

The plant *Alpinia nigra* (Zingiberaceae), is known for its traditional medicinal values and is abundantly available in Northeast (NE) India. Various phytochemicals have been reported from different parts of the plants. 3,5-dihydroxy-7,4'- dimethoxyflavone (DHF) is one of the flavonoids previously reported from our group (Gupta et al., 2021) from the leaf extracts of *A. nigra*. In the current thesis work, the UV-visible study of the compound DHF in organic solvents and water was studied which revealed that DHF is non-polar in nature and poorly water soluble. Therefore, in our present work we studied the solubility of DHF in different pH and we tried to enhance the aqueous solubility of DHF in different surfactant micelles with namely SDS, CTAB and Tween 20 as a function of pH.

The investigation into the absorption spectra of DHF across a range of organic solvents and aqueous environments has unveiled a tripartite pattern consisting of three distinct absorption bands. Specifically, these bands are referred to as Band I (363-370 nm), Band II (263-270 nm), and Band III (330 nm). Notably, in an aqueous medium, the absence of any discernible absorption band underscores the compound's limited solubility within water. Exploring the solubility of DHF across a spectrum of pH values (ranging from 2 to 13) has led to an intriguing revelation. The compound exhibits its most pronounced absorbance within the highly alkaline domain of pH 13, and this phenomenon is accompanied by a red shift of the absorption peak from 365 nm to an extended wavelength of 406 nm. The examination of DHF's solubility in aqueous solutions, facilitated by various surfactant micelles (including SDS, CTAB, and Tween 20), has been conducted in relation to pH variation. Within this context, a meticulous exploration of the time-dependent stability of DHF within diverse surfactant micellar environments, under varying pH conditions, has yielded insightful outcomes. Notably, the compound's stability has been observed to diminish in the realm of higher alkaline pH, consequently resulting in structural alterations over prolonged exposure to alkaline conditions. The investigation into the degradation kinetics of DHF under highly alkaline pH, following a 96-hour incubation period, has provided an illuminating perspective on the compound's behaviour. Specifically, the findings underscore a propensity for degradation within this markedly alkaline environment, reinforcing the dynamic interplay between DHF and its environment.

In addition to scrutinizing the solubility characteristics of DHF within distinct surfactant micellar systems, the impact of DHF upon Hen Egg White Lysozyme (HEWL) aggregates across varying pH conditions, namely pH 2, pH 5, and pH 12.2 were investigated. The outcomes of this investigation have illuminated noteworthy insights. Evidently, DHF exhibits pronounced interactions with HEWL aggregates when situated within an acidic environment of pH 2. This interaction notably inhibits aggregate fibril formation. However, it is noteworthy that DHF's inhibitory influence is not extended to amorphous aggregates at pH 5. Conversely, under the distinctly alkaline conditions at pH 12.2, DHF's inhibitory impact on HEWL aggregates is of a milder nature. This observation aligns with the compound's propensity to moderately impede the formation or stability of these aggregates. These outcomes possess substantial significance and furnish a heightened comprehension of the conceivable mechanisms underpinning DHF's capacity to impede the process of amyloid fibrillation. This study provides new avenues in the realm of screening and identifying novel compounds with the capability to modulate amyloid aggregation processes.

Furthermore, the effect of DHF on colon cancer cells SW480 and HCT116 was studied. The results suggested that DHF does not show cytoxicity towards normal human keratinocyte cells (HaCaT) compared to cancer cells SW480 and HCT116 by MTT (3-(4,5-Dimethylthiazol-2-yl)-2,5-Diphenyltetrazolium Bromide) assay. Cells were treated with varying concentrations of DHF, and its effects were evaluated through cell viability assays, cell proliferation assay, and migration assay. To gain insights into the underlying mechanisms, we performed Western blot analysis to assess the expression levels of key proteins involved in cell migration and proliferation which includes E-cadherin, N-cadherin and CXCR4. DHF was found to be non-cytotoxic against normal HaCaT cells. Significant suppression of migration in both the cancer cells on treatment with DHF in dose dependent manner was observed. DHF upregulated the expression of E-cadherin while downregulating the expressions of N-cadherin and CXCR4 in both the cell lines. In addition to DHF, we included kaempferol as a comparative agent due to its structural relationship, as DHF is a derivative of kaempferol. Kaempferol has been extensively reported to exhibit a range of anticancer activities. DHF showed significant dose dependent inhibition of cell proliferation in both the cell lines. Collectively, our findings underscore the potent anticancer properties of DHF, in inhibiting colon cancer cell migration and proliferation. These results provide motivation to explore the diverse potential of flavonoids in cancer therapy and encourage continued research into harnessing natural compounds for combating cancer.

Table of Contents

8

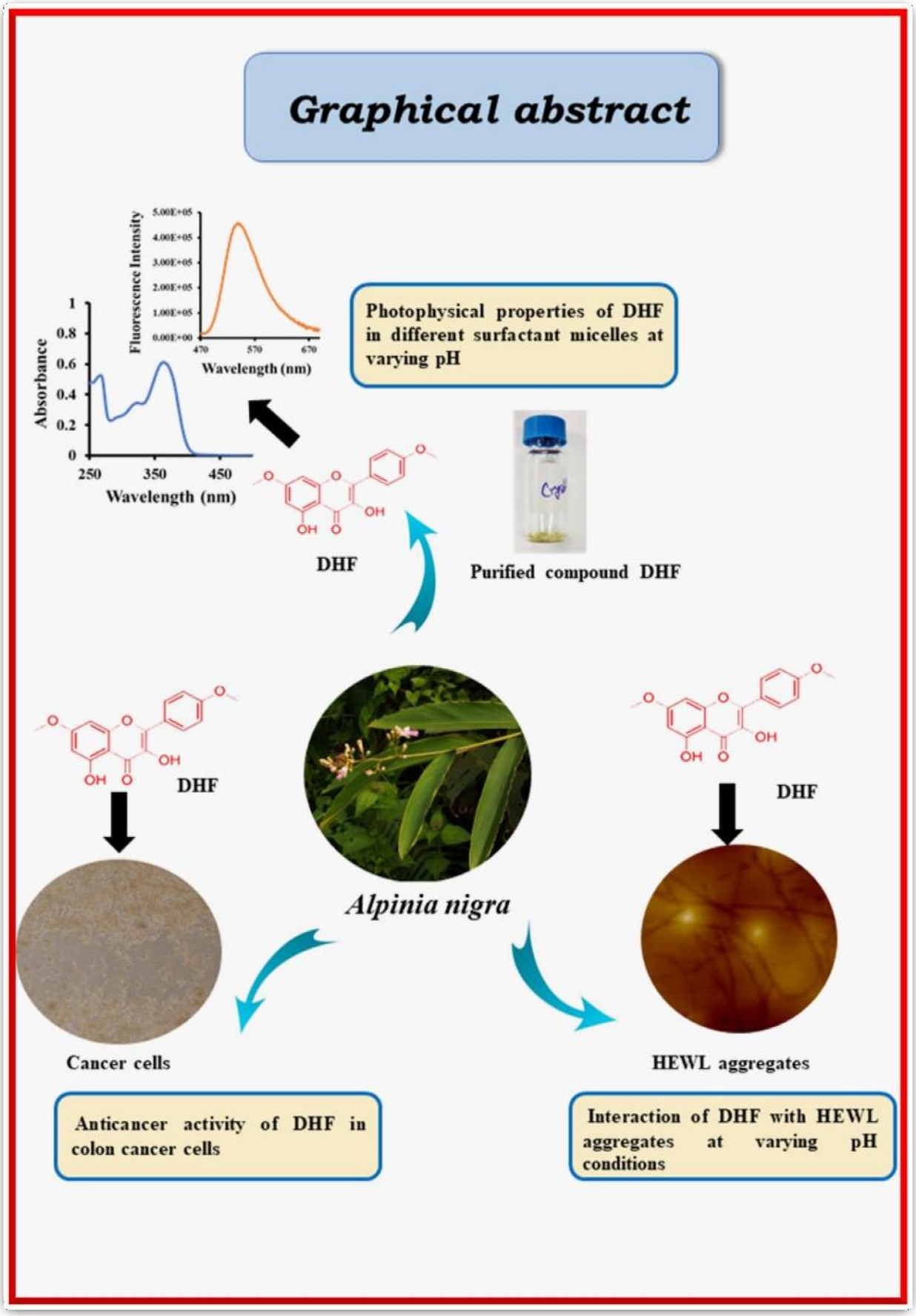
Graphical abstract
Fluorescence Intensity
Wavelength (nm)
Absorbance
Wavelength (nm)
Photophysical properties of DHF in different surfactant micelles at varying pH
DHF
Purified compound DHF
DHF
DHF
Alpinia nigra
Cancer cells
HEWL aggregates
Anticancer activity of DHF in colon cancer cells
Interaction of DHF with HEWL aggregates at varying pH conditions

Chapter1

Introduction and Review of Literature

1.1 Introduction

Natural polyphenols are primarily botanical compounds featuring a phenolic hydroxyl structure, widely prevalent in the plant kingdom (Lewandowska et al., 2013). This diverse group encompasses flavonoids, phenolic acids, tannins, and other substances, known for their robust antioxidative properties. These compounds effectively neutralize free radicals within the human body, playing a pivotal role in preventing cardiocerebral disorders and retarding the aging process. Polyphenols not only exhibit potent antioxidative characteristics (Zhang et al., 2013) but also demonstrate anticancer (Noratto et al., 2009), bacteriostatic (Ng et al., 2019), hepatoprotective (Callcott, 2019), anti-infective (Pešić et al., 2019), cholesterol-lowering (Liu et al., 2018), and immune-enhancing (Cuevas et al., 2013) properties. Furthermore, they exert preventive effects against various biological activities, including type 2 diabetes (Xiao et al., 2013). Flavonoids are a family of plant natural products derived from the phenylpropanoid metabolic pathway, which contains a C15 benzene ring structure of C6-C3-C6 and phenolic group at different locations. They reveal a variety of biological actions, but are well recognized for its antioxidant properties. Flavonoids are categorized into numerous subgroups based on structural properties such as the amount of hydroxyl or methyl groups and the heterocyclic ring oxidation, such as flavanones, flavones, isoflavones, stilbenes, chalcones, aurones, dihydroflavonols, anthocyanins, and so on. (Liu et al., 2021).

India boasts a rich spectrum of traditional medical systems, where plants play a central role in the majority of these practices. Ayurveda, Homeopathy, Siddha, Unani, and Tibetan medical traditions are reported to incorporate approximately 8000 plant species in their therapeutic approaches, showcasing the profound botanical knowledge deeply rooted in these ancient healing traditions (Khajuria et al., 2021). In plants, secondary metabolites play a vital role in potential defence mechanism especially in the chemical conflict between plants and pathogens, to attract pollinators, allelopathic agents, UV-light shielding of the leaves and various signal transduction (Ahmed et al., 2017).

Apart from medicinal properties, natural product has attracted great interest due to their use as dyes, polymers, fibers, glues, oils, waxes, flavouring agents, and perfumes. The term “secondary metabolites” was first quoted by A. Kossel in the year 1891, while he described that they hold less significance in plant life. The discovery of natural products has increased exponentially in recent decades, from just a handful of compounds per year in the 1940s to an average of over 1,600 per year in the last two decades. This surge is attributable to a number of factors, including the growing recognition of the therapeutic potential of natural products,

the development of more sophisticated analytical tools, and the refinement of compound isolation and structure determination techniques. In the early days of natural product research, scientists were limited by the rudimentary analytical tools available at the time. This made structure determination extremely challenging and time-consuming, often requiring years of painstaking work. However, the success of early therapeutic leads from nature, such as penicillin and streptomycin, spurred a surge of interest in the field. This led to the development of more sophisticated analytical tools, such as high-performance liquid chromatography (HPLC), nuclear magnetic resonance (NMR) spectroscopy, and mass spectrometry. The invention of 2D NMR methods in the mid-1980s was a particularly significant breakthrough, revolutionizing the process of compound isolation and structure determination (Pye et al., 2017). With the advancement in discovery of natural products; addressing their specific biological activities; exploring their importance in various other fields; their ethnopharmacological values has promoted further investigations of plant secondary metabolites for effective drug discovery.

In response to environmental stress, plants commonly synthesize secondary metabolites, which have demonstrated significant therapeutic benefits for humanity owing to their diverse pharmacological properties (Roy et al., 2022). These natural products exhibit an extraordinary range of structural and physicochemical diversity, coupled with potent pharmacological activities, making them invaluable resources in medicinal research. Despite their occasional fluorescence, often perceived as a curiosity by chemists, natural products possess exceptional molecular and biological attributes. Fluorescence, although perceived as a peculiarity, serves as a valuable asset in the study and development of these metabolites in both fundamental and applied life sciences. However, systematic investigations into fluorescent natural products have been relatively limited on a global scale, marking an area with untapped potential for further exploration and discovery (Duval and Duplais, 2017). Additionally, its utility extends to various domains including food technology, the dyeing industry, pesticide development, polymer synthesis, and other diverse applications (Senthilkumar et al., 2023).

Polyphenols' photophysical and photochemical activity is of significant interest for possible therapeutic uses (Kelm et al., 2000; Psotova et al., 2006). Polyphenol photophysical characteristics, such as optical absorption and fluorescence, are greatly influenced by the solvent and pH of the solution. Favaro et al., (2007) investigated the acido- and iono-chromic characteristics of apigenin and luteolin, which are responsible for the color changes seen with age and have applications in diagnostics and art conservation. In ordered media such as liposomes (Mignet et al., 2012; Sengupta et al., 2004), bile salt media (Selvam and Mishra,

2011), and cyclodextrins (Mojr et al., 2010), the optical absorption and fluorescence characteristics of fisetin, another flavonoid polyphenol, display two emission peaks.

In 2015, Tu Youyou was awarded the Nobel Prize in Physiology and Medicine for her ground-breaking discovery of artemisinin and dihydroartemisinin, marking a significant milestone in the realm of antimalarial drugs (Su and Miller, 2015). This achievement underscored the profound potential of plant-based components in drug discovery, highlighting their vital role in the field. The success of artemisinin is not an isolated case but rather a small fragment of the vast array of plant-derived compounds with potential therapeutic value. Notably, the National Cancer Institute (NCI) in the USA has channelled substantial efforts into exploring plant-based compounds for cancer treatment. Their Cancer Moonshot^{SM} project, designed to accelerate cancer research and enhance therapeutic options for patients, focuses extensively on phytochemicals. Within this initiative, the NCI has curated a comprehensive collection of natural products and their purified chemical constituents, facilitating researchers in their quest to discover novel anticancer drugs (Ashraf, 2020).

Numerous natural compounds derived from plants have demonstrated potential as therapeutic agents for several neurodegenerative diseases including Alzheimer's disease due to their anti-amyloid aggregation properties. Despite their effectiveness, the precise mechanisms underlying their activity remain unclear. Many of these natural compounds are observed to directly interact with diverse amyloid species, including oligomers and fibrils. This interaction induces conformational changes in beta-sheet assemblies, leading to the formation of non-toxic aggregates, thereby making them promising candidates for Alzheimer's disease treatment. Flavonoids, particularly myricetin and quercetin, are neuroprotective in Alzheimer's disease (AD) through a variety of mechanisms (Bu et al., 2016).

The majority of plant polyphenols exhibit a non-polar nature, impacting their solubility, stability, and bioavailability within biological systems (Mondal et al., 2016). Additionally, these compounds are chemically unstable, reactive, and prone to degradation due to external factors such as temperature, chemical processing, and oxidation (Chang et al., 2022). Consequently, extensive research efforts are focused on developing efficient carrier systems to safely deliver these molecules to specific targets within cells and tissues.

One notable technique involves encapsulation within self-assembling surfactant micelles. This method serves to shield drug-like molecules from adverse environmental conditions while facilitating their absorption. Molecular-level studies examining the interactions between drugs and micelles play a crucial role in predicting various pharmacological and pharmacokinetic properties of diverse drugs, thereby influencing their

efficacy (Saraf et al., 2018). Furthermore, these micelles are recognized for their ability to augment the bioactivity of phenolic compounds (Chat et al., 2011; Kwaśniewska & Kiewlicz, 2022).

In our current investigation, our primary emphasis is placed on *Alpinia nigra*, a plant species within the Zingiberaceae family. The family Zingiberaceae is widely studied for its important medicinal values and its major contribution in Indian Ayurvedic medicine. Gingers are annual or perennial rhizomatous herbs and are known for their use in various products such as spices, drugs, perfumes etc. The family Zingiberaceae consists of various important genera having their medicinal values such *as Alpinia, Amomum, Curcuma, Elettaria, Hedychium, Kaempferia and Zingiber* (Kumar et al., 2013). The family Zingiberaceae is rich in metabolites such as flavonoids, tannins and some terpenoids which have therapeutic properties against various cancer, neurodegenerative diseases, heart disease and several forms of other diseases.

A. nigra (Gaertn.) Burtt is a perennial and aromatic rhizomatous herb with medicinal properties. It is widely distributed in China, India, Srilanka and other Southeast Asian countries (Panizzi et al., 2002). In many traditional dishes it is widely used as a flavouring agent and spice. In Assam it is commonly named as "Tora" and the aqueous extract from its rhizome and shoot is used as folk medicine to treat various health problems such as bone weakness, jaundice, gastric ulcers etc (Tushar et al., 2010). Report suggests that the seed extracts have effective antibacterial properties (Ghosh et al., 2013), the rhizome extracts have anti-inflammatory effects (Das and Qais, 2012), the ethanolic shoot extract showed anthelmintic effects (Roy and Swargiary, 2009), also cytotoxic and analgesic effects of leave extracts were reported from the plant (Ahmed et al., 2015).

The plant *A. nigra* has remained relatively unexplored in scientific research. Consequently, our present investigation was initiated with the primary objective of isolating a remarkably pure compound, namely 3,5-dihydroxy-7,4'- dimethoxyflavone (DHF), belonging to the flavonoid class. This compound was meticulously extracted from mature leaves of *A. nigra* using organic solvents. Subsequent to its isolation, our research aims to explore its photophysical attributes in the presence of diverse surfactant micelles and to evaluate its potential biological activity.

1.2 Advancement in natural product research

Natural products present distinct attributes when compared to traditional synthetic molecules, offering both advantages and complexities in the realm of drug discovery. Developing drug leads from natural products can be particularly challenging, especially when intricate synthetic pathways are involved (Atanasov et al., 2021). Moreover, natural product-based drug leads are often pinpointed through phenotypic assays, and unravelling their precise molecular mechanisms can be a time-intensive endeavour (Corson and Crews, 2007). Fortunately, significant progress has been made in refining screening assays, utilizing innovative techniques such as induced pluripotent stem cells and gene editing technologies. These advancements contribute substantially to elucidating the modes of action of active compounds, enhancing our understanding of their therapeutic potential (Moffat et al., 2017; Shi et al., 2017).

Classical research in the field of natural product-based drug discovery commences with the biological screening of 'crude' extracts, aiming to identify a bioactive 'hit' extract. Subsequently, this extract undergoes further fractionation to isolate the active natural products. The process of bioactivity-guided isolation is inherently laborious and encumbered with limitations; however, various strategies and technologies have been devised to address these challenges (Allard et al., 2018; Hubert et al., 2017). For instance, in order to create libraries compatible with high-throughput screening, crude extracts can be pre-fractionated into sub-fractions that are better suited for automated liquid handling systems.

Metabolomics emerged as a powerful approach for the simultaneous analysis of multiple metabolites in biological samples. This method offers precise insights into the metabolite composition within natural product extracts. It aids in prioritizing natural products for isolation, expedites dereplication, and assists in annotating unknown analogues and new natural product scaffolds. Metabolite profiling typically involves the use of advanced techniques such as nuclear magnetic resonance (NMR) spectroscopy or high-resolution mass spectrometry (HRMS), often in combination with upstream liquid chromatography (LC) (Eugster et al., 2011) methods like LC-HRMS. These techniques, such as LC-HRMS, prove instrumental in separating numerous isomers present in natural product extracts. Dereplication of secondary metabolites in bioactive extracts involves determining molecular mass and formula, followed by cross-referencing in literature or structural natural product databases

enriched with taxonomic information. Proprietary databases like the Dictionary of Natural products play a pivotal role by compiling metadata that are challenging to extract from the literature. These databases offer valuable links to the biological sources of natural product structures (Stavrianidi, 2020).

Furthermore, advancements in our understanding of biosynthetic pathways for natural products and the development of sophisticated tools for genome analysis and manipulation are pivotal drivers in modern natural product-based drug discovery. Biosynthetic genes in the genomes of natural product-producing organisms are identifiable due to their clustering in the genomes of bacteria and filamentous fungi. Many natural products are built upon polyketide or peptide cores, and their biosynthetic pathways involve enzymes such as polyketide synthases (PKSs) and nonribosomal peptide synthetases (NRPSs). These enzymes are encoded by large genes with highly conserved modules, enabling their identification and manipulation for tailored drug discovery efforts (Ziemert et al., 2016).

1.3 Pitfalls in plant medicinal research

Medicines made out of plant-based products have been used by man since ages. These have helped him stand the test of time by enriching him with immunity against several commonly occurring disease such as cold, fever, joint pains etc. India has been the host to development of a few traditional systems of medicine. These systems include Ayurveda and Unani, which are based upon the use of plant-based medicines to cure common ailments. However, no scientific records are available to decide the effectivity and the identity of these plants. This has led to doubts and concerns being raised over the use of plant-based medicines, alongside a few other reasons. Other reasons being (i) several herbs known by the same name have different scientific identity, (ii) Even if they do have the same scientific identity or origin, they differ based upon the topography they are exposed to and grown in, (iii) various stages of processing the plant-based medicines cause variations in the effectiveness and the safety, (iv) frequent unavailability of these medicine create a lot of disorder and chaos, and (v) the bar for standard in the field of herbal medicines aren't specifically set. These pitfalls have delayed the inculcation of some well-known traditional medicine recipes into modern medicinal system (Gupta, 1994).

Commercially traded raw herbal drugs are subject to regulation and control through diverse measures, varying across countries. Among these measures, species protection stands out as a paramount consideration in the international trade of medicinal plants. The Convention on International Trade in Endangered Species of Wild Fauna and Flora (CITES), an

international treaty proposed by the World Union Conservation (WUC), has established rigorous protocols to regulate international trade, ensuring the trade of specimens without jeopardizing their survival. In India, the escalating demand from herbal industries has led to unscientific extraction of medicinal plants from the wild, constituting approximately 80 percent of the extraction (Ved and Goraya, 2007). This rampant extraction has resulted in the overexploitation of resources, posing a grave threat to the survival of these species and severely impacting the livelihoods of communities dependent on these resources. The inaccessibility to potent ayurvedic raw drugs has further exacerbated the situation, leading to adulteration and substitution with closely related or similar-looking species, thereby compromising the quality of these herbal (Unnikrishnan et al., 2020).

The escalating global utilization of plant-based medicines is accompanied by significant challenges. Foremost among these challenges are the emergence of allergic reactions associated with these medicines, the ambiguity surrounding their precise clinical efficacy and appropriate dosage, as well as the attitudes of patients towards their utilization. These factors collectively contribute to the decline in the field of plant medicinal research. Natural medicine is widely perceived as safe, with minimal adverse drug reactions (ADRs). However, despite their natural origin, Chinese herbs, if improperly utilized, can pose risks. For instance, Ginseng, renowned for its purported benefits in prolonging life and enhancing sensory functions, may yield adverse outcomes with excessive consumption. Instead of the intended effects, excessive usage can lead to adverse reactions affecting the nervous and digestive systems. In severe cases, it may even prove fatal (Zeng and Jiang, 2010).

1.4 Plant secondary metabolites

Plants synthesize a large diversified group of low molecular weight compounds. These compounds help plants withstand extreme environments and to colonize. Low molecular weight organic compounds can be distributed, with respect to prospective function, as primary metabolites, secondary metabolites (also known as specialized metabolites) and plant hormones (Lazar, 2003). As they are known for their biological significance, plant secondary metabolites have been in use, as traditional medicines, for over centuries now. In today's era, they have been put to use in several sectors such as pharmaceutics, cosmetics, fine chemicals, or more recently nutraceuticals. Recently, surveys have also shown that 25% of the molecules used in the pharmaceutical industry are known to be of plant-based origin (GF, 1991).

Plant secondary metabolites can also be further classified into four major classes: terpenoids, phenolic compounds, alkaloids and sulphur-containing compounds. For a long time, the production of plant secondary metabolites has been based on the field cultivation of medicinal plants. However, due to the difficulties in cultivating plants which have particular biotopes, scientists and biotechnologists have been led to consider plant cell, tissue and organ cultures as alternatives to the production of plant secondary metabolites from plant cultivation (Bourgaud et al., 2001). In this discourse, we delve comprehensively into the multifaceted realm of flavonoids and their myriad applications in details.

Flavonoids and their various applications

Flavonoids are a diverse group of phytochemicals abundantly found in the plant kingdom. They are also known as secondary metabolites and plays crucial roles in plant defence mechanisms and development. During specific stress conditions, secondary metabolites can regulate various pathways and also act as toxins and antibiotics against harmful pathogens. Flavonoids are also well known for imparting colour and fragrance in flowers (D'Arcy, 2022). These are widely found among fruits, vegetables etc (Lee et al., 2009). Flavonoids were first isolated from orange in 1930 and were named as 'Vitamin P'. This was successfully done by a Hungarian physiologist Szent-Gyorgyi (Coppock and Dziwenka, 2016). Flavonoids were mass popularized after the discovery of the 'French Paradox'. It suggested the prevention of cardiovascular diseases, evident in the Mediterranean natives, due to the consumption of red wine, known to be a rich source of flavonoids (Tapas et al., 2008). The structure of flavonoids is a 15-carbon skeleton comprising of two phenyl rings named A and B linked via a heterocyclic 4H-pyrane ring named C (**Fig. 1.1**). Modification to this basic structure, through different level of oxidation and substituents to the ring C, is responsible for the existence of different classes of flavonoids (**Fig. 1.2**). Polyphenols are known to possess radical scavenging properties. The magnitude of these activities is directly pronounced by the number of hydroxyl atoms in the aromatic B-ring (Lee et al., 2009).

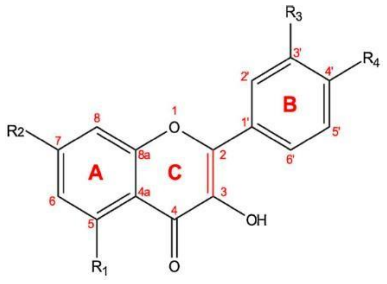

Fig. 1.1: Basic structure and numbering scheme of Flavonoids (Zeng and Jiang, 2010).

Polyphenols, have been known to generate reactive oxygen species (ROS) under certain circumstances, which can react with molecular oxygen, when auto-oxidation occurs, and produce superoxide anion radicals (O2•-) which gives rise to a pro-oxidant effect (Metodiewa et al., 1999). Flavonoids can go a step further as they have the ability to give a hydrogen atom from their catechol structure to O2•− produced during auto-oxidation to produce hydrogen peroxide (Miura et al., 1998). Report suggests that metal phenolic networks could break peroxide into reactive species, which in turn can be used in water clean-up (Tardy et al., 2018). Polyphenols are being considered as potential compounds to influence the major cellular processes involved with neurodegeneration. Among polyphenols, specifically interesting cases arise for flavonoids, which are abundantly found in food and beverages (Wang and Joseph, 1999). Certain observations have prompted researchers to develop seemingly lot of interests in flavonoids, for instance, regular intake of wild blueberry juice was found to enhance, in older adults several aspects of memory, reduced depressive symptoms and lowered glucose levels. In plants, flavonoids are the dictators for the colour and scent of flowers, to attract pollinators and scattering of fruits, to help in germination of spores, seeds, and the development of seedlings (Griesbach and Austin, 2005).

Flavonoids are known to act as UV filters. They also protect the plant from several abiotic and biotic factors (Takahashi et al., 2004). Flavonoids exhibit the role of UV absorption and plays important role in plant protection against these radiations. Research encompassing a diverse spectrum of species, including *Arabidopsis, Ligustrum vulgare, Vitis vinifera,* and *petunia*, has yielded new insights, elucidating the pivotal role of UV light in stimulating the biosynthesis of flavanol compounds (Agati et al., 2011; Berli et al., 2010; Kusano et al., 2011; Ryan et al., 2002; Stracke et al., 2010). Frost hardiness and resistibility to drought are also controlled by flavonoids and may play a functional role in adapting a plant to heat and freezing conditions. Flavonoids are also known for their antioxidant properties which solely depends on the functional group and its position around the nuclear structure. The free radical scavenging activity of flavonoid is influenced by its hydroxy groups position in the catechol B-ring and pyran C-ring (D'Amelia et al., 2018). Various subclasses of flavonoids such as flavon-3-ol, flavones and flavanones are reported to exhibit effective antiviral properties against HIV 1 and HIV 2 immunodeficiency (Tajammal et al., 2022). It has been also reported that flavonoid exhibits antibacterial activity against *Propionibacterium acnes* which causes skin acne (Tungmunnithum et al., 2018). Flavonoids are further subdivided into: flavones, flavonols, flavanones, flavanonols, flavanols **(Fig. 1.2)**.

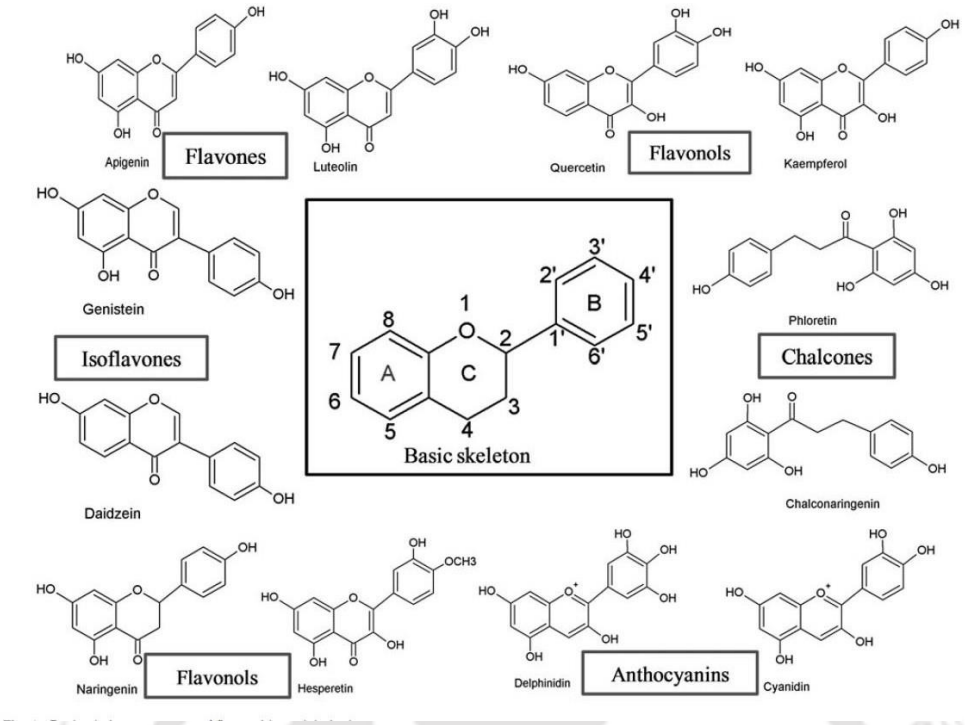

Fig. 1.2: Basic skeleton of flavonoids and their classes (Panche et al., 2016)

Over the course of time, several speculations revealed that flavonoids are known to possess anti-oxidizing, anti-microbial, anti-tumour, and anti-inflammatory properties. These findings have only fuelled the pace in research in the field of flavonoids. The biological activities of various flavonoids have been listed in **Table 1.1**.

Table 1.1: Biological activities of various flavonoids

Flavonoid	**Biological activity**	**Reference**
Silymarin	Effective against neurodegenerative diseases; inhibits Aβ aggregation	Liu et al., 2021; Roghani et al., 2010; Yin et al., 2011
Naringin	acetylcholinesterase inhibitor	Remya et al., 2014
Naringenin	acetylcholinesterase inhibitor	Sachdeva et al., 2014
Baicalein	modulates metabolic balance between glutamate and GABA	Yu et al., 2012
Rutin	Activation of MAPK, ERK2, and PI3K pathways.	Magalingam et al., 2013

Quercetin	Increases the antioxidant defenses GSH and SOD and increases the dopamine levels Decreases extracellular b-amyloidosis, tauopathy, astrogliosis, and microgliosis by decrease BACE1-mediated cleavage of APP (into CTFb)	Haleagrahara et al., 2013
Apigenin	Induces neurogenesis via ER a and b	Zhao et al., 2013
Genistein, daidzein, quercetin	Human Breast cancer	Han et al., 2001; Pouget et al., 2001
Quercetin, myricetin, chalcones	Human Leukemia	Petrides et al., 1990; Shi et al., 2001 Chung et al., 1999; Csokay et al., 1997
Diosmetin	Anticancer activity	Androutsopoulos et al., 2009
Dihydromyricetin	Anticancer activity	Wu et al., 2013
Theaflavin	Antibacterial activity	Vijaya et al., 1995

Anticancer properties of flavonoids

Flavonoids have been reported to exhibit anticancer properties against various cancers; Reports suggest that flavonoids are capable of inhibiting the proliferation of tumour cells by inhibiting the formation of ROS, cyclooxygenase-2 and 5-lipoxygenase enzymes (Ginwala et al., 2019). Kaempferol have been reported to show activity against breast cancer cell (MCF-7), human osteosarcoma, lung and stomach cancer cells (Kozłowska and Szostak-Węgierek, 2022). Kaempferol have also shown to cause apoptotic cell death in endometrial cancer by suppressing 17β-estradiol-induced Bcl-2 and survivin expression (Chuwa et al., 2018), it has been also reported to induce autophagy in human hepatic cancer cells (Huang et al., 2013). Quercetin is reported to downregulate the expression of antiapoptotic molecules Bcl-2, Bcl-xL and upregulating proapoptotic molecules such as caspase-3, caspase-9, Bid, Bad, Bax and cytochrome C, resulting in inhibition of human metastatic ovarian cancer cell PA-1 cells growth (Teekaraman et al., 2019).

1.5 Anti-amyloidogenic properties of polyphenols

Proteins stand as paramount macromolecules, comprising elongated sequences of amino acids vital for cellular activities. Their diverse structures and functions are orchestrated by ribosomes, cellular machinery producing these biomolecules. The linear covalent arrangement of polypeptides by ribosomes eventually acquires specific native conformations. Protein folding, a process intricately governed by amino acid sequences, enables polypeptides to adopt their unique, functional native structures through physical mechanisms (Finkelstein et al., 2017). However, the transformation of peptides and proteins into distinctive amyloid fibrils constitutes a fundamental factor underlying several neurodegenerative disorders (Chiti and Dobson, 2006). The various stages of protein aggregate formation have been depicted in **Fig. 1.3.**

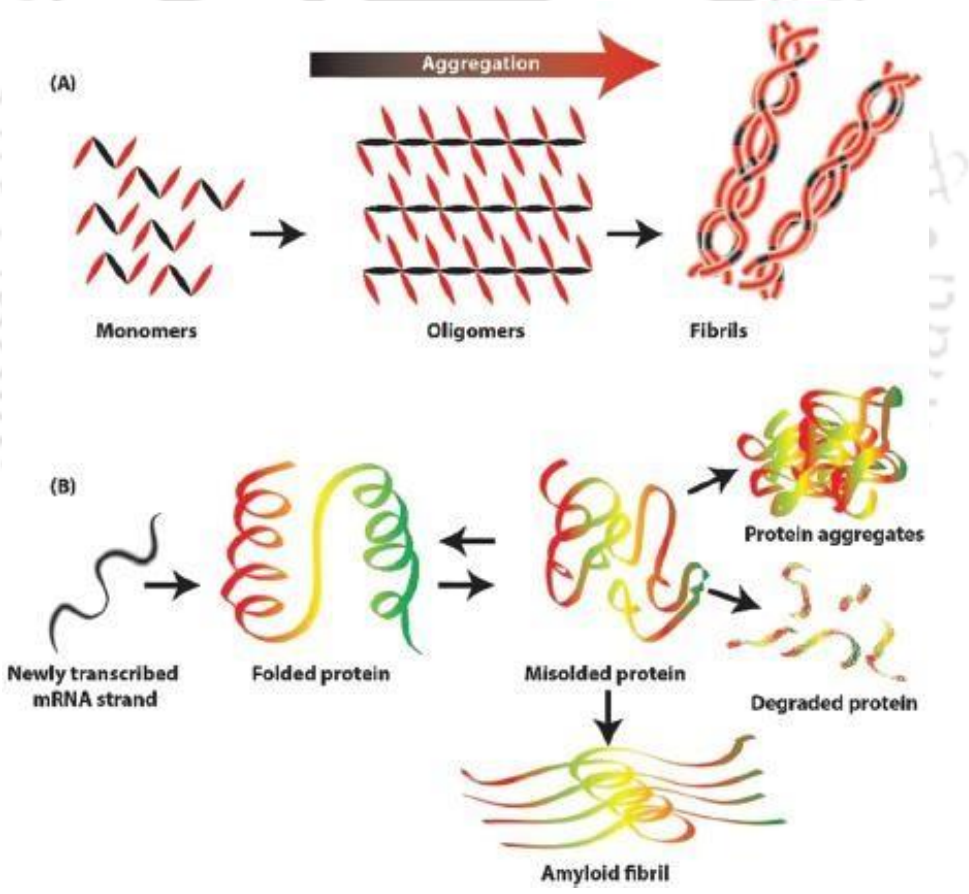

Fig. 1.3: (A) Diagrammatic representation of the steps for the formation of aggregation. (B) Depicted events shows the misfolded proteins or amyloid fibrils can form protein aggregate or refold back to the native structure (Rajan et al., 2021).

Distinct protein aggregates are typically specific to particular diseases, whether occurring within the central nervous system (CNS) or in peripheral tissues. Amyloid beta (Aβ)

and tau aggregates are hallmarks of Alzheimer's disease (Duyckaerts et al., 2009), whereas alpha-synuclein (α-syn) is the central player in Parkinson's disease (Samii et al., 2004). Prion disorders, also known as transmissible spongiform encephalopathies (TSE), are characterized by misfolded prion protein (PrPSC) aggregates (Hetz and Soto, 2003). Amyotrophic lateral sclerosis (ALS) cases show superoxide dismutase 1 (SOD1) and TAR DNA binding protein (TDP-43) aggregates (Taylor et al., 2016). Huntington's disease is defined by the accumulation of huntingtin protein (htt), which is prone to aggregation owing to glutamine-rich region expansions (polyQ), resulting in the formation of neuronal inclusion bodies (Ross and Tabrizi, 2011). AA amyloidosis is a peripheral illness characterized by aberrant deposition of insoluble serum amyloid A protein (SAA) in the liver, spleen, and kidney (Westermark et al., 2015). Islet amyloid polypeptide (IAPP or amylin) accumulates in pancreatic beta cells in type 2 diabetes (T2D) (Mukherjee et al., 2015). Transthyretin amyloidosis is a slowly progressing disorder characterized by the build-up of misfolded transthyretin (TTR) in the peripheral nerve system, resulting in peripheral neuropathy (Sekijima, 2015). Regardless of the illness, protein aggregation development follows a common seeding-nucleation kinetic model that involves soluble intermediate species, protofibril formation, and the build-up of insoluble fibrillar aggregates (Morales et al., 2013; Moreno-Gonzalez et al., 2011).

Polyphenols represent an extensive category of naturally occurring chemical compounds, however synthetic and semi-synthetic structures containing one or more aromatic phenolic rings have also been identified. Polyphenols sourced from natural products like green tea, grapes, and red wine have demonstrated the ability to mitigate protein aggregation both *in vitro* and *in vivo* (Ngoungoure et al., 2015). The past decade has witnessed profound research focus on diminutive natural compounds abundant in aromatic groups, particularly polyphenols. The allure of these entities lies in their natural origin, prevalent in food and herbal extracts, ensuring widespread availability, stability, minimal adverse effects, and convenience (Dhouafli et al., 2018).

Curcumin (1E,6E)-1,7-bis(4-hydroxy-3-methoxyphenyl) hepta-1,6-diene-3,5-dione, is a yellow compound naturally occurring in turmeric. Renowned for its multifaceted properties, including anticancer, antioxidant, and antiviral activities, curcumin has also been extensively investigated for its anti-aggregation capabilities in proteins. Studies have demonstrated curcumin's efficacy in mitigating the aggregation of proteins such as HEWL, Aβ, insulin, lysozyme, synuclein, and prion protein (Folch et al., 2018; Sgarbossa, 2012). Notably, its lipophilic nature enables curcumin to permeate the blood-brain barrier, allowing it to interact

with amyloids, disrupting their oligomeric structures and impeding amyloid production (Ringman et al., 2005). Curcumin operates through diverse mechanisms on various proteins, encompassing the prevention of conformational alterations, disaggregation of formed aggregates, and inhibition of fibril formation (Ahsan et al., 2015; Ghosh et al., 2015). The effect of curcumin on HEWL aggregates is shown in **Fig. 1.4.**

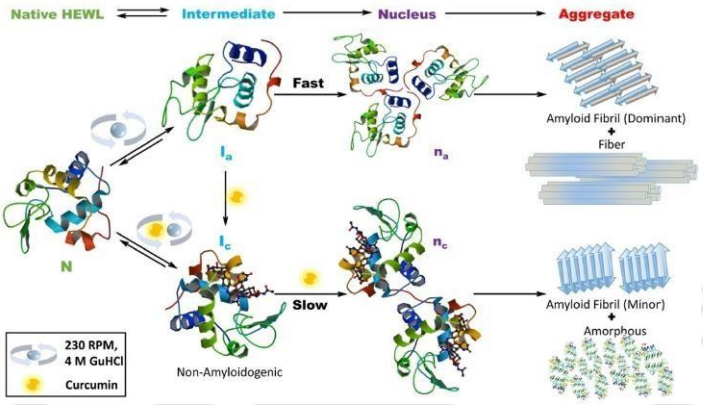

Fig. 1.4: Schematic model of the effect of curcumin on the aggregation of Hen egg white lysozyme, as model of globular proteins (Ahmad et al., 2017).

Tannic acid, a water-soluble polymeric polyphenol composed of phenolcarboxylic and gallic acids, functions as a dose-dependent inhibitor of β-amyloid fibrillization (Ono et al., 2004). Another polyphenol, primarily found in green tea, (-)-epigallocatechin-gallate (EGCG) (Cádiz-Gurrea et al., 2014), has demonstrated diverse biological activities such as antibacterial, antioxidant, neuroprotective, and anticancer properties both *in vitro* and *in vivo* (Amrati et al., 2021; Betts et al., 2015). EGCG exhibits promising effects in inhibiting proteins like Ab, tau, aSyn, IAPP, TTR, and Htt, although the underlying mechanisms remain elusive. Polyphenolic inhibition extends to IAPP, insulin, and β-amyloid inhibited by phenolsulfonphthaleine, and -synuclein inhibited by baicalein (Höppener et al., 2000; Zhu et al., 2004). Moreover, compounds like exifon, myricetin, hypericin, gossypetin, purpurogallin, pentahydroxybenzophenone, and epicatechin gallate have demonstrated inhibition of β-amyloid and tau protein (Porat et al., 2006). Squalamine, a natural substance with anticancer and antiviral potential, significantly influences α-synuclein aggregation by competitively binding with the lipid membrane (Perni et al., 2017). Gallic acid, sourced from green tea leaves, emerges as a dual regulator of amyloid and metal-induced aggregation, suggesting potential avenues for metal-based treatments in neurodegenerative disorders (Khan et al., 2019).

1.6 UV-visible spectroscopy of polyphenols

Molecules exhibit intricate charge and spin distributions, coupled with dynamic electric and magnetic fields that undergo transformations upon interaction with light. When a molecule absorbs energy, an electron transitions occurs from an occupied orbital to a vacant orbital possessing higher potential energy. Generally, the transition from the Highest Occupied Molecular Orbital (HOMO) to the Lowest Unoccupied Molecular Orbital (LUMO) predominates. Most molecules feature lowest-energy occupied molecular orbitals corresponding to s bonds, characterized by relatively lower energy levels. In contrast, nonbonding (n) orbitals carrying unshared pairs manifest at slightly higher energy states. The utmost energy levels are occupied by empty antibonding orbitals (π * and σ *) (Cantor and Schimmel, 1980; Pavia et al., 2014). The electronic energy levels and transitions are shown in **Fig. 1.5**.

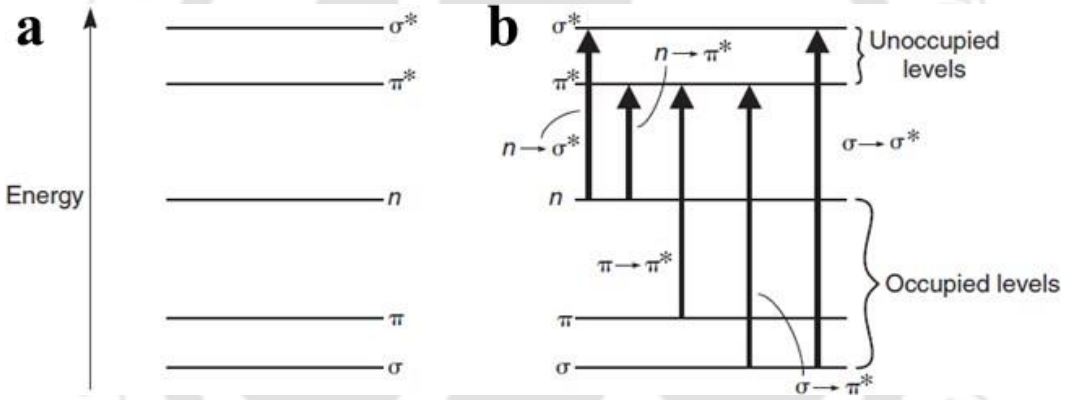

Fig. 1.5: Electronic energy levels and transitions (Pavia et al., 2014)

A σ orbital arises from the amalgamation of two s atomic orbitals, a combination of one s and one p atomic orbital, or the alignment of two p atomic orbitals with collinear symmetry, forming what is referred to as a σ bond. Conversely, when two p atomic orbitals overlap laterally, they create a π orbital, giving rise to a π bond. In molecules like ethylene (CH2=CH2), carbon atoms are bonded through a combination of an s and a p bond. In this context, when a photon holding adequate energy interacts, it can elevate one of the π electrons to an antibonding orbital denoted as π*. This transition, known as π- π*, necessitates a significant energy input, particularly in the far-field spectrum. Contrastingly, a much higher energy input is imperative for the promotion of an σ electron (Valeur and Berberan-Santos, 2012).

Within molecular configurations, heteroatoms like oxygen or nitrogen can harbour non-bonding electrons within their respective orbitals, denoted as n orbitals. It is crucial to note that

a non-bonding electron possesses the capacity to transition into an antibonding orbital, transformation is represented as n- π*(Valeur and Berberan-Santos, 2012).

Aromatic compounds frequently undergo transitions within conjugated systems marked by π-π* transitions, as well as transitions due to the substituent nature denoted as n- π*. Notably, polyphenols, in contrast to monocyclic compounds, exhibit extended conjugation, causing a convergence of electronic energy levels. This phenomenon reduces the energy threshold for transitions, leading to bathochromic shifts and hyperchromism (Pavia et al., 2014).

The UV/Vis spectra of polyphenols are frequently attributed to electronic transitions occurring within p-type molecular orbitals (MOs), the characteristics of which vary along the molecular backbone based on the subclass. Elevated molar absorption coefficients, indicative of strong transitions, stem from several factors: (i) significant coefficients in the linear combination of atomic orbitals (LCAO), (ii) extensive molecular topology, and (iii) topological resemblance in the contributing orbital (Gierschner et al., 2012). In the realm of flavonoids, the LUMO clusters are typically situated either directly on the carbonyl group or are diffusely spread across the molecular moiety encompassing the carbonyl group. Simultaneously, the HOMO clusters exhibit delocalization predominantly within the B ring. This distinctive arrangement engenders intramolecular charge transfer phenomena during the HOMO-LUMO transition, unveiling the nuanced electronic dynamics within these compounds (Markovic and Tosovic, 2015). An example depicting the energy and HOMO and LUMO for quercetin and its glucosides is shown **(Fig. 2.6)**.

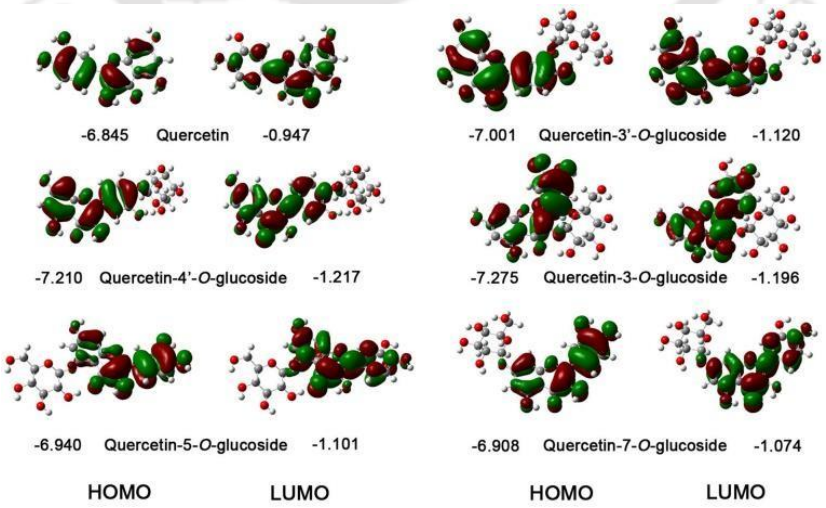

Fig. 1.6: The energy and distribution of HOMO and LUMO for quercetin and its glucosides in the gas phase (Zheng et al., 2017).

The nonbonding n orbitals, possessing lower energy levels than the p orbitals, are precluded from engagement in electronic transitions, as observed in previous studies involving monohydroxy-flavones, specifically flavonols (Cornard et al., 1997). The HOMO demonstrates an antibonding disposition concerning the interring bond, harmonizing with the rotational dynamics of the B ring in relation to the chromone segment. In contrast, the LUMO exhibits a bonding character pertinent to the same bond. The prominent peak within the long-wave spectrum predominantly stems from the HOMO-LUMO transition, constituting a significant majority, surpassing 51% of the overall spectral contribution. This involvement diminishes substantially in subsequent transitions. During the HOMO-LUMO transition, electronic charge density migrates from the B ring to the $C4{=}O_2$ bond. In other transitions, charge transfer occurs from one aromatic ring, traversing through carbon (C), to the adjacent aromatic ring (Cornard et al., 1997). At long wavelengths, flavones, flavonols, and isoflavones universally exhibit the HOMO-LUMO and HOMO-1-LUMO transitions. Due to their modest energy disparities and spatial distinctions, these transitions underpin the most robust absorption bands in flavones and flavonols. Notably, the presence of a potent hydrogen bond diminishes the HOMO-LUMO gap in flavonols, causing the absorption band linked to the HOMO-LUMO electronic transition to manifest at wavelengths longer than observed in flavones. In the realm of isoflavones, weak conjugation between the HOMO and LUMO clusters, coupled with heightened energy discrepancies, leads to the emergence of a subtle shoulder in their electronic transitions (Tošović and Marković, 2017).

1.7 Plant polyphenols in focus: overcoming drug-delivery complexities

In recent years, there has been a notable upsurge in the exploration of alternative medicines and the medicinal applications of natural products, particularly those derived from plants. Phytochemicals, comprising diverse compounds, find utility in various forms such as conventional foods, dietary supplements, pharmaceuticals, cosmetics, and medical devices, contingent upon the characteristics of the final product (Hoffman, 2015). Governments, international organizations, and industries are actively engaged in the search for potential medicinal herbs and natural products, viewing them as abundant sources of novel medicinal compounds. Remarkably, a substantial number of newly licensed chemical entities in the past two decades have been small-molecule natural products (SMNPs) or SMNP-derived entities. This resurgence in interest surrounding plant derivatives can be attributed to various factors,

including the amplified adverse effects associated with conventional treatments (Benowitz, 1996; Danishefsky, 2010).

However, the use of these plant-derived compounds presents challenges that hinder patient compliance. Factors such as potent odour and unpalatable taste contribute to these challenges. Additionally, issues like low solubility, slow dissolution rates, and instability at high pH levels significantly diminish their therapeutic efficacy, necessitating high dosages for meaningful impact (Puglia et al., 2017). According to the "Lipinski rule" (Biasutto et al., 2014; Lipinski, 2001), their reduced absorption correlates with their polarity and substitution groups. On the other hand, it is critical to evaluate the compound's cell permeability as well as its water solubility. Polyphenols are characterized as (1) having high solubility but poor cell membrane permeability, (2) having low solubility and low cell membrane permeability, and (3) having low solubility but good cell membrane permeability (Hu et al., 2017).

The low aqueous solubility of many drugs is a major challenge in drug delivery, as it is associated with low oral bioavailability (Bansal et al., 2011). To counter this challenge, the utilization of nanosized drug carriers, including polymeric nanoparticles, liposomes, dendrimers, and micelles, has emerged as a promising approach. These carriers can enhance the delivery of drugs to their target tissues and increase their bioavailability by many folds (Mishra et al., 2010; Oerlemans et al., 2010).

Specific examples of delivery methods that have already made an impact:

- Nanoparticle

Nanoparticle systems are emerging as a powerful tool for drug delivery. Nanoparticles can protect drugs from enzymatic degradation (Khan et al., 2006), alter their pharmacokinetics (Schluep et al., 2009), reduce their toxicity (Italia et al., 2007), and provide controlled release over extended periods of time (Grabovac and Bernkop-Schnürch, 2007). Within the realm of drug delivery systems, there exist diverse types of nanoparticles, one category is self-assembled nanoparticles. These nanocarriers typically exhibit a hydrophobic core and a hydrophilic shell, rendering them superior for drug delivery purposes (Kataoka et al., 2012; Yokoyama et al., 1991). Another category comprises polymeric nanoparticles, known for their controlled and sustained release properties (Reis et al., 2006), subcellular size, and compatibility with tissues and cells (Panyam and Labhasetwar, 2003). Researchers have explored various

nanoparticle types in chemoprevention, employing compounds such as narigenin (Sulfikkarali et al., 2013), curcumin (Bisht et al., 2007), and epigallocatechin gallate (Siddiqui et al., 2009).

- Liposomes

Liposomes, spherical nanovesicles comprising natural phospholipids and cholesterol, offer a versatile platform for drug delivery. Capable of encapsulating drugs with varying solubilities or lipophilicities either within their aqueous core or at their bilayer interface, liposomes serve as effective carriers (Sharma and Sharma, 1997). Furthermore, they have demonstrated efficacy as immunological adjuvants (Gregoriadis, 1990). Liposomes derived from natural lipids possess unique attributes, being biodegradable, biologically inert, weakly immunogenic (Van Rooijen and van Nieuwmegen, 1980), and eliciting minimal antigenic or pyrogenic responses (Campbell, 1983). Their unique properties make them promising candidates for immunological adjuvants and drug carriers in a variety of biomedical applications.

- Niosomes

Niosomes, minute vesicular structures composed of cholesterol and nonionic surfactants, mirror the architecture and functionality of liposomes (Chandu et al., 2012). However, they offer distinct advantages, including reduced costs, enhanced stability, and heightened adaptability. These nanostructures exhibit the capability to encapsulate a diverse array of therapeutic agents, encompassing both hydrophilic and hydrophobic drugs (Aqil et al., 2013). Niosomes can be administered through various routes such as oral, topical, transdermal, or parenteral, among others. Niosomes have demonstrated remarkable abilities, enhancing the oral bioavailability of poorly absorbed drugs, augmenting skin penetration, and regulating drug delivery rates. Additionally, they prove instrumental in targeted drug delivery, directing medications precisely to specific tissues and cells. In summary, niosomes emerge as a compelling alternative to liposomal drug carriers, showcasing multifaceted medical applications owing to their unique properties (Aqil et al., 2013).

- Cyclodextrins

Cyclodextrins represent distinctive molecules featuring a 'pseudo-amphiphilic' structure. Cyclodextrins are produced by the enzymatic degradation of starch, and several members of this family are widely used in pharmaceutical and allied applications. Cyclodextrins have a lipophilic inner cavity and a hydrophilic outer surface. This unique structure allows cyclodextrins to form noncovalent inclusion complexes with a wide variety of guest molecules (Challa et al., 2005). The hydrophobic inner cavity of cyclodextrins can accommodate poorly water-soluble molecules, while the hydrophilic outer surface facilitates the solubility of the complex in the aqueous environment (Thompson, 1997).

- Micelles

Micelles are self-assembled spherical structures formed by amphiphilic molecules, such as lipids or polymers, in aqueous solutions (Kataoka et al., 2012). Micelles can encapsulate and deliver a wide range of therapeutic agents, including both hydrophilic and hydrophobic drugs. The drug is well protected from degradation and inactivation within the micellar core, which can result in improved bioavailability and retention. The release of drugs from polymeric micelles is governed by a variety of factors, including micelle stability, drug diffusion rate, partition coefficient, and copolymer biodegradation (Kwon and Okano, 1996). Other factors that can influence drug release include the drug concentration within the micelles, molecular weight, physicochemical properties, and location within the micelles (Teng et al., 1998). The micelle delivery system has shown great promise in preclinical and clinical studies, with seven different polymeric micelle formulations of antitumor drugs in clinical trials (Gong et al., 2012).

Encapsulation of hydrophobic drug molecules within surfactant micelles is a popular strategy for enhancing their solubility in aqueous media (Talat et al., 2019). The critical micelle concentration (CMC) of surfactants is influenced by a number of factors, including interactions between the drug and carrier materials. These interactions can also impact the loading efficiency, drug stability, and targeted delivery. Of paramount importance are two key parameters governing the interactions of drug molecules with surfactant micelles: (a) the drug-micelle binding constant, and (b) the partition coefficient at the micelle-water interface (Čudina et al., 2008; Talele et al., 2016).

In the following discussion, we delve into the intricacies of surfactant-based drug carriers, shedding light on their vital role in enhancing drug solubility and facilitating targeted delivery.

Surfactants

Surfactants, also known as surface-active agents, are organic compounds with a dual nature. Surfactants are organic compounds composed of distinct parts: a lyophobic section, insoluble in specific solvents, and a lyophilic segment, which is soluble. This dual characteristic renders surfactants amphipathic, exhibiting both hydrophobic and hydrophilic properties (Moroi, 1992). At concentrations surpassing the CMC, these molecules organize into micelles. In this arrangement, the hydrophilic head of the surfactant molecule interacts with water or polar solvent molecules, while the hydrophobic tail engages in hydrophobic interactions (Saha et al., 2023). Surfactants can be classified into various types based on the nature of their head groups, showcasing their diverse applications and fundamental role in interfacial phenomena. The systematic classification of surfactant is depicted in **Fig. 1.7**.

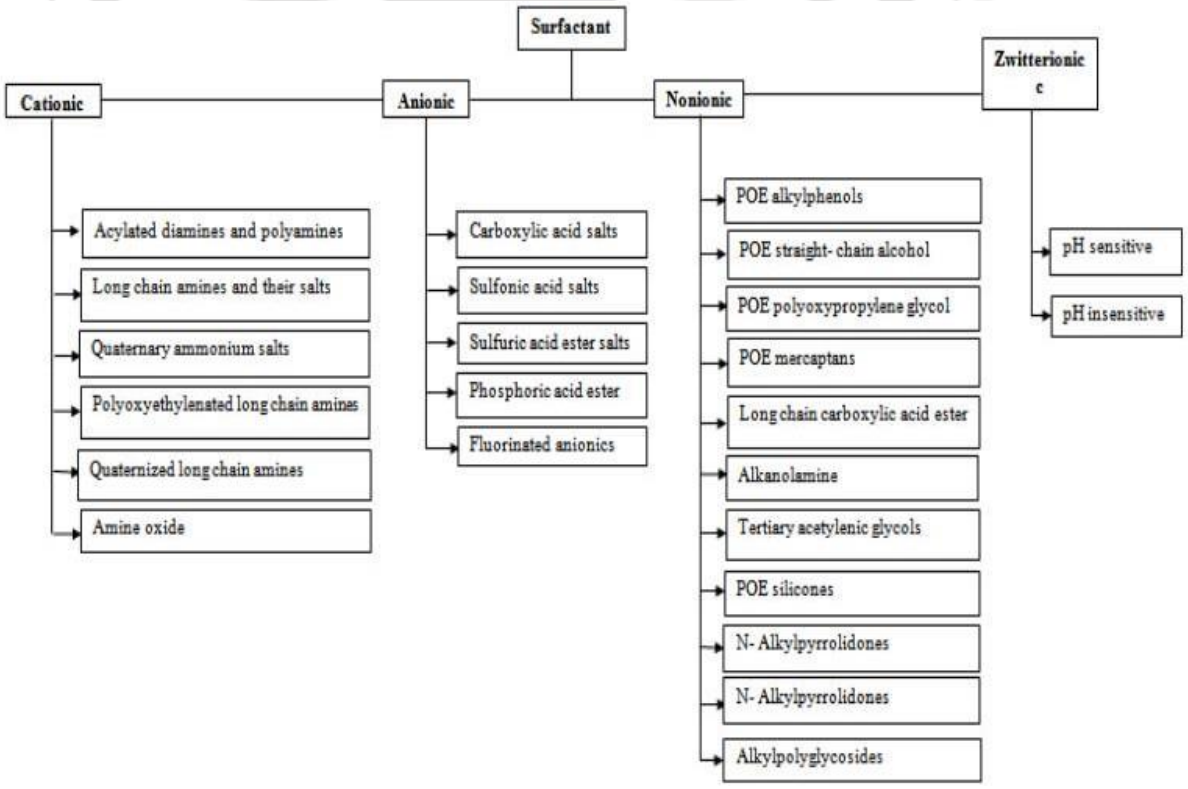

Fig. 1.7: Systematic classification of surfactants (Tiwari et al., 2018).

Some common types of surfactants include:

- Cationic surfactants, characterized by their positively charged hydrophilic head groups, dissociate in water, generating a positive charge at the head and a correspondingnegatively charged counter ion. Examples include cetyltrimethylammonium bromide (CTAB), cetylpyridinium chloride (CPC), benzethonium chloride (BTC), and tetradecyltrimethylammonium bromide (TTAB).

- Anionic surfactants feature negatively charged hydrophilic heads. Upon dissolutionin water, they yield negatively charged ionic heads and positively charged counter ions. Commonly used anionic surfactants incorporate sulfate, sulfonate, phosphate, and carboxylate functional groups. Sodium dodecyl sulfate (SDS) and sodium lauryl sulfate(SLS) are notable examples, recognized for their solubilizing properties and lowtoxicity.

- Nonionic surfactants are characterized by hydrophilic heads demonstrating minimal ionization in aqueous solutions due to their non-dissociative nature. Despite this, they exhibit compatibility with other surfactants, often serving as co-surfactants. Consequently, they find extensive utility in petroleum industries and environmental applications. Examples include tween, coco glucoside, and cetearyl oliveate.

- Zwitterionic surfactants, unique in their ability to exhibit either cationic or anionic charges based on the solvent pH, possess hydrophilic groups carrying both positive and negative charges concurrently. Sulfobetaine, $RN^{+}(CH_3)_2CH_2CH_2SO_3^{-}$ exemplifies this category.

Surfactants operate through three fundamental mechanisms: roll-up, emulsification, and solubilization. The roll-up mechanism entails the reduction of interfacial surface tension between oil/solution and surface/solution, effectively removing the oil. Emulsification involves the creation of a simple oil emulsion by minimizing oil/solution interfacial tension. Solubilization occurs when solute molecules interact

with surfactants in the solvent, leading to the liquefaction of the solute and theformation of a pure and homogeneous solution (Suhail et al., 2019). It is worth noting that the presence of salts in the solution significantly influences surfactant characteristics, affecting micelle shape, size, critical micelle concentration (CMC), and interfacial behaviour (Hooshyar and Sadeghi, 2015). Despite the critical role of surfactants, limited research has explored the impact of different salts on plant polyphenols in surfactant systems.

The amphiphilic nature of surfactants renders them versatile for various industrial applications, including medicines, corrosion inhibitors, detergents, de-emulsifiers, wetting agents, oil recovery enhancers, pharmaceutical formulations, and drug delivery systems. Furthermore, surfactants have emerged as vital components in nanotechnology, serving as stabilizers for hydrophobic inorganic nanomaterials such as carbon nanotubes, graphene, transition metal dichalcogenides, and black phosphorus (Shaban et al., 2020). Biotechnological applications include their use as extractants and solubilizers for proteins, pulmonary surfactants to enhance lung capacity in infants with acute respiratory syndrome, and bile salts crucial for digestion. Additionally, surfactants find innovative applications in environmental remediation, specifically in degrading pesticides and capturing CO_2, as well as in creating specialized coatings and materials with enhanced underwater adhesion for efficient implantation of bio-electronic devices. Furthermore, they serve as sensors and self-assembled monolayers, contributing significantly to diverse fields, including materials chemistry, biochemistry, and nano-electronics (Basu et al., 2023).

1.8 Zingiberaceae

Zingiberaceae plants are also commonly known as gingers. They are believed to exist in about 50 genera and 1300 species worldwide distributed mainly over the tropical parts of South Asia (Delin and Larsen, 2000). These plants mainly grow in wet places and are rarely found in secondary forest regions. However, certain plants can thrive under extremely sunny and high-altitude conditions.

Essential oils are a type of metabolites in herb plants. Zingiberaceae herbs essential oils are known to be rich in α-terpineol, 1,8-cineole, (E)-methyl cinnamate, terpinen-4-ol, camphor, α-pinenes and β-pinenes (Santos et al., 2015). The fruits as well as rhizomes are known to be aromatic as well as analeptic in nature. Some of them are put to dietary use whereas others are

used to produce a constricting and transudating juice (Kumar et al., 2013).

Zingiberaceae plants are used in traditional medicines and are also known to possess anticancer, antioxidative, anti-inflammatory, antiplatelet, anti-ulcer, anticonvulsive and analgesic properties (Zhang et al., 2023). Turmeric (*Curcuma longa*) is one of the most well-known Zingiberaceae species, and its main compound, curcumin, is known for its anti-inflammatory, antioxidant, antidiabetic, and anticancer properties. Other important genera in the Zingiberaceae family with medicinal properties include *Alpina* and *Amomum* (Kumar et al., 2013).

1.9 Alpinia nigra

Alpinia nigra (Gaertn.) B.L. Burtt, is a perennial aromatic herb which is rhizomatous in nature. It is well known for its medicinal properties and it is also known as Tora (Assamese), Jongly Ada or Tara, Galangal, False Galangal, Black-Fruited, Kala etc. It is abundantly distributed in China, Bangladesh, India, Srilanka and other Southeast Asian countries (Cragg and Newman, 2005; Delin and Larsen, 2000).

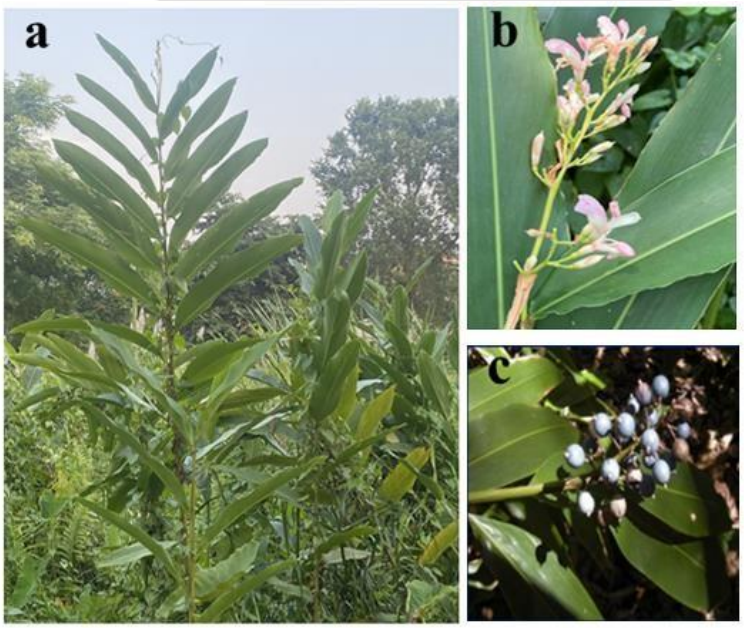

Fig. 1.8: (a) *A. nigra* plant photographed at IIT Guwahati campus, (b) flower of *A. nigra*, (c) Seeds of *A. nigra*

A. nigra **(Fig. 1.8)** grows well in moist, swampy areas and also near the river side. The underground stem consists of rhizome and the aerial stem also called the pseudo-stem is mainly the leaf sheath with an approximate height of 3.08 meters. The leaves are sessile, alternate, simple elongated, entire, and acute at base, apex of the plant is tiny petiole and very long leaf sheath. The type of inflorescence shown is panicle and the in-floret have involucre bract which

are asymmetrical. The flowers are fertile, white-pink in colour, asymmetric, 3 sepals and 3 lobes, 3 petals and 3 lobes. The stamens are flat in nature comprising a total number of 5 which are separated at the apex, Labellum obovate, Lateral staminodes subulate. It consists of a single pistil with inferior ovary, style is present in middle of the anthers. The anthers comprise of three carpels with stigma placed over it. Fruit comprises of plentiful seeds with thin pericarp and it is green in color at initial stage and black in color when gets matured and old (Delin andLarsen, 2000).

Taxonomy

Kingdom: Plantae

Order: Zingiberales

Family: Zingiberaceae

Subfamily: Alpinioideae

Tribe: Alpinieae

Genus: *Alpinia*

Species: *nigra*

A. nigra is used to prepare traditional delicacy among various tribes across different places and also it has been used as a folk medicine for various health issues such as intestinal parasitic infection, gastric ulcers, irregular menstruation, bone weakness and jaundice (Tushar et al., 2010), dyspepsia, bronchitis, and insect bites (Qiao et al., 2007). The presence of two flavone glycosides, astragalin and kaempferol-3-O-glucuronide have been reported from the phytochemical analysis of *A. nigra* (Ahmed et al., 2015). The role of *A. nigra* in traditional herbal system has been depicted in **Table 2.2** and the biological activities reported from *A. nigra* has been depicted in **Table 2.3**.

Table 1.2: Role of *A. nigra* in traditional herbal system

Plant Part	Remedies	References
Shoot and rhizome	Bone weakness, irregular menstruation, jaundice, and gastric ulcers	Tushar et al., 2010
Shoot	Anthelmintic properties	Roy and Swargiary, 2009
Rhizome	Fungal infections in the skin such as Pityriasis versicolor	White et al., 2014
Leaf and Root	Loss of sensation in hands and legs	Rahmatullah et al., 2010

Leaf, Rhizome, and root	Used in the treatment of heart diseases, wounds, eye diseases, stomach ulcer, body pain, rheumatism, dyspepsia, whooping colds in children, throat infection and fever	Bhunia and Mondal, 2012
Rhizome	Juice is used to cure cough	Baruah et al., 2018
Rhizome	Rheumatism and respiratory problems	Bhatt et al., 2018

Table 1.3: Biological activities reported for *A. nigra*

Plant Part	**Properties**	**References**
Leaves	Antioxidant and antimicrobial activity	Ahmed et al., 2015; Sahoo et al., 2013
	Analgesic, antibacterial, and cytotoxic effect	Ahmed et al., 2015
	Antidepressant effect	Sharmen et al., 2014
	Antidiabetic effect	Kabir et al., 2016
	Antioxidant and skin whitening (anti tyrosinase activity)	Janyapanich et al., 2019
	Thrombolytic effect	Sharmen et al., 2014
	Oxidative liver damage	Islam et al., 2016
Rhizome	Cytotoxic effect	Paul et al., 2015
	Inhibits the growth of Malassezia furfur and Microsporum gypseum, which cause dermal diseases in human.	Rajapaksha et al., 2017
	Antibacterial and Cytotoxic activity	Das and Qais, 2012
	Anticancer effects against both breast and cervical cancer cell lines	Sahoo et al., 2018

Seeds	Antibacterial	Ghosh et al., 2013; Sahoo et al., 2013
	Antioxidant and antibacterial properties	Ghosh et al., 2013
	Antidiabetic properties	Ghosh and Rangan, 2014
	Anti-leishmanial activity	Ghosh et al., 2017

1.10 Phytoconstituents present in *A. nigra*

Phytochemicals from *A. nigra* have been traditionally used in many countries to cure various diseases. According to reports, the hydrodistillation of *A. nigra's* various components produced translucent oil from the seeds and flowers that are yellowish oil for the leaves, and reddish-brown oil with a distinctive smell as obtained from rhizomes. On a dry weight basis, yields of *A. nigra's* seeds, flowers, leaves, and rhizomes were estimated to be at 0.76%, 0.06%, 0.23%, and 0.18%, respectively (Ghosh et al., 2014). Kanjilal et al., (2010) reported 18 components for leaf and rhizome essential oil. The major component in *A. nigra* leaves was found to be 1,8-cineole (Kanjilal et al., 2010). Whereas, in contrast to (Kanjilal et al., 2010) β- caryophyllene was reported to be the major component of leaf essential oil. The essential oil reported from *A. nigra* contains terpenoids of the class mainly monoterpenes and sesquiterpenes (Zou et al., 2016). The essential oil derived from *A. nigra* were found to possess potential antioxidant activities and rhizome essential oil has been reported to show most effective free radical scavenging properties. Also antibacterial properties have been reported for the essential oils derived (Ghosh et al., 2014). Presence of two types of natural diterpenes have been reported from the seed extracts of *A. nigra* which are diterpenes I:(E)-labda-8(17),12-diene-15,16-dial and II:(E)-8β,17-epoxylabd-12-ene-15,16-dial respectively. Both of the diterpenes were found to inhibit α-glucosidase and α-amylase by molecular docking studies which suggests these compounds to be potential herbal drug against diabetes (Ghosh and Rangan, 2014). Further antibacterial properties of both the compounds against three Gram positive and four Gram negative bacteria have been reported (Ghosh et al., 2014). Compound (E)-labda-8(17), 12-diene-15, 16-dial was found to inhibit the growth of *C. albicans* and also its effect on erythrocytes was studied which suggested its maximum dosage for IV administration to be 0.44mg/mL (Chakrabartty et al., 2021). Another research group reported the presence of two bioactive flavones glycosides astragalin and kaempferol-3-O-glucuronide from *A. nigra* seeds (Qiao et al., 2007). The compound astragalin has been reported to show anthelmintic properties against *Fasciolopsis buski* by acting over the enzymes such as acid and alkaline phosphatase

and resulting in surface ultrastructural changes of the parasite. The various essential oil reported from *A. nigra* leaves are listed in **Table 1.4** and the compounds reported from *A. nigra* seeds are listed in **Table 1.5** and structures of some of the major essential oils are shown in **(Fig. 1.9)**.

Table 1.4: Essential oil content in leaves of *A. nigra* (Ghosh et al., 2014)

Compound	**% of Essential Oil**
α-Pinene	6.4
α-Thujene	0.1
Camphene	0.3
β-Pinene	13.8
Sabinene	0.2
β-Myrcene	0.3
Limonene	0.3
1,8-Cineole	0.5
γ-Terpinene	0.1
α-Copaene	0.1
2-Nonanol	0.1
Camphor	0.1
Linalool	0.1
Pinocarvone	0.1
Isocaryophyllene	0.1
β-Caryophyllene	47.7
Myrtenal	0.1
trans-Pinocarveol	0.1
α-Humulene	7.5
γ-Muurolene	0.2
α-Terpineol	0.4

Borneol	0.1
Drima-7,9(11)-diene	0.4
Germacrene D	0.2
β-Selinene	0.2
α-Selinene	0.1
(E,E)-α-Farnesene	0.1
δ-Cadinene	0.1
δ-Cadinene	0.1
Myrtenol	0.1
(E)-Anethol	1.2
Isocaryophyllene oxide	0.3
Caryophyllene oxide	4.3
(E)-Nerolidol	3.6
Humulene epoxide-II	1.1
Neointermedeol	0.1
Fokienol	0.1
α-Cadinol	0.1
Selin-11-en-4α-ol	0.2
Caryophylla-2(12),6(13)-dien-5β-ol(= Caryophylladienol I)	0.5
Caryophylla-2(12),6(13)-dien-5α-ol (=Caryophylladienol II)	1.6
14-Hydroxy-β-caryophyllene	0.1
Caryophylla-2(12),6-dien-5α-ol (= Caryophyllenol I)	0.3
Caryophylla-2(12),6-dien-5β-ol (=Caryophyllenol II)	0.9

Geranyl linalool	0.4
Phytol	1.0
Hexadecanoic acid	0.6

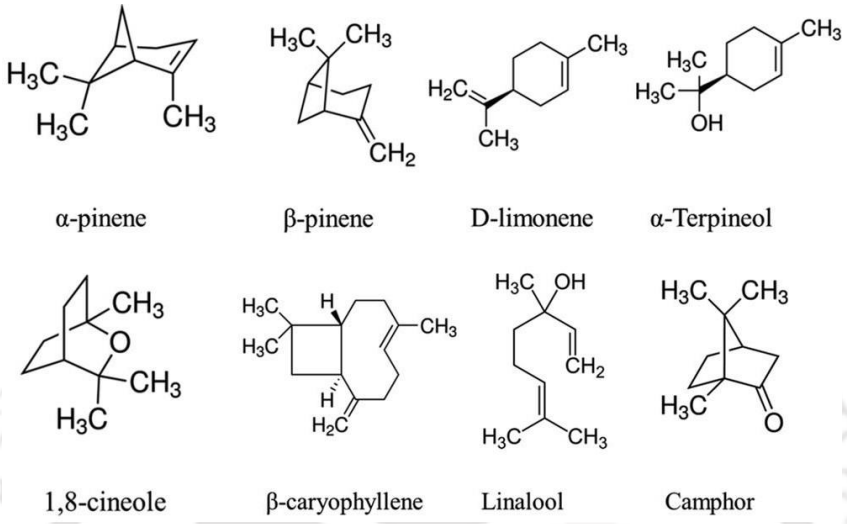

Fig.1.9: Structure of some major essential oil available in *Alpinia nigra* (Van et al., 2021)

Table 1.5: List of compounds isolated from *A. nigra* seeds

S.No.	Compound	Structure	Family of compounds	Reference
1.	(E)-labda-8(17), 12-diene-15, 16-dial	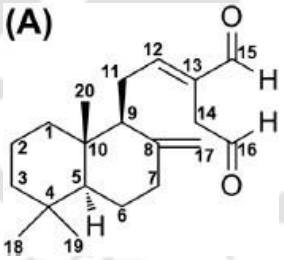	Labdane diterpene	Ghosh and Rangan, 2014
2.	(E)-8β ,17- Epoxylabd-12-ene-15, 16-dial	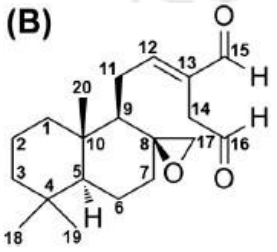	Labdane diterpene (epoxy derivative)	Ghosh and Rangan, 2014

3.	Astragalin	**R= glc** 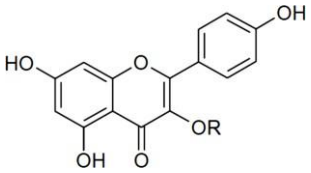	Flavone glycoside	Qiao et al., 2007
4.	kaempferol-3-O-glucuronide	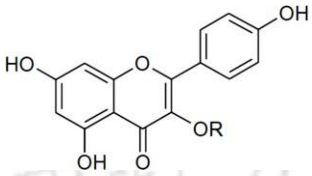 **R= glcUA**	Flavone glycoside	Qiao et al., 2007

1.11 3,5-dihydroxy-7,4'- dimethoxyflavone (DHF)

Flavonoid DHF **(Fig. 1.10)** isolated from the leaf extract of *A. nigra* is the main focus of this thesis work. DHF is a Kaempferol derivative in which the hydroxy groups at position 4'and 7 in Kaempferol is replaced by methoxy groups. This compound is found in bee glue and has been detected in several plant species including *Betula exilis, Zingiber mekongense*, and *Alpinia flabellata*. It is the conjugate acid of 7,4'-O-dimethylkaempferol 3-olate and possesses functional similarities with kaempferol (NCBI:pubchem., 2023). DHF has been reported to exhibit the phenomenon of Excited-state intramolecular proton-transfer (ESIPT) (Portugal et al., 2006). The various biological activity reported from DHF are listed in **Table 1.6**.

Fig. 1.10: Structure of 3,5-dihydroxy-7,4'- dimethoxyflavone (DHF)

Table 1.6: Biological activities of DHF reported:

Bioactivity	**Target molecule**	**Result**	**References**
Oestrogen activity	MVLN cell line	EC50 (M): 62.7 × 10−8	Ying et al., 2014

Anti-HIV-1 activity	HIV-1 reverse transcriptase	33.6% inhibition at 200 µg/ml	Chareonkla et al., 2011
Antioxidant and α-Glucosidase Inhibitory assay	DPPH and porcine α-amylase	Antioxidant activity: 65.5 %, IC_{50}- 86.1 µM Alpha glucosidase inhibition: 51.2%, IC_{50}value: 78.74 µM	Jani et al., 2015
Antioxidant activity and Enhances collagen production	DPPH and L929 fibroblast cells	IC_{50}=39.0 µM and 51.7 µg/mL on treatment with 10 µM DHF	Sudsai et al., 2016
Antibacterial and Anti-HIV-1 activity	S. aureus and HIV-1 Integrase	Moderate inhibition only of Gram-positive bacteria strain with MIC/MBC of 64/>256 µg/ml	Sudsai et al., 2017
Antioxidant, anti-tyrosinase and anti-inflammatory activities	DPPH;Tyrosinase; TNF-α and p-NF-κB	Potent antioxidant activity at different conc. of DHF (30 µM- 60 µM); inhibition of Tyrosinase at 60 µM DHF; inhibition of TNF-α and the	Gupta et al., 2021

		activation of Nuclear factor-κB (NF-κB) in dose dependent manner

Further purification and structural characterization of bioactive compound DHF from the leaf extracts of *A. nigra* was carried out earlier (Gupta et al., 2021).

1.12 Objectives of the thesis work

A. nigra, a plant renowned for its medicinal properties yet insufficiently explored, current study focuses on isolating a pure compound, DHF, from its leaves. Within the framework of our present study, we have embarked upon the isolation of a pure compound, namely 3,5-dihydroxy-7,4'- dimethoxyflavone (DHF), from the leaves of *A. nigra*. Our comprehensive inquiry extends to unravelling the nuanced physical and chemical attributes inherent to DHF. An extensive exploration into its photophysical properties was undertaken, with a deliberate consideration of varying pH conditions. Moreover, we have probed the interactions of DHF with surfactant micelles of differing charge characteristics, Sodium dodecyl sulfate (SDS), Cetyltrimethylammonium Bromide (CTAB), and Tween20. These investigations were conducted under systematically modulated pH conditions, enriching our understanding of DHF's behaviour in these distinct environments.

DHF is categorized among flavonoids, a class of compounds documented for their demonstrated anti-aggregation properties against amyloid fibres. However, curiously, its specific anti-aggregation potential remains uncharted. As such, our study seeks to fill this critical knowledge gap by investigating DHF's capacity to interact with protein aggregates, specifically those of HEWL, across a spectrum of pH levels, spanning pH 2, pH 5, and pH 12.2. Despite various reported biological activities of DHF, its potential as an anticancer agent against colon cancer, particularly concerning cell lines HCT116 and SW480, remains unexplored.

This extensive study not only sheds light on the nuanced physicochemical attributes of DHF but also uncovers its promising therapeutic potential in combating colon cancer. By bridging gaps in our understanding, this research paves the way for future advancements in both flavonoid research and targeted cancer therapies.

Therefore, the objectives of thesis work were decided as follows:

1. Extraction, purification and subsequent investigations on the photophysical properties of 3,5-dihydroxy-7,4'- dimethoxyflavone (DHF) in various organic solvents, pH and aqueous surfactant micelles by UV-visible and fluorescence spectroscopy
2. Studying the interaction of DHF with HEWL aggregates at varying pH conditions
3. Studying the anticancer activity of DHF in colon cancer cells

Chapter 2

Extraction, purification, and subsequent investigations on the photophysical properties of 3,5-dihydroxy-7,4'-dimethoxyflavone (DHF) in various organic solvents, pH and aqueous surfactant micelles by UV-visible and fluorescence spectroscopy

2.1 Introduction

Flavonoids are polyphenolic compounds also known as plant secondary metabolites which are ubiquitously present in different variety of fruits, vegetables, and plant-based products. They are extensively studied due to their potent therapeutic properties against several metabolic diseases such as cancer, anti-inflammatory, antimicrobial and cardiovascular diseases (Sahu and Mishra, 2022). The biosynthesis of Flavonoids is under the photoregulation influence of both UV and blue radiation at various points. Additionally, the efficient absorption of flavonoids in the 290-400 nm range (cinnamoyl part) and 240-285 nm range (benzoyl part) has been ascribed to their role in providing protection against UV-induced damage in plants (Christoff et al., 1996).

Flavonols represent a specific subgroup of Flavonoids characterized by a double bond between carbon atoms C2 and C3, along with a carbonyl group located at the C4 position. The yellow coloration exhibited by flavonols is attributed to the presence of a large conjugated double bond system, which allows them to absorb light in the visible range. Their absorption spectrum is particularly prominent around 340-380 nm, thereby enabling them to attract insects that are sensitive to ultraviolet (UV) light (Murkovic, 2016). Flavonols are reported to exhibit photoinduced excited-state intramolecular proton transfer (ESIPT). It has a dual fluorescence behaviour which is mainly environment-sensitive. The phenomenon of ESIPT observed in 3-Hydroxyflavone has been hypothesised to occur between 3-hydroxy (3-OH) group and the neighbouring C4 carbonyl group within the γ-pyrone ring. The number of hydroxy groups present in a flavonol significantly impacts its photophysical characteristics (Sahu and Mishra, 2022). Flavonols have been documented to possess antioxidant properties, and it has been observed that a majority of diseases can be attributed to oxidative stress. This emphasizes the substantial potential of flavonols as health-promoting compounds, owing to their ability to counteract oxidative damage and its associated adverse effects.

Compound 3,5-dihydroxy-7,4’- dimethoxyflavone (DHF) is a Kaempferol derivative in which the hydroxy groups at position 4’and 7 in Kaempferol are replaced by methoxy groups. It belongs to the flavonol group of flavonoid and it is a conjugate acid of a 7,4’-O-dimethylKaempferol 3-olate (NCBI:pubchem., 2023). DHF has been reported to exhibit the phenomenon of ESIPT (Portugal et al., 2006). Various biological activities of DHF has been reported such as: estrogenic activity (Ying et al., 2014); antibacterial and anti-HIV (Sudsai et al., 2017); and antioxidant; anti-tyrosinase; anti-inflammatory properties (Gupta et al., 2021).

A majority of drugs or molecules with therapeutic properties exhibit a non-polar character. The solubility of a drug stands as a pivotal determinant influencing drug release and bioavailability. Certain drugs exhibit pH-dependent solubility, manifesting alterations in solubility in response to varying pH levels; notable examples encompass verapamil hydrochloride, papaverine hydrochloride, dipyridamole, trimethoprim, and divalproex sodium (Bassi and Kaur, 2010).

The utilization of amphiphile-based micellar solutions for drug delivery presents an efficacious strategy for conveying non-polar drugs to their intended targets. The hydrophobic core of the micelle facilitates the solubilization of water-insoluble drugs, enabling targeted delivery. Diverse drug carriers encompassing soluble polymers, insoluble natural and synthetic polymers, micro particles, cells, cell ghosts, lipoproteins, liposomes, and amphiphilic polymer-derived micellar systems are broadly used (Ahmad et al., 2014).

This chapter is focused to investigating the solubility behaviour and photophysics of DHF within various charged surfactant micellar environments, considering pH as a variable. The time dependent stability of DHF was examined in distinct surfactant micelles across varying pH conditions using absorption and fluorescence spectroscopic techniques. Additionally, the process of DHF degradation under alkaline pH conditions was explored.

2.2 Materials and methods

2.2.1 Sample collection

Mature leaves of *A. nigra* were collected from IIT Guwahati campus and the leaves were shade dried. The dried leaves were grinded into fine powder which was followed by further extraction.

2.2.1 Hot solvent Soxhlet extraction by organic solvents

In the present study, dried leaves powder of *A. nigra* was subjected for hot organic solvent extraction using Soxhlet extractor. The extraction of the same sample was carried out sequentially based on the increasing polarity gradient of the solvents starting with non-polar (n-hexane), semi-polar (ethyl acetate, EtOAc) and polar (Methanol, MeOH) respectively. The Ethyl acetate extract was further used as crude for isolating the compound.

2.2.2 Isolation and purification of compound from Ethyl acetate crude extract by normal phase column chromatography

The ethanolic crude extract was further subjected to chromatography in silica gel (60-120 mesh, Merck India) using glass column (3 x 50 cm) and was eluted by step-wise gradient of ethyl acetate in hexane. Various fractions were collected and left for slow evaporation. The fraction which formed crystals was then subjected to further purification based on its solubility.The compound was first treated with hexane to remove any impurities that is soluble in hexanesince the crystals were not readily soluble in hexane. After removing the impurities with hexane, it was subsequently followed by dissolving in acetone and adding deionised water which was kept for 3-4 days at room temperature for recrystallization. The crystals were recovered after 3-4 days and washed with deionised water to remove any impurities. The compound is readily soluble in ethyl acetate and it was allowed to recrystallize by dissolving in ethyl acetate and allowed for slow evaporation. The recrystallized compound was further washed with hexane and its purity was checked using analytical TLC plates.

2.2.3 TLC and High-performance liquid chromatography for purity analysis

TLC of the purified compound was carried out in Merck Silica gel 60 F_{254} aluminium sheet. The mobile phase used was 20% ethyl acetate in hexane. The spot was visualized under iodine fume.

The final purity of the compound was estimated by analytical reverse phase- HPLC (Shimadzu) using C18 (250x4.6mm, 5 microns pore size) column. The sample injection volume was 30 µL, and elution was performed at 1.0 mL/min flow rate with 5-100% gradient of water in acetonitrile (0-45min). The program was run for 45 minutes with UV-Vis Detector (SPD-20A) set at wavelength 363 nm. Data was procured and processed using Shimadzu lab solutions.

2.2.4 High resolution mass spectrometry (HR-MS)

Mass spectra were measured in High resolution mass spectrometer (HR-MS) Agilent QTQF 6520 with electron spray ionization (ESI) technique and was matched with the reported spectra for molecular mass. For the mass spectral analysis, 0.5 mg of the pure compound DHF was dissolved in 1 mL of acetonitrile (HPLC grade). The spectra of mass were recorded in positive ESI mode.

2.2.5 Nuclear magnetic resonance (NMR)

Nuclear magnetic resonance (NMR) was achieved by dissolving 5mg of the purified compound in 600 µL of $CDCl_3$ (deprotonated solvent) and then transferred to 5mm NMR tubes using 0.2 µ syringe filter. The structure of the compound was characterized by (1H, 13 C) NMR (Bruker ASCEND 500) and matched with the previously reported NMR spectra.

2.2.6 UV-Visible Absorption Spectra of DHF in various organic solvents

UV-Vis Absorption studies of DHF in different organic solvents based on polarity which includes Hexane, Ethanol (EtOH), Methanol (MeOH), Ethyl acetate (EtOAc), Acetonitrile, Dimethyl sulfoxide (DMSO) and Water (H_2O) were carried out in Perkin Elmer Lambda 25 spectrophotometer, in the range of 250-500 nm. The organic solvents used for the experiments were HPLC grade.

Molar extinction coefficient (ε) of DHF in ethanol was determined from slope of absorbance Vs. concentration of DHF (20 µM, 30 µM, 40 µM, 50 µM and 60 µM) plots. DHF dissolved in ethanol stock was used to carry out all the absorption and fluorescence-based study.

2.2.7 Absorption of DHF in different pH

UV-Vis Absorption spectra of DHF in different pH was investigated- pH 2 (glycine buffer), pH 3 (glycine buffer), pH 5 (Citrate buffer), pH 7 (phosphate buffer), pH 8 (phosphate buffer), pH 9 (carbonate buffer), pH 11 (carbonate buffer), pH 12 (0.01N NaOH) and pH 13 (0.1 N NaOH). DHF stock was prepared in ethanol and DHF (20 µM) was added to each pH and the absorption spectrum was recorded. The ethanol concentration in each sample was kept to be ≤ 2% (v/v).

2.2.8 Solubility of DHF in different pH

The solubility of DHF in different pH (7-13) was tested by UV-Vis Absorption spectra, 100 µM DHF was added in each pH. The samples were vortexed and centrifuged at 12000 rpm for 2 minutes, the supernatant was collected and the remaining pellet were dissolved in 1mL of DMSO. The supernatant and pellet fractions absorption spectra were recorded.

2.2.9 Time dependent stability of DHF in alkaline pH

The stability of DHF in alkaline pH were observed at different time interval i.e., 0 hr, 24 hrs, 48 hrs, 72 hrs and 96 hrs respectively. DHF at concentration of 50 μM was dissolved in each pH (11, 12, 13) and the absorption spectra were recorded at different time interval at room temperature.

2.2.10 Stability of DHF in surfactant micelles in different pH

The stability of DHF at different time interval (0 hr, 24 hrs, 48 hrs, 72 hrs and 96 hrs) was monitored in different surfactant micelles SDS (20 mM), CTAB (5 mM) and Tween 20(0.5 mM) in different pH (2-13) respectively. The surfactant micelles were prepared in different pH by vortexing followed by incubation for 15 minutes at room temperature. DHF at different concentrations (10 μM, 20 μM, 30 μM, 40 μM and 50 μM) were added to each surfactant micelles and vortexed for 10 minutes and incubated for 1 hour before measuring the absorption spectra of the samples at different time intervals. Absorption of DHF at wavelengths 270, 330 and 365 nm was plotted against different concentration of DHF in surfactant for different pH.

2.2.11 Reversibility assay of DHF from alkaline pH to neutral pH

The reversibility assay of DHF incubated for 96 hrs in alkaline pH 13 followed by transfer to pH 7 was investigated by UV-Vis absorption spectra. DHF with concentration 100 μM was added to pH 13 and incubated for 96 hrs. After 96 hours 100 μL of the sample was added to pH 7 (50 mM phosphate buffer) and 20mM SDS in pH 7(50 mM phosphate buffer) in to make up to a final volume of 1 mL. The final concentration of DHF in each solution was 10 μM.

2.2.12 Degradation analysis of DHF in alkaline pH by TLC

The degradation of DHF in alkaline pH 13 was investigated by TLC, 20 μL of the sample was loaded in TLC plate. The mobile phase used was 50% hexane in ethyl acetate and 0.1 % triethylamine in ethylacetate and the bands were spotted under iodine fume.

2.2.13 Degradation analysis of DHF in alkaline pH by HPLC

The degradation of DHF in alkaline pH (9, 13) after 96 hrs of incubation at room temperature was investigated by HPLC. DHF with concentration 200 μM was added to each condition: pH 13, pH 9, 20 mM SDS in pH 13, 20 mM SDS in pH 9, 5 mM CTAB pH 9, 5 mM CTAB in pH 13, 0.5 mM Tween 20 in pH 9 and 0.5 mM Tween 20 in pH 13. The samples were incubated for 96 hours at room temperature. After 96 hours of incubation the samples were diluted to 50

μM each in dH_2O and the pH was adjusted below pH 10 by adding 1 N HCl. The samples were filtered using 0.2 μ syringe filter. For control, sample of freshly prepared DHF at 50 μM dissolved in acetonitrile was used for analysis. RP- HPLC (Shimadzu) was used along with C18 (250x4.6 mm, 5 microns pore size) column for the analysis. A linear gradient of 0-30 % acetonitrile in water containing 0.1% TFA was applied for 20 minutes. It was followed by 2 minutes isocratic elution with 30% acetonitrile. Hereafter, a linear gradient of 30-100% acetonitrile was applied for 10 minutes. Isocratic elution of 100% acetonitrile was applied for another next 10 minutes. Isocratic elution of 50% acetonitrile was used for another 22 minutes. The rate of elution was 0.7 mL/min.

2.2.14 Investigation of fluorescence properties of DHF in organic solvents and alkaline pH

The fluorescence spectra of DHF was measured in organic solvents ethanol, ethyl acetate and hexane. The excitation slit was kept at 2 nm and the emission slit was kept at 15 nm for all the samples for fluorescence measurement. DHF with concentration 2.4 μM with OD ≤ 0.04 was used for each solvent. The excitation wavelength was kept at 365 nm and the emission was collected in the range 470- 690 nm in Horiba FluoroMax Plus 4C spectrofluorometer. The fluorescence spectra of DHF was also measured in alkaline pH (9, 10, 11) against ethanol, at λ_{ex} 365 nm and λ_{ex} 406 nm. The emission was collected at 470- 690 nm, the concentration of DHF and the excitation and emission slits were kept similar as per above samples.

2.2.15 Time dependent investigation of fluorescence properties of DHF in surfactant micelles in different pH

The fluorescence of DHF was investigated in three differently charged surfactant micelles- SDS (20 mM), CTAB (5 mM) and Tween 20 (0.5 mM) at different pH. The micelles were prepared beyond the cmc in different pH and were mixed by vortexing properly and incubated at room temperature for 15 minutes. DHF with concentration 2.4 μM was added to each micelle in different pH and mixed by vortexing for 10 minutes. The samples were incubated for 1 hour at room temperature before analysis in spectrofluorometer at different time interval (0 hr, 24 hrs, 48 hrs, 72 hrs and 96 hrs).

2.3 Results and Discussions

2.3.1 TLC and HPLC analysis

The compound extracted and isolated from the ethyl acetate extract of *A. nigra* leaves with the help of silica gel (mess size 60-120) column chromatography. The compound was assessed for its purity by TLC and RP-HPLC. In TLC the mobile phase used was 20% ethyl acetate in hexane **(Fig. 2.1 a)**. Further the purity was confirmed by Reverse phase- HPLC. HPLC is used to detect the nature of analyzed sample (polar or non-polar) obtained from their retention time data and the UV detector ascertain the purity of the isolated compound by giving the characteristic pattern of the peak (Kumar, 2017). The compound was obtained at a retention time of 8.7 min at 263 nm detection. With the above-mentioned purification procedure, 95-99% purity was obtained **(Fig. 2.1 b)**.

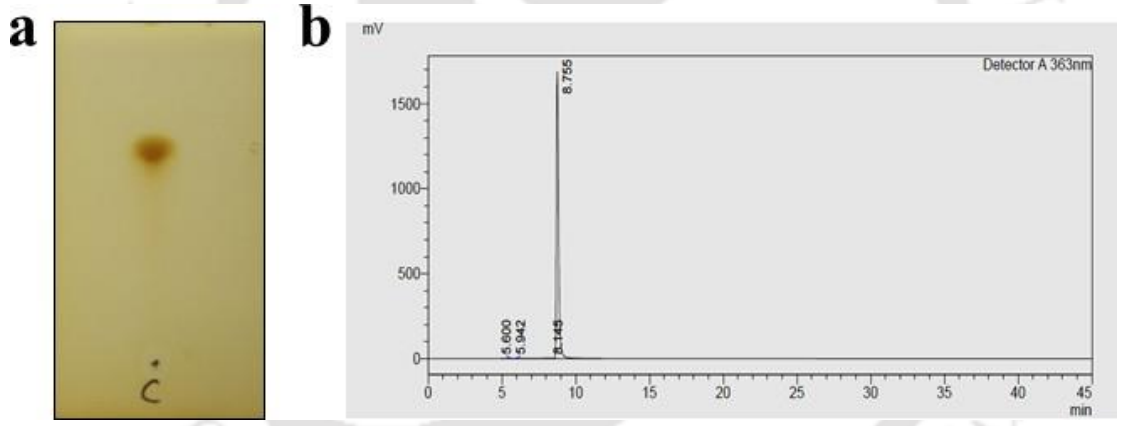

Fig. 2.1: (a) TLC of DHF using 20% Ethyl acetate in hexane as solvent system; (b) HPLC chromatogram of DHF showing retention time at 8.75 minutes.

2.3.2 High Resolution- Mass Spectrometry (HR-MS)

HR-MS was performed to estimate the mass of the compound. The molecular ion in positive mode $[M+H]^+$ peak was obtained at m/z 315.0904 **(Fig. 2.2)**. Therefore, the molecular mass of DHF is 314.0904 Da.

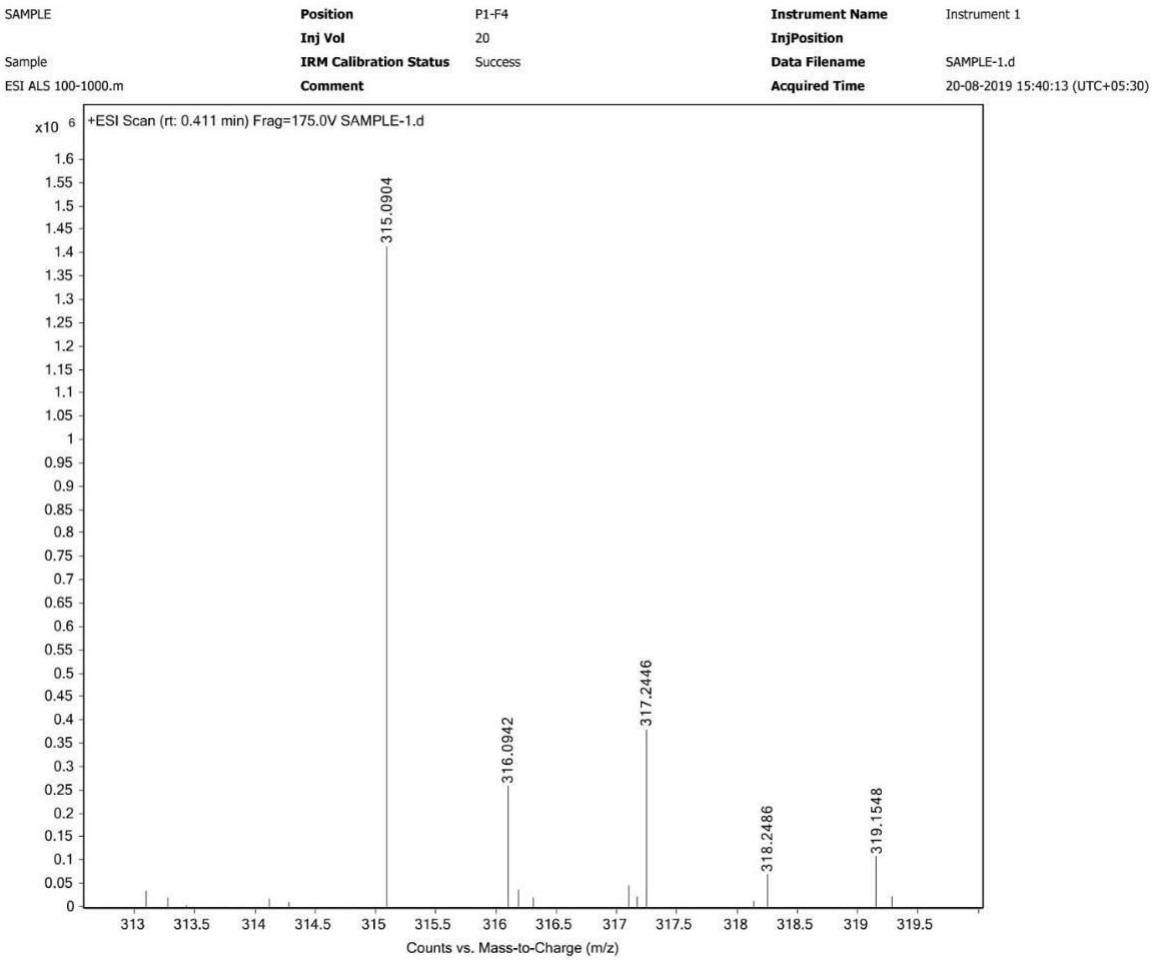

Fig. 2.2: HR-MS spectra of compound

2.3.3 NMR

The structure of the compound was elucidated by 1H **(Fig. 2.3)** and 13C NMR **(Fig. 2.4)**. The ^{1}H NMR spectra of the isolated compound revealed four peaks at δ (ppm) = 6.49 (s, 1H, *J* = 2.06 Hz, H-6), 6.50 (d, 1H, *J* = 2.06 Hz, H-8) and 6.38 (s,1H, 3-OH), 11.74 (s, 1H, 5-OH); Two doublets at δ = 7.03 (d, 2H, *J* = 8.94 Hz, H-3', H-5') and δ = 8.19(d, 2H, *J* = 8.94 Hz, H-2', H-6'); Two singlets peaks at δ = 3.89 (s, 6H, 4'-OCH3, 7-OCH3).

The ^{13}C NMR spectrum revealed the presence of two peaks at δ (ppm) =55.85 (7-OCH_3) and 55.43 (4'-OCH_3) are linked to an oxygen atom in —OCH_3 group. and other carbon peaks are δ175.20 (C-4), 165.73 (C-7), 161.17(C-5),160.84 (C-4'), 156.86 (C-9), 145.72 (C-2),135.67 (C-3), 129.40 (C-2',6'), 123.22 (C-1'), 114.11 (C-3',5'), 103.96 (C-10), 97.90(C-6), 92.23 (C-8).The compound was found to be 3,5- dihydroxy- 7,4'- dimethoxy flavone (DHF) **(Fig. 2.5)**. The compound was previously reported from a different species of the same family,

Zingiber phillipseae (Hsiang and Yusoff, 2012), The structural confirmation was further validated by matching the reported NMR spectra.

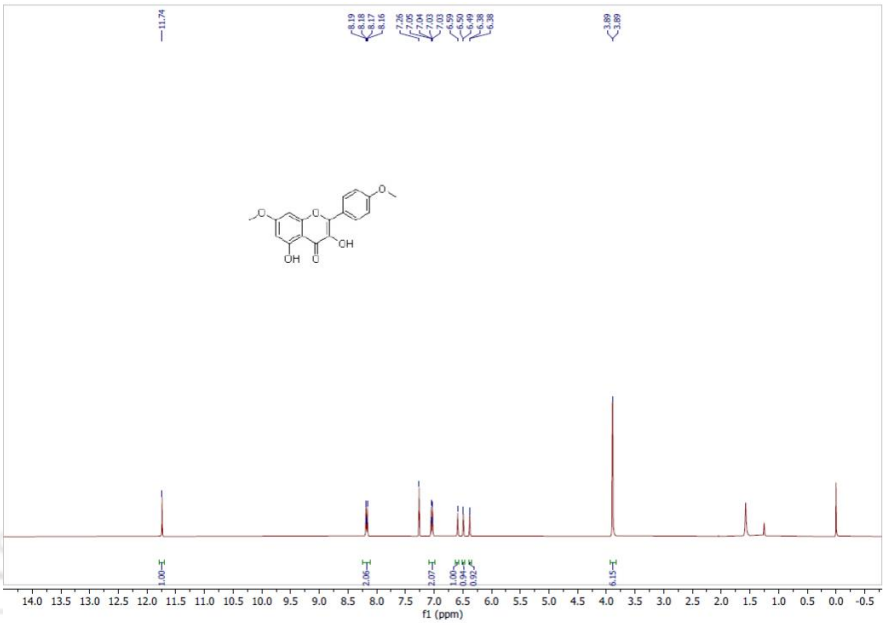

Fig. 2.3: 1D NMR, ^{1}H NMR spectra of 3,5-dihydroxy-7,4'-dimethoxyflavone. **^{1}H NMR** (400 MHz,$CDCl_3$) δ 11.74 (s, 1H, 5-OH), δ 8.19(d, 2H, *J* = 10 Hz, H-2', H-6'), δ 7.03 (d, 2H, *J* = 7 Hz, H-3', H-5'), δ 6.50 (1H,J=3.0 Hz, H-8), δ 6.49(1H,d,J=2.5Hz, H-6), δ 6.38 (s,1H, 3-OH) and δ 3.89 (s, 6H, 4'-OCH_3, 7-OCH_3).

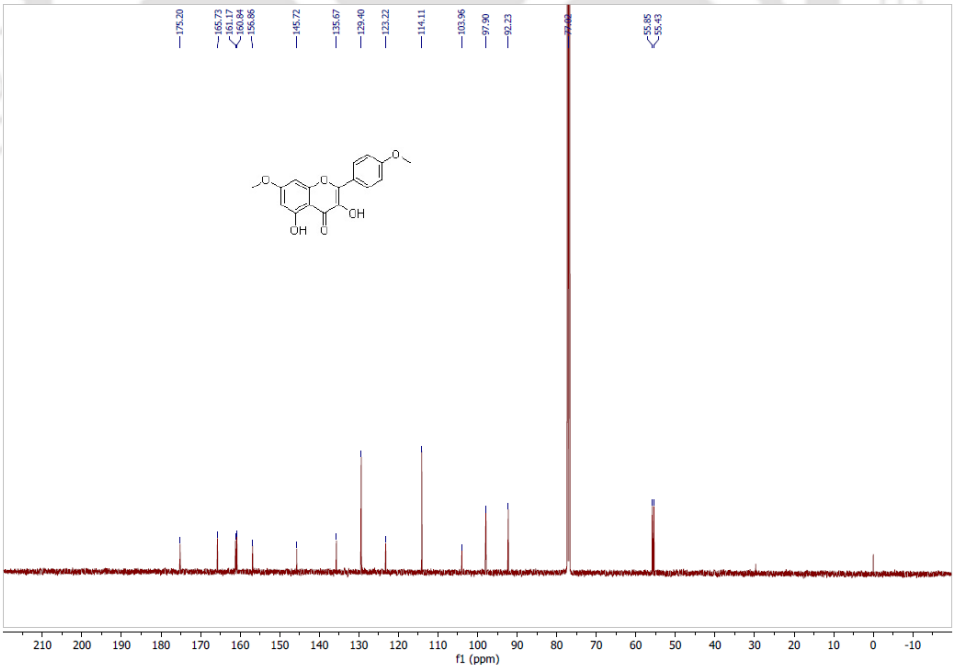

Fig. 2.4: ^{13}C NMR Spectra of 3,5-dihydroxy-7,4'-dimethoxyflavone. **^{13}C NMR** ($CDCl_3$) δ175.20 (C-4), 165.73 (C-7), 161.17(C-5),160.84 (C-4'), 156.86 (C-9), 145.72 (C-2),135.67 (C-3), 129.40 (C-2',6'), 123.22 (C-1'), 114.11 (C-3',5'), 103.96 (C-10), 97.90(C-6), 92.23 (C-8), 55.85 (7-OCH_3) and 55.43 (4'-OCH_3).

Fig. 3.5: Structure of 3,5-dihydroxy-7,4'- dimethoxyflavone (DHF).

2.3.4 Spectroscopic properties of DHF in organic solvents and aqueous medium at different pH

The absorption spectrum of DHF within the UV-Vis spectral range was investigated in various solvents, including hexane, ethyl acetate, ethanol, methanol, acetonitrile, dimethyl sulfoxide, and water **(Fig. 2.6)**. Notably, in the aqueous medium, DHF exhibited a conspicuous absence of spectral bands, indicative of its pronounced insolubility in water. In contrast, within organic solvents, DHF consistently manifested a tripartite band pattern of resonance, exhibiting remarkable uniformity across the solvent spectrum. Band I, spanning the wavelength range of

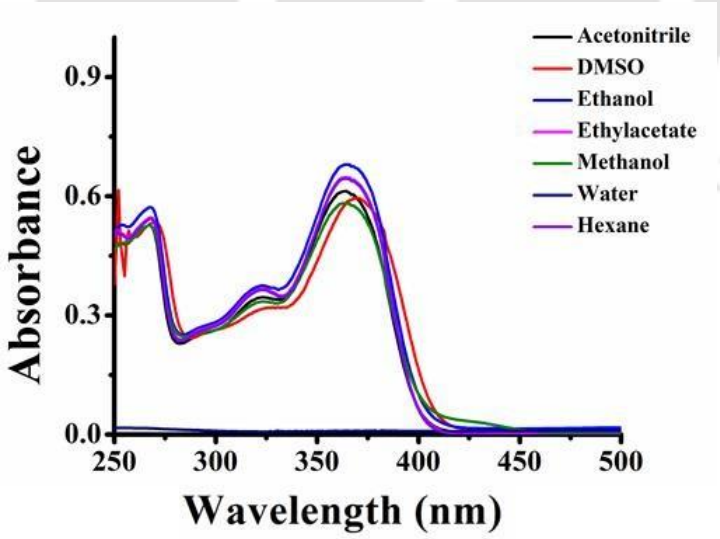

Fig. 2.6: Absorption spectra of 30 μM DHF in organic solvents.

363-370 nm, can be attributed to the chromophoric B-ring, intricately conjugated with the C-ring (the cinnamoyl system). Band II, residing within the 263-270 nm region, is associated with

the molecular architecture of rings A and C, which in turn is connected to the benzoyl system. Meanwhile, Band III, positioned at 330 nm, corresponds to the absorption emanating from the hydroxycinnamoyl moiety. It is noteworthy that Bands I and II are conceivably ascribed to π-π* electronic transitions, elucidating the underlying molecular processes governing DHF's spectral behavior in these solvents.

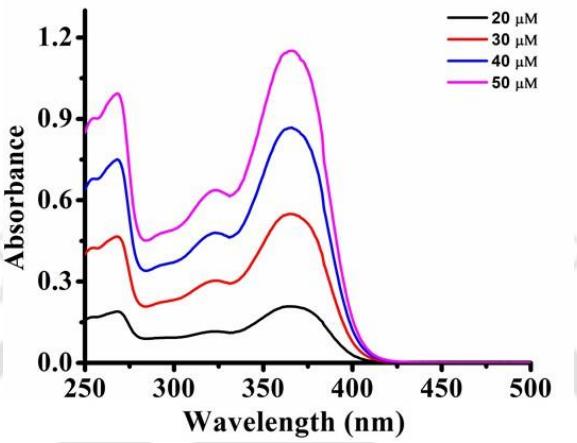

Fig. 2.7: Absorption spectra of DHF (20 µM, 30 µM, 40 µM and 50 µM) in ethanol

The absorption spectra of DHF with concentrations 20 µM, 30 µM, 40 µM and 50 µM in Ethanol **(Fig. 2.7)** was observed and the molar extinction coefficient (Ɛ) of DHF was determined in ethanol **(Fig. 2.8)**, $Ɛ_{270\ nm}$ =19167 $M^{-1}cm^{-1}$, $Ɛ_{330\ nm}$= 12220 $M^{-1}cm^{-1}$, $Ɛ_{365\ nm}$= 15123 $M^{-1}cm^{-1}$ **(Table 2.1)**. The $Ɛ_{365\ nm}$ in ethanol was used to calculate the stock concentration for all the other experiments.

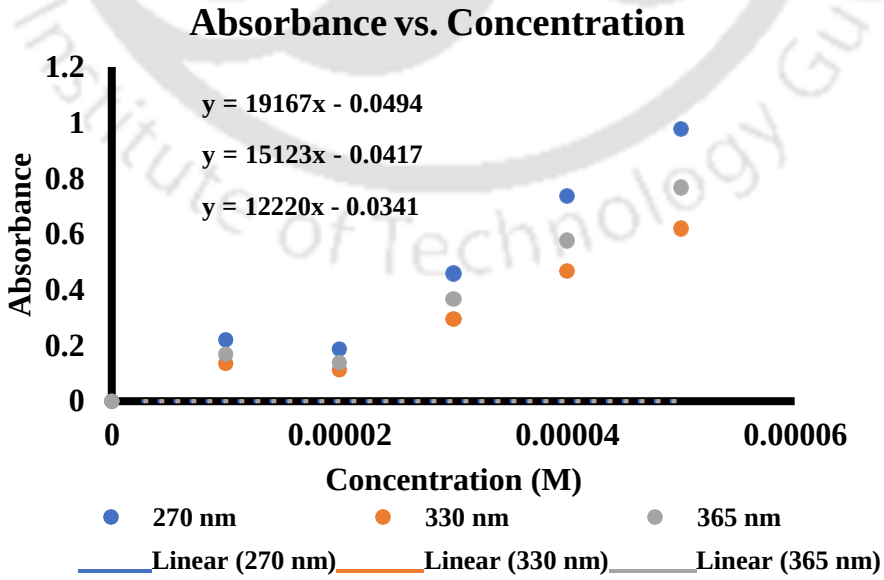

Fig 2.8: Molar extinction coefficient (Ɛ) calculation of DHF in ethanol at wavelengths 270, 330 and 365 nm

Table 2.1: Molar extinction Coefficient of DHF in Ethanol at 270, 330, and 365 nm.

Wavelength	Molar Absorptivity ($M^{-1} cm^{-1}$)
270 nm	19167
330 nm	12220
365 nm	15123

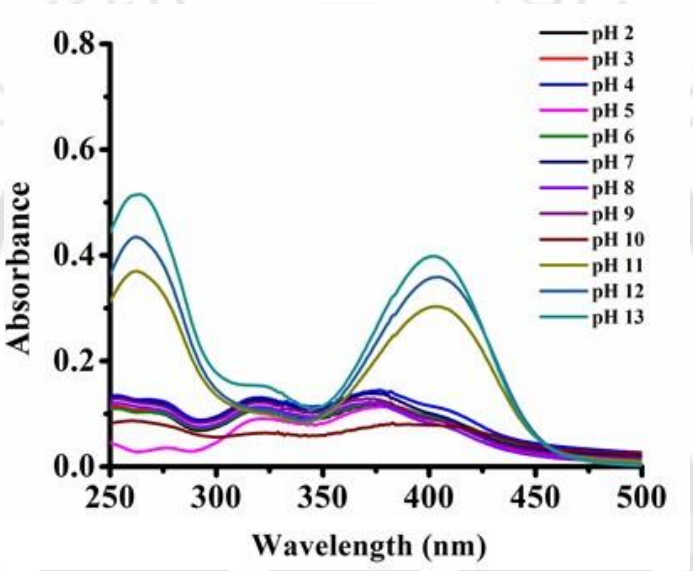

Fig. 2.9: Absorption spectra of 20 μM DHF in different pH (2-13)

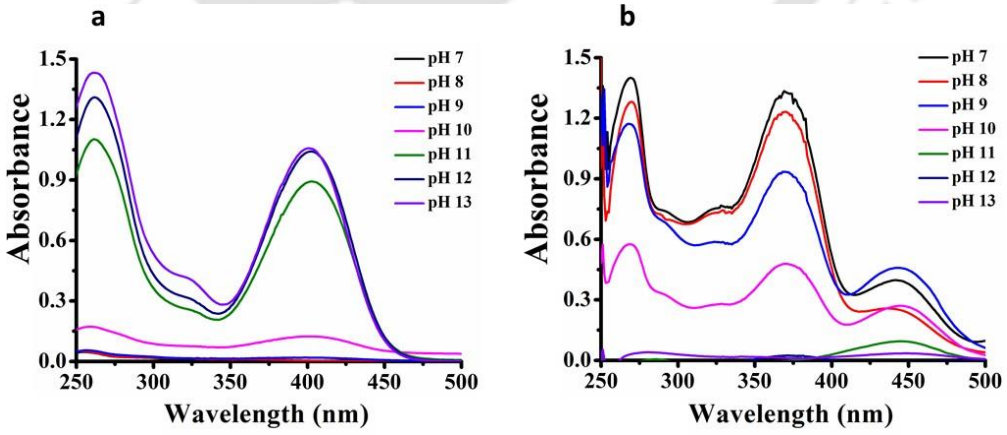

Fig. 2.10: (a) Absorption spectra of DHF in pH 7-13, after collecting the supernatant subsequent to centrifugation, (b) Absorption spectra of DHF in pH 7-13 of the remaining pellet after centrifugation, dissolved in DMSO.

The absorption spectra of DHF in different pH was investigated which suggested that DHF shows very less absorption in pH (2-10) **(Fig. 2.9)**, DHF showed higher absorption in alkaline pH (11, 12 and 13) with a red shift in Band I (365 nm) to 406 nm **(Fig 2.9)**. From the absorption spectra it can be observed that DHF is more soluble in higher alkaline pH. To further confirm the solubility, we investigated the absorption spectra of DHF in pH 7- pH 13 **(Fig 2.10 a)** by collecting the supernatant after centrifugation of insoluble sample which showed the similar pattern as previously found. The absorption spectra of remaining pellet which was dissolved in DMSO depicted highest absorbance in pH 7 followed by pH 8, pH 9, pH 10 and very negligible absorbance in pH 11, pH 12 and pH 13 **(Fig. 2.10 b)**. Thus, based on the absorption spectra it could be concluded that DHF is more soluble in higher alkaline pH 13 followed by pH 12 and pH 11.

2.3.5 Time dependent stability of DHF in Alkaline pH

The absorption spectra of DHF in alkaline pH (11, 12, 13) was investigated after incubation at room temperature for different time interval 0, 24, 48, 72 and 96 hrs which revealed that the

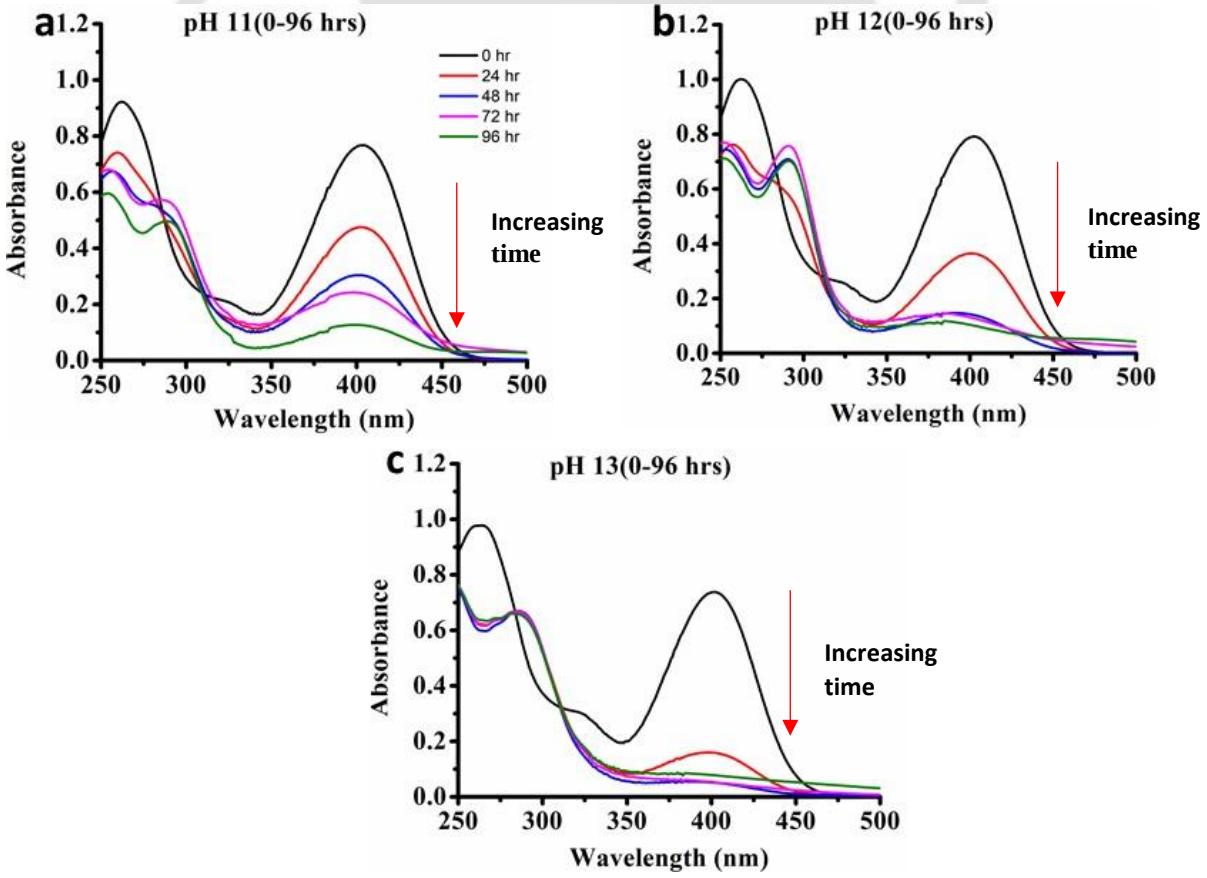

Fig. 2.11: Absorption spectra of 50 µM DHF in different time interval (0, 24, 48, 72 and 96 hrs) at alkaline pH (a) pH 11, (b) pH 12 and (c) pH 13.

band I (365 nm) which is red shifted to 406 nm decreased and vanished in alkaline pH after 96 hours and the reaction was catalysed faster in pH 13 **(Fig. 2.11 a)** followed by pH 12 **(Fig. 2.11 b)** and pH 11 **(Fig. 2.11 c)**.

The absorption spectra in alkaline pH at different time interval of incubation suggests that DHF is not stable at higher alkaline pH. DHF undergoes colour change from bright yellow **(Fig. 2.12 a)** to almost colourless after 96 hrs of incubation at pH 13 **(Fig. 2.12 b)**.

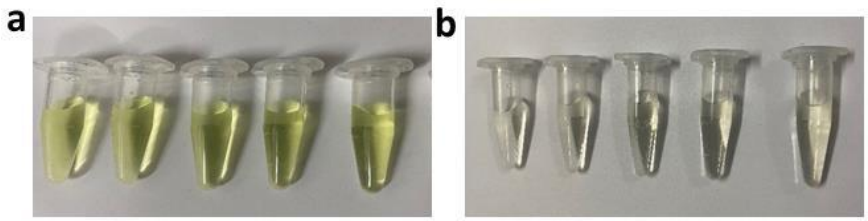

Fig. 2.12: (a) DHF in pH 13 at 0 hr , (b) DHF in pH 13 at 96 hrs.

When phenolic compounds are dissolved in a NaOH solution, their absorption spectra red shift between 200 and 360 nm, according to research (Dearden and Forbes, 1959). The absorption spectra and extinction coefficients of these phenols are observed to be influenced by a variety of factors, including solvent properties, the presence of electron-donating substituents on the benzene rings, intra- and intermolecular hydrogen bonding, steric influences, and the formation of pH-dependent resonance forms with modified conjugation compared to the original compounds (Dearden and Forbes, 1959).

2.3.6 Stability of DHF in different charged surfactant micelles

The limited water solubility of DHF arises from its inherent hydrophobic character. Beyond solubility, a crucial aspect of comprehending DHF's behavior pertains to its stability within diverse pH environments. Such insights hold the key to enhancing its advantageous attributes and safeguarding it against degradation.Through the examination of DHF's spectral characteristics when encapsulated within distinct micellar systems at varying pH levels, we gain valuable insights into the microenvironment that DHF molecules encounter within these intricately structured surfactant micelles. This investigation serves as an illuminating window into DHF's behavior, shedding light on its intricate interactions within these specialized environments.

The absorption spectra of DHF (10 μM, 20 μM, 30 μM, 40 μM and 50 μM) was investigated in three different charged surfactant micelles – 20 mM SDS, 5 mM CTAB and 0.5

mM T20 in different pH for different time intervals (0 hr, 24 hrs, 48 hrs, 72 hrs and 96 hrs). DHF exhibited enhanced absorbance at pH 2 in all the different surfactant micelles compared to pure aqueous medium and it was stable upto 96 hrs of incubation **(Fig. 2.13)** and similar trend was observed for pH 3 **(Fig. 2.14)** and for pH 5 **(Fig. 2.15)**. DHF exhibits three main absorption bands, Band I (363-370 nm), Band II (263-270 nm) is and Band III (330 nm). SDS micelles, CTAB micelles and T20 micelles do not exert any changes in these bands in pH 2, pH 3 and pH 5. DHF consists

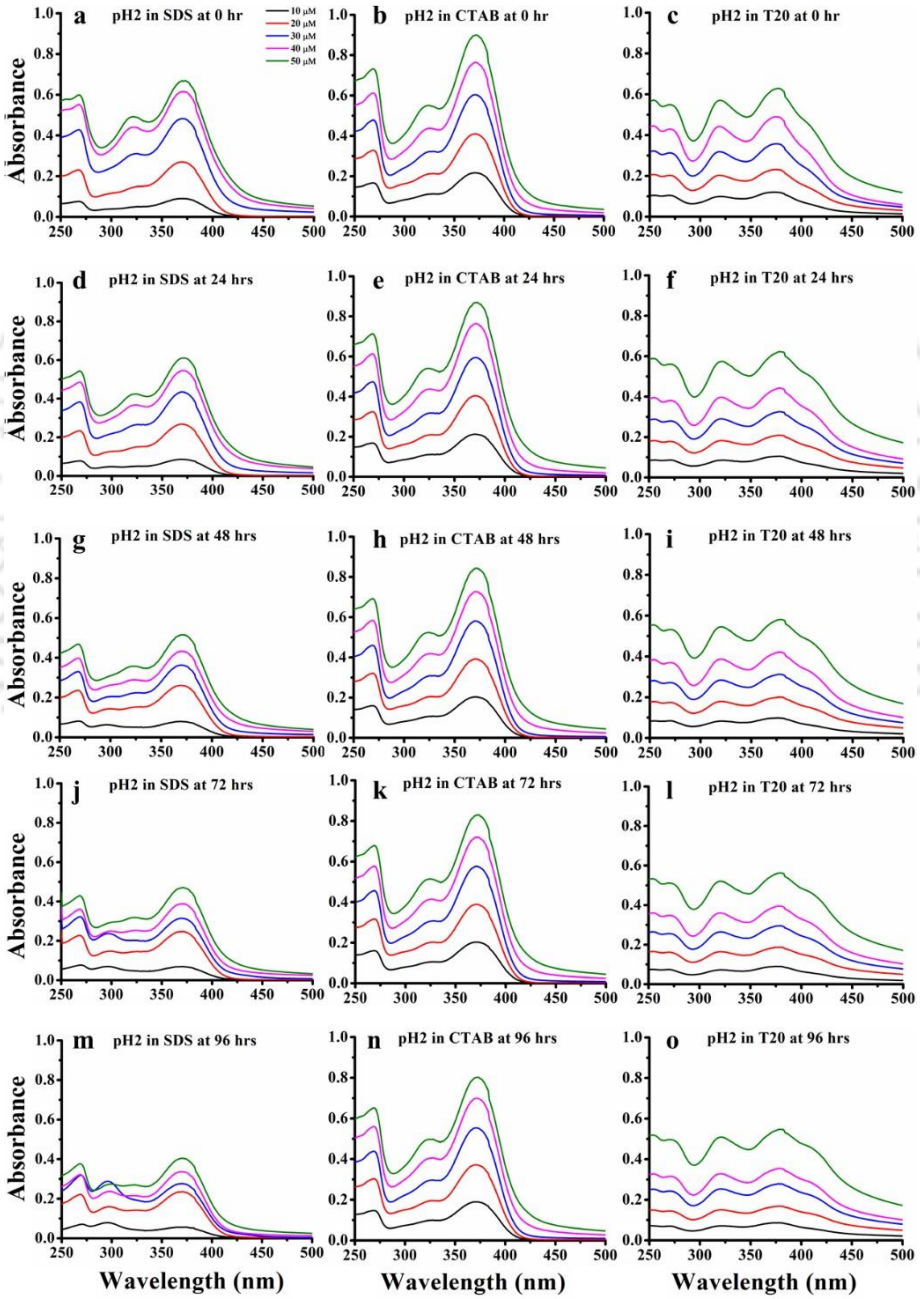

Fig. 2.13: Absorption spectra of DHF in pH 2 in (a) SDS at 0 hr, (b) CTAB at 0 hr, (c)T20 at 0 hr, (d) SDS at 24 hrs, (e) CTAB at 24 hrs, (f) T20 at 24 hrs, (g) SDS at 48 hrs, (h) CTAB at 48 hrs, (i) T20 at 48 hrs, (j) SDS at 72 hrs, (k) CTAB at 72 hrs, (l) T20 at 72 hrs, (m) SDS at 96 hrs, (n) CTAB at 96 hrs, (o) T20 at 96 hrs.

of aromatic rings and it is poorly soluble in aqueous media. However, DHF shows enhanced absorption in all the surfactant micelles in pH 2, pH 3 and pH 5 which suggests the possibility of DHF to be extracted into the micelles through hydrophobic interaction.

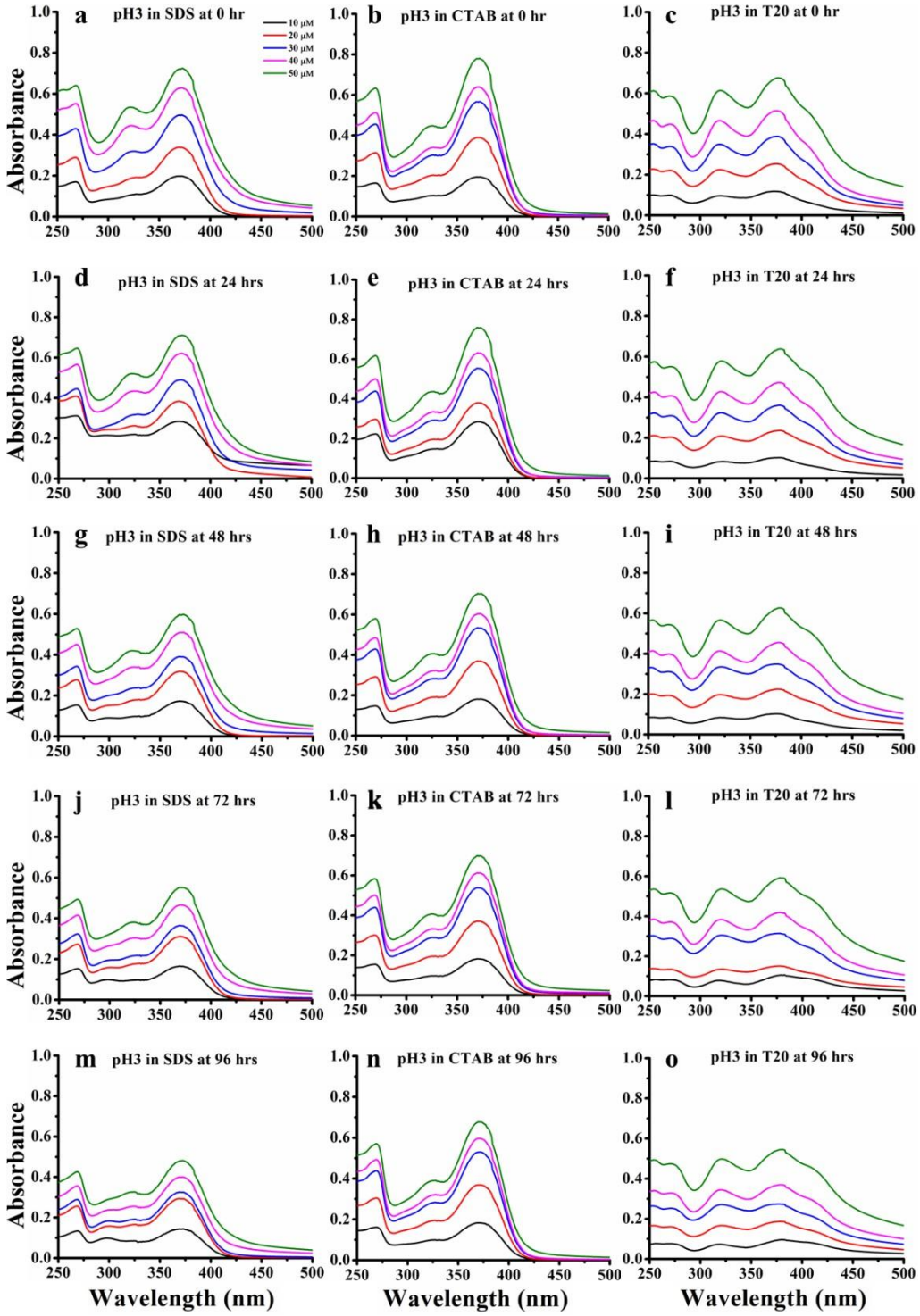

Fig. 2.14: Absorption spectra of DHF in pH 3 in (a) SDS at 0 hr, (b) CTAB at 0 hr, (c)T20 at 0 hr, (d) SDS at 24 hrs, (e) CTAB at 24 hrs, (f) T20 at 24 hrs, (g) SDS at 48 hrs, (h) CTAB at 48 hrs, (i) T20 at 48 hrs, (j) SDS at 72 hrs, (k) CTAB at 72 hrs, (l) T20 at 72 hrs, (m) SDS at 96 hrs, (n) CTAB at 96 hrs, (o) T20 at 96 hrs.

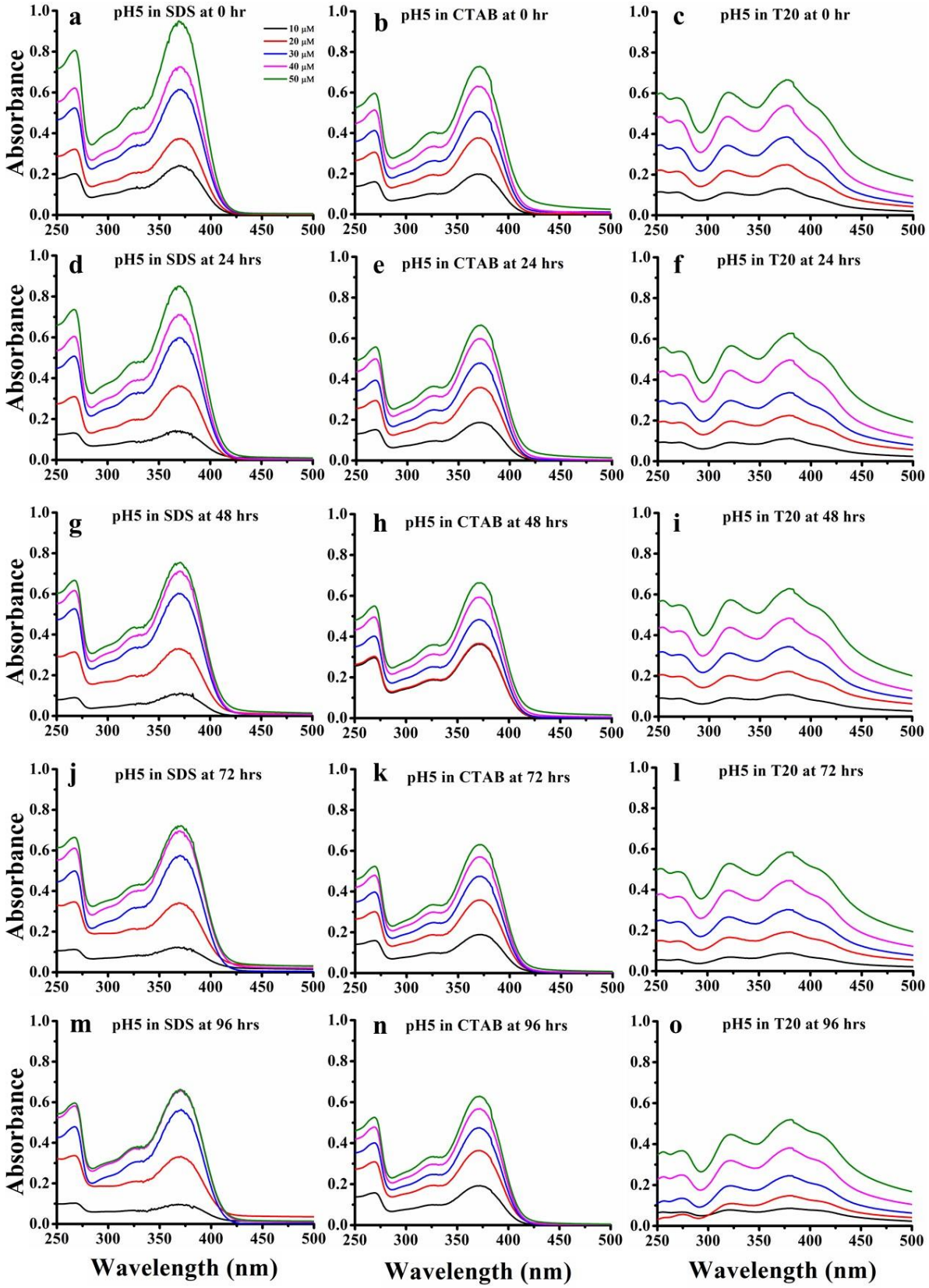

Fig. 2.15: Absorption spectra of DHF in pH 5 in (a) SDS at 0 hr, (b) CTAB at 0 hr, (c)T20 at 0 hr, (d) SDS at 24 hrs, (e) CTAB at 24 hrs, (f) T20 at 24 hrs, (g) SDS at 48 hrs, (h) CTAB at 48 hrs, (i) T20 at 48 hrs, (j) SDS at 72 hrs, (k) CTAB at 72 hrs, (l) T20 at 72 hrs, (m) SDS at 96 hrs, (n) CTAB at 96 hrs, (o) T20 at 96 hrs.

At pH 7, DHF exhibited similar trend as above-mentioned pH conditions in SDS and T20 surfactant micelles **(Fig. 2.16)** but an additional shoulder peak at around 424 nm was observed in presence of CTAB micelles in pH 7 **(Fig. 2.16 b, e, h, k, n)**. The overlap of DHF absorption

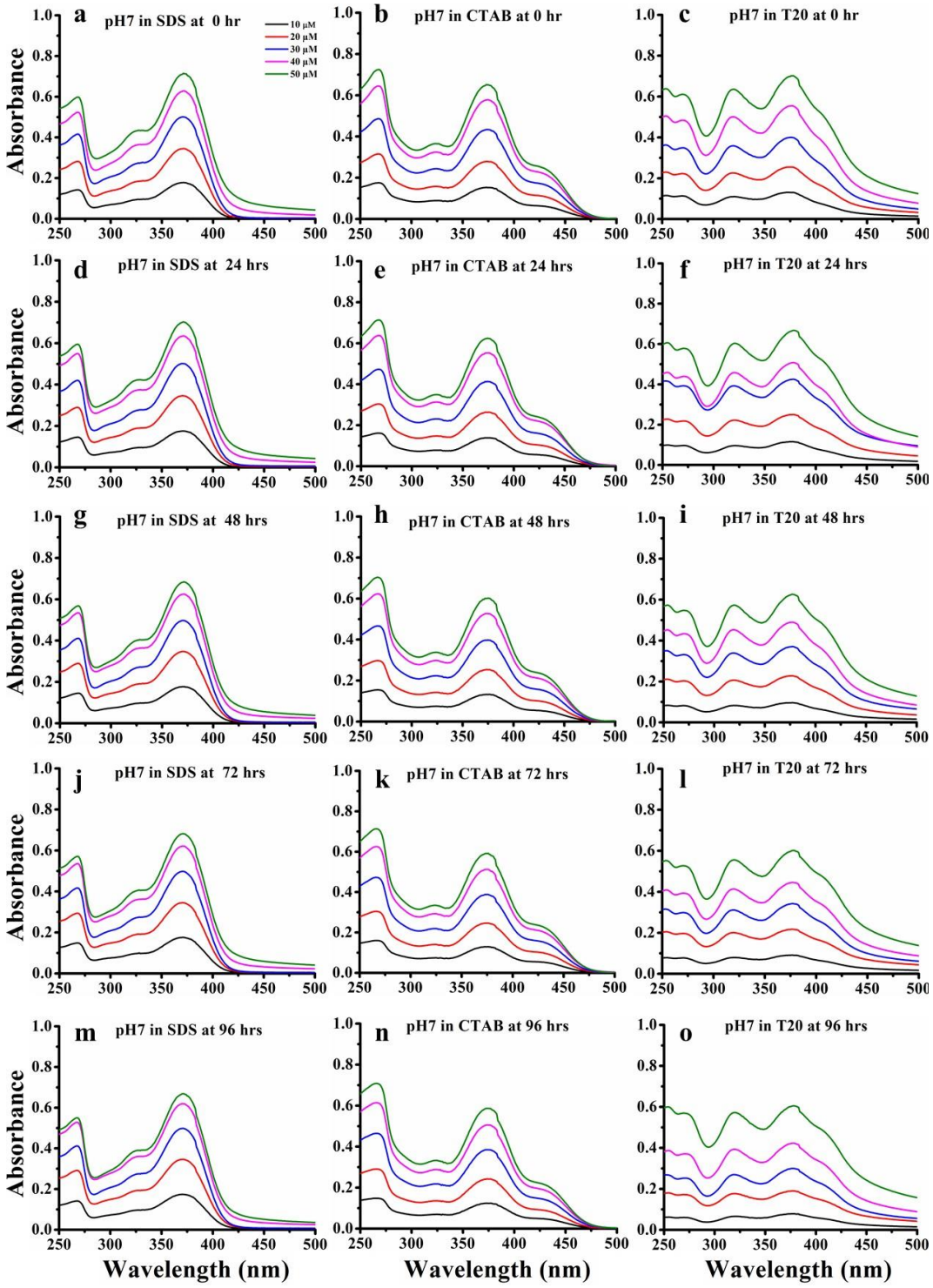

Fig. 2.16: Absorption spectra of DHF in pH 7 in (a) SDS at 0 hr, (b) CTAB at 0 hr, (c)T20 at 0 hr, (d) SDS at 24 hrs, (e) CTAB at 24 hrs, (f) T20 at 24 hrs, (g) SDS at 48 hrs, (h) CTAB at 48 hrs, (i) T20 at 48 hrs, (j) SDS at 72 hrs, (k) CTAB at 72 hrs, (l) T20 at 72 hrs, (m) SDS at 96 hrs, (n) CTAB at 96 hrs, (o) T20 at 96 hrs.

spectra between SDS and CTAB is shown in **(Fig. 2.17 a)** which clearly indicates the presence of 424 nm shoulder peak in CTAB micelles at pH 7. The molar extinction coefficient (ε) of DHF at 424 nm in presence of SDS and CTAB micelles **(Fig. 2.17 b)** is shown which showed increased ε in CTAB micelles compared to SDS micelles.

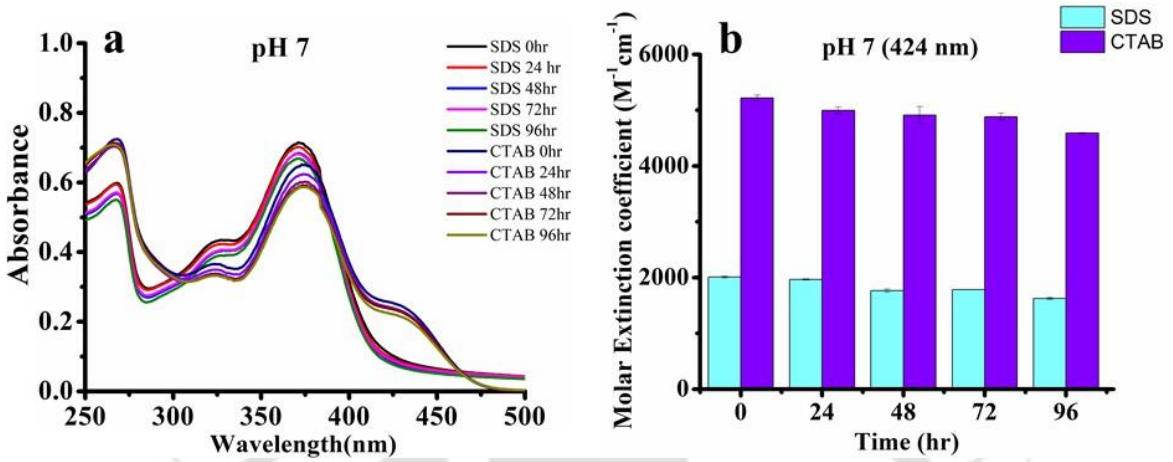

Fig. 2.17: (a) Absorption spectra of DHF at pH 7 in SDS and CTAB at different time intervals ((0, 24, 48, 72 and 96 hrs) (b) Molar extinction coefficient of DHF in 424 nm at pH7 in SDS and CTAB at different time intervals (0, 24, 48, 72 and 96 hrs).

DHF at pH9 in SDS and T20 micelles **(Fig. 2.18)** showed enhanced solubility and stability compared to aqueous medium but in CTAB micelles the absorption spectra at 365 nm is red shifted to 425 nm **(Fig. 2.18 b)** and the intensity of the peak gradually decreases with increasing incubation time period **(Fig. 2.18 b, e, h, k, n)**. The red shift observed in CTAB micelles at pH 9 could be due to large density of positive charges in CTAB micelles creating more alkaline behaviour. Similar phenomenon has been observed in flavonoid mammeigin (MMG) at pH 9, which exist as a deprotonated anionic form in CTAB micelles due to large density of positive charges and can interact with the positively charged CTAB head group at surface of CTAB micelle via electrostatic attraction (Senthilkumar et al., 2023).

The absorption spectra of DHF at pH 11 in all the different surfactant micelles showed enhanced absorbance **(Fig. 2.19)**. In SDS micelles, at pH 11 the 365 nm peak was red shifted to 406 nm peak **(Fig. 2.19 a)** and the intensity of peak decreased with respect to time **(Fig. 2.20 a, d, g, j, m)**. Also, in presence of CTAB micelles at pH 11, the 365 nm peak was red shifted to 425 nm peak **(Fig. 2.19 b)** and the intensity of the peak decreased with respect to increasing incubation time **(Fig. 2.19 b, e, h, k, n)**. The absorption spectra of DHF at pH 11 in T20 showed that the 356 nm peak was red shifted to 406 nm peak **(Fig. 2.19 c)** and the red shifted peak was stable upto 96 hrs of incubation **(Fig. 2.19 c, f, i, l, o)**. It has been reported that flavonoid

quercitin undergoes ionization of the OH group at C3 (C-ring) position which resulted in the red shift of the aborption maximum at pH between 9.0 and 11.0 (Jurasekova et al., 2014).

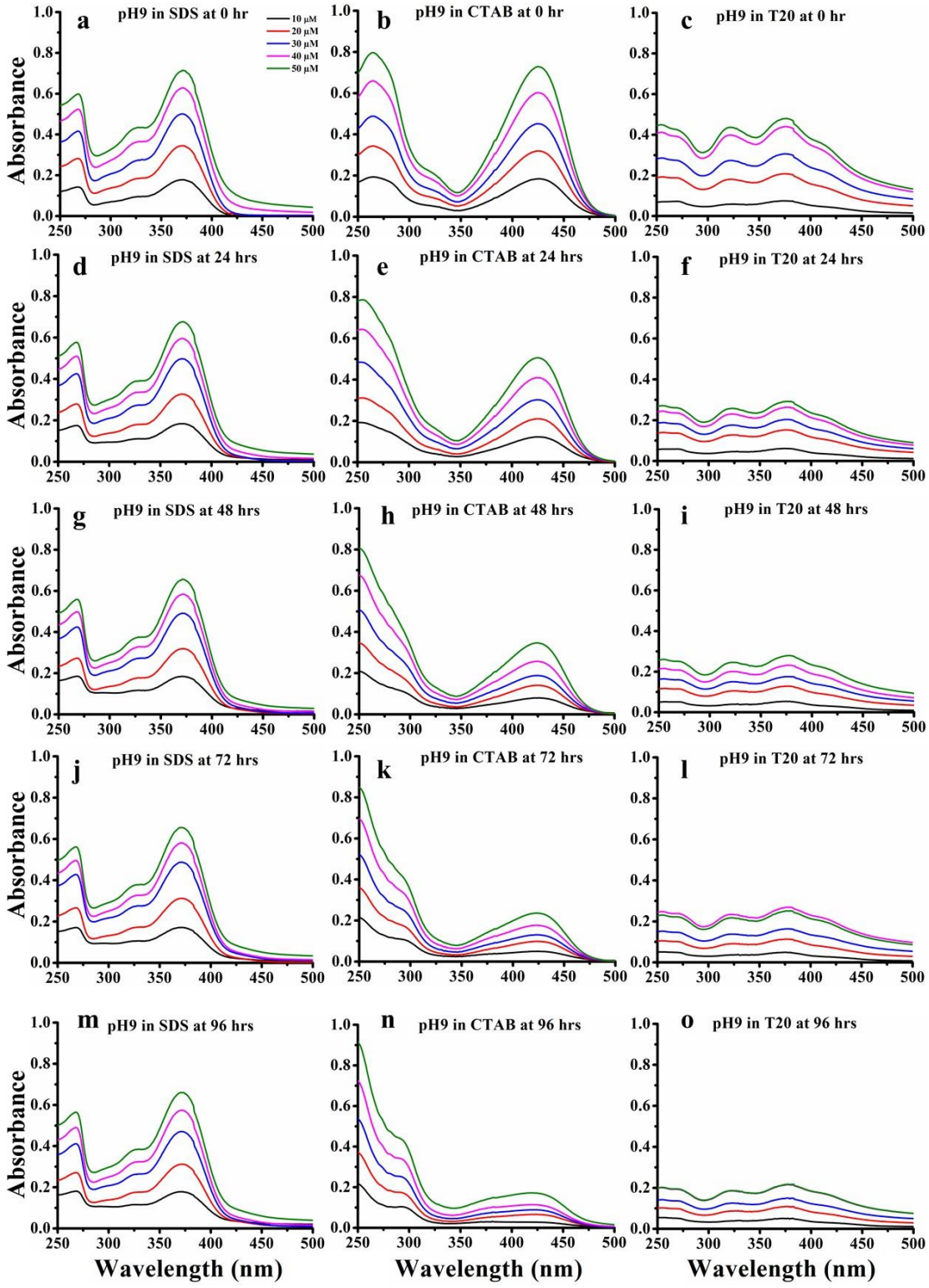

Fig. 2.18: Absorption spectra of DHF in pH 9 in (a) SDS at 0 hr, (b) CTAB at 0 hr, (c)T20 at 0 hr, (d) SDS at 24 hrs, (e) CTAB at 24 hrs, (f) T20 at 24 hrs, (g) SDS at 48 hrs, (h) CTAB at 48 hrs, (i) T20 at 48 hrs, (j) SDS at 72 hrs, (k) CTAB at 72 hrs, (l) T20 at 72 hrs, (m) SDS at 96 hrs, (n) CTAB at 96 hrs, (o) T20 at 96 hrs.

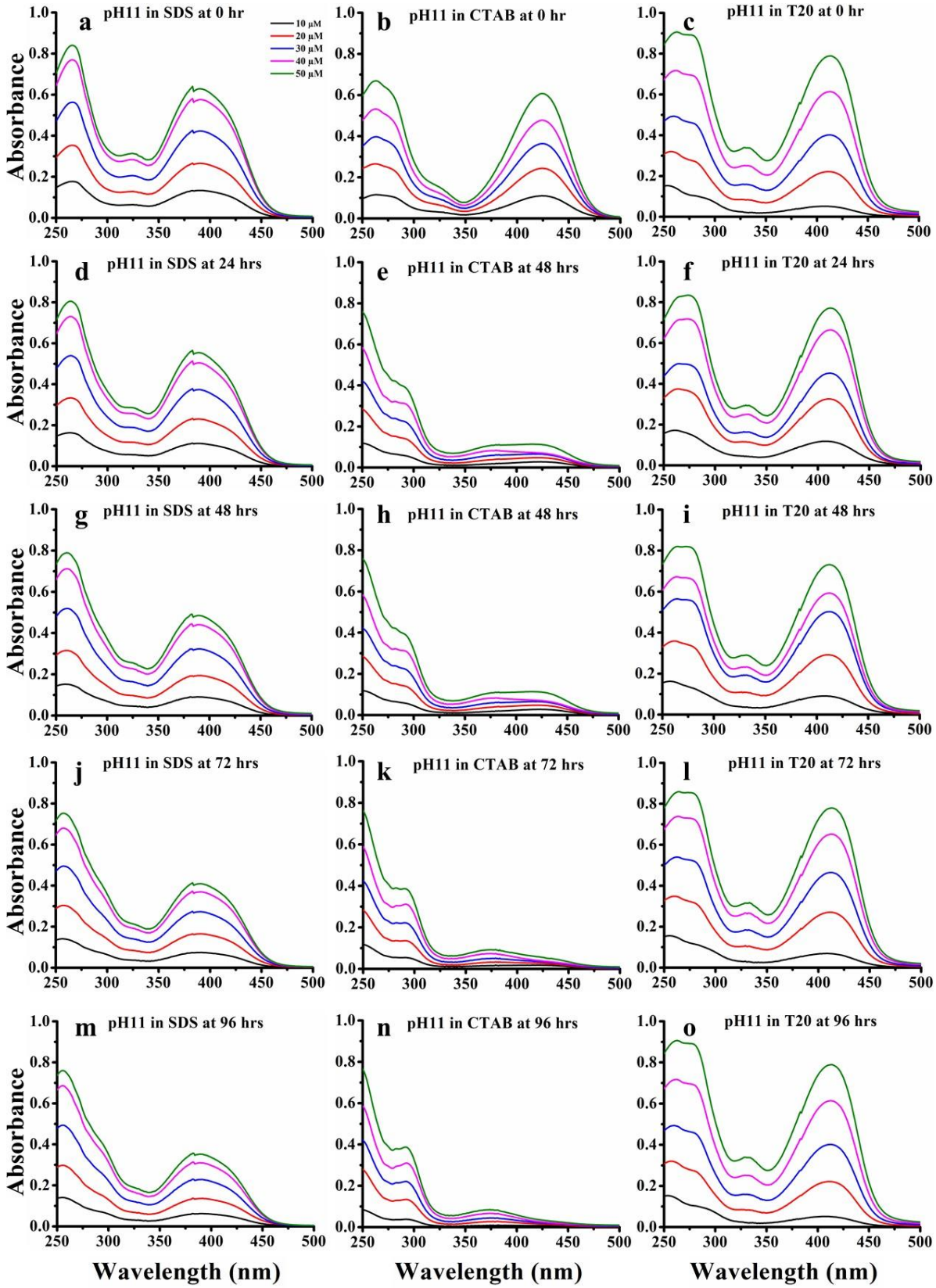

Fig. 2.19: Absorption spectra of DHF in pH 11 in (a) SDS at 0 hr, (b) CTAB at 0 hr, (c)T20 at 0 hr, (d) SDS at 24 hrs, (e) CTAB at 24 hrs, (f) T20 at 24 hrs, (g) SDS at 48 hrs, (h) CTAB at 48 hrs, (i) T20 at 48 hrs, (j) SDS at 72 hrs, (k) CTAB at 72 hrs, (l) T20 at 72 hrs, (m) SDS at 96 hrs, (n) CTAB at 96 hrs, (o) T20 at 96 hrs.

At pH 13, the absorption spectra of DHF in SDS showed red shift of the peak 365 nm to 406 nm **(Fig. 2.20)** and the peak disappears completely with increasing incubation time upto 96 hrs **(Fig. 2.20 a, d, g, j, m)**, similarly in CTAB micelles the 365 nm peak is red shifted to 425 nm

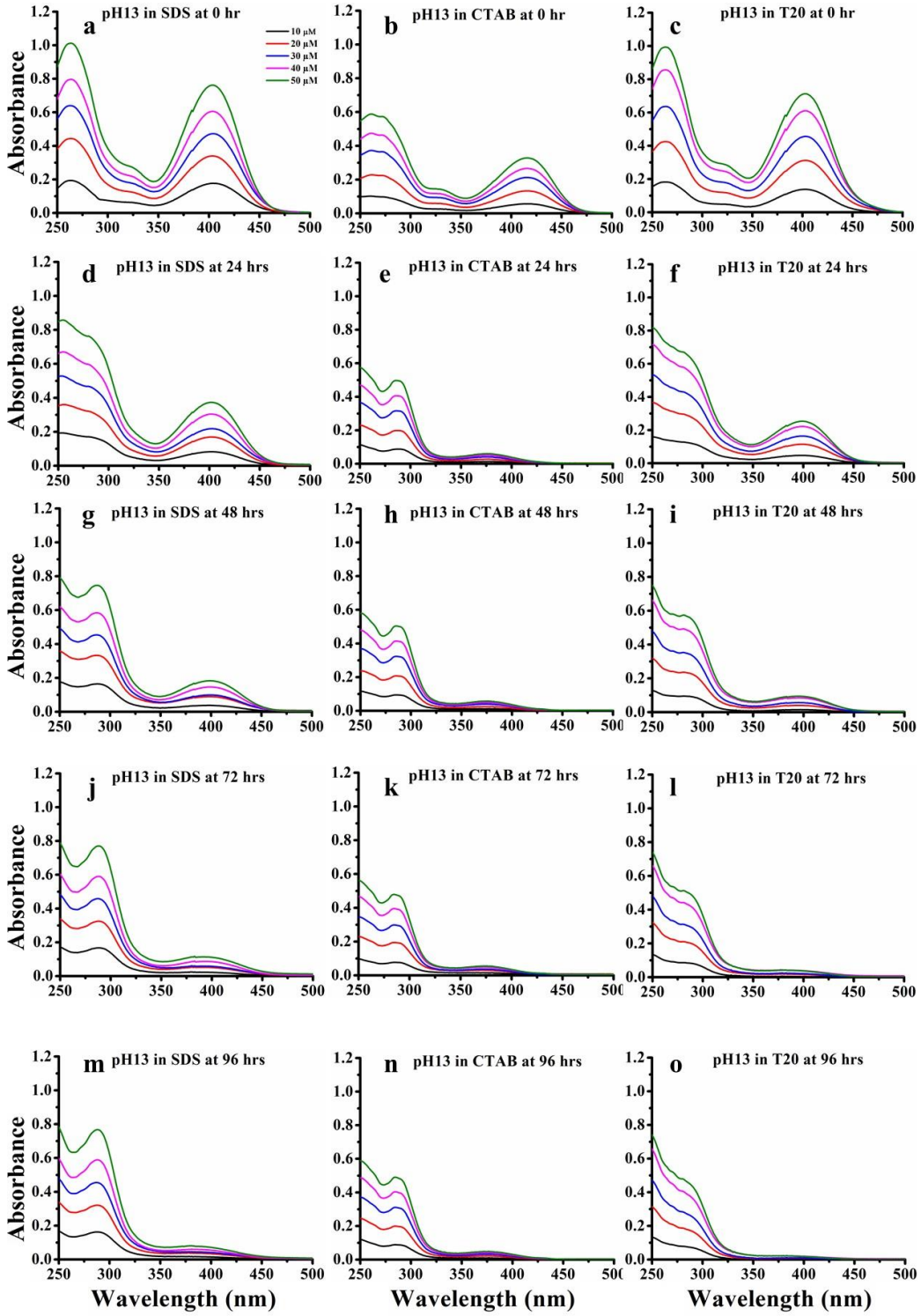

Fig. 2.20: Absorption spectra of DHF in pH 13 in (a) SDS at 0 hr, (b) CTAB at 0 hr, (c)T20 at 0 hr, (d) SDS at 24 hrs, (e) CTAB at 24 hrs, (f) T20 at 24 hrs, (g) SDS at 48 hrs, (h) CTAB at 48 hrs, (i) T20 at 48 hrs, (j) SDS at 72 hrs, (k) CTAB at 72 hrs, (l) T20 at 72 hrs, (m) SDS at 96 hrs, (n) CTAB at 96 hrs, (o) T20 at 96 hrs.

(Fig. 2.20 b) and the peak disappears **(Fig. 2.20 e, h, k, n)** and in T20 micelles also it was observed that 365 nm peak was redshifted and disappears after 96 hours **(Fig. 2.20 o).** In Quercitin, it has been observed that at pH 13 it undergoes autoxidation affecting mainly the C-ring and resulting in fragmentation, dimerization and polymerization which makes it instable at higher alkaline pH (Jurasekova et al., 2014). Therefore, it could be concluded that the solubility of DHF was enhanced in all the three surfactant micelles at pH 7 and pH 9. DHF was not stable in higher alkaline pH even in the presence of micelles.

The comparative plot of 50 µM DHF in alkaline pH (9, 11, 13) at different time interval (0-96 hrs) in different surfactant micelles were plotted **(Fig. 2.21)** which shows that DHF is more stable at pH 9 in SDS micelles **(Fig. 2.21 a)** compared to DHF in CTAB **(Fig. 2.21 b)** and T20 **(Fig. 2.21 c)** micelles. DHF at pH 11 in SDS micelles **(Fig. 2.21 d)** shows instablity.

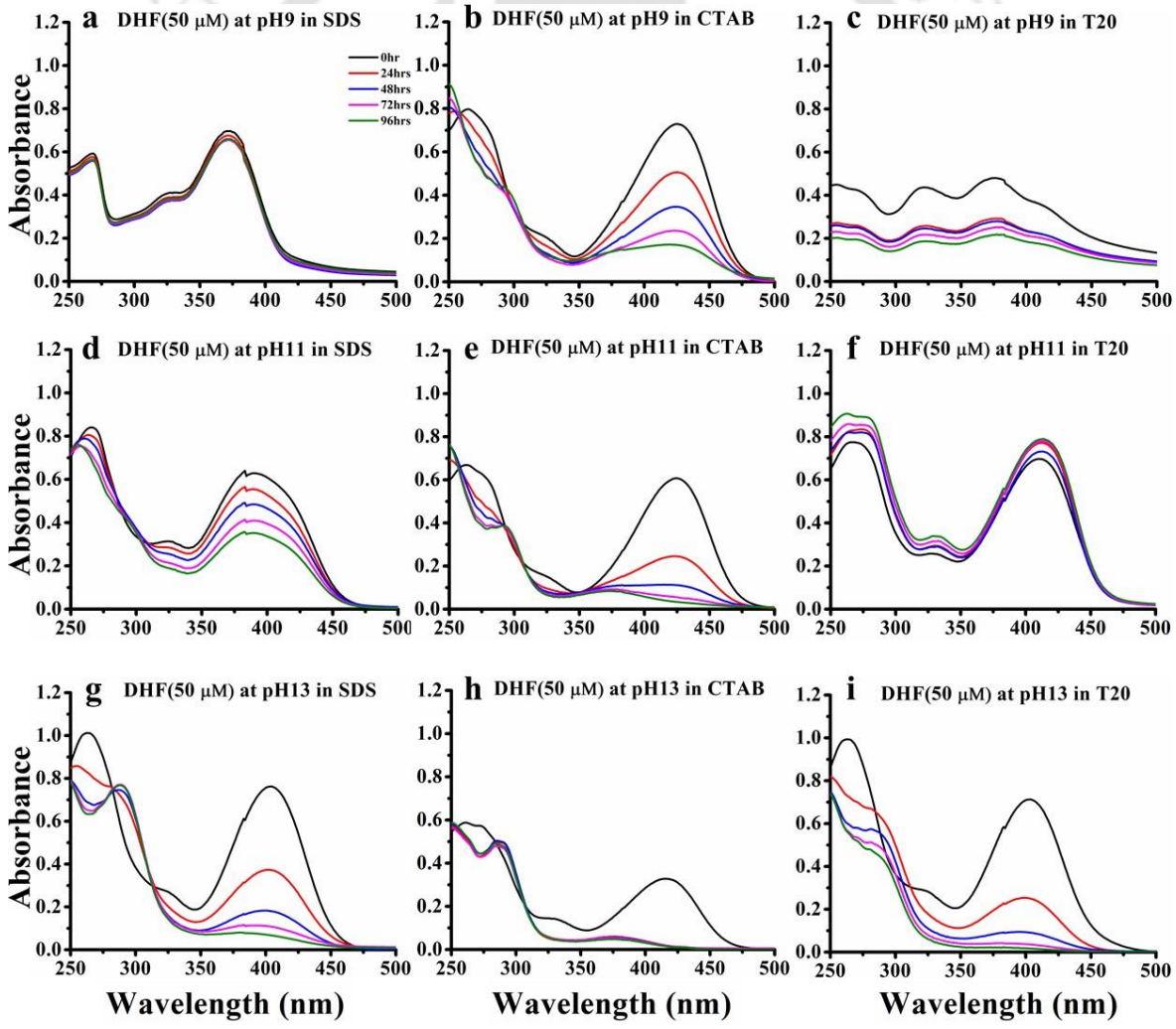

Fig. 2.21: Absorption spectra of 50 µM DHF at different time interval (0, 24, 48, 72 and 96 hrs) in (a) pH9 in SDS, (b) pH9 in CTAB, (c) pH9 in T20, (d) pH 11 in SDS, (e) pH 11 in CTAB, (f) pH 11 in T20, (g) pH 13 in SDS, (h) pH 13 in CTAB, (i) pH 13 in T20.

DHF in CTAB micelles **(Fig. 2.21 e)** showing highest level of transition and instability. DHF shows red shift of absorption maximum in T20 micelles **(Fig. 2.21 f)** and exhibits higher stability. At pH 13, DHF shows instability in all the sufactant micelles with CTAB micelles **(Fig. 2.21 h)** showing the faster kinetics compared to SDS **(Fig. 2.21 g)** and T20 **(Fig. 2.21 i)** micelles.

The molar extinction coefficient (Ɛ) of DHF in presence of different surfactant micelles as a function of pH was calculated in different wavelengths. At 270 nm the Ɛ of DHF in pH 2

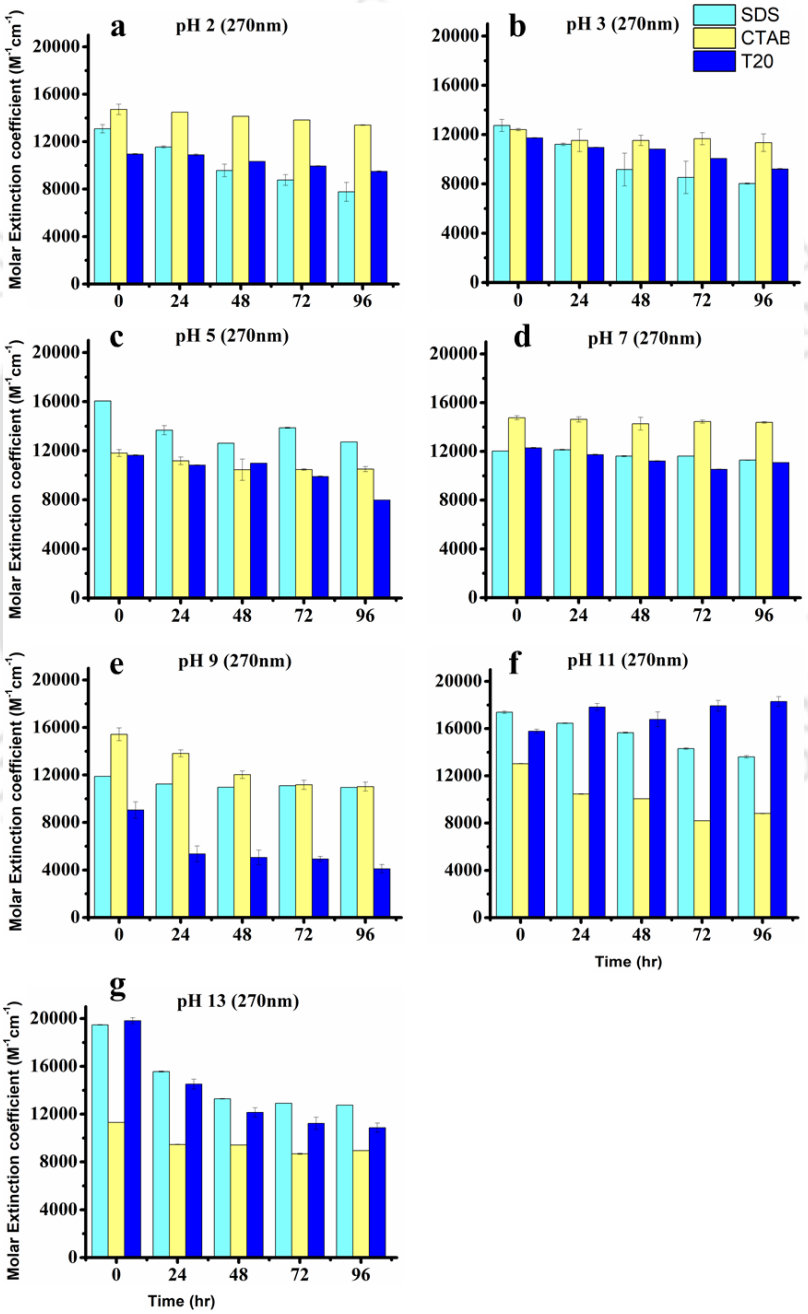

Fig. 2.22: Molar extinction coefficient (ε) of DHF at 270 nm at different time interval (0, 24, 48, 72 and 96 hrs) in SDS, CTAB and T20 in (a) pH 2, (b) pH 3, (c) pH 5, (d) pH 7, (e) pH 9, (f) pH 11, (g) pH 13.

in SDS depicted decrease in value with increasing incubation time. DHF at pH 2 in CTAB micelles showed stable and highest Ɛ value compared to SDS and T20 micelles, DHF in pH 2 in T20 depicted lesser Ɛ value compared to SDS and CTAB micelles **(Fig. 2.22 a)**. Similar trend was observed in pH 3 at 270 nm **(Fig. 2.22 b)** and at pH 5 SDS showed highest Ɛ value followed by CTAB and T20 at 270 nm **(Fig. 2.22 c)**. At pH 7, the Ɛ value of DHF was highest in CTAB micelles followed by SDS and T20 **(Fig. 2.22 d)** at 270 nm. At pH 9, DHF showed highest Ɛ value in CTAB micelles which gradually decreases with increasing incubation time followed by SDS with better stability compared to CTAB micelles. In T20 it showed the least Ɛ value which gradually decreases with increasing incubation time **(Fig. 2.22 e)**. The Ɛ value of DHF in pH 11 revealed that in SDS micelles it decreases with increase in incubation time. Similary it decreases in CTAB micelles at a faster rate. In T20 micelles the Ɛ value is quite stable at 270 nm **(Fig. 2.22 f)**. The Ɛ value of DHF in pH 13 at 270 nm decreases graduallyin all the surfactant micelles with increase in incubation time **(Fig. 2.22 g)**.

The molar extinction coefficient of DHF at 330 nm in pH 2 revealed that in SDS micelles the Ɛ value decreases with time but in CTAB and T20 micelles it remains stable with time **(Fig. 2.23 a)**. In pH 3 at 330 nm, it is observed that the Ɛ value in SDS decreases with time, in CTAB micelles it remains stable, while the decrease in intensity was lesser in T20 micelles compared to SDS and CTAB **(Fig. 2.23 b)**. Similar trend was observed in pH 5 for all the surfactant micelles **(Fig. 2.23 c)**. In pH 7 at 330 nm, Ɛ value in SDS almost remained stable, CTAB showed the least Ɛ value and T20 showed highest Ɛ value **(Fig. 2.23 d)**. In pH 9 at 330 nm, the Ɛ value in SDS micelles were stable; CTAB showed the least values and in T20 the Ɛ value decreased gradually with time **(Fig. 2.23 e)**. Ɛ value in SDS micelles in pH 11 decreased gradually with time, while CTAB depicted similar trend. In T20 micelles Ɛ value displayed a rising trend was **(Fig. 2.23 f)**. In pH 13 at 330 nm, the Ɛ value in all the surfactant micelles decreased gradually with increased incubation time **(Fig. 2.23 g)**.

At 365 nm, the molar extinction coefficient of DHF in pH 2 revealed that CTAB has the highest stable Ɛ value followed by SDS micelles displaying gradual decrease in Ɛ value with respect to time and finally T20 showing the least Ɛ value and gradual decrease with respect to time **(Fig. 2.24 a)**. In pH 3 at 365 nm it was observed that the Ɛ value of DHF in CTAB was highest followed by SDS and T20 where it decreased with increase in incubation time **(Fig. 2.24 b)**. In pH 5 **(Fig. 2.24 c)** and pH 7 **(Fig. 2.24 d)** at 365 nm, DHF showed similar trend in the Ɛ value where SDS showed the highest, followed by CTAB and T20. In pH 9 at 365 nm,

the Ɛ value in SDS was highest and stable with respect to time, CTAB showing the least Ɛ value and T20

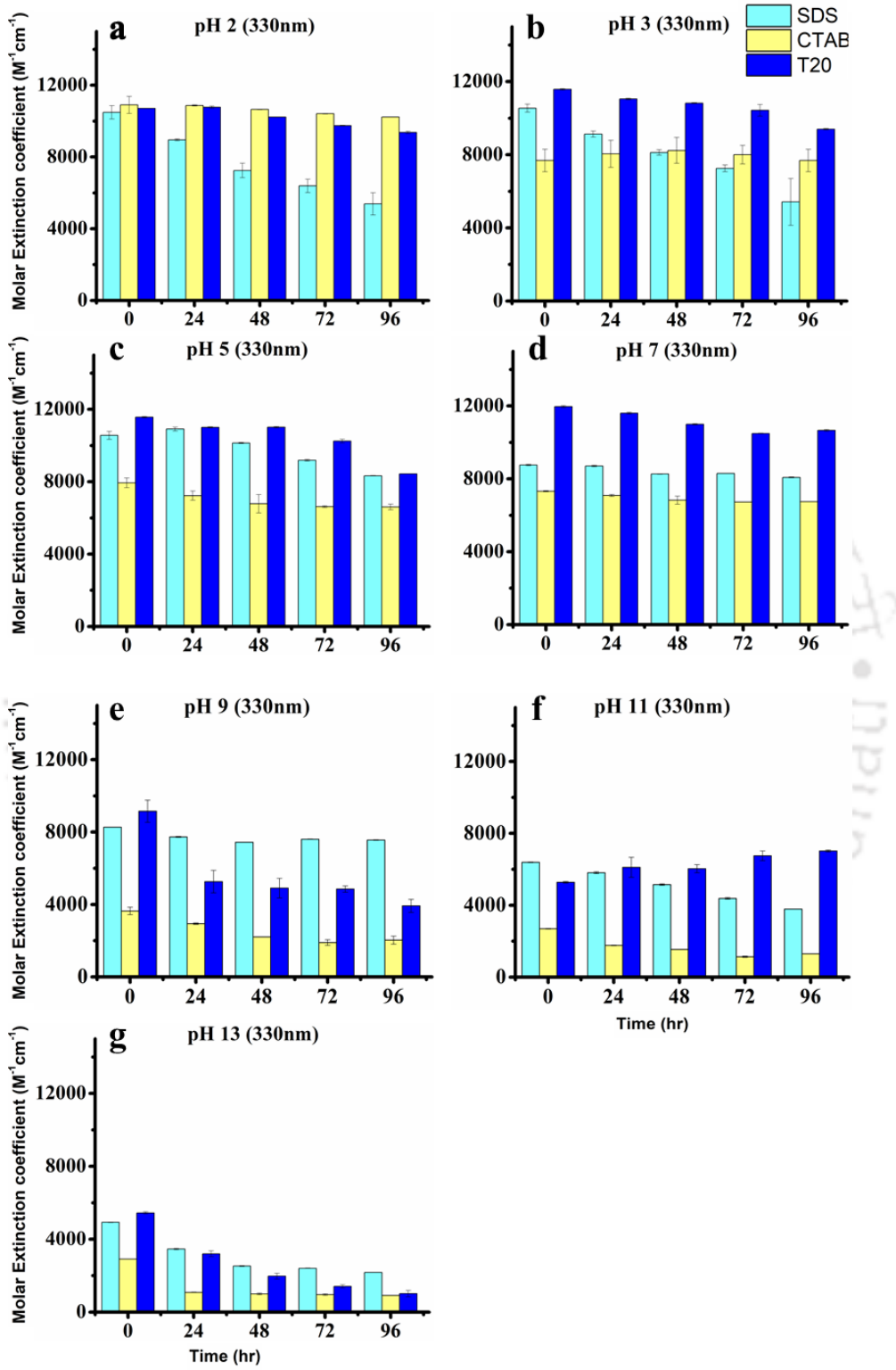

Fig. 2.23: Molar extinction coefficient (ε) of DHF at 330 nm at different time interval (0, 24, 48, 72 and 96 hrs) in SDS, CTAB and T20 in (a) pH 2, (b) pH 3, (c) pH 5, (d) pH 7, (e) pH 9, (f) pH 11, (g) pH 13

showing higher Ɛ value than CTAB with gradual decrease with respect to time **(Fig. 2.24 e)**. In pH 11 at 365 nm, the Ɛ value in T20 micelles showed better stability compared to SDS and CTAB, while CTAB along with SDS depicted the least Ɛ value **(Fig. 2.24 f)**. In pH 13 at 365 nm, the Ɛ value of DHF decreased gradually with respect to increase in incubation time in all the different surfactant micelles **(Fig. 2.24 g)**.

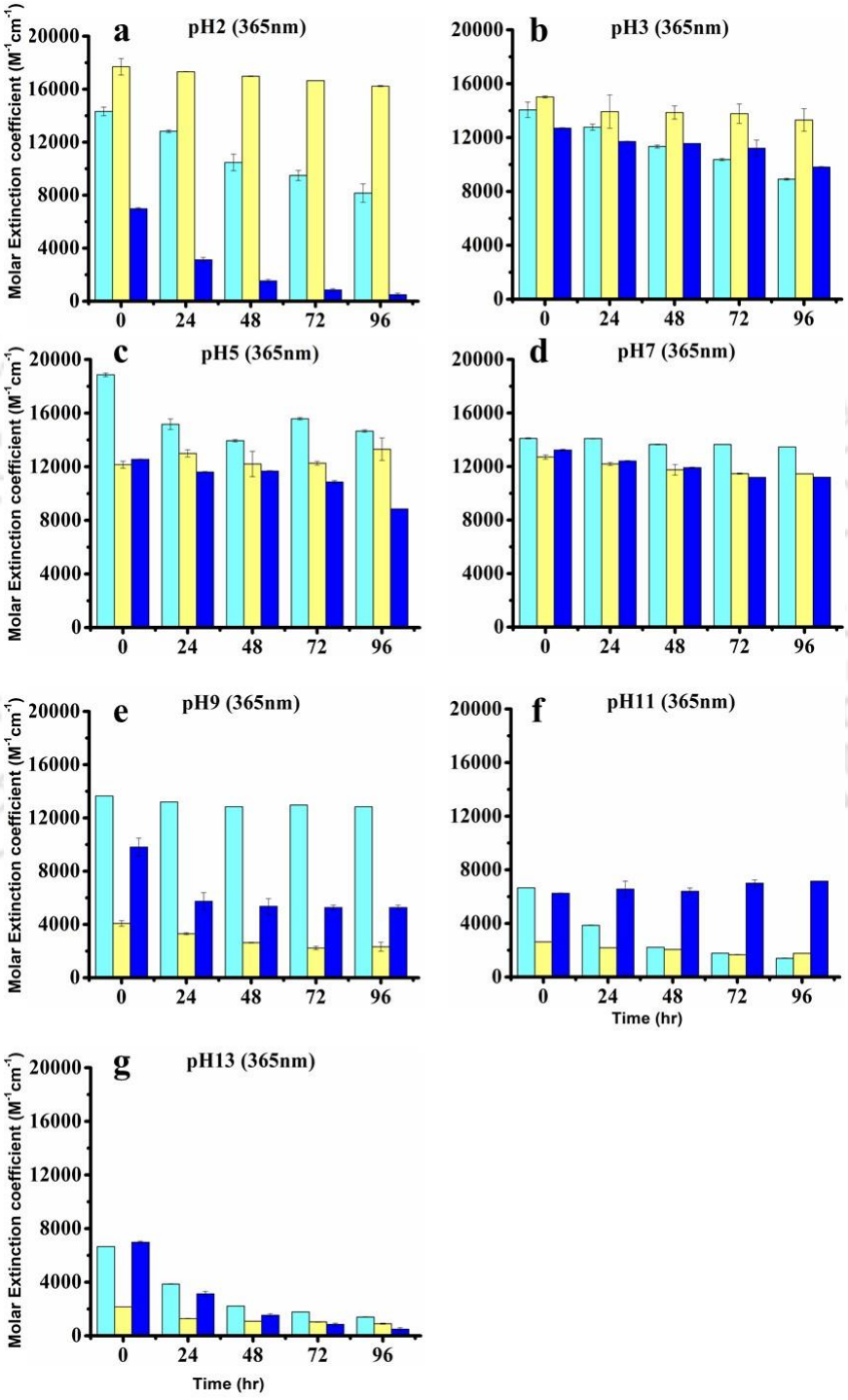

Fig. 2.24: Molar extinction coefficient (ε) of DHF at 365 nm at different time intervals (0, 24, 48, 72 and 96 hrs) in SDS, CTAB and T20 in (a) pH 2, (b) pH 3, (c) pH 5, (d) pH 7, (e) pH 9, (f) pH 11, (g) pH 13.

The molar extinction coefficient of DHF calculated at 406 nm revealed that in pH 2 T20 showed the highest and stable Ɛ value followed by SDS and CTAB. The Ɛ value in SDS was least stable **(Fig. 2.25 a)**. In pH 3 **(Fig. 2.25 b)** and pH 5 **(Fig. 2.25 c)** it was revealed that T20 showed the highest Ɛ value followed by SDS and CTAB. In pH 7 at 406 nm, T20 showed the highest Ɛ value followed by CTAB and SDS **(Fig. 2.25 d)**. In pH 9 at 406 nm, CTAB exhibited highest

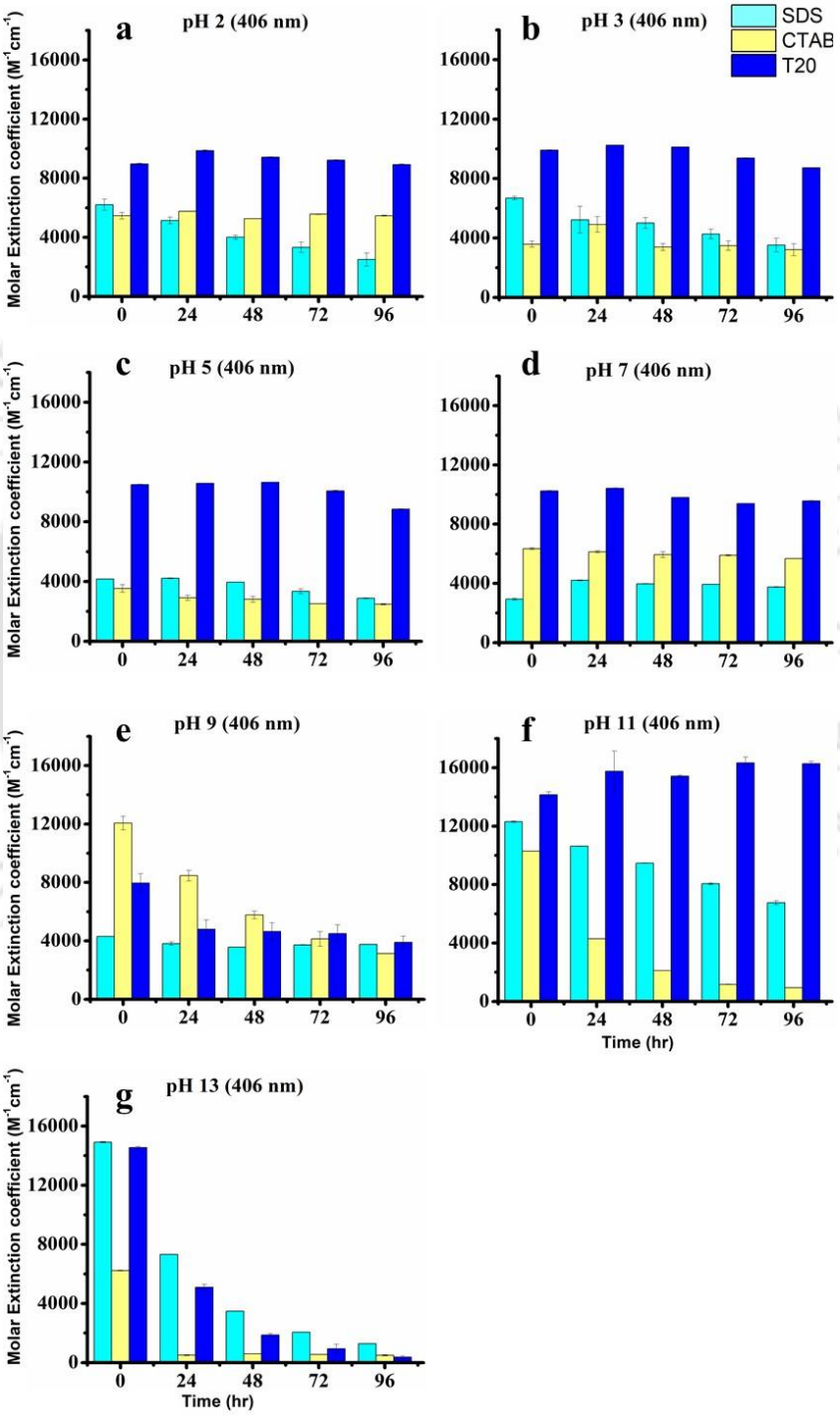

Fig. 2.25: Molar extinction coefficient (ε) of DHF at 406 nm at different time interval (0, 24, 48, 72 and 96 hrs) in SDS, CTAB and T20 in (a) pH 2, (b) pH 3, (c) pH 5, (d) pH 7, (e) pH 9, (f) pH 11, (g) pH 13.

Ɛ value followed by T20 and SDS with gradual decrease in Ɛ with respect to time in CTAB and T20 surfactant micelles **(Fig. 2.25 e)**. In pH 11 at 406 nm, the Ɛ value of DHF in T20 micelles is highest and stable followed SDS and CTAB displaying a gradual decrease in Ɛ with respect to time **(Fig. 2.25 f)**. In pH 13 at 406 nm, the Ɛ value of DHF gradually decreases in all the surfactant micelles with respect to time **(Fig. 2.25 f)**.

The molar extinction coefficient of DHF calculated at 450 nm revealed that at pH 2 **(Fig. 2.26 a)**, pH 3 **(Fig. 2.26 b)** and pH 5 **(Fig. 2.26 c)** showed similar trend where Ɛ value in T20 micelle

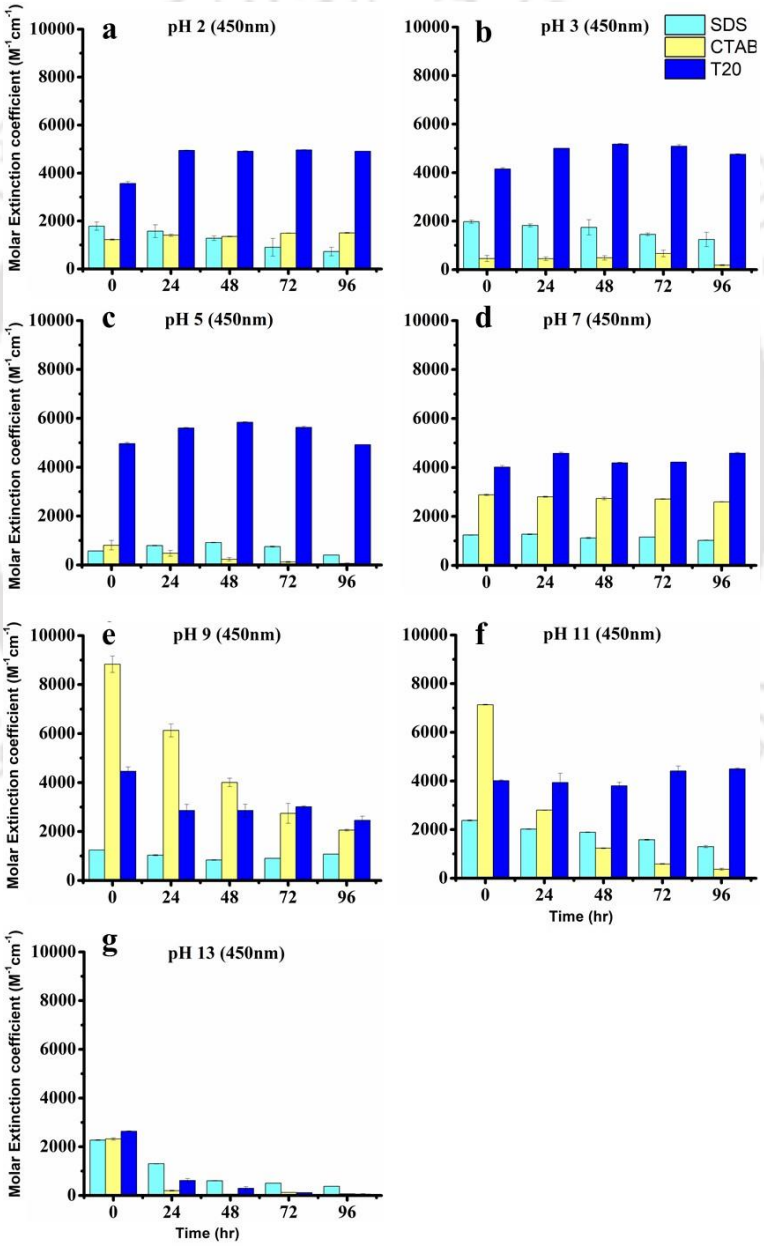

Fig. 2.26: Molar extinction coefficient (ε) of DHF at 450 nm at different time interval (0, 24, 48, 72 and 96 hrs) in SDS, CTAB and T20 in (a) pH 2, (b) pH 3, (c) pH 5, (d) pH 7, (e) pH 9, (f) pH 11, (g) pH 13.

is highest and stable followed by SDS and CTAB micelles. In pH 7 at 450 nm, the Ɛ value of DHF is highest in T20 micelle followed by CTAB and SDS **(Fig. 2.26 d)**. In pH 9 at 450 nm, the Ɛ value in CTAB micelle was highest with gradual decrease in Ɛ with respect to time follwed by T20 and SDS **(Fig. 2.26 e)**. In pH 11 at 450 nm, CTAB showed the highest Ɛ valuewith gradual decrease in Ɛ with respect to time followed by T20 micelle showing better stabilityand SDS showing least Ɛ value with gradual decrease in Ɛ with respect to time **(Fig. 2.26 f)**. InpH 13 at 450 nm, the Ɛ value of DHF gradually diminishes to zero in all the surfactant micelleswith respect to time **(Fig. 2.26 g)**.

2.3.7 Reversibility assay of DHF in Alkaline pH

The reversibility assay of DHF incubated in pH 13 for 96 hours followed by transfer to pH 7 in 50mM phosphate buffer (pH 7) and 20 mM SDS in 50mM phosphate buffer (pH 7) by UV absorption spectra revealed that DHF undergoes irreversible changes in higher alkaline pH (pH 13). The native absorption spectrum of DHF showing λmax at 365nm undergoes a red shift in alkaline pH 13 to 406 nm. This peak completely disappears after 96 hours even after bringing back to neutral pH 7, while a peak around 295 nm **(Fig. 2.27)** is observed. This suggests that DHF might have undergone degradation or permanent structural changes during prolonged exposure to alkaline pH.

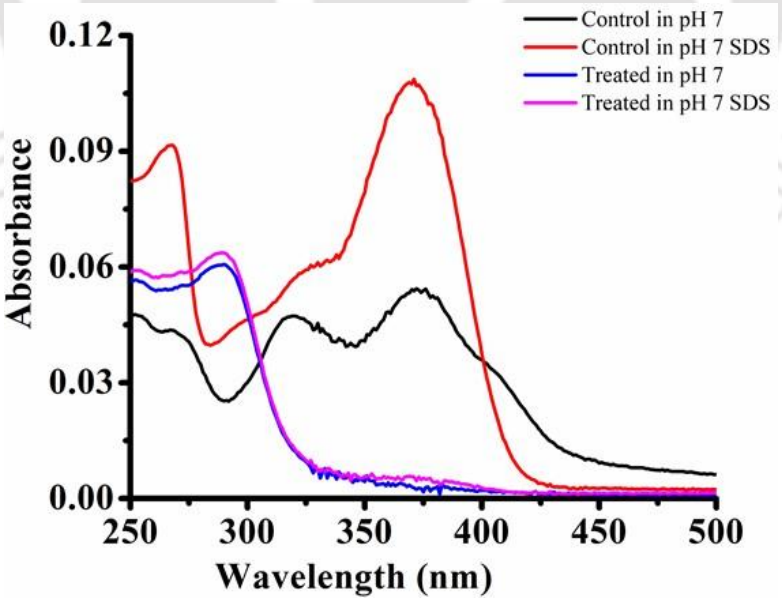

Fig. 2.27: Absorption spectra of DHF control in pH 7 and pH 7 (20mM SDS) and DHF incubated for 96 hours in pH 13 and neutralizing in pH 7 alone and pH 7(20mM SDS).

2.3.8 Degradation analysis of DHF in pH 13 by TLC and HPLC

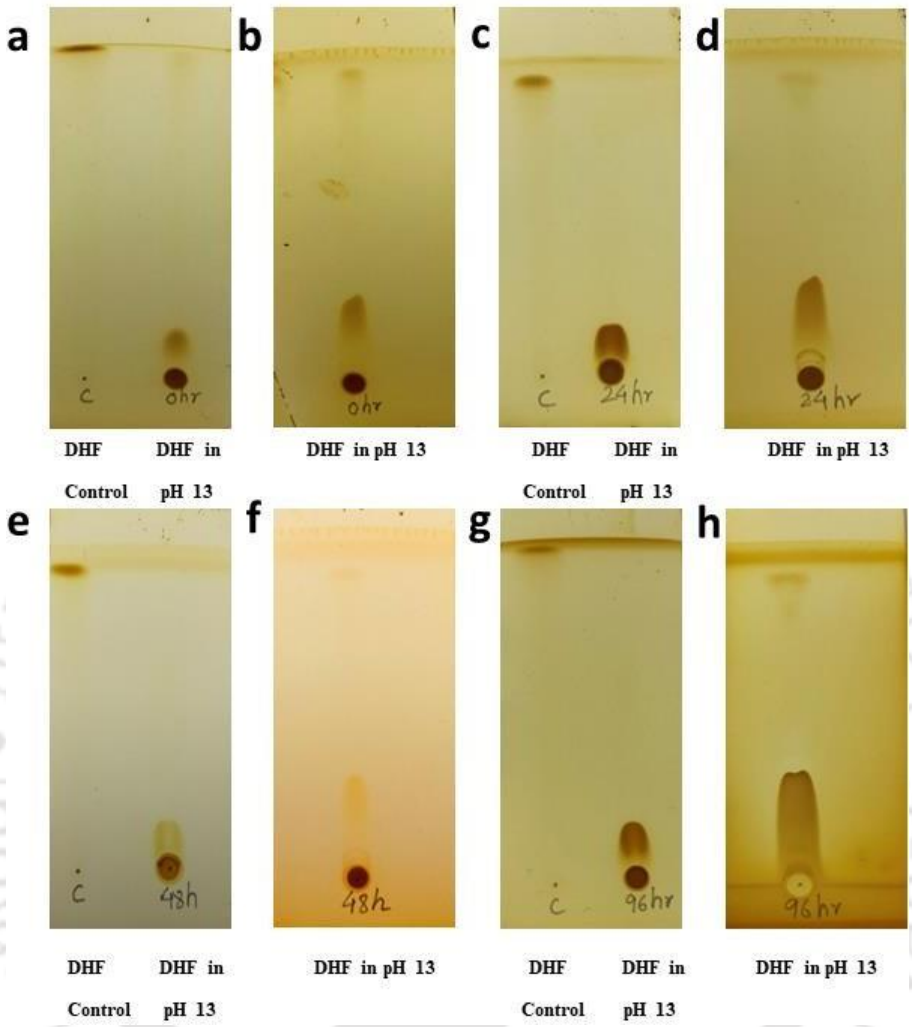

Fig. 2.28: TLC image of DHF incubated in pH 13 at different time interval (a) 0 hr, mobile phase(50% ethylacetate in hexane), (b) 0 hr, mobile phase(Pure ethylacetate), (c) 24 hr , mobile phase(50% ethylacetate in hexane), (d) 24 hr , mobile phase(Pure ethylacetate), (e) 48 hr, mobile phase(50% ethylacetate in hexane), (f)48hr, mobile phase(Pure ethylacetate), (g) 96 hr, mobile phase(50% ethylacetate in hexane), (h) 96 hr, mobile phase(0.1%triethylamine in ethylacetate).

The TLC analysis of DHF conducted under alkaline conditions with a pH of 13 **(Fig. 2.28)**, has revealed a notable phenomenon. Unlike the native, undisturbed DHF, which exhibits a solitary peak when analyzed on the TLC plate, DHF subjected to incubation in the strongly alkaline pH 13 environment **(Fig. 2.28a and b)** exhibits multiple peaks even at the initial time point (0 hours). This observation strongly suggests the occurrence of degradation processes. Upon further examination, it becomes evident that, after 24 hours of incubation, both the pristine, untouched DHF and the DHF exposed to pH 13 **(Fig. 2.28c and d)** no longer exhibit

a distinct single band but instead show a smeared appearance on the TLC plate. This smeared pattern persists even when DHF is incubated for 48 hours **(Fig. 2.28e and f)** and for an extended duration of 96 hours **(Fig. 2.28g and h)** within the alkaline pH 13 environment. These findings suggest that DHF undergoes a fragmentation process when exposed to the strongly alkaline pH 13 conditions, leading to the formation of multiple peaks on the TLC plate over time.Moreover, the progressive transformation of the TLC profiles from distinct bands to smeared patterns underscores the dynamic nature of this degradation process.

The HPLC chromatogram revealed valuable insights into the behavior of DHF under various experimental conditions. In its native state, DHF exhibits a single peak when subjected to detection at wavelengths of 365 nm and 295 nm, with a retention time of approximately 39.9 minutes **(Fig. 2.29 and Fig. 2.30)**. However, when DHF is subjected to a 96-hour incubation in a pH 9 environment **(Fig. 2.31)**, the resulting chromatogram reveals a reduced number of peaks. Notably, a major peak emerges with a retention time of around 43 minutes, accompanied by a minor peak at approximately 39.27 minutes. In stark contrast, DHF incubated under highly alkaline pH 13 conditions for the same duration **(Fig. 2.32)** exhibits a considerably more complex profile, characterized by multiple peaks. Among these, two major peaks are discerned, with retention times of 42.9 minutes and 6.9 minutes, in addition to several minor peaks. This discrepancy strongly suggests that DHF degradation occurs more rapidly in the highly alkaline pH 13 environment compared to pH 9.

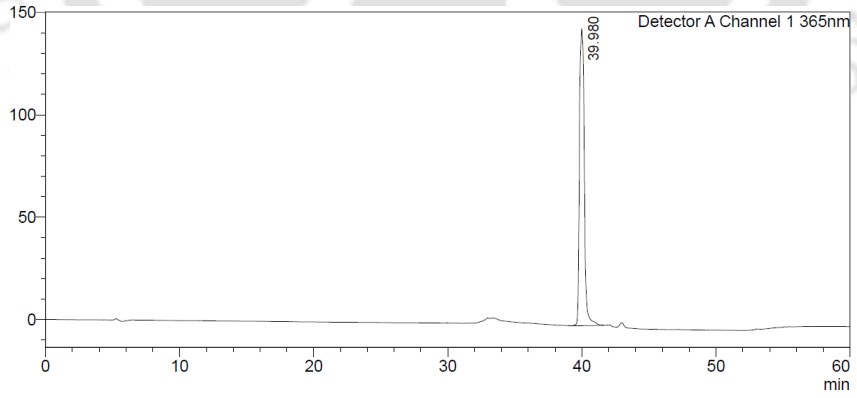

Fig. 2.29: HPLC peak of control DHF at 365 nm.

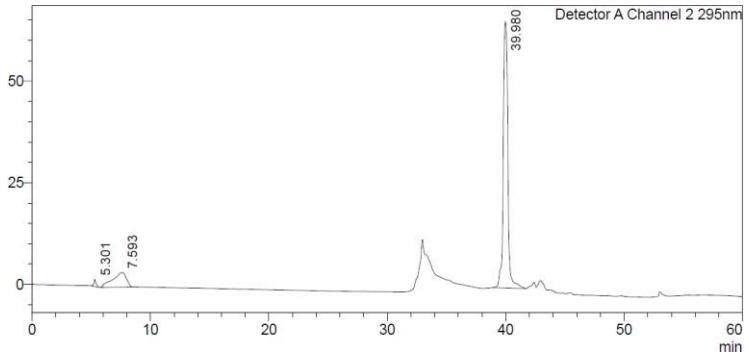

Fig. 2.30: HPLC peak of control DHF at 295 nm.

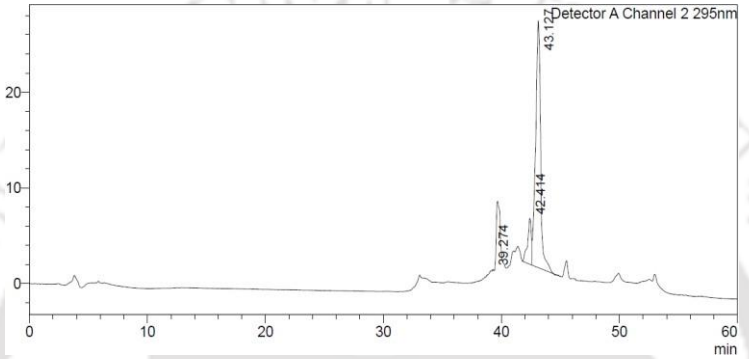

Fig. 2.31: HPLC analysis of DHF incubated in pH9 for 96 hours.

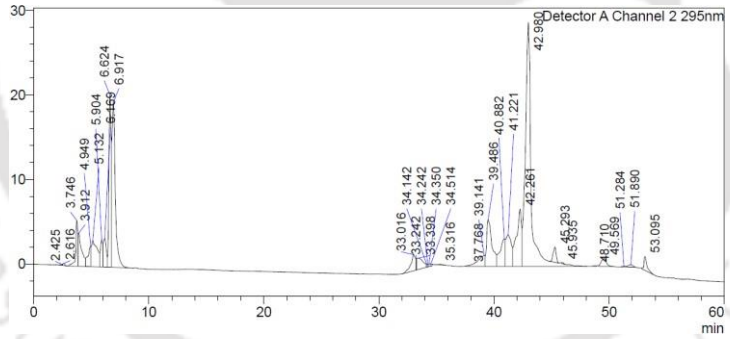

Fig 2.32: HPLC analysis of DHF incubated in pH13 for 96 hours.

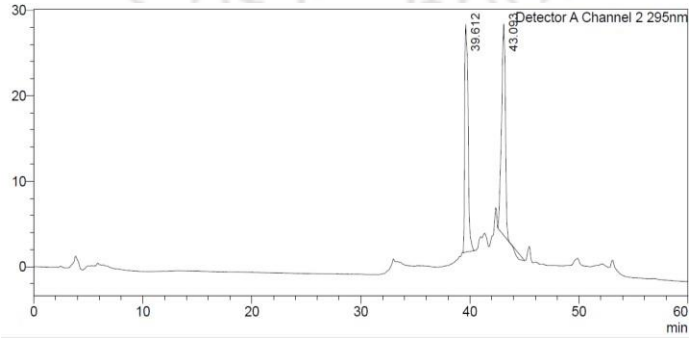

Fig. 2.33: HPLC analysis of DHF incubated in pH 9 SDS for 96 hours.

Similar observations were made when DHF was exposed to surfactants. In the presence of 20 mM SDS at both pH 9 and pH 13, distinct chromatographic profiles were obtained. Under pH 9 conditions **(Fig. 2.33)**, the chromatogram exhibited only two major peaks with retention times of 39.6 minutes and 43 minutes. Conversely, at pH 13 **(Fig. 2.34)**, the chromatogram displayed multiple peaks, including four major ones with retention times at 21.2 minutes, 21.7 minutes, 33 minutes, and 39.5 minutes, alongside numerous minor peaks. This outcome indicates that DHF degradation is accelerated in the presence of SDS and an alkaline environment.

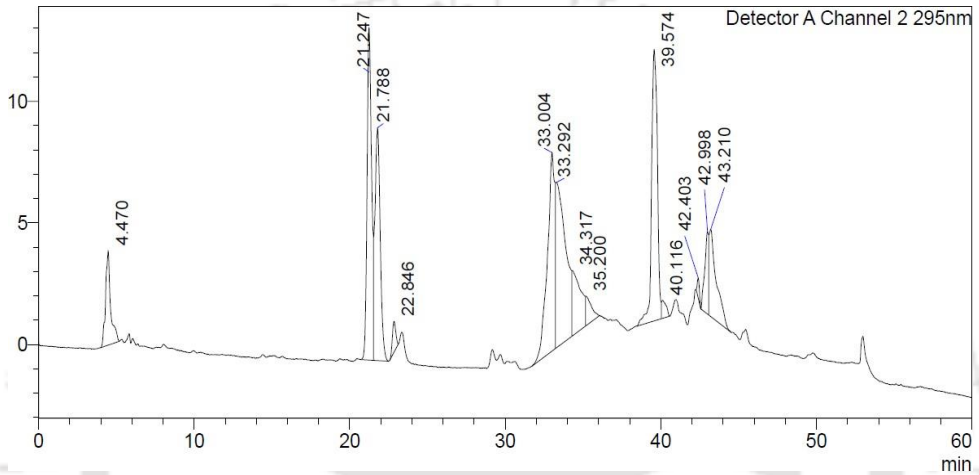

Fig. 2.34: HPLC analysis of DHF incubated in pH 13 SDS for 96 hours.

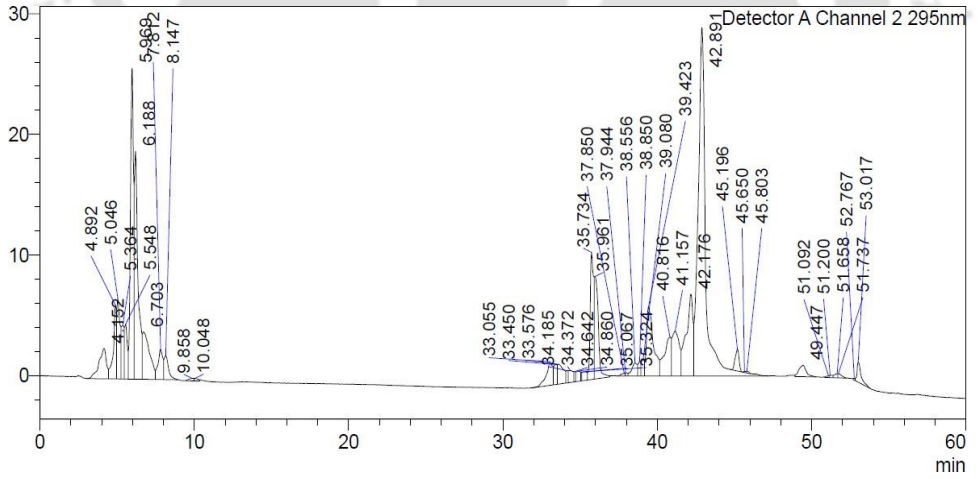

Fig. 2.35: HPLC analysis of DHF incubated in pH 9 CTAB for 96 hours.

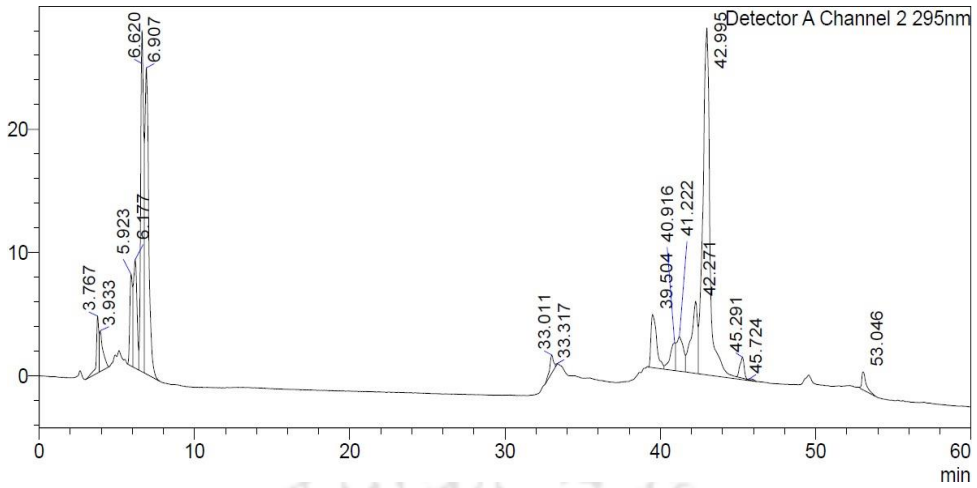

Fig. 2.36: HPLC analysis of DHF incubated in pH 13 CTAB for 96 hours

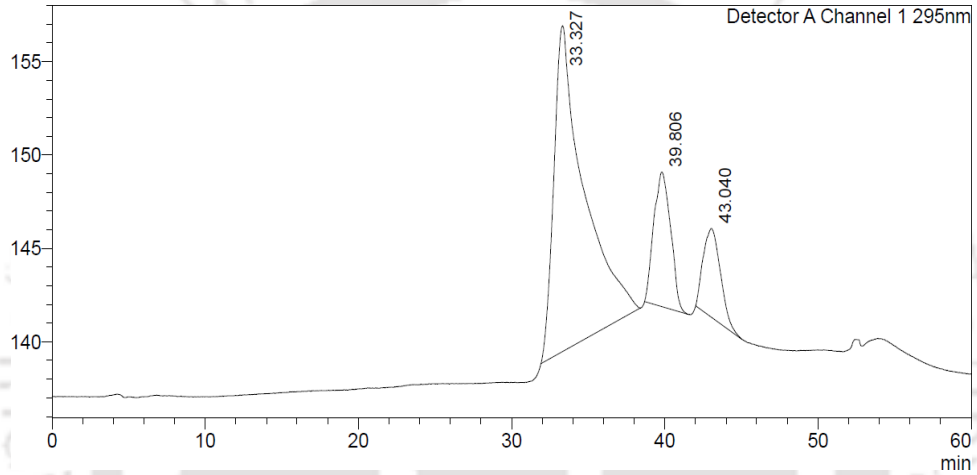

Fig. 2.37: HPLC analysis of DHF incubated in pH 9 Tween20 for 96 hours.

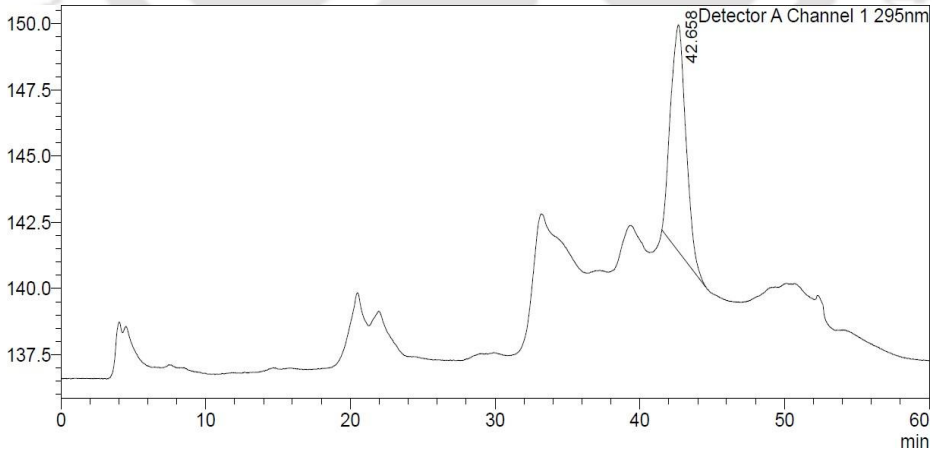

Fig. 2.38: HPLC analysis of DHF incubated in pH 13 Tween20 for 96 hours.

A similar trend was observed when DHF was exposed to 5 mM CTAB. In pH 9 **(Fig. 2.35)** and pH 13 **(Fig. 2.36)**, both conditions resulted in multiple peaks, albeit with slightly different retention times. Notably, the degradation rate in pH 9 with CTAB was found to be

higher than that observed with SDS and pH 9 alone, possibly attributed to the cationic charges of CTAB contributing to a more alkaline environment. Finally, when DHF was exposed to 0.5 mM Tween 20, pH 9 **(Fig. 2.37)** and pH 13 **(Fig. 2.38)**, the chromatograms displayed distinct peaks. Although both conditions yielded multiple peaks, the number of peaks was comparatively lower than those observed with SDS and CTAB. Therefore, it could be concluded that DHF undergoes degradation in CTAB at pH 9 at a faster rate compared to other surfactant and pH alone which is possibly due to its cationic charges imparting more alkaline nature to the surroundings.

2.3.9 : Fluorescence study of DHF in organic solvents and alkaline pH

The fluorescence measurement of DHF in different organic solvent was carried out, which revealed weak fluorescence intensity of DHF in organic solvents excited at 365 nm **(Fig. 2.39)**. DHF was also excited at 365 nm in alkaline pH (9, 10, 11) which gave weak fluorescence intensity **(Fig. 2.40 a).** Further it was also excited at 406 nm which revealed a slightly higher increase in fluorescence intensity at pH 11 followed by pH 10 and pH 9 in comparison to excitation at 365 nm **(Fig. 2.40 b)**.

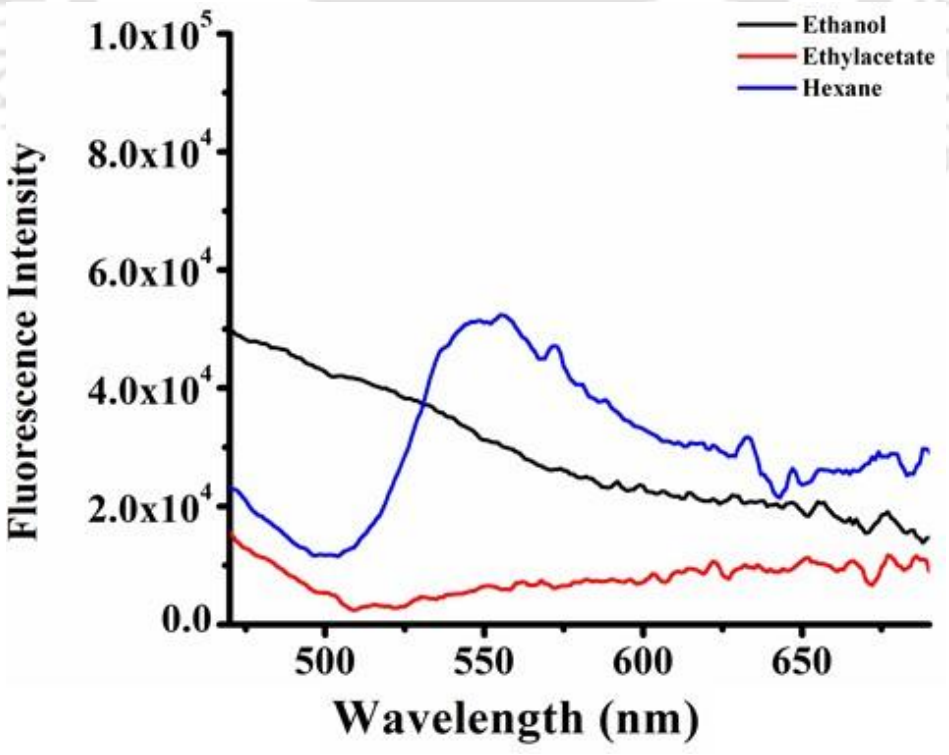

Fig. 2.39: Fluorescence spectra of DHF in organic solvents

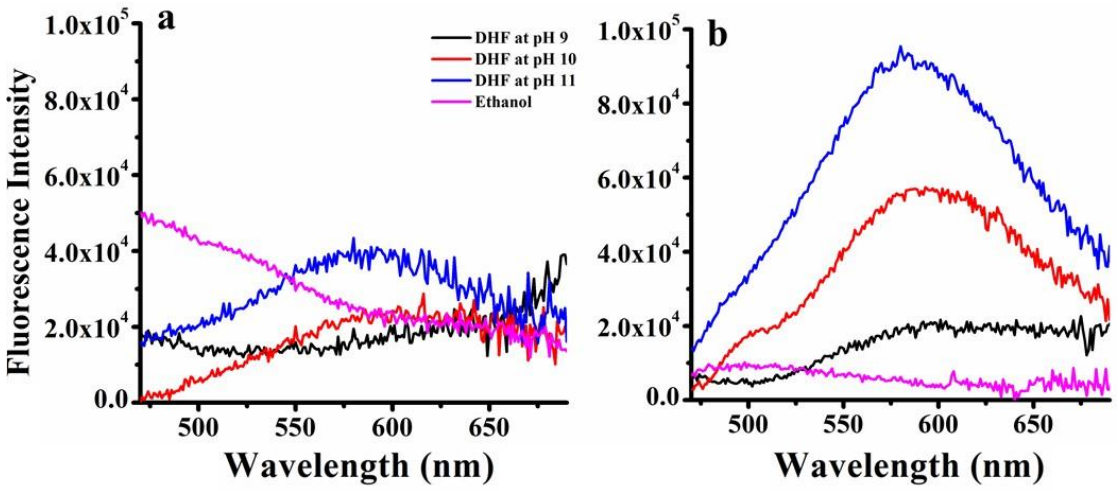

Fig. 2.40: (a) Fluorescence spectra of DHF in alkaline pH and ethanol excited at 365 nm (b) Fluorescence spectra of DHF in alkaline pH and ethanol excited at 406 nm

2.3.10 Time dependent fluorescence study of DHF in different surfactant micelles as a function of pH

The fluorescence spectra of DHF in three different surfactant micelles SDS, CTAB and Tween 20 was investigated, which revealed that DHF showed increased fluorescence intensity in all the three surfactant micelles at all different pH compared to organic solvents and alkaline pH alone when excited at 365 nm. The hydrophobic chains inherent to surfactant molecules possess the capacity to engage in interactions with both flavonoid compounds and water molecules, facilitated by the formation of hydrogen bonds (Kumar and Pandey, 2013). Notably, these flavonoid-surfactant interactions involve two distinct types of forces: long-range electrostatic forces and short-range hydrophobic forces. Long-range forces entail the binding of oppositely charged species, resulting in ion pair formation, while short-range forces encompass the binding and penetration processes (Shah et al., 2021). DHF showed higher fluorescence intensity in pH 2 and pH 3 in presence of CTAB micelles compared to SDS and Tween 20 **(Fig. 2.41 and 2.42)**.

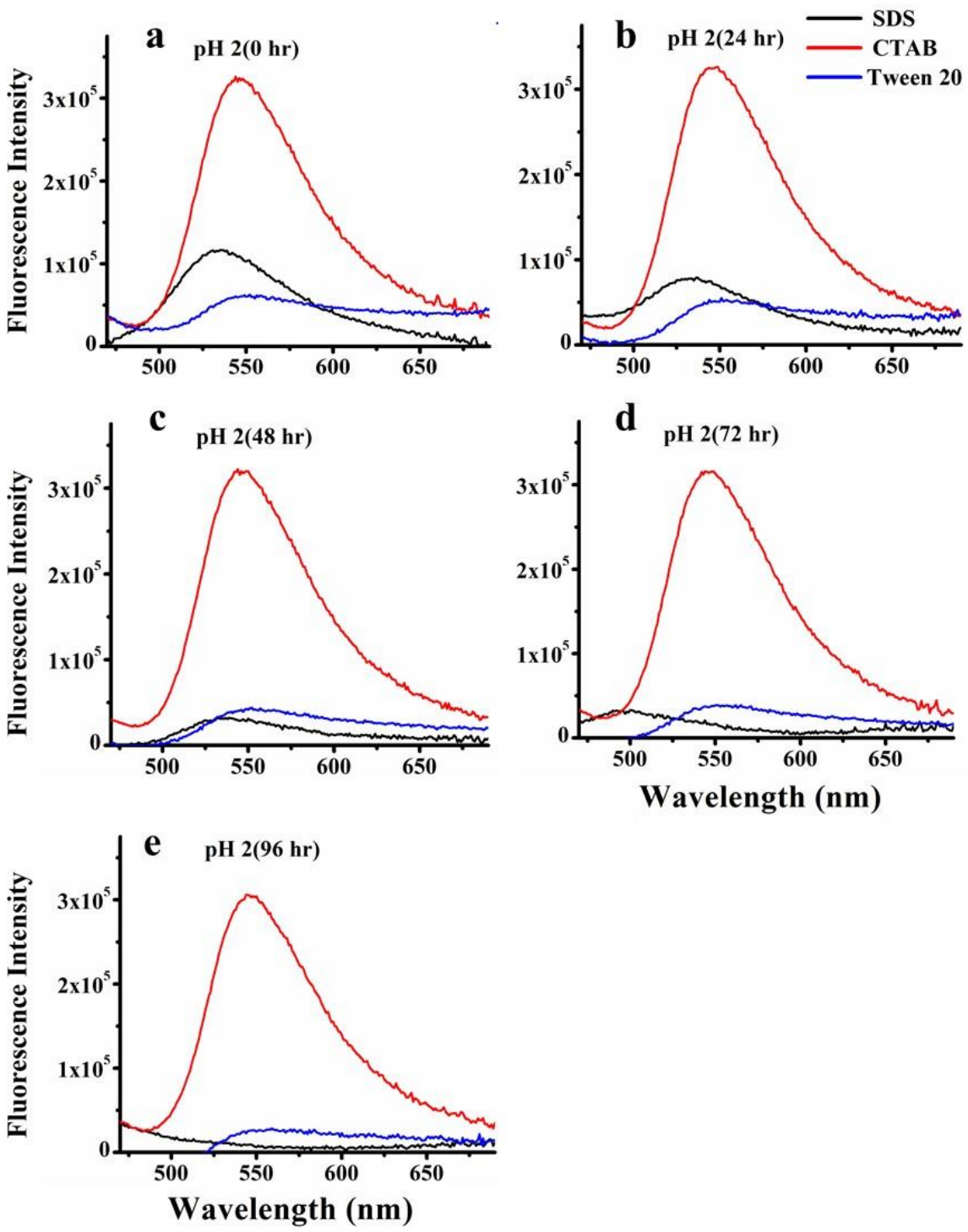

Fig. 2.41: Fluorescence spectra of DHF in SDS, CTAB and T20 micelles at pH2 excited at 365 nm in (a) 0 hr, (b) 24 hrs, (c) 48 hrs, (d) 72 hrs, (e) 96 hrs.

This observation implies a robust interaction between DHF and CTAB micelles at acidic pH levels, overshadowing the interactions observed with SDS and Tween 20 micelles under similar conditions. Further scrutiny of the fluorescence peaks within SDS micelles revealed a characteristic emission at 530 nm, while within CTAB micelles at pH 2 and pH 3, this peak

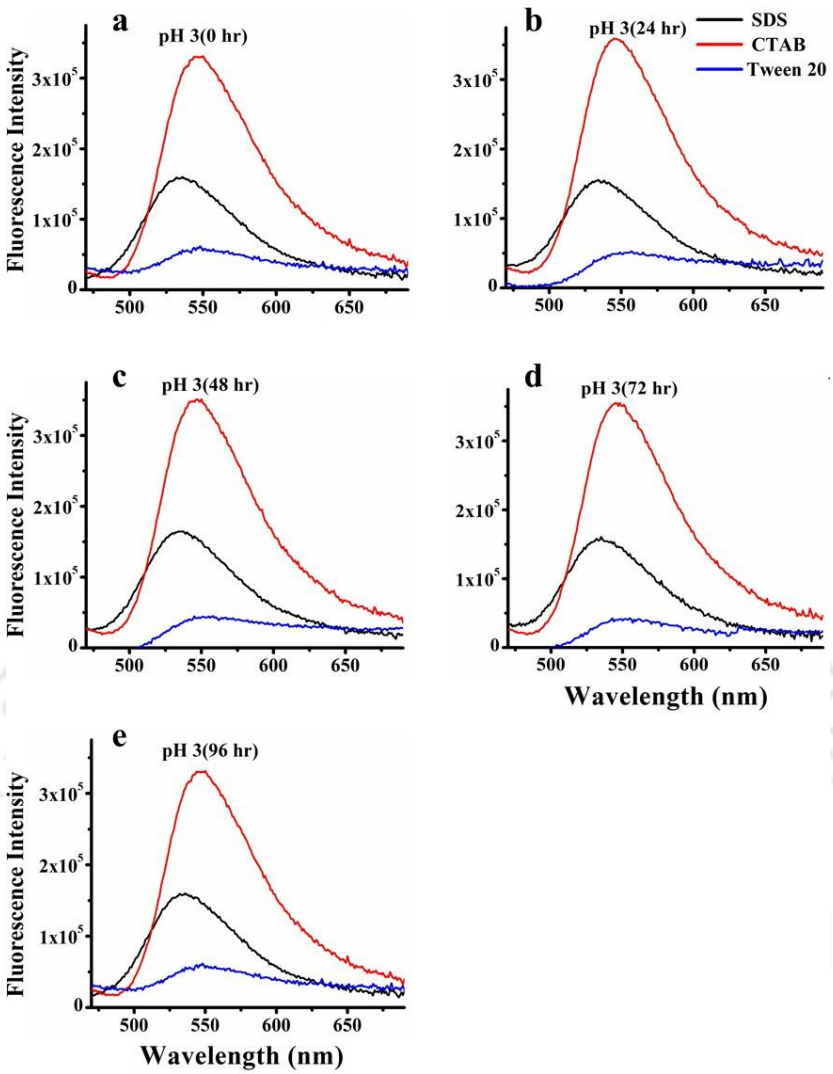

Fig. 2.42: Fluorescence spectra of DHF in SDS, CTAB and T20 micelles at pH3 excited at 365 nm in (a) 0 hr, (b) 24 hrs, (c) 48 hrs, (d) 72 hrs, (e) 96 hrs.

exhibited a discernible shift to 549 nm. This spectral alteration underscores the distinctive behaviour of DHF within CTAB micelles under acidic conditions. Such an alteration was not evident in the case of SDS micelles and Tween 20 micelles. This phenomenon is reminiscent of similar findings concerning quercetin, where the emission peak position in SDS micelles remained unaltered. Consequently, the principal driving force behind quercetin's solubilization within SDS micelles is ascribed primarily to hydrophobic forces. In stark contrast, within CTAB micelles, the fluorescence spectra of quercetin exhibited a notable shift to approximately 550 nm, coupled with an escalated fluorescence intensity, when compared to its behaviour within SDS micelles. This implies that quercetin forms a more robust interaction with CTAB micelles as opposed to SDS micelles. The interaction of quercetin with CTAB micelles has been attributed to a combination of electrostatic and hydrophobic interactions, signifying a

more intricate interplay of forces governing solubilization within this particular micellar environment (Liu and Guo, 2006).

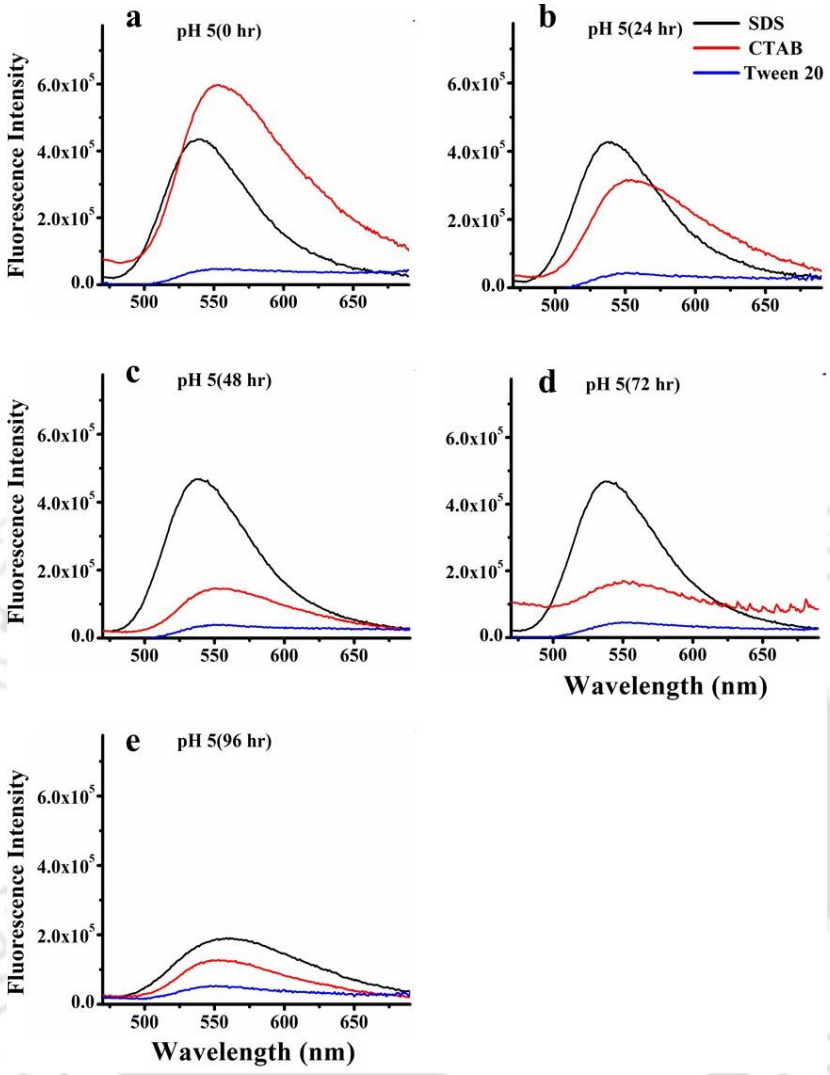

Fig. 2.43: Fluorescence spectra of DHF in SDS, CTAB and T20 micelles at pH5 excited at 365 nm in (a) 0 hr, (b) 24 hrs, (c) 48 hrs, (d) 72 hrs, (e) 96 hrs.

In pH 5 DHF showed more fluorescence intensity in SDS compared to CTAB micelles except at 0 hr, whereas in Tween 20 it was comparatively less **(Fig. 2.43)**. In pH 7 DHF showed more fluorescence in CTAB micelles compared to SDS. DHF in Tween 20 showed the lowest intensity. Fluorescence intensity decreased with time at pH 5. In pH 7, emission peaks of DHF in CTAB micelles red shifted to 578 nm compared to SDS at 545 nm **(Fig. 2.44)**. The red shift could be possibly due to the tautomer of DHF formed due to the phenomenon of excited-state intramolecular proton transfer (ESIPT) reaction as DHF is already reported to exhibit ESIPT (Portugal et al., 2006). Similar result has been observed for flavonoid fisetin, which exhibited

red shift in CTAB micelles due to ESIPT (Liu and Wu, 2015). The fluorescence intensity remained neatly constant at pH 7 in all the surfactant micelles **(Fig. 2.44).**

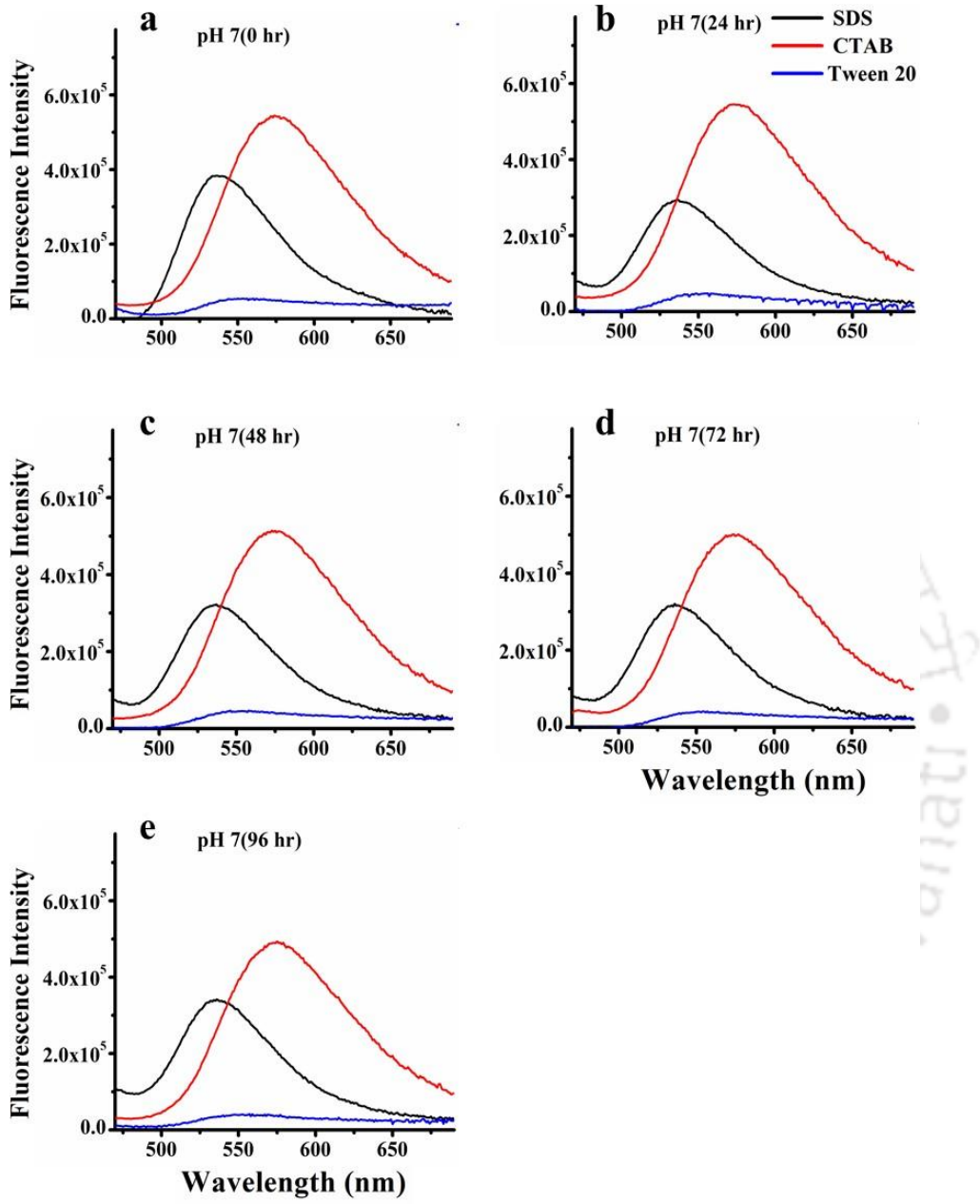

Fig. 2.44: Fluorescence spectra of DHF in SDS, CTAB and T20 micelles at pH7 excited at 365 nm in (a) 0 hr, (b) 24 hrs, (c) 48 hrs, (d) 72 hrs, (e) 96 hrs.

DHF showed higher fluoresence in CTAB micelles at pH 9 when excited at 365 nm compared to SDS and tween 20 micelles **(Fig. 2.45)**. DHF showed highest fluorescence intenstiy at pH 9 in CTAB micelles when excited at 425 nm **(Fig. 2.46 and 2.47).**

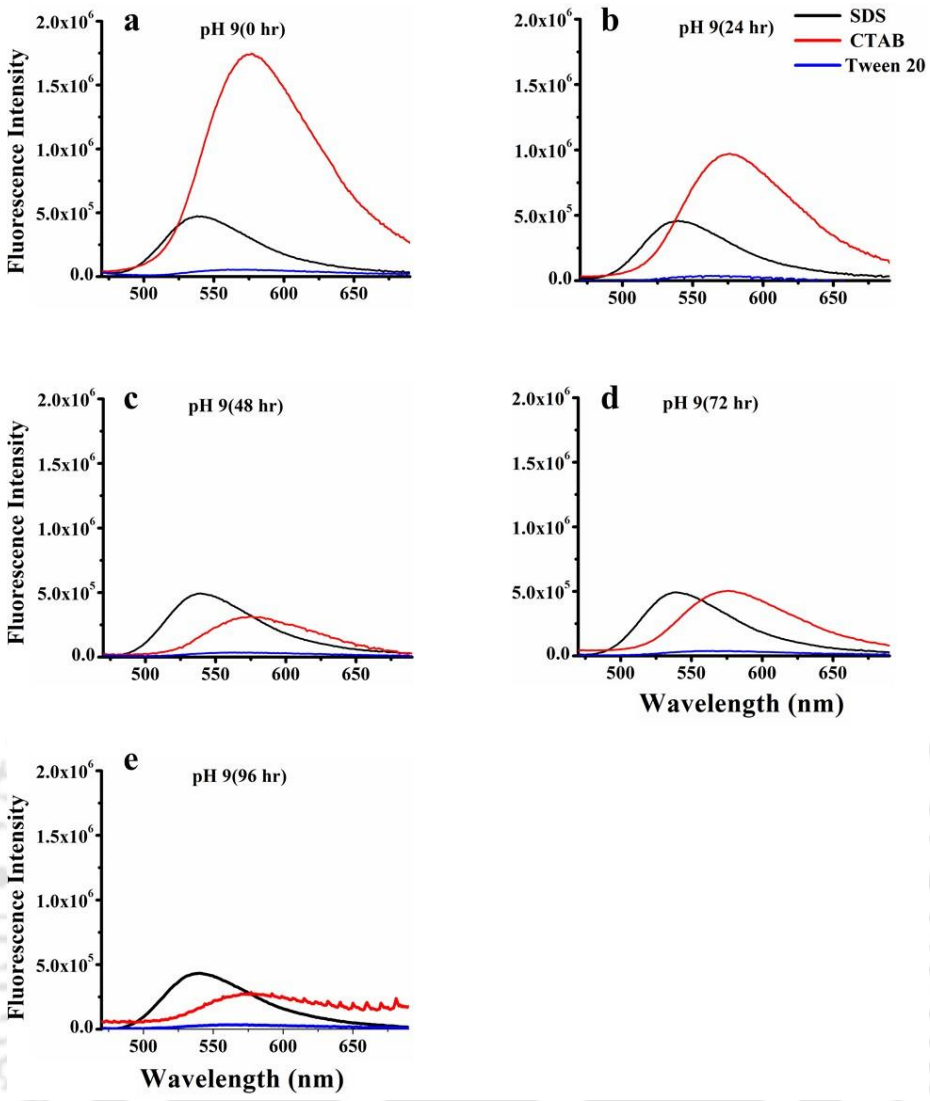

Fig. 2.45: Fluorescence spectra of DHF in SDS, CTAB and T20 micelles at pH9 excited at 365 nm in (a) 0 hr, (b) 24 hrs, (c) 48 hrs, (d) 72 hrs, (e) 96 hrs.

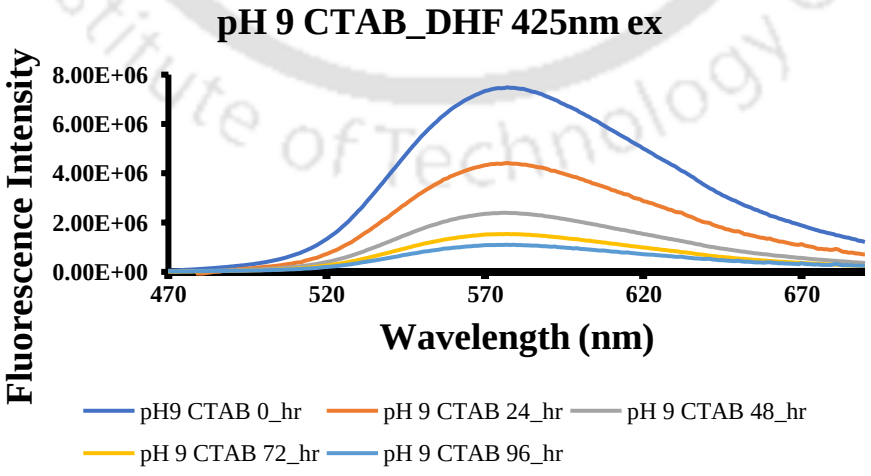

Fig. 2.46: Fluorescence spectra of DHF in different 0.5 mM CTAB in pH 9 excited at 425 nm

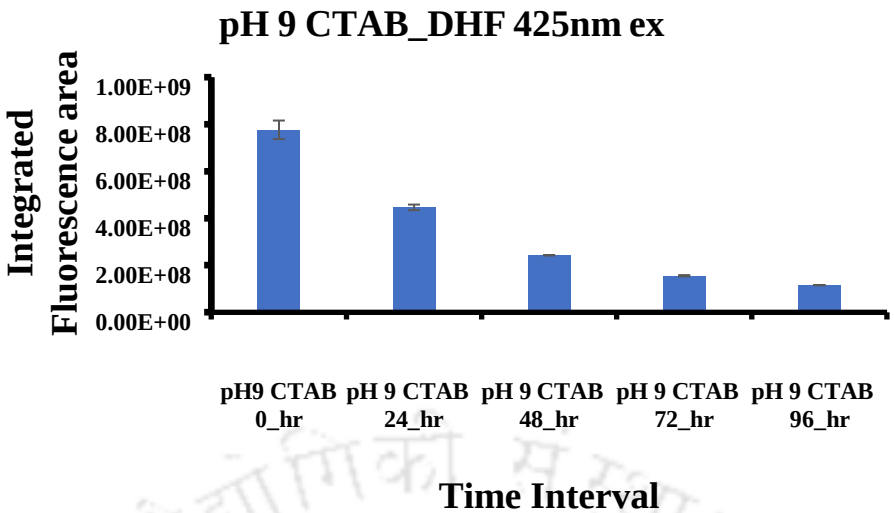

Fig. 2.47: Integrated Fluorescence intensity of DHF in 0.5 mM CTAB in pH 9 excited at 425 nm.

DHF also showed higher fluorescence intensity in CTAB micelles in pH 11 **(Fig. 2.48)** and pH 13 **(Fig. 2.49)** compared to SDS and Tween 20 on excitation at 365 nm. The fluorescence spectra in pH 9, 11 and 13 were not stable, as the intensity decreased with respect to time in all

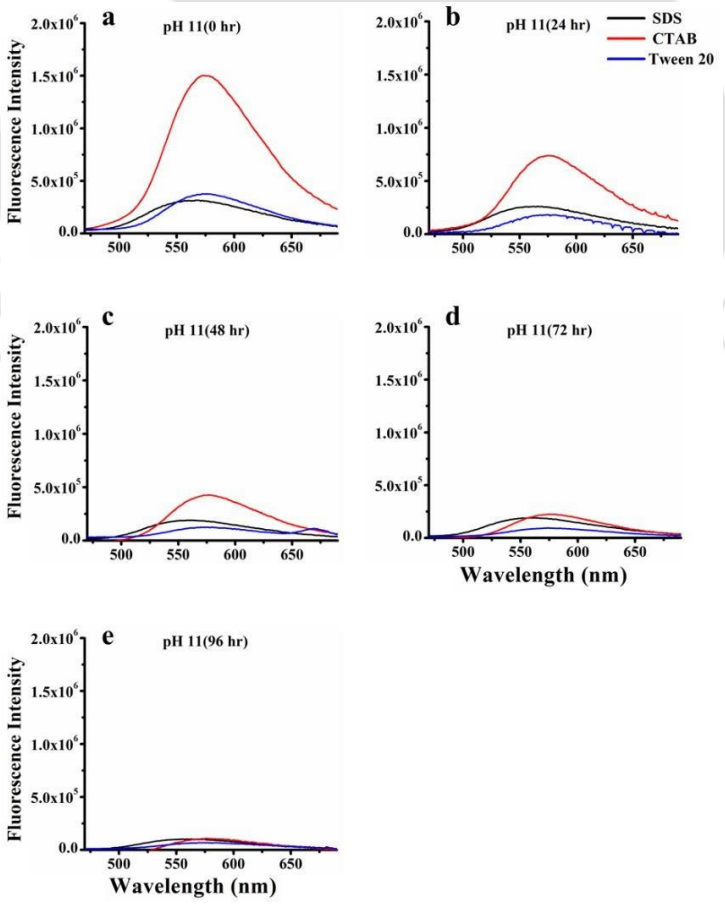

Fig. 2.48: Fluorescence spectra of DHF in SDS, CTAB and T20 micelles at pH11 excited at 365 nm in (a) 0 hr, (b) 24 hrs, (c) 48 hrs, (d) 72 hrs, (e) 96 hrs.

the three surfactant micelles. Also, in pH 13, the fluorescence intensity of DHF disappears after 24 hours of incubation in all the surfactant micelles which is due to degradation of compound DHF.Therefore, it could be concluded that DHF gives better fluorescence intensity in sufactant micelles. DHF gives highest fluorescence intensity in CTAB micelles in pH 2, 3 and 7 compared to SDS and Tween 20.

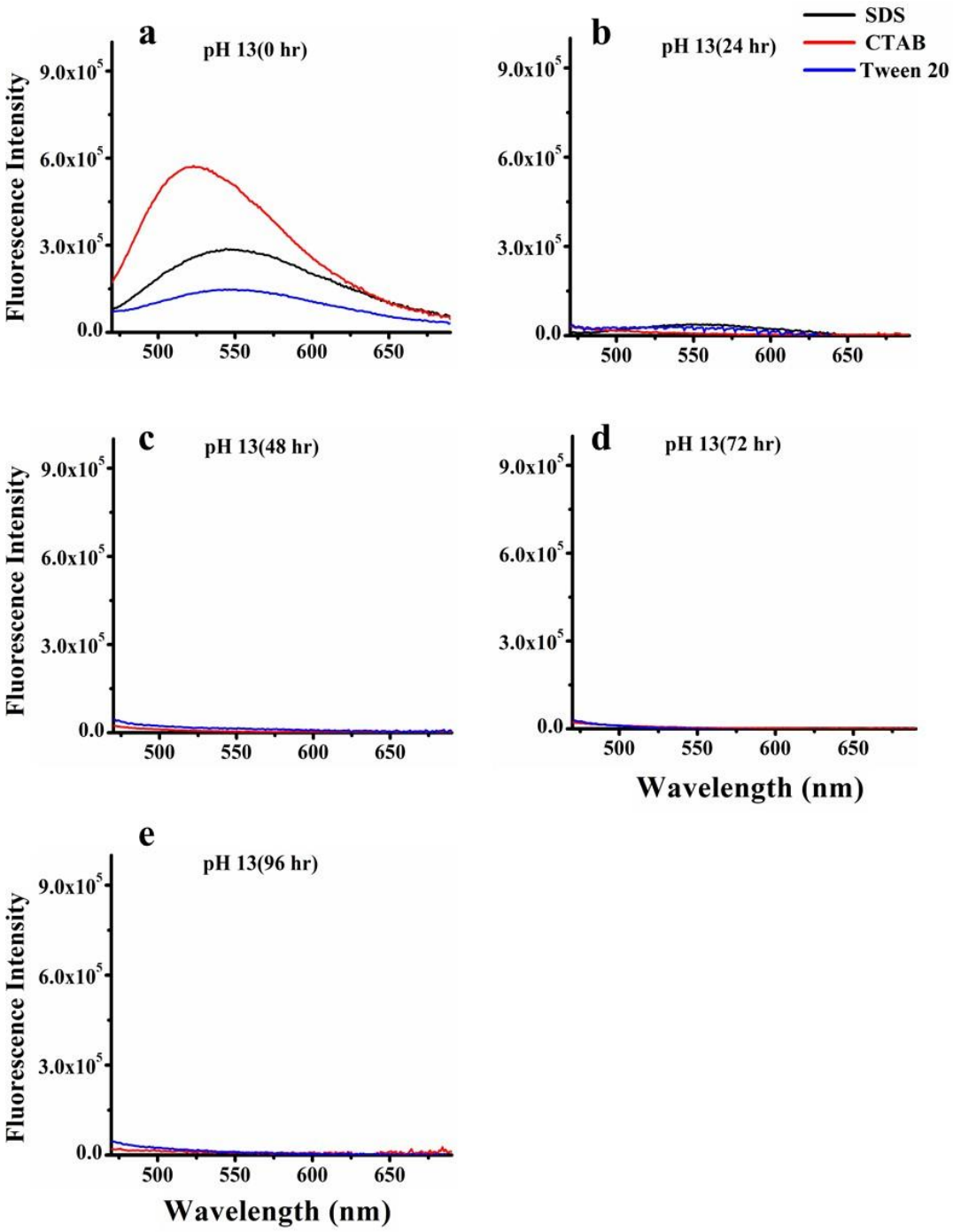

Fig. 2.49: Fluorescence spectra of DHF in SDS, CTAB and T20 micelles at pH13 excited at 365 nm in (a) 0 hr, (b) 24 hrs, (c) 48 hrs, (d) 72 hrs, (e) 96 hrs.

2.4 Conclusions

The absorption spectra of DHF revealed that DHF shows poor solubility in water, while it exhibited improved solubility in higher alkaline pH. However, in alkaline pH (pH 13), DHF displayed instability and undergoes degradation with time which was confirmed by HPLC and TLC. Interestingly, DHF exhibited increased solubility when introduced into three different surfactant micelles: SDS, CTAB, and Tween 20, across varying pH levels in an aqueous environment. Moreover, DHF showcased enhanced fluorescence intensity within all three surfactant micelles in comparison to both organic solvents and aqueous media. Notably, CTAB micelles influenced DHF degradation, as evidenced by shifts in absorption spectra and HPLC analysis. Particularly, CTAB micelles exhibited superior fluorescence intensity for DHF at pH 2, 3, and 7, surpassing the fluorescence levels observed in SDS and Tween 20 micelles. This series of observations highlights the intricate interplay between DHF, its solubility, and fluorescence properties in the presence of different surfactant micelles and pH conditions.

Chapter 3

Studying the interaction of DHF with HEWL aggregates at varying pH conditions

3.1 Introduction

Proteins achieve their full functional capacity by adopting precise three-dimensional conformations in their native state. Throughout the process of protein folding, ribosomal synthesis gives rise to proteins that traverse structural intermediates prior to attaining their native conformation. Occasionally, these intermediates may undergo misfolding, leading to configurations that deviate from the native state. The energy barrier between the native and non-native configurations is minimal, rendering native protein unfolding possible under circumstances of environmental stress. During protein folding, hydrophobic residues that are typically buried in the interior of the native conformation become exposed within misfolded intermediates. The exposure of these hydrophobic regions serves as a catalyst for protein aggregation (Tyedmers et al., 2010). The resultant aggregates exhibit variability in solubility, manifesting as either soluble or insoluble forms, with the insoluble aggregates adopting either an amorphous or fibrillar morphology contingent upon the protein milieu. Aggregation processes encompass both reversible and irreversible outcomes, the former predominantly arising from the self-assembly of protein entities, potentially instigated by alterations in the protein solution's pH or ionic strength (Mahler et al., 2009). The misfolding of proteins, leading to the formation of intracellular or extracellular aggregates, followed by their deposition in afflicted tissues, can result in severe degenerative conditions encompassing a group of disorders termed amyloidosis. The successful identification of therapeutic drugs aimed at impeding the fibrillogenesis of amyloidogenic proteins holds significant importance for the treatment of diverse diseases. Consequently, the identification and development of efficacious small molecule inhibitors represent a promising domain of scientific investigation. Notably, naturally occurring polyphenols have emerged as particularly potent agents displaying effective anti-amyloidogenic activity (He et al., 2014).

Hen egg white lysozyme (HEWL) serves as paradigmatic model protein to investigate protein aggregation and to study its inhibition by small molecules. HEWL has been reported to show aggregation under different conditions, including acidic and alkaline pH environments, absence of disulfide bonds, presence of ethanol, and exposure to guanidine hydrochloride (Ravi et al., 2014). Several natural polyphenols, such as (−)-epicatechin gallate (Ghosh et al., 2013), myricetin (He et al., 2014), curcumin, and kaempferol (Borana et al., 2014), have been reported to exhibit inhibitory effects on the aggregation of HEWL.

Our research group recently conducted a comprehensive investigation into the intrinsic UV/Visible absorbance properties of a highly charged protein known as α3C, which notably lacks any aromatic amino acids in its structure (Prasad et al., 2017). Subsequently, meticulous time-dependent density functional theory (TDDFT) calculations on the three-dimensional conformation of α3C were carried out. These calculations shed light on the presence of specific Lysine-Glutamate interactions within the protein. Intriguingly, the findings indicated that the intrinsic absorption phenomenon in α3C is primarily driven by charge transfer processes occurring within the charged residues. This phenomenon has been coined as "Protein Charge Transfer Spectra (ProCharTS)."

In the present chapter, we have investigated the effect of DHF on HEWL aggregates at pH 2, pH 5 and pH 12.2. Here, ProCharTS absorption was employed to analyze the impact of DHF on aggregates of HEWL. Previous research has already utilized ProCharTS absorption to probe HEWL aggregation, revealing a consistent elevation in ProCharTS absorption within HEWL aggregates as compared to the monomeric HEWL (Ansari et al., 2018). Additionally, the study revealed a reduction in ProCharTS absorption upon the inhibition of HEWL aggregates through treatment with iodoacetamide, a compound known for its capacity to hinder reactive thiol groups. Additionally, the observation of intrinsic fluorescence or intrinsic deep-blue/blue luminescence emanating from monomeric proteins (Guptasarma, 2008), oligomeric proteins (Bhattacharya et al., 2017), protein crystals (Shukla et al., 2004), and amyloid aggregates (Chan et al., 2013) has provided encouraging insights into this domain. ProCharTS has been utilized as an innovative label-free technique for the detection of both initial oligomerization events and subsequent fibril assembly during the protein aggregation process (Ansari et al., 2018). It leverages information concerning the proximal interactions between particular charged groups of Lysine and Glutamate residues in protein aggregates.

Furthermore, it is worth noting that light scattering phenomena originating fromfibrillar structures will not interfere with our ProCharTS investigations. This is because we specifically work with soluble oligomeric aggregates and place our primary focus on the initialstages of aggregation kinetics. Generally, light scattering arises from higher-order, insoluble fibrillar aggregates and mature fibrils. Consequently, the potential for interference with ProCharTS is exceedingly minimal. Even if some interference were to occur due to preformedfibrils in the oligomeric state, its contribution would be negligible and would unlikely exert a substantial influence on our ProCharTS analysis.

3.2Materials and methods

3.2.1 HEWL aggregation at pH 2 and effect of DHF

HEWL (Sigma Aldrich, India) stock was prepared in deionised water and the concentration was determined using the extinction coefficient at $\lambda_{280\ nm}$ (37,970 $M^{-1}cm^{-1}$). The aggregation of HEWL with concentration 1.36 mM was carried out in 10mM glycine buffer at pH 2. DHF with concentration 20 μM ,50 μM and 80 μM was incubated in presence of 1.36 mM HEWL and without HEWL in pH 2 for 10 days. The samples were incubated incubated at 65 °C with intermittent mixing for 10 days. At the end of each day 100 μL aliquots of sample were collected and stored at 4 °C. The incubated samples were diluted to 100 μM in the same buffer and centrifuged at 10,500 rpm for 4 minutes and the supernatant was collected for further analysis (Ansari et al., 2018).

3.2.2 HEWL aggregation at pH 5 and effect of DHF

The aggregation of HEWL with concentration 100 μM was carried out in 0.1 M citrate buffer at pH 5. DHF with concentration 20 μM ,50 μM and 80 μM was incubated in presence of 100 μM HEWL and without HEWL in pH 5 for 5 days. The samples were incubated at 65 °C with intermittent mixing for 5 days. At the end of each day aliquots of sample were collected and stored at 4 °C. The samples were centrifuged at 10,500 rpm for 4 minutes and the supernatant was used for further analysis (Ansari et al., 2018).

3.2.3 HEWL aggregation at pH 12.2 and effect of DHF

The aggregation of HEWL with concentration 120 μM was carried out in 50 mM phosphate buffer at pH 12.2. DHF with concentration 20 μM ,50 μM and 80 μM was incubated in presence of 120 μM HEWL and without HEWL in pH 12.2 for 5 days at room temperature. At the end of each day aliquots of sample were stored at 4 °C for further analysis (Ansari et al., 2018).

3.2.4 UV-visible absorption spectra

The absorption spectra of the aggregated protein samples incubated with different concentrations of DHF were recorded using a double beam spectrophotometer (Perkin Elmer Lambda 25 spectrophotometer) at room temperature (25 °C). The absorption spectra were recorded from 325 nm to 800 nm (1 nm bandwidth; 480 nm $minute^{-1}$ scan speed) and all the samples were repeated in triplicates and average of at least two measurements are shown.

3.2.5 ThT Fluorescence assay

The aggregated protein sample with 10 μM concentration was mixed with 20 μM of ThT in pH 8.5 Gly-Gly buffer. The concentration of ThT was measured by using the extinction coefficient 26620 $M^{-1}cm^{-1}$ at 416 nm. The samples were vortexed properly and the spectrum was measured immediately. The excitation wavelength was kept at 450 nm with a slit width of 2 nm and the emission spectrum was collected from 470 nm to 550 nm with a slit width of 10 nm. The area under the emission spectrum was calculated from 470 nm to 550 nm after substraction of the blank spectrum without ThT. All fluorescence measurements were done in triplicate in a 2 mL quartz cuvette with a 10 mm path length using a Fluoromax-4 Spectrofluorometer (Jobin-Yvon Horiba Inc., USA).

3.2.6 ANS binding assay

The aggregated protein sample with 5 μM concentration was diluted in the same buffer used for protein aggregation and was mixed with 10 μM ANS. The ANS stock was prepared in deionised water and the concentration was determined by using the extinction coefficient of 4950 $M^{-1}cm^{-1}$ at 350 nm. Steady-state fluorescence emission spectrum of ANS was recorded from 400 to 600 nm after excitation at 380 nm (excitation slit width 1 nm and emission slit width 10 nm). The area under the emission spectrum was calculated from 400 nm to 600 nm after substraction of the blank spectrum without ANS. All fluorescence measurements were done in triplicate in a 2 mL quartz cuvette with a 10 mm path length using a Fluoromax-4 Spectrofluorometer (Jobin-Yvon Horiba Inc., USA).

3.2.7 Atomic Force Microscopy

The aggregated HEWL protein samples in presence of DHF after incubation for 10 days in pH 2 was diluted to 2 μM concentration in deionised water. In a cleaved sheet of mica, 12 μL of the diluted sample was added and allowed to dry at room temperature. The samples were imaged in air under AAC or MAC MODE (non-contact) PICO PLUS^{TM} AFM purchased from Molecular Imaging, USA. Cantilever type PPP-MFMR-20 (resonance frequency, 60—70 kHz; Nano sensors) was used for MAC mode, while type PPP-NCL-50 (resonance frequency, 150 kHz; Molecular Imaging) was used for AAC mode. AFM images with at least 5 scans for each sample condition was acquired.

3.3 Results and Discussions

3.3.1 ProCharTS absorbance to detect aggregation inhibition of HEWL by DHF in pH 2, pH 5 and pH 12.2

The investigation of HEWL's aggregation through ProCharTS absorbance reveals a gradual increase in absorbance as the aggregate concentration rises. This phenomenon indicates a significant augmentation in the formation of new contacts among the charged residues within the aggregates compared to the monomeric state. It is of significance to highlight that prior research endeavors have utilized the evaluation of absorbance specifically at wavelengths of 220 nm and 257 nm as a method to closely observe and track the early phases of aggregation in Aβ (Paul et al., 2016). The alterations observed in the absorbance at 220 nm predominantly originate from variations in the amide groups within the peptide backbone. Meanwhile, the shifts in absorbance at 257 nm can be attributed to perturbations in the π-π^* transitions of phenylalanine residues, induced by environmental changes occurring during the aggregation process. Furthermore, it is pertinent to note that a prior study had documented the conformational transition of poly-L-Lysine, wherein it shifted from a random coil configuration to a β-sheet structure (Rosenheck and Doty, 1961). Nevertheless, our primary investigative emphasis is directed toward the extended wavelength region of the UV-Visible spectrum, specifically spanning from 300 nm to 800 nm. Within this spectral range, the dominant influence on absorption patterns stems from the ProCharTS. Moreover, it is noteworthy that the analysis of ProCharTS absorbance has been effectively harnessed to scrutinize the conformational changes occurring in a variety of Intrinsically Disordered Proteins (IDPs) and our research team has previously conducted an absorbance study utilizing ProCharTS on HEWL at a pH 2, 5 and 12.2 (Ansari et al., 2018).This technique effectively captures the redistribution of proximal charges within the side chains and backbones of these proteins induced by structural modifications. Computational investigations on the structural transformations of Aβ peptides and analogous polypeptides also suggest that charge transfer is a viable method for scrutinizing conformational variations in amyloid aggregation (Grisanti et al., 2017, 2020; Jong et al., 2019; Serrano-Andrés and Fülscher, 2001).In the context of di and tripeptides of phenylalanine (Phe) undergoing aggregation, an elevation in optical absorbance in the 400-650 nm range has been observed, as reported by (Apter et al., 2021). Thisobservation is attributed to the interaction between Phe residues forming the core of the aggregated assembly (Singh et al., 2020). Consequently, it is anticipated that the charged residues neighboring Phe will also come into contact during the aggregation process, resulting

in the redistribution and heightened interaction of charged moieties in aggregates compared to monomers. Consequently, ProCharTS is poised to effectively monitor the kinetics of aggregation in such systems.

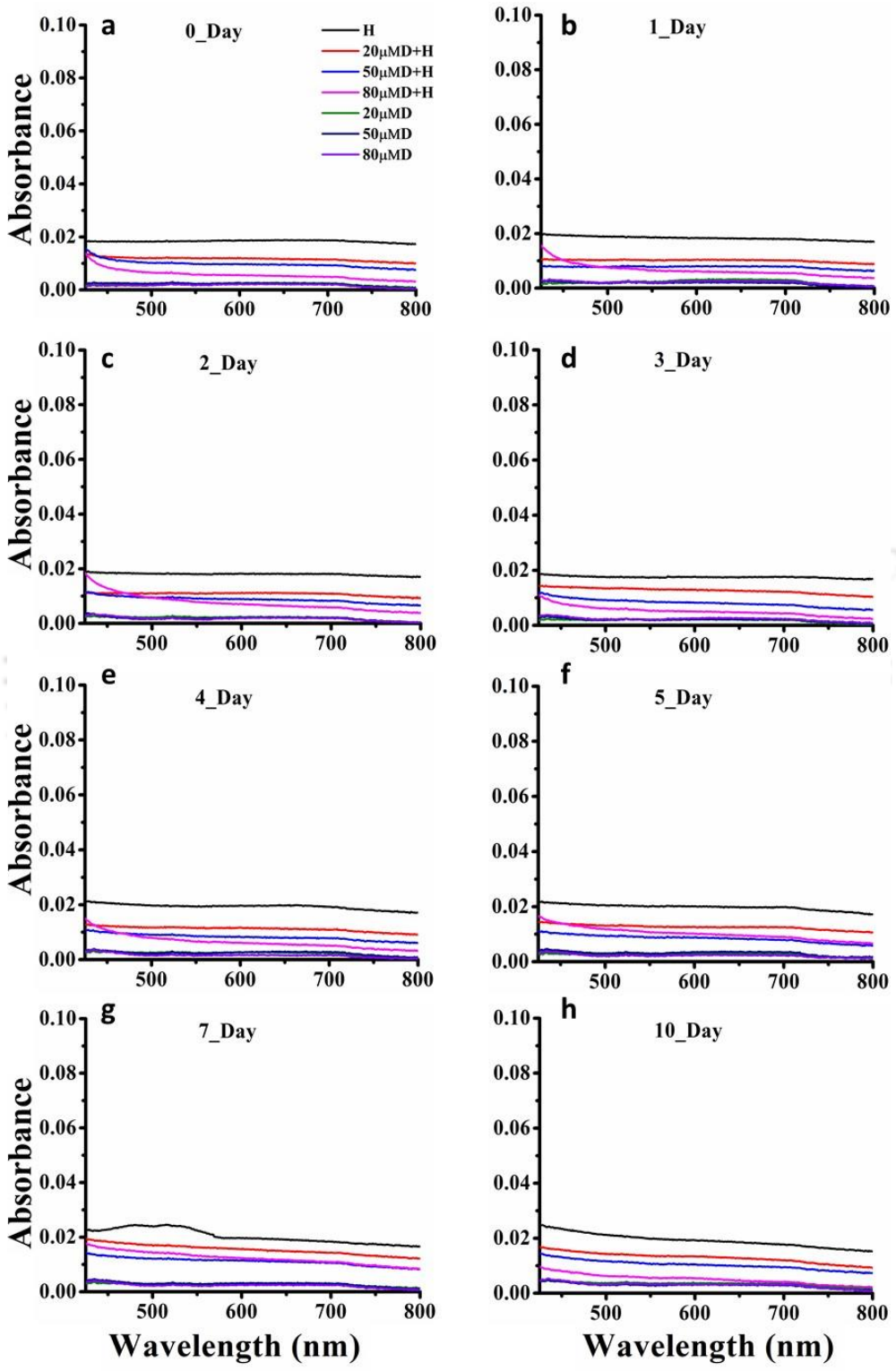

Fig. 3.1: UV visible absorption spectra of HEWL aggregates incubated with different concentration (20 μM, 50 μM and 80 μM) DHF in pH 2 for 10 days. H-HEWL, D-DHF

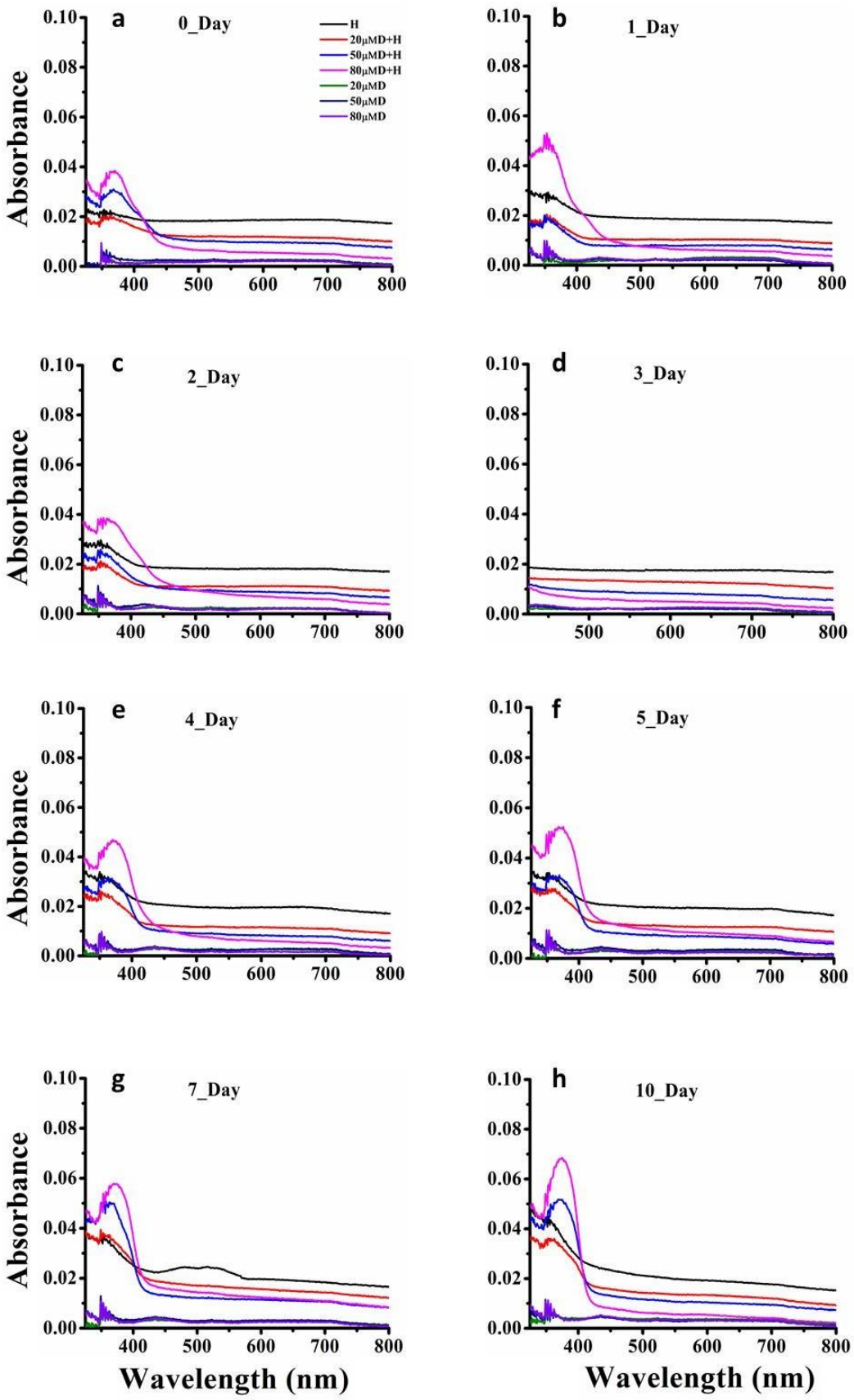

Fig. 3.2: UV visible absorption spectra of HEWL aggregates incubated with different concentration (20 μM, 50 μM and 80 μM) DHF in pH 2 for 10 days plotted from 325-800 nm. H-HEWL, D-DHF

The absorption spectra analysis of Hen Egg White Lysozyme (HEWL) aggregates incubated with varying concentrations of DHF at pH 2 **(Fig. 3.1 a-h)** indicated a potential masking effect of DHF on the anticipated ProCharTS absorption inhibition **(Fig. 3.2 a-h)**. This masking effect is likely due to the inherent absorption characteristics of DHF, particularly in the wavelength range of 365-370 nm. Consequently, the spectral analysis was plotted from 425 nm to 800 nm to mitigate this interference. It is worth noting that prior research has documented a similar phenomenon in the interaction between procyanidin B3 and lysozyme. Specifically, this interaction leads to a noteworthy reduction in the intensity peak of lysozyme at 200 nm, accompanied by a conspicuous shift in its maximum absorption wavelength from 200 nm to 205 nm. This spectral transformation can be attributed to the substantial absorbance exhibited by procyanidin B3 around the 200 nm region. These observations provide strong indications of structural alterations within the peptide backbone of lysozyme, potentially involving unfolding processes and changes in the local microenvironment's hydrophobic properties. These changes are believed to arise from the robust binding affinity between procyanidin B3 and lysozyme (Poklar Ulrih, 2017).

Notably, across all investigated time points (ranging from 0 to 10 days), the absorbance of HEWL is consistently lower in the presence of DHF at all concentrations (20 μM, 50 μM, and 80 μM) compared to HEWL in isolation. This consistent reduction in absorbance strongly suggests that DHF exerts an inhibitory influence on the fibrillation process of HEWL. Remarkably, at the 10-day time point **(Fig 3.1 h)**, it becomes evident that the lowest absorbance of HEWL aggregates is achieved when incubated with 80 μM DHF, followed by 50 μM DHF and 20 μM DHF. This concentration-dependent trend underscores the dose-dependent impact of DHF on HEWL fibrillation. Previous research findings have indicated a similar dose-dependent phenomenon in the context of lysozyme fibrillation inhibition induced by gallic acid (Konar et al., 2017). Additionally, it has been documented that the presence of HEWL aggregate inhibitor iodoacetamide leads to a significant reduction in ProCharTS absorption. This reduction is attributed to a pronounced decrease in the interactions between charged residues within HEWL, thereby contributing to the observed suppression of ProCharTS (Ansari et al., 2018).

The absorption spectra of HEWL aggregates, as elucidated by ProCharTS, were meticulously examined within the wavelength range of 425 nm to 800 nm, considering the intrinsic absorbance of DHF, which manifests in the vicinity of 365-370 nm. Notably, our investigation into the ProCharTS absorption spectra of HEWL incubated at pH 5 with varying concentrations

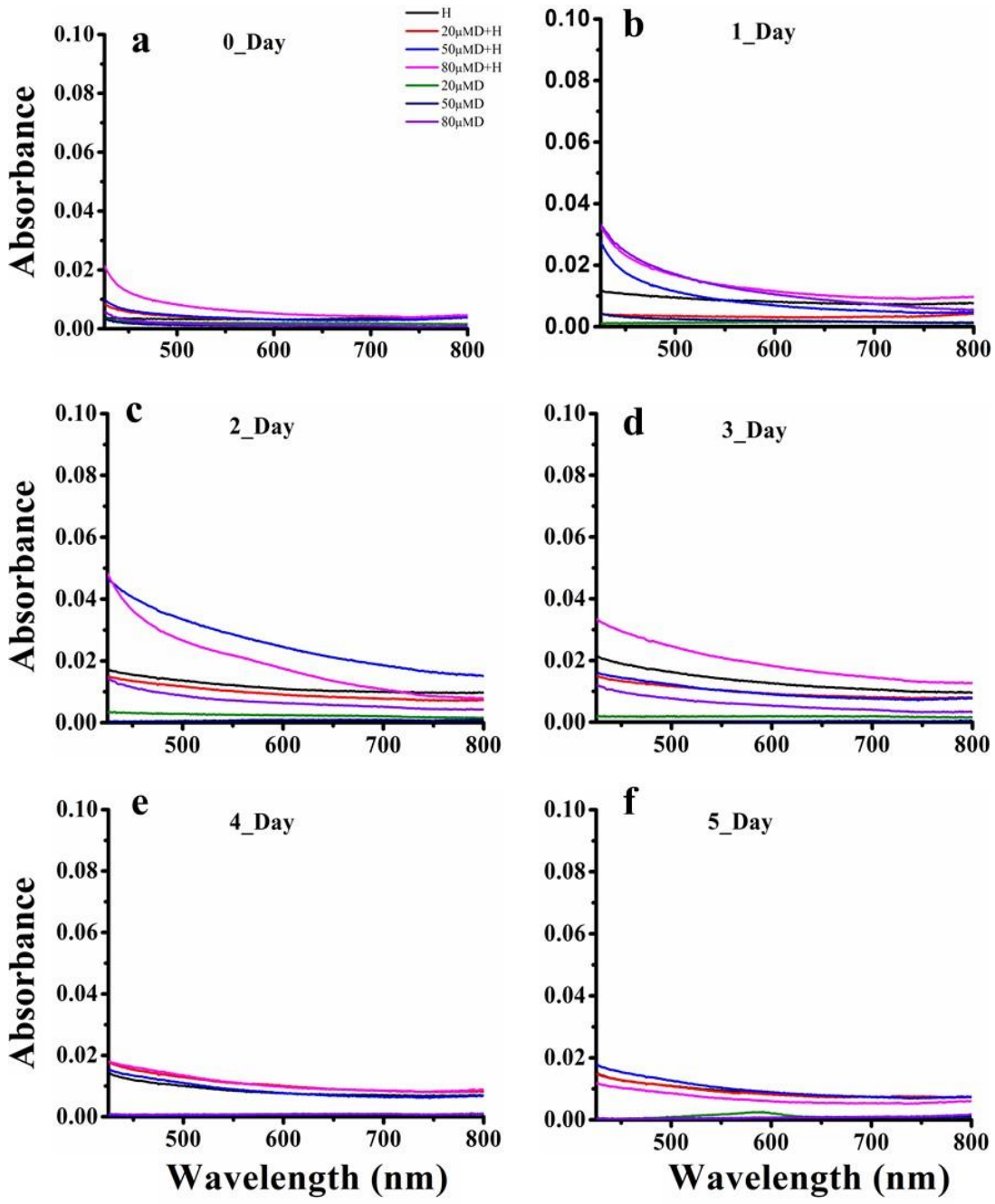

Fig. 3.3: UV visible absorption spectra of HEWL aggregates incubated with different concentration (20 μM, 50 μM and 80 μM) DHF in pH 5 for 5 days. H-HEWL, D-DHF

of DHF (20 μM, 50 μM, and 80 μM) revealed intriguing insights. While our findings suggested a discernible, albeit mild, inhibitory effect with all three concentrations of DHF when compared to HEWL aggregates in pH 5 alone **(Fig. 3.3)**, an intriguing observation emerged. The observed absorbance patterns across different time points **(Fig. 3.3 a-f)**, presented a rather enigmatic picture. Contrary to expectations, no consistent trend in absorbance was discernible, casting uncertainty upon the prospect of DHF effectively mitigating HEWL aggregation under these

conditions. This intriguing observation prompts us to consider the nuances of HEWL aggregation under distinct pH environments. It is well-documented that HEWL aggregation dynamics differ significantly between pH 2 and pH 5, with the latter representing a milder milieu. At pH 2, the aggregation pathway yields more structured fibrils, while at pH 5, smaller aggregates predominate (Ansari et al., 2018). In light of these disparities, our results imply that DHF may not exert its inhibitory influence as effectively on the formation of smaller HEWL aggregates at pH 5, in contrast to its more pronounced inhibition of structured fibril formation observed at pH 2.

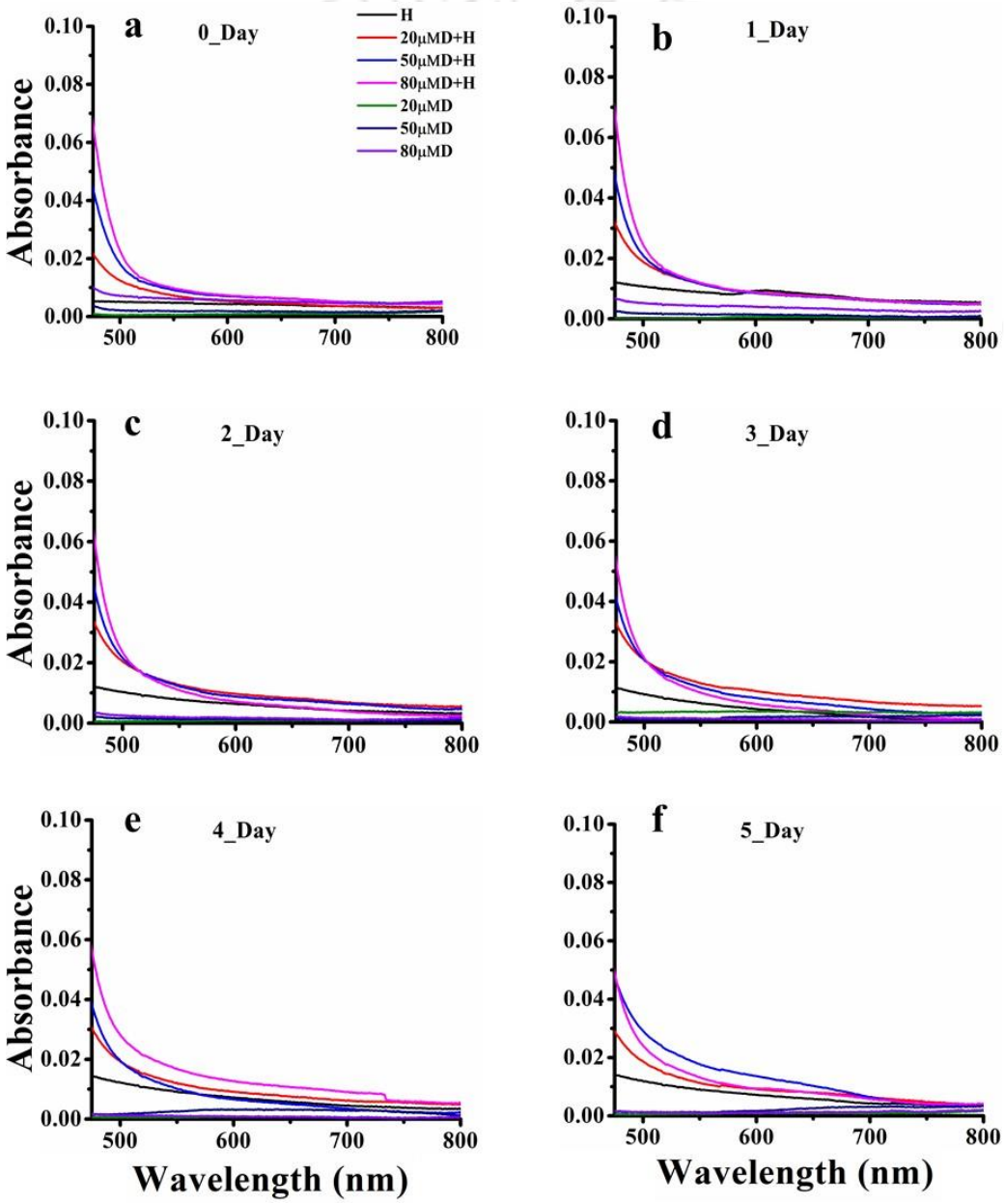

Fig. 3.4: UV visible absorption spectra of HEWL aggregates incubated with different concentration (20 μM, 50 μM and 80 μM) DHF in pH 12.2 for 5 days. H-HEWL, D-DHF

The ProCharTS absorption spectra analysis of HEWL aggregates at an alkaline pH of 12.2 has been thoughtfully executed over a spectral range spanning from 475 nm to 800 nm. This strategic selection of the spectral window stems from the well-documented red shift of DHF's intrinsic absorbance in response to an alkaline pH environment, shifting from its typical 365 nm to 406 nm as discussed in Chapter 3. Notably, within the pH 12.2 milieu **(Fig. 3.4)**, DHF exhibits intrinsic absorbance exclusively within the boundaries of 406 nm, with no consequential intrinsic absorbance observable beyond the 475 nm threshold. Intriguingly, our comprehensive investigation into the ProCharTS absorption spectra of HEWL aggregates within this highly alkaline context yielded compelling findings. As the incubation period extended from 0 to 5 days **(Fig. 3.4 a-f)**, the progression of fibril formation within HEWL aggregates remained notably uninterrupted. The process of fibril formation by HEWL at pH 12.2 has been previously documented by our group (Ravi et al., 2014). The progressive augmentation observed in the absorption spectra can be attributed to the heightened intermolecular interactions occurring among the charged residue side chains within the aggregates, as contrasted with the monomeric state (HEWL at day 0). A discerning observation emerges: in comparison to HEWL aggregates in isolation, DHF did not show decrease in absorbance spectra **(Fig. 3.4 f)**. These intriguing outcomes hint at a crucial insight. It is conceivable that DHF, within the confines of the pH 12.2 milieu, may not exhibit a robust capacity to effectively inhibit the formation of HEWL aggregates. This observed phenomenon might be attributed to structural alterations undergone by DHF in alkaline pH environments, potentially disrupting its structure-activity relationship and rendering it less efficacious in impeding HEWL aggregation dynamics under these specific conditions.

3.3.2. Thioflavin T (ThT) fluorescence studies

Thioflavin T (ThT) serves as a valuable probe in the realm of scientific investigation, particularly in the context of identifying and scrutinizing the formation of amyloid fibers. This unique compound has found application in the diagnosis of several pathological conditions, including Alzheimer's disease, Parkinson's disease, and type II diabetes. Notably, the conformational transition towards β-sheet-rich fiber structures represents a pivotal event in the aggregation of distinct proteins associated with specific diseases. It is worth highlighting that ThT fluorescence exhibits a notable spike in quantum yield upon binding to these β-sheet-rich fibers, thus affording researchers a powerful means to discern and monitor these pathological processes (Wolfe et al., 2010). ThT fluorescence emission, detected at a wavelength of 485 nm

upon its interaction with amyloid β-strands, served as a robust means to track the dynamic progression of fibril formation kinetics (Levine III, 1993).

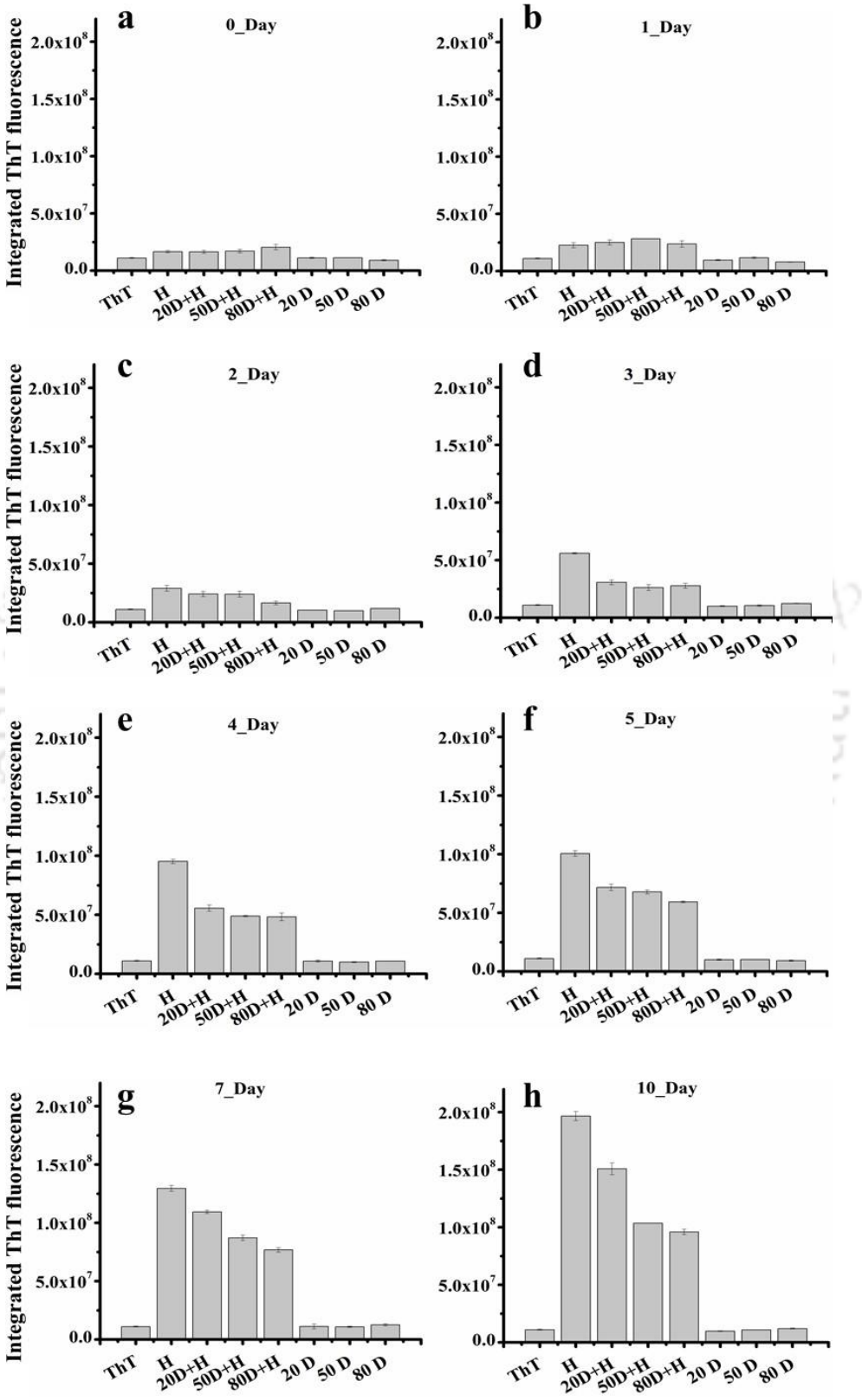

Fig. 3.5: Integrated Thioflavin T fluorescence of HEWL aggregates incubated with different concentrations of DHF (20 μM, 50 μM and 80 μM) in pH 2 for 10 days. H-HEWL, D-DHF

The Thioflavin T (ThT) fluorescence assay was employed to monitor the aggregation dynamics HEWL in the presence and absence of varying concentrations (20 μM, 50 μM, and 80 μM) of DHF in pH 2 incubated at 65 °C **(Fig. 3.5 a-Fig. 3.5 h)**. This aggregation profile served as a control, facilitating the examination of whether DHF had the capacity to intervene or influence the aggregation of HEWL. The findings reveal a progressive increase in HEWL fluorescence from day 3 to day 10 **(Fig. 3.5 d -Fig. 3.5 h)**. Furthermore, these findings align harmoniously with the concept of nucleation-dependent polymerization that characterizes the aggregation behavior of amyloidogenic proteins. This phenomenon suggests the gradual formation of structured fibrils within an acidic pH environment (pH 2), leading to extended incubation periods due to which ThT binds to these fibrillar structures, resulting in augmented fluorescence. In the presence of DHF at the specified concentrations, a notable and dose-dependent reduction in ThT fluorescence is observed, contrasting with HEWL aggregates without DHF **(Fig. 3.5 d, e, f, g, h)**. This outcome underscores the inhibitory effect of DHF on HEWL fibril formation, which persists across all concentrations tested. Particularly, the most significant inhibition of HEWL fibrils occurs when exposed to 80 μM DHF on days 5 **(Fig. 3.5 f)**, 7 **(Fig. 3.5 g)**, and 10 **(Fig. 3.5 h)**. Nonetheless, it is noteworthy that ThT fluorescence in the presence of DHF remains significantly lower compared to HEWL aggregates in isolation, underscoring the partial inhibition effect of DHF on HEWL fibril formation.

The ThT fluorescence assay conducted on HEWL aggregates at pH 5 incubated at 65 °C revealed that the presence of varying concentrations (20 μM, 50 μM, and 80 μM) of DHF did not yield any noteworthy reduction in ThT fluorescence **(Fig. 3.6)**. Under pH 5 conditions, HEWL predominantly generates amorphous aggregates of smaller size, as opposed to the formation of fibrillar structures (Ansari et al., 2018). These findings not only corroborate the utility of ProCharTs absorbance but also underscore its applicability as a label-free probe for tracking both the aggregation process and its inhibition. Conversely, in the pH 2 environment, the ThT fluorescence assay conducted on HEWL aggregates unveiled that DHF had the capacity to substantially inhibit fibril formation. Interestingly, under these conditions, DHF failed to inhibit the development of amorphous aggregates. This observation implies that DHF plays a pivotal role in modulating the aggregation pathway, steering it away from fibrillar aggregation toward the amorphous aggregation pathway. Previously documented reports have noted that ThT fluorescence does not exhibit elevation in the presence of amorphous aggregates (Kumar et al., 2014). Likewise, the intricate interplay between amorphous and fibrillar

structural elements, along with the existence of alternate aggregation pathways, has been documented in prior studies involving various aggregating proteins (Huang et al., 2000).

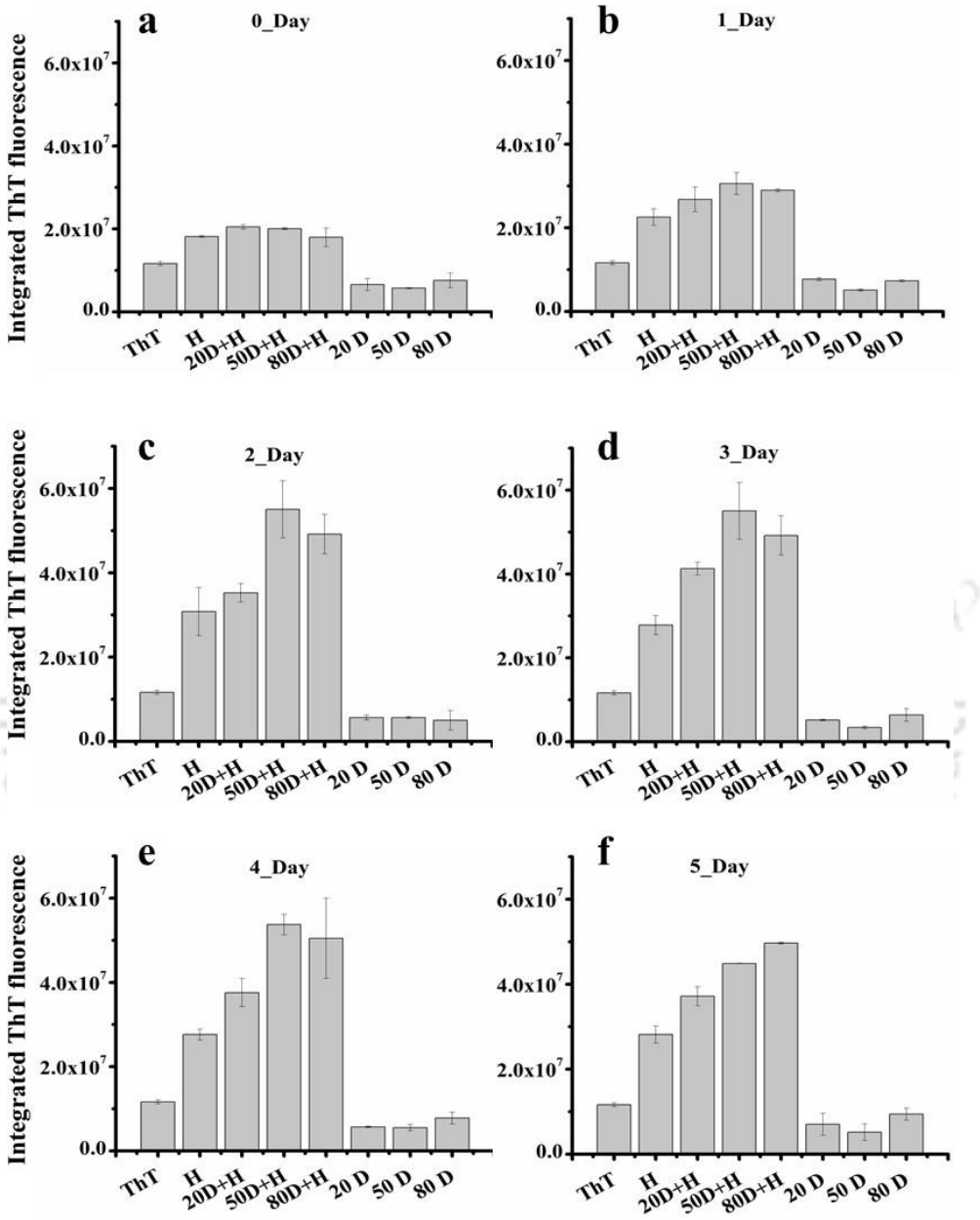

Fig. 3.6: Integrated Thioflavin T fluorescence of HEWL aggregates incubated with different concentrations of DHF (20 μM, 50 μM and 80 μM) in pH 5 for 5 days. H-HEWL, D-DHF

The ThT fluorescence assay was employed to monitor the aggregation dynamics of HEWL in the presence and absence of varying concentrations (20 μM, 50 μM, and 80 μM) of DHF in pH 12.2 incubated at room temperature **(Fig. 3.6a-f).** The ThT fluorescence assay discloses a notably heightened fluorescence intensity within the HEWL aggregates at pH 12.2 **(Fig. 3.6)**,

when juxtaposed with the monomeric HEWL state at day 0 **(Fig. 3.7 a)**. This observation strongly suggests the emergence of a fibrillar morphology in the HEWL aggregates **(Fig. 3.7 b-f)**. In contrast, there is a marginal reduction in the ThT fluorescence intensity of HEWL aggregates in the presence of varying concentrations of DHF, although this effect is not particularly pronounced. Specifically, a dose-dependent effect is conspicuously absent in contrast to results in pH 2 **(Fig. 3.5)**. This phenomenon could potentially be attributed to the structural instability of DHF under alkaline pH conditions, as expounded upon in Chapter 2, leading to a compromised functionality due to structure-activity relationships.

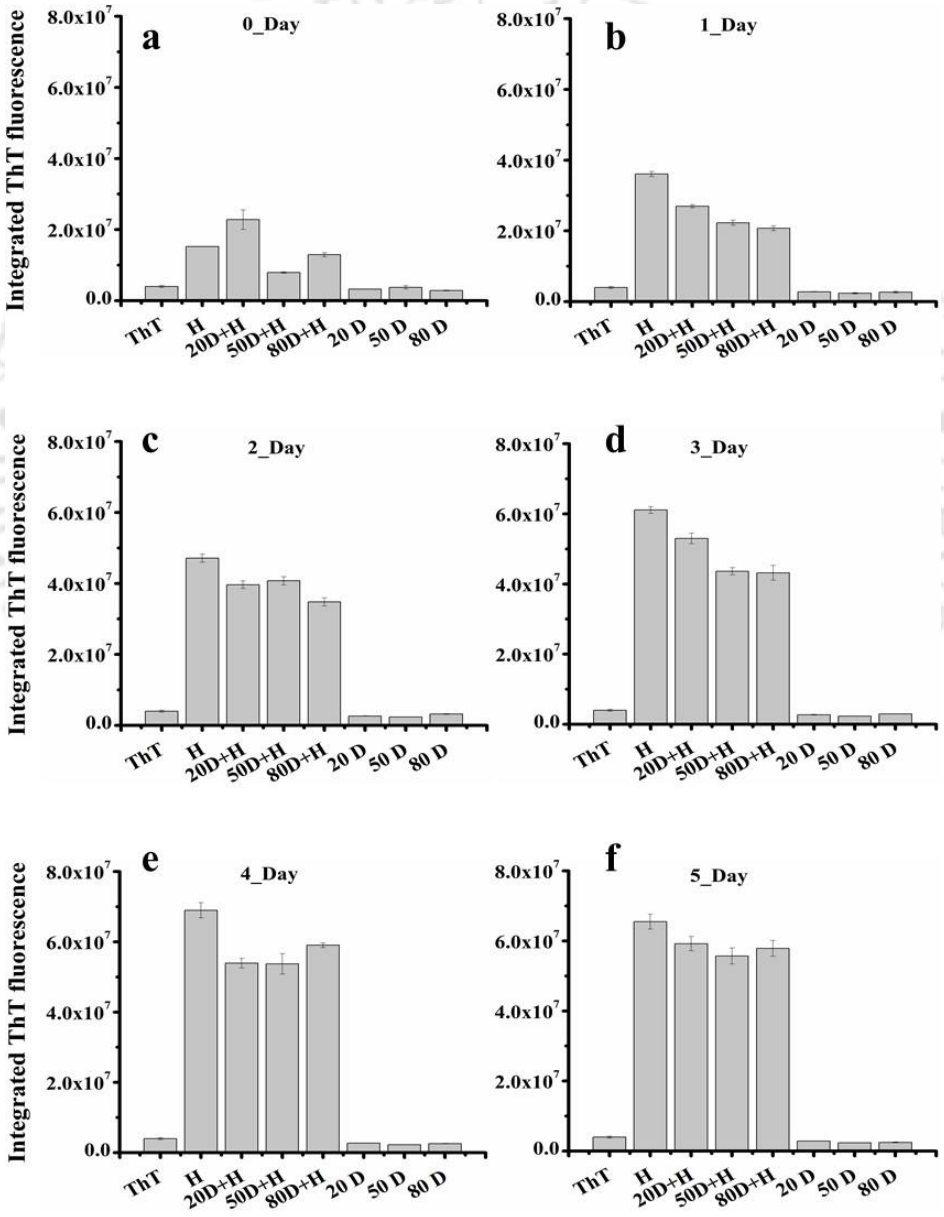

Fig. 3.7: Integrated Thioflavin T fluorescence of HEWL aggregates incubated with different concentrations of DHF (20 μM, 50 μM and 80 μM) in pH 12.2 for 5 days. H-HEWL, D-DHF

3.3.3 ANS Fluorescence studies

ANS serves as an extrinsically applied fluorescent probe, finding broad utility in the comprehensive characterization of proteins across diverse conformational states. The elevation in ANS fluorescence within the context of a molten globule state serves as a discernible marker, signifying the exposure of hydrophobic protein clusters. Notably, ANS demonstrates an augmented fluorescence signal, primarily centred around 480 nm, upon its interaction with the hydrophobic cores of proteins, in stark contrast to its subdued fluorescence emission while in a free state within an aqueous milieu. When excited at 380 nm, ANS yields minimal fluorescence output at approximately 480 nm under these specific experimental conditions. ANS serves as an extrinsically applied fluorescent probe, extensively employed for the characterization of proteins across diverse conformational states. The augmentation in ANS fluorescence within the milieu of a molten globule state signifies the exposition of hydrophobic clusters within the protein structure (Guliyeva and Gasymov, 2020).

The ANS fluorescence assay unveiled a noteworthy augmentation in fluorescence intensity for HEWL aggregates at pH 2, in contrast to the negligible ANS fluorescence exhibited by freshly prepared monomeric HEWL at day 0, a fluorescence level akin to that of blank ANS. This observation can be attributed to the significant unfolding of HEWL, a process that entails the exposure of hydrophobic moieties, subsequently leading to the gradual escalation of ANS fluorescence intensity. Remarkably, when varying concentrations of DHF at 20 μM, 50 μM, and 80 μM were introduced, HEWL aggregates exhibited a reduction in ANS fluorescence intensity compared to their counterparts without DHF **(Fig 3.8)**. This reduction in fluorescence can likely be ascribed to the ability of DHF to mitigate the exposure of HEWL's internal hydrophobic groups, rendering the aggregation process more arduous. Importantly, these findings from the ANS fluorescence assay are in consonance with the outcomes obtained through ThT assays, affirming their consistency and supporting the overall conclusions.

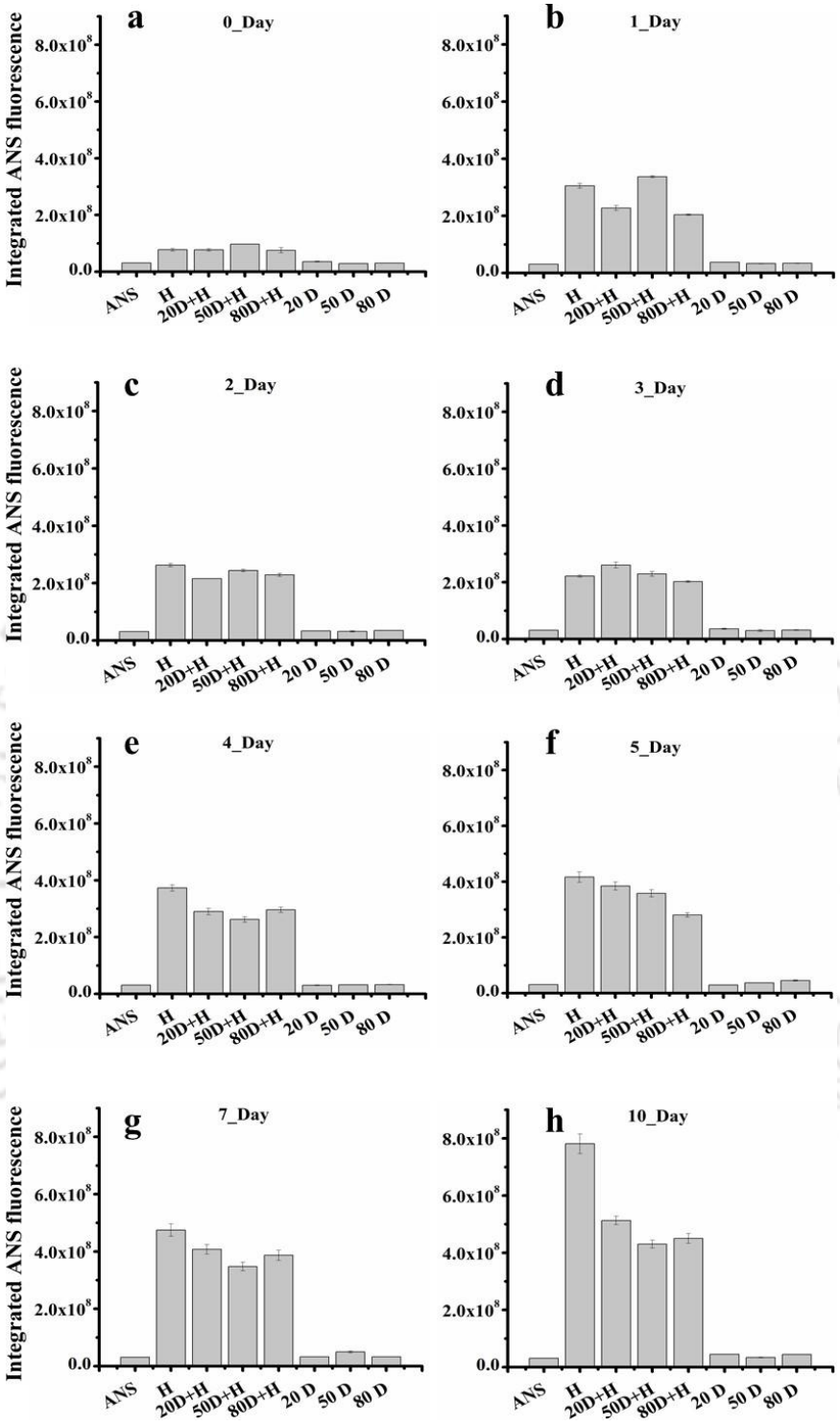

Fig. 3.8: Integrated ANS fluorescence of HEWL aggregates incubated with different concentrations of DHF (20 μM, 50 μM and 80 μM) in pH 2 for 10 days. H-HEWL, D-DHF

Nonetheless, when scrutinizing the ANS fluorescence assay results for HEWL at pH 5 **(Fig. 3.9)**, a notable trend emerges. It becomes apparent that the ANS fluorescence intensity within HEWL aggregates remains relatively constant across varying concentrations of DHF – specifically, at 20 μM, 50 μM, and 80 μM. Only a subtle decrease in ANS fluorescence intensity

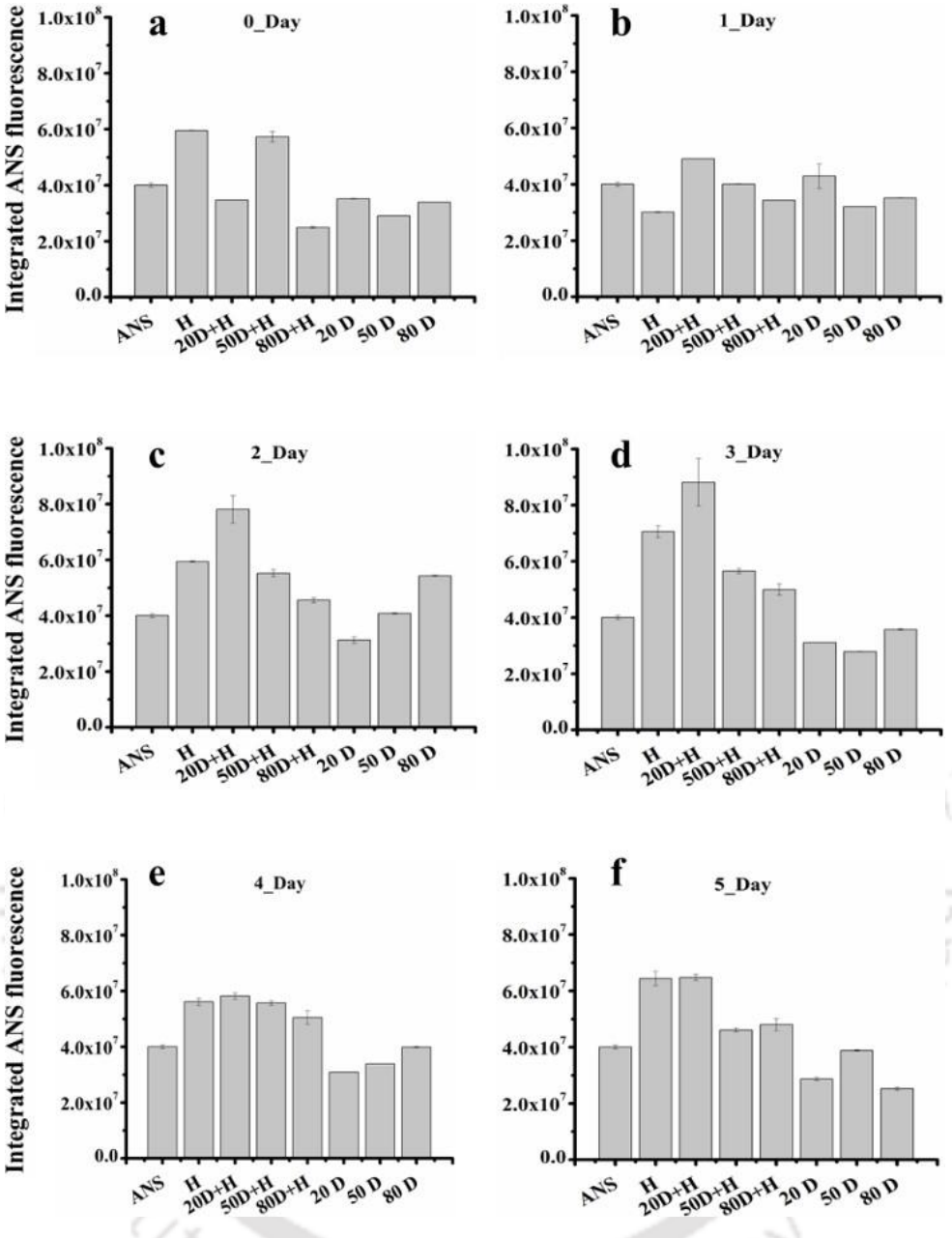

Fig. 3.9: Integrated ANS fluorescence of HEWL aggregates incubated with different concentrations of DHF (20 μM, 50 μM and 80 μM) in pH 5 for 5 days. H-HEWL, D-DHF

becomes evident in HEWL aggregates exposed to 50 μM and 80 μM DHF, during the incubation period spanning from the second to the fifth day **(Fig 3.9 c-f)**. This intriguing observation can be rationalized by considering previous reports that have highlighted the heightened selectivity of ThT for fibrillar structures as compared to ANS. ThT has a propensity to preferentially bind to amyloid fibrils, whereas ANS, in contrast, interacts with hydrophobic regions present in both amorphous aggregates and amyloid fibrils (Vetri et al., 2007). Consequently, this subtle differentiation in binding preferences may elucidate our inability to detect any inhibitory effects exerted by DHF on HEWL aggregates at pH 5 when employing

the ThT assay. In contrast, ANS assay at pH 5 reveals a mild, dose-dependent inhibition of HEWL by DHF, likely attributable to the formation of amorphous aggregates of HEWL under these conditions.

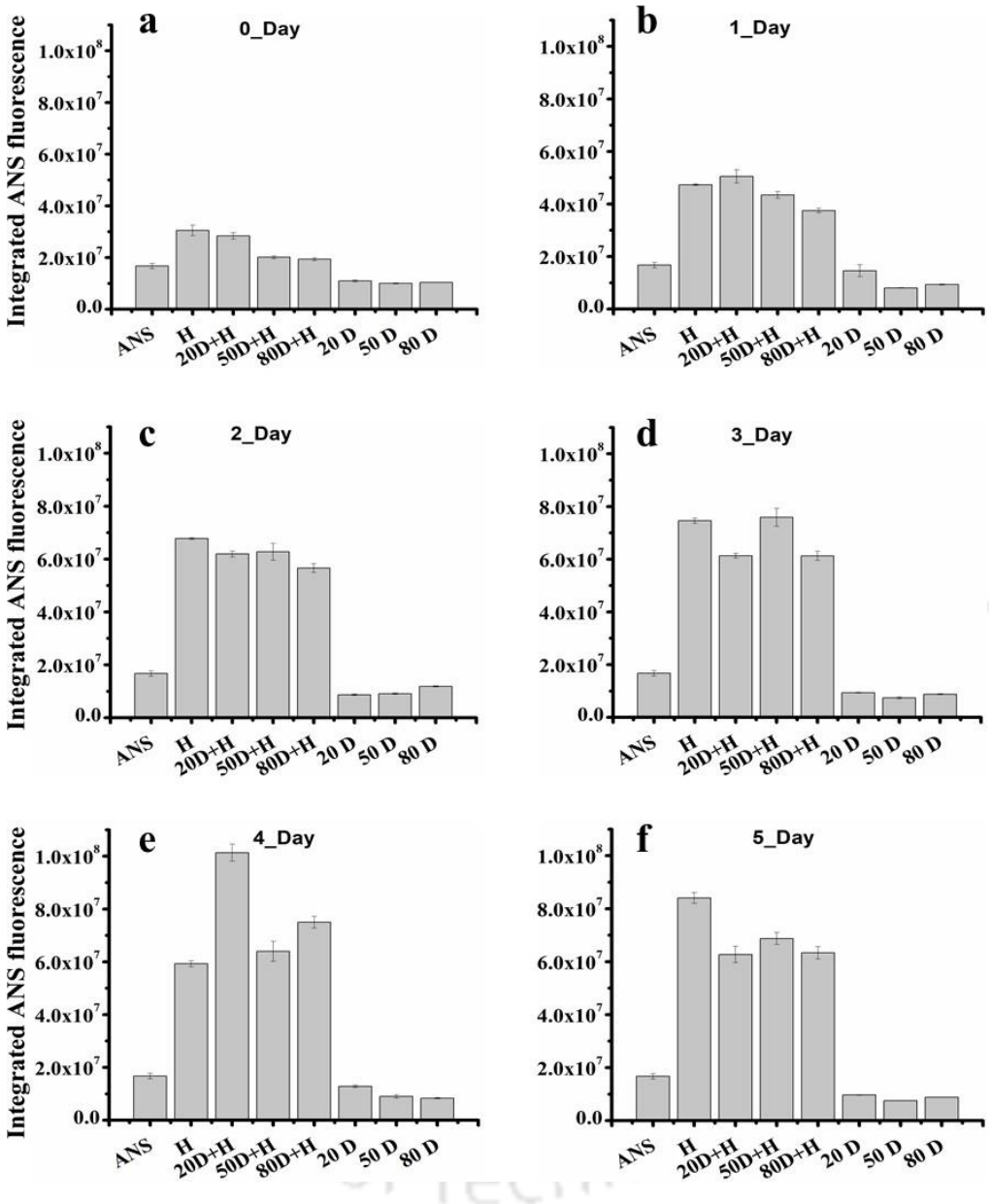

Fig. 3.10: Integrated ANS fluorescence of HEWL aggregates incubated with different concentrations of DHF (20 μM, 50 μM and 80 μM) in pH 12.2 for 5 days. H-HEWL, D-DHF

The ANS fluorescence assay applied to HEWL aggregates at a markedly alkaline pH of 12.2 has revealed a gradual increase in fluorescence intensity in comparison to the pristine monomeric HEWL at day zero **(Fig. 3.10 a)**. Remarkably, the introduction of varying concentrations of DHF – specifically, 20 μM, 50 μM, and 80 μM – did not elicit a significant reduction in ANS fluorescence **(Fig 3.10)**. It was only on the fifth day of incubation that a

modest decline in ANS fluorescence intensity within the HEWL aggregates became discernible in the presence of DHF **(Fig. 3.10 f)**. This intriguing set of results resonates the findings derived from ThT assay, indicating that DHF exerts only a mild inhibitory effect on HEWL aggregates at the alkaline pH of 12.2. This subtle inhibition is likely attributed to the inherent structural instability of DHF under alkaline conditions.

3.3.4 Observing the effects of DHF on HEWL fibrillogenesis by Atomic Force Microscopy

Collectively integrating insights from ProCharTS, ThT, and ANS assays, a compelling pattern emerges revealing the potent inhibitory influence of DHF on the formation of HEWL fibrils at pH 2. In pursuit of a more direct visual assessment of DHF's impact on fibril formation, we turned to AFM. The AFM images, as depicted in **(Fig. 3.11)**, illustrate three distinct scenarios: HEWL in its monomeric state **(Fig. 3.11a)**, HEWL aggregates incubated for a period of 7 days at pH 2 **(Fig. 3.11b)**, and HEWL aggregates subjected to the presence of 80 µM DHF over a duration of 10 days at pH 2 **(Fig. 3.11c)**.

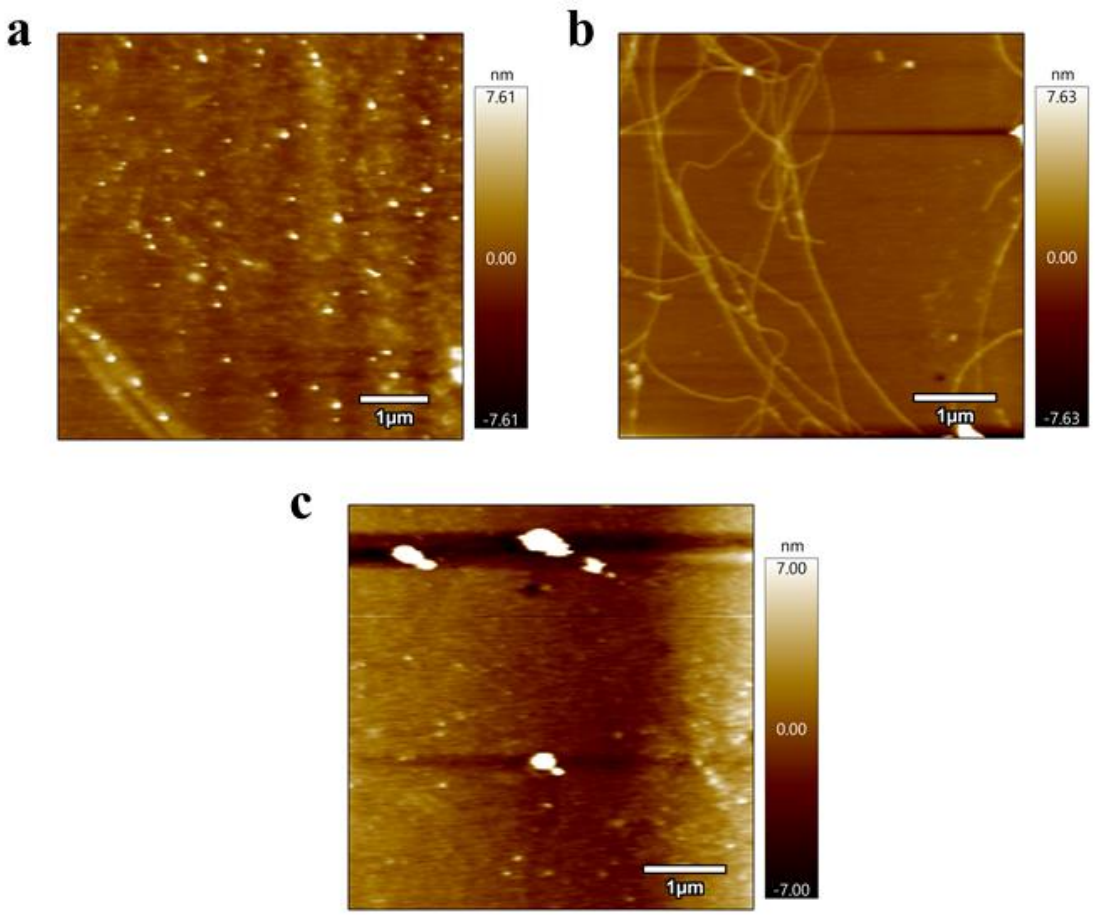

Fig. 3.11: AFM images of HEWL Monomer 2µM (a), 7_Day HEWL in pH 2 diluted to 2µM (b), 10_Day 80 µM DHF+HEWL in pH 2 diluted to 2µM (c).

A discernible outcome of this AFM analysis is the clear formation of mature HEWL amyloid fibrils in the absence of DHF **(Fig. 3.11 b)**. Conversely, when DHF is introduced, a starkly contrasting observation emerges. The fibrillar structures are notably suppressed within the HEWL aggregates, giving rise instead to amorphous aggregates characterized by a range of diameters surpassing those of the monomers **(Fig. 3.11 c)**. This collective body of evidence leads us to posit a hypothesis: DHF may engage with on-pathway intermediates, thereby effectively impeding the lateral assembly of oligomers, which is essential for the formation of larger fibrillar structures.

3.4 Conclusions

DHF exhibits robust inhibitory effects on the aggregation of fibrils in HEWL under acidic conditions (pH 2), resulting in the formation of more disordered and amorphous aggregates. This observation underscores DHF's capacity to modulate the aggregation process under specific pH conditions. However, it is important to note that DHF does not manifest significant inhibitory effects on HEWL aggregates at pH 5, thereby confirming its inability to impede the formation of amorphous aggregates in this pH range. Furthermore, DHF's efficacy in inhibiting HEWL fibrils is notably diminished at an elevated alkaline pH of 12.2. This attenuation in inhibitory activity is attributed to the inherent instability of DHF under such high alkaline pH conditions.

Chapter 4

Studying the anticancer activity of DHF in colon cancer cells

4.1 Introduction

Colon cancer has asserted its position as the second leading cause of cancer fatalities in the developed world and a major cause of death worldwide. Tumor recurrence and the risky spread of cancer to distant places following conservative surgery loom as fearsome foes, bearing the weight of death and foretelling a gloomy future (Gu et al., 2021). Consequently, ground-breaking therapeutic agents that combat metastasis becomes an urgent imperative, poised to illuminate a path towards heightened survival rates into the realm of colon cancer treatment.

Cancer invasion and metastasis involve an intricate cascade of events, encompasses a sequential series of cellular transformations, including disruption of intercellular adhesion, the infiltration of basal membranes and surrounding tissues, intravasation into either the bloodstream or lymphatic vessels, sustenance of viability within the circulatory system, and ultimately, the processes of extravasation followed by robust proliferation at nascent metastatic (Trinh et al., 2022). One of the key factors contributing to metastasis is the epithelial-mesenchymal transition (EMT). A key hallmark observed in the EMT of carcinoma cells is the transition from epithelial (E-cadherin), which is a cell-surface protein primarily associated with epithelial junctions, to neural cadherin (N-cadherin). This switching in cadherin expression contributes to the cellular changes observed during EMT (Kalluri and Weinberg, 2009). Furthermore, there is an upregulation of vimentin, an intermediate filament protein, which is typically highly expressed in mesenchymal cells (Jie et al., 2017).

A. nigra (Gaertn.) Burtt is an aromatic rhizomatous herb known for its various medicinal properties. Different parts of the plant contain a diverse range of bioactive compounds that contribute to its therapeutic benefits. In Assam it is commonly named as "Tora" and the aqueous extract from its rhizome and shoot has been a popular folk remedy for various health concerns, including bone weakness, jaundice, and gastric ulcers (Tushar et al., 2010). Reports suggests that its various extracts have demonstrated potent antibacterial (Ghosh et al., 2013), anti-inflammatory (Das and Qais, 2012) antihelmintic (Roy and Swargiary, 2009), cytotoxic, and analgesic effects (Ahmed et al., 2015). This remarkable plant holds great promise for future therapeutic applications.

In the present study, we investigated the anticancer activity of flavonoid 3,5-dihydroxy-7,4'- dimethoxyflavone (DHF) from *A. nigra*, previously reported from our lab group (Gupta et al., 2021). The focus of our study was to assess its effects on colon cancer cell lines, specifically HCT116 and SW480. Numerous biological activities have been documented for

DHF (3,5-dihydroxy-7,4'-dimethoxyflavone), including estrogenic activity as reported by (Ying et al., 2014). Additionally, Sudsai et al., (2017) demonstrated its potential as an antibacterial and anti-HIV agent. Furthermore, DHF has been recognized for its antioxidant, anti-tyrosinase, and anti-inflammatory properties, as evidenced in the study by Gupta et al., (2021).

Moreover, despite the numerous documented biological effects of DHF, its potential as an anticancer agent targeting colon cancer cells remains uncharted in prior research. DHF is a derivative of kaempferol and shares a structural resemblance with this well-recognized compound, which is renowned for its multifaceted anticancer attributes, including its established effectiveness against colon cancer. Since DHF is a derivative of kaempferol, a compound known for its diverse anticancer effects, we undertook a pioneering investigation to explore the impact of DHF on colon cancer cells. In the present chapter, the study unveils the pivotal role of DHF in colon cancer development, particularly in proliferation and migration.

4.2 Materials and methods

4.2.1 MTT Assay:

Day 1: Cell seeding

Cell lines were obtained and sub-cultured on Dulbecco's Modified Eagle Medium (DMEM) media. The cells were thus obtained were incubated in 5% CO_2 at 37°C. When the cells were 70-80% confluent, media was discarded and the cells were washed with 2 mL of 1X phosphate-buffered saline (PBS). The cells were trypsinized with 100 µL trypsin and incubated for 6 minutes until the cells were detached. About 2 mL of fresh medium was then added and the suspension was transferred to a clean falcon tube and centrifuged at 1200 rpm for 6 minutes at 4°C. The supernatant was then discarded and the pellet was dissolved in 1 mL of fresh medium. Nearly 20 µL of the suspension was then mixed with trypan blue in 1:1 ratio and the cell count were obtained by using the hemocytometer.

For cell count: cells/mL= Avg. cell count per square X 10^4 x dilution factor x 2 x 10^4

Stock preparation: Required cell count = 2000 cells/ 100 µL

Required volume = 20 mL

Roughly 100 µL of cell suspension was added to 96 well plates and these were incubated at 37°C and 5% CO_2 for 24 hours.

Day 2: Drug dilution

Stock concentration of 50 mM DHF in dimethyl sulfoxide (DMSO), 10 mM Kaempferol in DMSO, 10 mM 5 Fluorouracil in DH_2O was used. Concentration of DHF used for the treatment: 5 µM, 10 µM, 25 µM, 50 µM and 100 µM. A volume of 10 µL of MTT was introduced to the 0-hour plate and subjected to a 2-hour incubation period at 37°C under conditions of 5% CO_2. After 2 hours the content of the 0-hour plate was discarded and 100 µL of DMSO was added to each well.

The plate was then wrapped with aluminum foil and incubated for 15 minutes. After 15 minutes the absorbance was measured at 570 nm.

Day 3 and 4: Incubation at 37°C at 5 % CO_2 incubator.

Day 5: Detection/visualization

In each well of the 72-hour plate, precisely 10 µL of MTT was added, followed by a 2-hour incubation period at 37°C with a 5% CO_2 atmosphere. Subsequently, the plate contents were removed, replaced with 100 µL of DMSO, and then covered with foil followed by a 15 minutes incubation. After a further 1-hour interval, the absorbance was measured at 570 nm.

4.2.2 Cell death analysis by propidium iodide (PI) staining using flow cytometer

The plate containing HCT116 and SW480 cells were taken and the media was discarded, the cells were washed with PBS buffer. The cells were trypsinized and 2 mL of fresh media was added which was followed by centrifugation at 12000 rpm for 6 minutes at 4°C. After centrifugation, the supernatant was discarded and the pellet was mixed with 1mL of fresh medium, from this mixture 50 µL of cells were transferred to a 1.5 mL Eppendorf tube to which 50 µL trypan blue was added making the ratio of 1:1. From this mixture, 10 µL volume was loaded on to hemocytometer for the cell count using inverted microscope. A volume of 1 mL of cell suspension, containing a cell density of 5000 cells/mL, was introduced into each well of a 6-well culture plate. Subsequently, 1 mL of fresh cell culture media was added to each well to attain a final volume of 2 mL. The plate was then placed in a CO_2 incubator and incubated for a duration of 24 hours. After completion of 24 hours, cells are treated with different concentrations of DHF (50 µM and 100 µM) and Kaempferol 100 µM. The cells were then further incubated for 72 hours. After incubation, the cells in the 6 well plate were detached by trypsinization and collected in tubes. The cells were gently mixed and centrifuged at 4000

rpm for 10 minutes at 4°C and supernatant was discarded. The pellet was gently mixed and suspended in 1 mL PBS and centrifuged at 4000 rpm for 10 minutes at 4°C which was repeated twice. The collected pellet was then finally resuspended to 495 µL of PBS and kept in ice. A volume of 5 µL of PI was introduced into the sample, which was then incubated on ice for a period of 10 minutes. Subsequently, the sample was analyzed by flow cytometer (BD FACS Celesta^{TM}, Becton-Dickinson, New Jersey, USA).

4.2.3 Test for apoptosis

A total of $1x10^5$ HCT116 and SW480 cells were evenly distributed and cultured within individual wells of 6-well plates. These plates were then incubated for a duration of 24 hours at a controlled environment of 37°C within a 5% CO_2 incubator. After incubation, the cells were treated with DHF concentrations of 50 µM and 100 µM and incubated for 72 hours at CO_2 incubator. The cells in 6 well plates were then detached by trypsinization and were collected in tubes and mixed gently, which were then subjected to centrifugation at 4000 rpm for 10 minutes at 4°C. It was repeated twice with 1X PBS. The cells were centrifuged at 4000rpm for 10 minutes and resuspended in the binding buffer (100 µL) for each tube. The controlsused were unstained PI control, Annexin control and Double stained control. PI (2 µg/mL) andAnnexin 25 µL (2.5 µg/mL) each were added to the sample and the reading was done using flow cytometer (BD FACS Celesta^{TM}, Becton-Dickinson, New Jersey, USA).

4.2.4 Migration assay

The purpose of this assay was to look into the migration of HCT116 and SW480 cells after they were treated with DHF and Kaempferol. HCT116 and SW480 cells were seeded in 12 well plates with approximately 2 lakh cells per well and incubated in a CO_2 incubator. Upon the establishment of monolayers, cellular synchronization was achieved through the implementation of serum-deprived media, with a duration spanning 8 to 12 hours, preceding the initiation of the scratch or wound generation, which was meticulously executed using P200 pipette tips. The debris created during the scratch is removed by washing with 1 mL media and then replacing it with 5 mL media. Subsequently, cells were subjected to treatment with DHF concentrations of 50 µM and 100 µM, as well as a 100 µM dosage of kaempferol. The migration of the cells was assessed using an inverted microscope (Nikon T1-SM, Japan) to observe the difference in the area of the scratch wounds. The photos were taken at various time intervals beginning at 0 hour and ending after the control cells had completely migrated and the scratch

had healed. ImageJ software was used to analyze the images and determine the unhealed area at various time intervals.

4.2.5 Western blotting

Western blot analysis was performed to determine the expression profiles of distinct target proteins implicated in the migration of cancer cells, specifically HCT116 and SW480 cells, upon treatment with DHF and kaempferol. The experiment followed a series of rigorous protocol, encompassing the following methodological steps:

Cell seeding and treatment with DHF and Kaempferol

The plate containing HCT116 and SW480 cells were utilized and the media was discarded from the plate, and subsequent to a PBS wash, 200 µL of trypsin was added. The plates were then incubated in a 37°C CO_2 incubator for a duration of 3-5 minutes. Following incubation, 2mL of fresh media was introduced into the plates, and the cells were gently transferred to Falcon tubes. These tubes were subsequently subjected to centrifugation at 1200 rpm for 6 minutes at 4°C. Upon centrifugation, the supernatant was discarded, and the cell pellet was resuspended in 1 mL of fresh media. From this cell suspension, 20 µL was extracted and mixedwith an equal volume of trypan blue, achieving a 1:1 ratio. Cell counting was then performed employing a hemocytometer, with a final count of $3x10^5$ cells for each petriplate. Subsequently,2 mL of fresh DMEM media was added to each plate, making the total volume in each plate 3mL. All plates were then incubated for 24 hours at 37°C. After the incubation period, the mediawas removed from the plates and replaced with 2.9 mL of fresh media. A solution containing 50 mM DHF in (99.9%) DMSO and 50 mM Kaempferol in (99.9%) DMSO was diluted withinthe media. The cells were treated with DHF at concentrations of 50 µM and 100 µM, and Kaempferol at 100 µM, except for the control. Following this treatment, all plates were incubated for an additional 24 hours in a CO_2 incubator at 37°C, after which cell lysates were prepared.

Lysate preparation

The media in the petriplates was removed and each plate was gently washed with 1 mL of PBS. Following the PBS wash, 100 µL of lysis buffer was introduced into each plate. The resulting lysates were then transferred into 1.5 mL eppendorf tubes and subsequently subjected to centrifugation at 13,000 rpm for 15 minutes. After centrifugation, the supernatant was carefully collected, and the pellets were discarded.

Protein estimation

Protein estimation was done using Bradford protein assay (Bradford, 1976). Different dilutions of bovine serum albumin (BSA) from 2 mg/mL stock in lysis buffer was used to prepare the standard curve. The different dilutions of BSA prepared were: 20 µL of 2 mg/mL stock, 1 mg/mL, 0.5 mg/mL, 0.25 mg/mL and 0.125 mg/mL. In 95 µL of Bradford reagent, 5 µL of protein were added for each dilution which were then loaded in the wells of 96 well plates. Same procedure was followed for loading samples treated with DHF and Kaempferol along with control samples and the absorbance was measured at 595 nm. The graph for standard curve was plotted and the concentration of protein was estimated for each sample. Then 30 µg of each sample were loaded on separate wells on the gel after gel preparation for electrophoresisat 90 V. A resolving gel comprising 12% concentration and a stacking gel with 4% concentration, composed of a blend of deionized water, acrylamide bisacrylamide, Tris-HCl, ammonium persulfate, SDS, and N,N,N′,N′ -Tetramethylethylenediamine (TEMED), were prepared for running the protein samples. The protein samples were loaded on the wells for electrophoresis and after completion of electrophoresis, the stacking gel was removed. Then the blotting was done on nitrocellulose membrane, the gel and nitrocellulose membrane were sandwiched between the stacks and electroblotted at 1.3 A, 25 V for 30 minutes.

After blotting was completed, the membrane was stained with the ponceau stain to visualize the transferred proteins. Then washing was done thrice using 1x Tris-buffered saline with 0.1% Tween 20 (TBST) for 10-15 minutes each. After the wash the, the membrane was blocked with 2% milk in TBST for 2 hours in shaker and then washed thrice again with 1X TBST. The membrane was then incubated with the primary antibody at 4°C overnight. After the incubation, washing was done for three times with 1x TBST.

Then the membranes were incubated with anti-rabbit/anti-mouse secondary antibody for 2 hours at room temperature. The membranes were then washed with 1X TBST for three times for 10-15 minutes each. The blots were then developed with Bio Rad Chemi Doc through the software protocol.

4.2.6 Colony formation assay

The colony formation assay was conducted exclusively using plates containing HCT116 cells, chosen for their heightened sensitivity in cell proliferation and migration assays as opposed to the SW480 cell line. Initially, the growth media was removed from the plates, and the cells

were rinsed with PBS. Subsequently, the cells were treated with 200 µL of trypsin and incubated in a CO_2 incubator for 3-5 minutes. Following this, 2 mL of fresh DMEM media was added to the plate, and the cells were gently collected into Falcon tubes, which were then subjected to centrifugation at 1200 rpm for 6 minutes at 4°C. Upon centrifugation, the supernatant was discarded, and the cell pellet was resuspended in 1 mL of fresh media. To determine cell count, 50 µL of the suspended cell pellet was transferred to an Eppendorf tube, and 50 µL of trypan blue was added, resulting in a 1:1 ratio. From this mixture, 10 µL was loaded onto a hemocytometer for cell counting using an inverted microscope. Subsequently, 1 mL of cells was added to each well of a 6-well plate, with a target of 1500 cells per well. An additional 1 mL of fresh media was added to each well to achieve a final volume of 2 mL. The plate was then incubated in a CO_2 incubator for 24 hours and treated with varying concentrations of DHF (50 µM and 100 µM) and 100 µM of Kaempferol. Colony formation was monitored during this incubation period. Upon the formation of colonies, the media was removed from the plate, and a gentle wash with 1X PBS was performed. Subsequently, ethanol (70%) fixation was carried out at -20°C for 1 hour. Following fixation, 1 mL of 0.5% (w/v) crystal violet was added to each well for 2-3 minutes. The cells were then gently washed to remove excess stain, and photographs were taken for analysis.

4.3 Results and Discussions

4.3.1 Cell proliferation by MTT

Cell proliferation, a fundamental biological process, involves rapid multiplication of cells through division, crucial for proper growth, development, and maintenance of organisms, ensuring tissue and cellular homeostasis. This assay gauges the rate at which cell populations expand and serves as a valuable tool to assess drug effects, study growth factors, measure cytotoxicity, and explore cell activation contexts. Existing methodologies encompass assessments related to DNA synthesis, metabolic activity, proliferation-associated antigens, and ATP concentration (Romar et al., 2016).

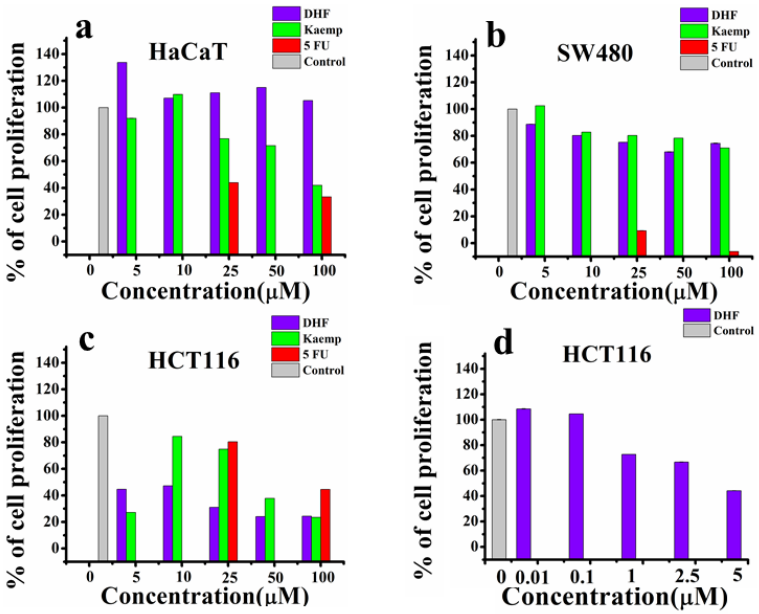

Fig. 4.1: Cell proliferation assay by MTT on treatment with DHF, Kaempferol and 5FU against three different cell lines :(a) HaCaT, (b) SW480 and (c) HCT116 (d) HCT116

In our study, employing the MTT assay, cell proliferation analysis was conducted across three distinct cell lines. Notably, HaCaT cells exhibited unhindered proliferation when exposed to DHF. Conversely, treatment with higher concentrations of kaempferol (25 μM, 50 μM, and 100 μM) led to notable inhibition rates of 24%, 29%, and 59%, respectively, while 5FU treatments at 25 μM and 50 μM resulted in substantial inhibition of proliferation by 57% and 67% in HaCaT cells (**Fig. 4.1 a**).

In both HCT116 and SW480 cell lines, DHF treatment significantly inhibited cell proliferation. In the case of SW480 cells, DHF treatments at higher concentrations (50 μM and 100 μM) led to inhibitions of 32% and 26%, whereas kaempferol treatments at 50 μM and 100 μM resulted in inhibitions of 22% and 30%. Strikingly, 5FU treatments at 25 μM and 100 μM resulted in substantial inhibitions of 91% and 94% **(Fig. 4.1 b)**.

HCT116 cells, when subjected to DHF concentrations (25 μM, 50 μM, and 100 μM), displayed inhibitions of 69%, 76%, and 76%, respectively. Kaempferol treatments at 50 μM and 100 μM exhibited significant inhibitions of 63% and 77%. Contrastingly, 5FU treatments at 25 μM and 100 μM resulted in 20% and 56% inhibition in HCT116 cells **(Fig. 4.1 c)**. The IC_{50} value of DHF for HCT116 cell line was calculated to be 3.75 μM using DHF concentrations (0.01 μM, 0.1 μM, 0.5 μM, 1 μM, 2.5 μM, 5 μM) as shown in figure **Fig. 4.1 d.**

Noteworthy is the variation in sensitivity among the cell lines. HCT116 cells exhibited heightened sensitivity to DHF in comparison to SW480, whereas SW480 cells displayed

higher susceptibility to 5FU compared to HCT116. Similar results have been discussed in caseof cell viability assay as well. Additionally, HCT116 cells manifested greater sensitivity to kaempferol compared to SW480, as depicted in Figure 5.2. These results underscore the diverse responses of distinct cell lines to the compounds studied, providing valuable insights into their potential therapeutic applications. Astragalin has been reported to impede cell proliferation in HCT116 cells through the induction of cell cycle arrest. Mechanistically, astragalin disrupts the NF-κB signaling pathways *in vitro* in a dose-dependent manner. Notably, it inhibits the nuclear translocation of NF-κB P65 protein stimulated by TNF-α. *In vivo* experiments employing nude mice demonstrated that oral administration of astragalin reduced the proliferation of xenograft HCT116 tumors and suppressed HCT116 tumor growth. This effectwas attributed to increased apoptotic cells within tumor tissues and inhibition of the NFκB signaling pathway (Yang et al., 2021).

Metformin, a well-known antidiabetic drug, displayed substantial growth inhibition in both HCT116 and SW480 CRC cell lines (Esra'a et al., 2021). In HCT116, metformin treatment led to a 25–30% decrease in proliferation (Mogavero et al., 2017). Silibinin, on the other hand, exhibited significant growth inhibition of SW480 cells in culture. Silibinin achieved this by decreasing the total cellular pool as well as the subcellular localization of β-catenin, a pivotal component in the Wnt/β-catenin signaling pathway. Silibinin's growth-inhibitory effect was specific to β-catenin down-regulation, as evidenced by HCT116 cells, which harbor wild-type APC but mutant β-catenin, failing to respond to silibinin treatment (Kaur et al., 2010).

Moreover, compound C, identified as an inhibitor of AMP-activated protein kinase (AMPK), displayed potent anti-proliferative activity across all four colorectal cancer cell lines: HCT116, DLD-1, SW480, and KM12C. Remarkably, compound C induced both apoptosis and autophagy in colorectal cancer cells, with apoptosis predominant in HCT116 and KM12C cells, and autophagy observed mainly in DLD-1 and SW480 cells (Yang et al., 2012). These findings underscore the diverse yet interconnected mechanisms through which these compounds exert their anti-proliferative effects, shedding light on potential avenues for targeted therapeutic interventions in colon cancer.

4.3.2 Cell death analysis by flow cytometry

The PI flow cytometric technique has been widely utilized in numerous experimental models to estimate apoptosis. Apoptotic cells are characterized by DNA fragmentation, leading to the

loss of nuclear DNA content. PI, a fluorochrome capable of binding and tagging DNA, allows for a quick and exact assessment of cellular DNA content by flow cytometric analysis, as well as the detection of hypodiploid cells (Riccardi and Nicoletti, 2006).

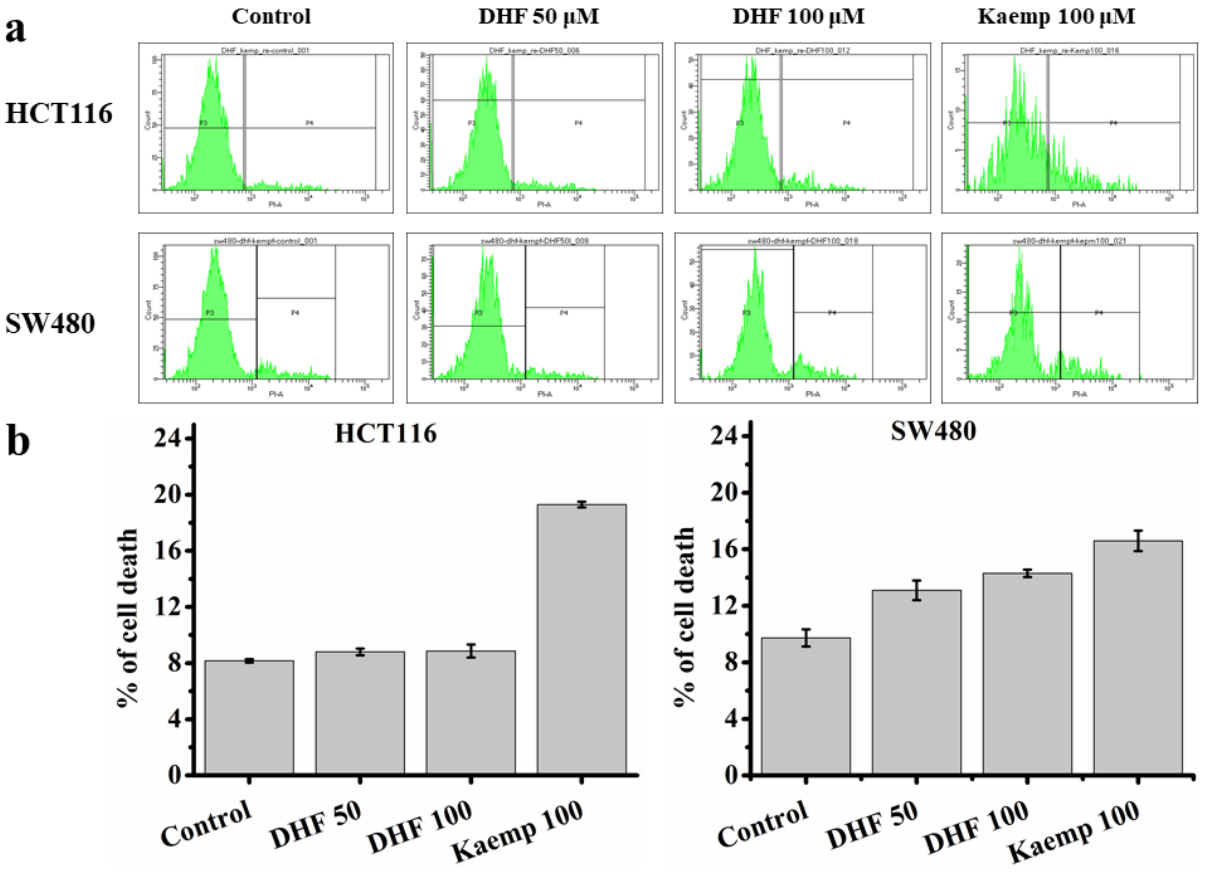

Fig 4.2: (a) Cell death analysis by propidium iodide dye on treatment with DHF (50 µM and 100 µM) and Kaempferol(100 µM) in HCT116 and SW480 cells, (b) Cell death percentage plotted against various. treatment in HCT116 and SW480 cells by PI-FACS with DHF (50 µM and 100 µM) and Kaempferol(100 µM).

The analysis of cell death in HCT116 cells employing PI dye revealed that there is no significant cell death. Cells treated with DMSO (control) exhibited 8% cell death, and upon treatment with 50 µM and 100 µM DHF, a marginal increase to approximately 8.8% cell death was observed. In contrast, exposure to 100 µM kaempferol led to a moderate elevation, resulting in approximately 20% cell death in HCT116 cells **(Fig. 4.2)**.

In SW480 cells, cells treated with DMSO (control) exhibited 9.7% cell death. Upon treatment with 50 µM and 100 µM DHF, a minor effect was observed, leading to only about 13% and 14% cell death, respectively. Similarly, treatment with 100 µM kaempferol induced a slight elevation, with approximately 16% cell death observed in SW480 cells **(Fig. 4.2)**. These findings shed light on the differential responses of HCT116 and SW480 cells to the treatments, providing valuable insights into the nuances of cell death mechanisms in these contexts.

Apoptosis is a critical mechanism of programmed cell death that is required for tissue equilibrium. It begins with a breakdown of the cell's plasma membrane, exposing phosphatidylserine (PS) residues on the outer leaflet. Annexin V has a high affinity for PS and is used as a reliable marker for detecting early apoptosis. To distinguish between dead and apoptotic cells, PI is used in conjunction with Annexin V.

The evaluation of cell death in SW480 and HCT116 cells, conducted through PI-Annexin staining, revealed a lack of significant cell death in response to both DHF and kaempferol treatments **(Fig. 4.3)**. Specifically, in HCT116 cells, the cells treated with DMSO (control) exhibited a modest 10.5% cell death. Following exposure to 50 µM and 100 µM DHF, only 11.4% and 8.1% cell death were noted, respectively. Similarly, treatment with 100 µM kaempferol resulted in a marginal 11.4% cell death in HCT116 cells.

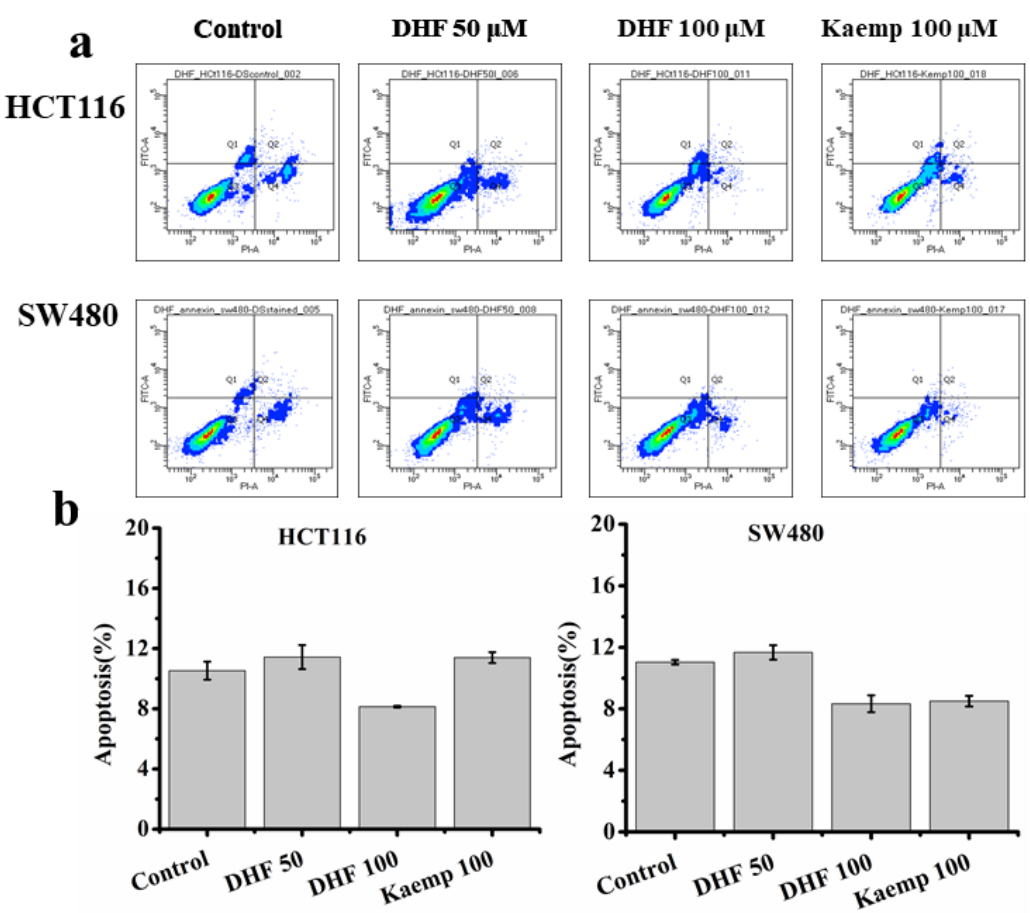

Fig 4.3: (a) Cell death analysis by PI-Annexin V dye on treatment with DHF (50 µM and 100 µM) and Kaempferol(100 µM) in HCT116 and SW480 cells (b) Cell death percentage plotted against various. treatment in HCT116 and SW480 cells by PI-Annexin V with DHF (50 µM and 100 µM) and Kaempferol(100 µM).

In SW480 cells, cells treated with DMSO (control) displayed 11% cell death. Subsequent treatments with 50 µM and 100 µM DHF showed 11.6% and 8.3% cell death,

respectively. Likewise, exposure to 100 μM kaempferol led to 8.5% cell death **(Fig. 4.3)**. Consequently, based on the results obtained from the cell death analysis assay, it can be concluded that neither SW480 nor HCT116 cells undergo apoptosis upon treatment with DHF.

Flavonoids have emerged as potent regulators of cell growth, operating through diverse mechanisms, including the modulation of oncogene and tumour suppressor gene expression, inhibition of critical signal transduction pathways such as Nrf, NF-κB, AP-1, Wnt/β-catenin, MAPK, and growth factors. These multifaceted actions extend to the induction of cell-cycle arrest and apoptosis, involving pivotal players like p53, Bcl-2, and caspase families (Huang et al., 2009).

In the context of SW480 cells, it has been documented that Epicatechin Gallate (ECG) plays a crucial role in stabilizing p53, an indispensable factor in apoptosis induction. Additionally, the activation of MAPKs (JNK and p38) mediated by p53 influences both phosphorylated p53 (p-p53) and total p53 levels. Disruption of this process and the subsequent induction of apoptotic cell death occur upon MAPKs inhibition, underscoring the intricate interplay between these pathways (Cordero-Herrera et al., 2013).

Isorhamnetin, in HCT-116 cells, exhibits a dual effect, inducing apoptosis and necrosis in a dose- and time-dependent manner (Jaramillo et al., 2010). Conversely, when metformin is combined with irinotecan, apoptosis isn't triggered in HCT116 and SW480 cells; instead, it prompts cell cycle arrest by halting progression at G1 and S phases. Notably, HCT116 cells exhibit heightened susceptibility to apoptotic cell death, as evidenced by Annexin V staining, further emphasizing the nuanced responses of different colon cancer cells to various treatments (Esra'a et al., 2021).

Sappanchalcone, at equimolar concentrations, demonstrates a pronounced impact on HCT116 cells compared to SW480 cells. It orchestrates apoptosis through intricate pathways, involving both caspase-dependent and caspase-independent mechanisms, illuminating the complexity of its regulatory role in colon cancer cells (Seo et al., 2020). These findings underscore the intricate web of molecular events orchestrated by flavonoids and their derivatives, highlighting the potential for targeted therapeutic interventions in colon cancer.

4.3.3 Effect of DHF on migration of HCT116 and SW480 cells

Traditional anti-cancer therapies have historically targeted cell proliferation processes, focusing on DNA replication and related events like cell cycle progression and apoptosis

evasion. However, these approaches often damage healthy self-renewing cells in tissues, causing significant side effects. The search for more selective targets has led to the exploration of cell motility, a fundamental component of invasion and neoangiogenesis, as a potential avenue. Investigating inhibitors with distinct mechanisms of action could offer novel strategies. Combining these inhibitors with conventional cytotoxic drugs may enhance treatment precision and efficacy, minimizing collateral damage to healthy tissues. This approach represents a paradigm shift, aiming to improve cancer therapies by harnessing the complexities of cell motility while optimizing the therapeutic potential of existing cytotoxic agents (Eccles et al., 2005).

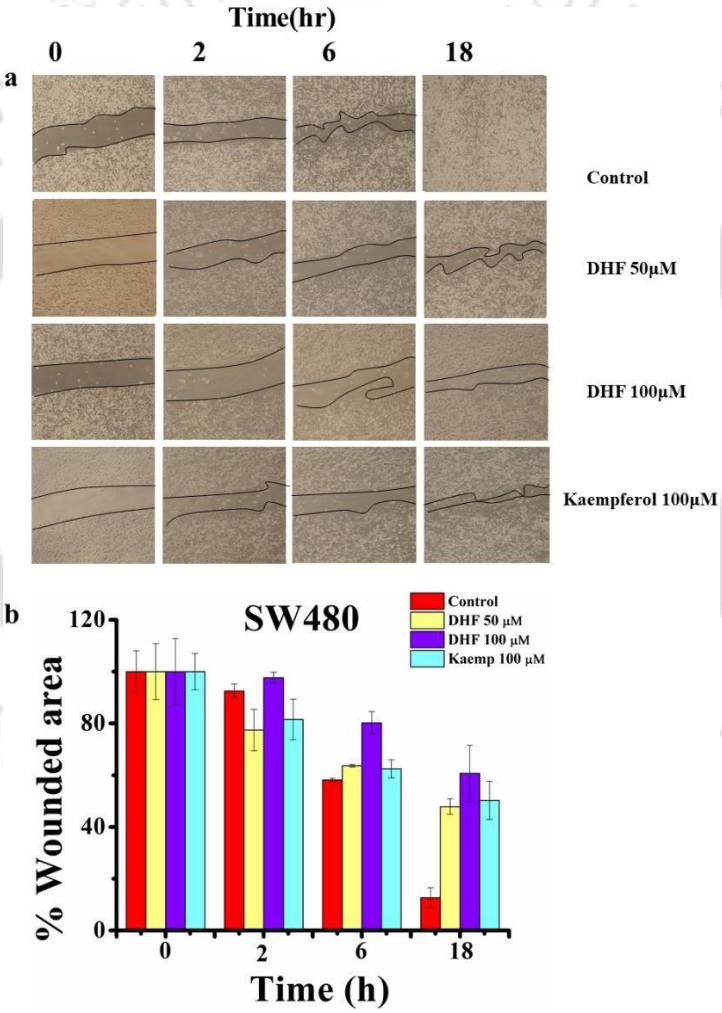

Fig. 4.4: (a) Migration assay of SW480 cells treated with DHF and Kaempferol at different time interval (0 hr-18 hrs), (b) unhealed area plotted against different time interval in SW480 cell.

Therefore, in our current investigation, we meticulously examined the impact of DHF on the migration abilities of colon cancer cells, specifically HCT116 and SW480. Employing a wound healing assay, we tracked cell migration progress over various time intervals.

When SW480 cells were treated with DHF at concentrations of 50 µM and 100 µM, a significant inhibitory effect on cell migration was observed. At different time points (0 hr, 2 hrs, 6 hrs, and 18 hrs), treatment with DHF at 50 µM resulted in remaining wound percentages of 100%, 77.4%, 63.6%, and 47.8%, respectively. Moreover, DHF at 100 µM exhibited even greater efficacy, with remaining wound percentages of 100%, 97.6%, 80.2%, and 60.7% across the same time intervals. Kaempferol at 100 µM, while slightly less effective than DHF, still significantly curtailed migration with remaining wound percentages of 100%, 81.5%, 62.4%, and 50.25% **(Fig. 4.4)**.

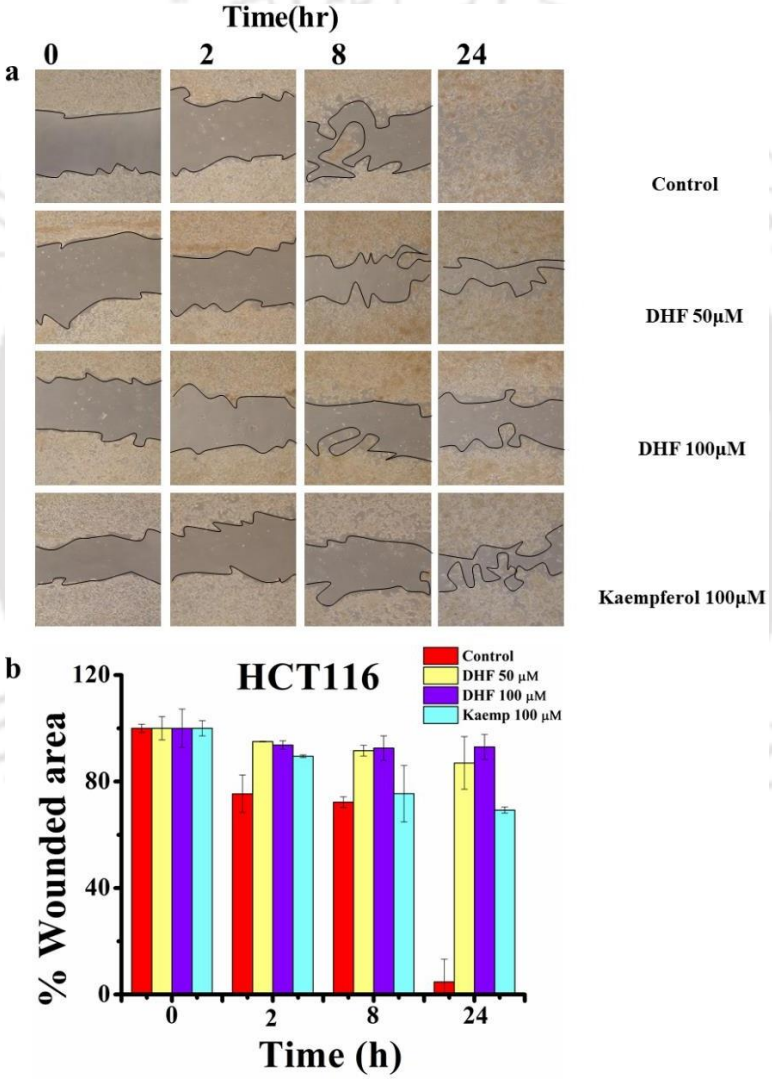

Fig. 4.5: (a) Migration assay of HCT116 cells treated with DHF and Kaempferol at different time interval (0 hr-24 hrs), (b) unhealed area plotted against different time interval in HCT116 cells

Similarly, in HCT116 cells, DHF, particularly at 100 µM, showcased remarkable efficacy in impeding cell migration. At different time points (0 hr, 2 hrs, 8 hrs, and 24 hrs), treatment with DHF at 50 µM resulted in remaining wound percentages of 100%, 95%, 91.5%, and 86.9%.

DHF at 100 μM displayed superior effectiveness, maintaining wound percentages of 100%, 93.6%, 92.5%, and 93%. Kaempferol at 100 μM also demonstrated significant inhibitory effects, with remaining wound percentages of 100%, 89.5%, 75.4%, and 69.2% **(Fig. 4.5)**.

Comparatively, both DHF and Kaempferol treatments substantially curtailed migration rates in both SW480 and HCT116 cells. Furthermore, it is noteworthy that the migratory slowdown in HCT116 cells was comparatively more pronounced than in SW480 cells. HCT116 showed more sensitivity towards DHF compared to SW480 cells. The findings indicate that DHF exerts direct influence on cellular growth and the biological characteristics of colon cancer cells. Similar observation has been reported for flavonoid baicalein where HCT116 cells were more sensitive compared to SW480 cells (Dou et al., 2018). Liquiritigenin, a flavonoid derived from Glycyrrhiza uralensis Fisch roots, has demonstrated inhibitory effects on HCT116 colorectal cancer cell invasion and epithelial-mesenchymal transition (EMT). This effect was attributed to the reduction of Runt-Related Transcription Factor 2 (Runx2) and the inactivation of the PI3K/AKT signaling pathway. Likewise, Pectolinarigenin, found in Cirsium chanroenicum (Nakai) Nakai, exhibited anti-migratory and anti-invasive properties in CT26 and HCT116 colorectal carcinoma cells. Its mechanism involved the downregulation of Matrix Metalloproteinase-9 (MMP-9) and phosphorylated Signal Transducer and Activator of Transcription 3 (STAT3). Notably, pectolinarigenin also curtailed abdominal metastasis in a murine colorectal cancer model.

It has been reported that genistin showcased anti-metastatic potential in SW480 colorectal cancer cells, primarily through the inhibition of the TTTY18/Akt pathway (Chen et al., 2020). In another study, Delphinidin exhibited anti-metastatic effects in human DLD-1, SW480, and SW620 colorectal cancer cells by targeting integrin/FAK signaling. This action was mediated by upregulating miRNA-204-3p (Huang et al., 2019). Luteolin, in HT-29 and SW480 cells, hindered migration and invasion by upregulating miR-384, which subsequently reduced the expression of Matrix Metalloproteinases 2, 3, 9, and 16 (Yao et al., 2019). Hispidulin, targeting PIM1 via inhibition of JAK2/STAT3 signaling, effectively curbed growth and metastasis in HT29 and SW480 colorectal cancer cells, and this effect extended to reducing colorectal cancer pulmonary metastasis in a xenograft animal model (Liu et al., 2018).

Moreover, the flavonoid GL-V9 exhibited significant dose-dependent reductions in colon cancer cell migration, invasion, and adhesion in HCT116 and SW480 cells (Gu et al., 2021). Astragalin, on the other hand, suppressed HCT116 cell migration by inhibiting the

expression of matrix metalloproteinases MMP-2 and MMP-9 (Yang et al., 2021). Another report suggests that the synergistic combination of naringenin and epicatechin effectively hindered cell migration and invasion in metastatic HCT116 and T84 cell lines (Dukel, 2023). These findings underscore the remarkable potential of flavonoids in impeding colon cancer metastasis, illuminating intricate molecular pathways that could pave the way for novel therapeutic strategies in combating this aggressive disease.

4.3.4 Effect of DHF on the expression profile of CXCR4, E-cadherin and N-cadherin

EMT plays a crucial role in the advancement and metastasis of various cancer types, including colon cancer. This process is characterized by the reduction in the presence of the epithelial cell junction protein E-cadherin, which leads to the destabilization of adherens junctions. In stage III colorectal cancer, a diminished expression of E-cadherin is linked to a poorer prognosis. EMT is also linked to the activation of genes encoding proteins like C-cadherin, which facilitate adhesion among mesenchymal cells (Vu and Datta, 2017). Furthermore, existing literature indicates that heightened levels of CXCR4 expression in colorectal cancer patients correlate with more advanced tumor stages and an elevated risk of both recurrence and distant metastasis (Goïta and Guenot, 2022). Therefore, to determine whether migration of HCT116 and SW480 cells on treatment with DHF and Kaempferol were associated with CXCR4, E-cadherin and N-cadherin, western blotting was performed.

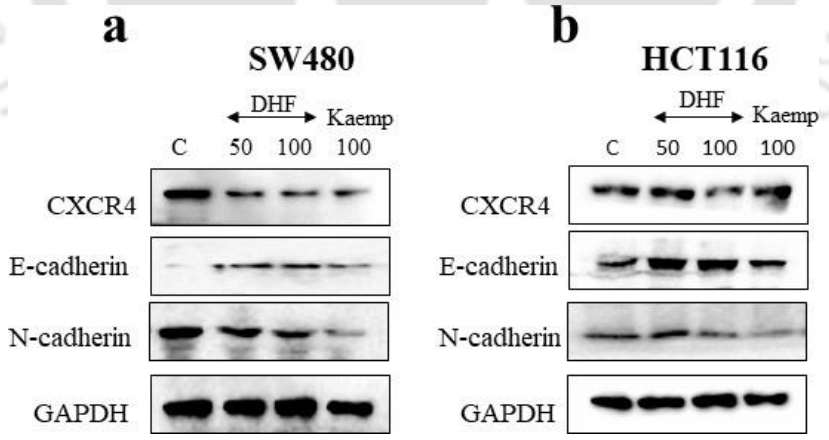

Fig. 4.6: (a) Expression profile of CXR4, E-cadherin, N-cadherin and GAPDH in HCT116 cell line, (b)Expression profile of CXR4, E-cadherin, N-cadherin and GAPDH in SW480 cell line

In HCT116 cell line it has been observed that the expression of CXCR4 has been downregulated on treatment with 100 μM DHF, N-cadherin expression has also been downregulated on treatment with 100 μM DHF and also with 100 μM Kaempferol, whereas E

cadherin expression has been upregulated on treatment with 50 μM and 100 μM DHF, also treatment with 100 μM Kaempferol upregulated the expression of N-cadherin in HCT116 cells **(Fig. 4.6 a)**.

The expression of CXCR4 on treatment with DHF (50 μM and 100 μM) and Kaempferol 100 μM was downregulated in SW480 cells, the expression of N-cadherin was also downregulated on treatment with DHF and Kaempferol at about same concentration, whilethe expression of E-cadherin was upregulated on treatment with DHF and kaempferol **(Fig 4.6b)**.

In SW480 cells, the results demonstrate a reduction in CXCR4 (**Fig. 4.7 a)** expression levels relative to GAPDH when treated with DHF at concentrations of 50 μM and 100 μM, as well as when treated with Kaempferol at 100 μM. It reveals a noteworthy increase in E-cadherin (**Fig. 4.7 b**) expression fold change upon treatment with 50 μM DHF, followed by an even greater

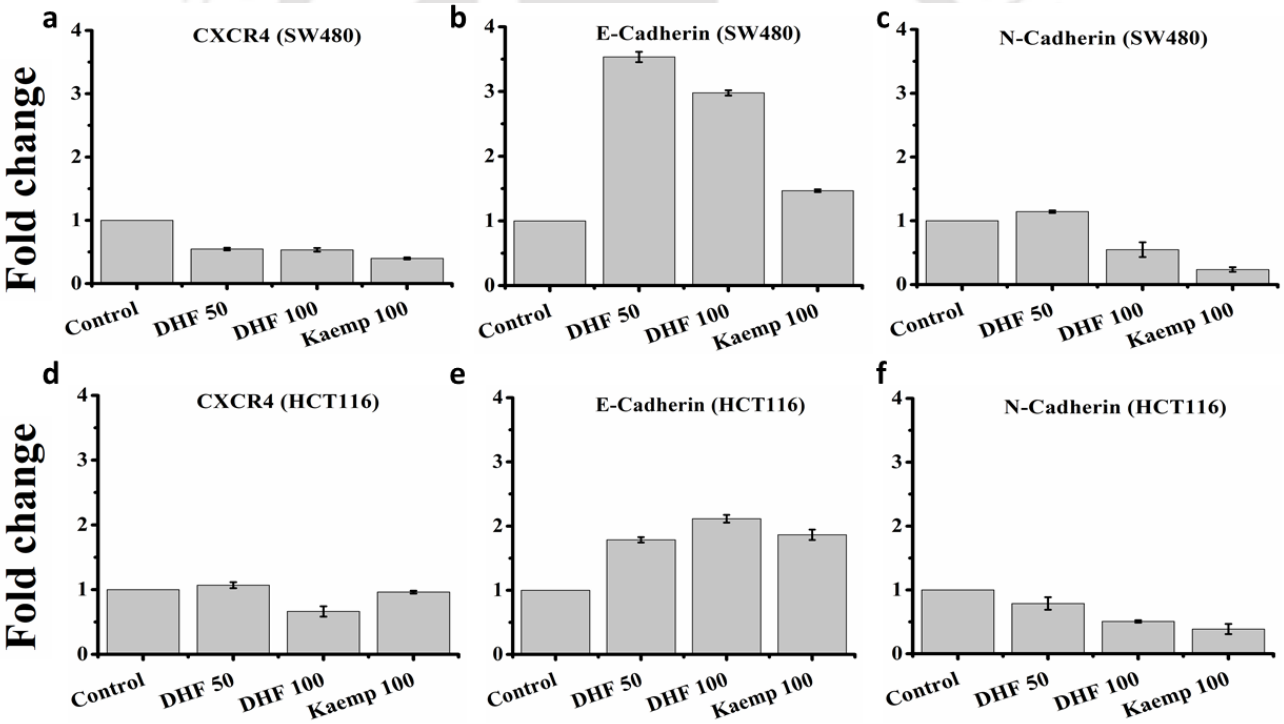

Fig. 4.7: Fold change in protein expression with respect to GAPDH in (a) CXCR4 in SW480 cells, (b) E-Cadherin in SW480 cells, (c) N-Cadherin in SW480 cells, (d) CXCR4 in HCT116 cells, (e) E-Cadherin in HCT116 cells, (f) N-Cadherin in HCT116 cells

increase with 100 μM DHF, and a similar effect with 100 μM Kaempferol. The data suggests that there is no substantial change in N-cadherin (**Fig. 4.7 c)** expression fold change when treated with 50 μM DHF. However, treatment with 100 μM DHF leads to a decrease in fold change, and the same pattern is observed with 100 μM Kaempferol treatment as well. In prior studies, it was observed that the introduction of exogenous miR-146a led to the suppression of

CXCR4 expression in SW480 cells. This suppression coincided with a decrease in the expression of genes associated with EMT and a subsequent reduction in the rate of cell migration (Afshar-Khamseh et al., 2021). Our finding also suggests that DHF is effective in inhibiting the migration rate of SW480 cells by downregulating the expression of N- cadherin and upregulating the expression of E-cadherin.

In HCT116 cells, the expression fold change of CXCR4 relative to GAPDH remains relatively stable when treated with 50 μM DHF but decreases notably when treated with 100 μM DHF **(Fig. 4.7 d)**. However, there is no significant change in expression fold change when exposed to 100 μM Kaempferol. It reveals an increase in E-cadherin **(Fig. 4.7 e)** expression fold change relative to GAPDH upon treatment with 50 μM DHF, 100 μM DHF, and 100 μM Kaempferol. The result indicates a substantial decrease in C-cadherin **(Fig. 4.7 f)** expression fold change concerning GAPDH when treated with 100 μM DHF and 100 μM Kaempferol, with a slight decrease observed with 50 μM DHF treatment. Our findings imply that DHF hinders migration in HCT116 cells through the downregulation of CXCR4 and N-cadherin expression, while concurrently upregulating the expression of E-cadherin. It has been reported that colon cancer metastasis can be inhibited by silencing CXCR4 (Marchesi et al., 2004). Also, it has been reported that All-trans retinoic acid (ATRA) triggers the activation of E-Cadherin expression through promoter hypomethylation, enabling Sp1 binding to its recognition sites within human colon carcinoma HCT116 cells. Consequently, this process enhances cell-to-cell interactions, diminishes cell migration, and leads to the downregulation of Vimentin and Fibronectin levels in HCT116 cells (Woo and Jang, 2012). Demonstration of N-cadherin downregulation has revealed its ability to instigate cell cycle arrest, subsequently leading to apoptosis, as well as diminished invasiveness and reduced tumour formation (Li et al., 2010).

The comparative analysis of expression fold changes in both cell types reveals a more pronounced downregulation of CXCR4 in SW480 cells compared to HCT116 cells. Additionally, the fold change indicating upregulation of E-cadherin is notably more significant in SW480 cells in contrast to HCT116 cells. Conversely, the fold change indicating downregulation of N-cadherin is more substantial in the case of HCT116 cells when compared to SW480 cells (**Fig. 4.7**).

Therefore, these results indicate that DHF has a downregulating effect on CXCR4 and N-cadherin expression in both the cell lines. Whereas, DHF upregulates the expression of E-cadherin in both HCT116 and SW480 cells. Therefore, it could be concluded that DHF inhibits

the migration of HCT116 and SW480 cells by downregulating the expression of CXCR4 and N-cadherin while upregulating the expression of E-cadherin in a dose dependent manner.

4.3.5: Colony formation assay

Apart from proliferation, the survival of cancer cell is also important. Therefore, to investigate the survival potential of HCT116 in presence of DHF and Kaempferol colony formation assay was performed. We performed colony formation assay only in HCT16 cells based on the cell proliferation and migration assay result which showed that HCT116 cells were more sensitive compared to SW480 cells. This assay is based on the ability of a single cell to grow into a colony.

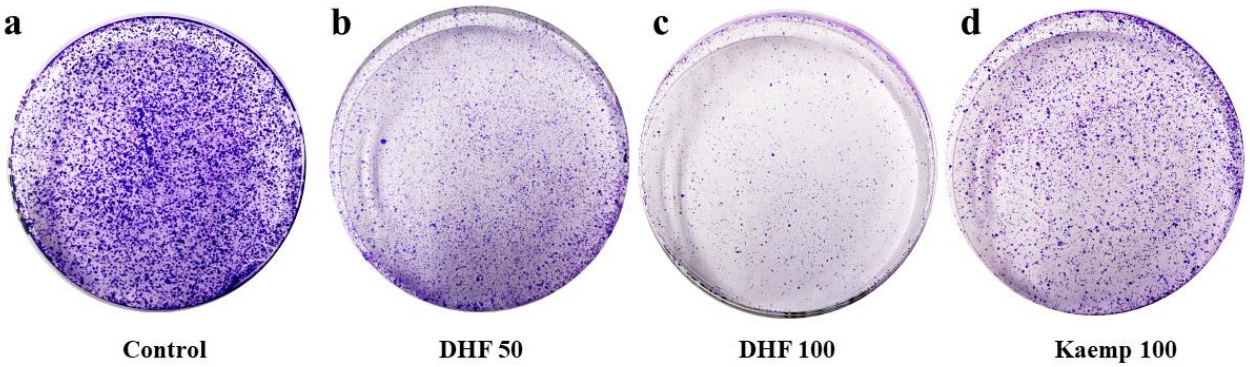

Fig. 4.8: Colony formation assay in HCT116 cells in presence of (a) Control (DMSO), (b) 50 µM DHF, (c) 100 µM DHF, (d) 100 µM Kaempferol

The ability of each cell to undergo unlimited division is tested in this assay (Franken et al., 2006). The colony forming efficiency of HCT116 cells were analysed on treatment with DHF (50 and 100 µM) and Kaempferol (100 µM) with respect to control (DMSO 99.9%). It has been observed that the colony formation efficiency of HCT116 cells were significantly reduced in presence of 50 µM DHF **(Fig. 4.8 b)**, 100 µM DHF **(Fig. 4.8 c)** and 100 µM Kaempferol **(Fig 4.8 d)** compared to control **(Fig. 4.8 a)**. The highest reduction in colony formation was observed in treatment with 100 µM DHF followed by 50 µM DHF and 100 µM Kaempferol. The result suggests that DHF reduces the colony formation efficacy of HCT116 cells thereby affecting its cell proliferation and might play important role in suppressing cell migration in HCT116 cells. It has been reported that the potent inhibitory effects of the methanolic extract derived from *Eclipta alba* on crucial aspects vital for cancer cell growth and proliferation. Specifically, this extract effectively hampers the ability of cancer cells to form colonies and impedes their migratory potential, crucial processes linked to metastasis. These inhibitory effects were notably observed in HCT116 cells (Nelson et al., 2020). Metastasis, a multifaceted

biological phenomenon involving cancer cell invasion and migration, stands as a prominent factor contributing to cancer-related mortality. Consequently, diverse research groups are diligently exploring potential drug candidates to inhibit metastasis, aiming to curtail tumour growth effectively (Khan et al., 2016).

4.4 Conclusions

In our study, it was observed that DHF does not exhibit cytotoxic effects on normal cells. In contrast, in colon cancer cell lines, DHF demonstrates a moderate impact, inducing cell death and inhibiting cell proliferation. Notably, DHF significantly impedes cell migration in colon cancer cell lines by upregulating E-cadherin expression and concomitantly downregulating CXCR4 and N-cadherin expression. Furthermore, DHF significantly diminishes the colony formation efficiency of HCT116 cells. These findings collectively underscore the potential of DHF as a promising therapeutic agent in the context of colon cancer treatment, showcasing its specific inhibitory effects on cancer cell proliferation, migration, and colony formation.

SUMMARY

3,5-dihydroxy-7,4'- dimethoxyflavone (DHF) was isolated and purified from the mature leaves of *Alpinia nigra*. The absorption spectra of DHF, when subjected to a diverse array of organic solvents, divulged the presence of three distinct absorption bands localized at 270 nm, 330 nm, and 365 nm. However, DHF conspicuously exhibited an absence of appreciable absorption peaks in water, thereby depicting its poor water solubility and non-polar nature. The meticulous examination of DHF's solubility across a spectrum of pH conditions (ranging from 2 to 13) yielded profound insights. Within the ambit of acidic pH, DHF exhibited poor solubility. Contrarily, under the alkaline influence of pH 13, the compound exhibited its highest degree of solubility, a phenomenon accentuated by a significant red shift of the absorption peak from 365 nm to a discernibly extended wavelength of 406 nm. Elucidating the compound's behaviour within surfactant micellar systems in relation to solubility and stability unveiled intriguing observations. DHF exhibited an enhanced solubility within all different (SDS, CTAB and T20) surfactant micelles across the pH (2-13) spectrum, surpassing its solubility levels in organic solvents. Nonetheless, in the presence of higher alkaline pH, DHF's stability was perturbed, leading to its degradation, even in the protective context of surfactant micelles. The fluorescence study of DHF shed light on its emission characteristics in differing environments. DHF exhibited weak fluorescence intensity within organic solvents and under alkaline pH conditions upon excitation at 365 nm. In contrast, a time-dependent fluorescence analysis of DHF within surfactant micellar systems, across various pH (2-13) conditions, unveiled a heightened fluorescence intensity. Notably, this enhancement was significantly pronounced when compared to both organic solvents and alkaline pH solutions, when excited at 365 nm. Remarkably, DHF exhibited highest fluorescence intensity in the presence of CTAB micelles at pH 9, particularly when excited at 425 nm. The objective of this study resided in increasing the understanding of DHF's chemical attributes, with the ultimate aspiration of harnessing its health-enhancing potential by averting susceptibility to environmental degradation. This study provides insights into better understanding of DHF solubility and stability. Further research along this path hold promise in not only shaping functional food products enriched with bioactive constituents but also in establishing the therapeutic properties inherently harboured by DHF.

Furthermore, interaction between DHF and Hen Egg White Lysozyme (HEWL) aggregates, conducted under different pH conditions of 2, 5, and 12.2, has uncovered intriguing

revelations. At pH 2, DHF exhibited interaction with HEWL, notably manifesting an inclination to inhibit the progression of aggregate fibrillation. Conversely, under the conditions of pH 5, DHF's inhibitory influence was confined to a lack of efficacy against amorphous HEWL aggregates. Notably, at alkaline pH 12.2, DHF exhibited a mild hindrance of HEWL aggregates, indicating a partial attenuation of its functional attributes owing to potential degradation in the higher alkaline pH. Within the confines of the current investigation, DHF emerges as a potent suppressor of amyloid fibrillation within the HEWL aggregates at pH 2. Moreover, our findings suggest an intriguing facet: DHF appears potent with the capacity to modulate the fibrillation trajectory of the protein, steering it towards the formation of amorphous aggregates throughout the aggregation process. By shedding light on these intricate interactions, this study not only augments our comprehension of DHF's potential therapeutic applications but also furnishes a framework for the systematic exploration of novel compounds with inhibitory attributes.

Lastly, the effect of DHF on colon cancer cells HCT116 and SW480 was studied by cell viability assays, cell proliferation assay, and migration assay and western blotting of specific proteins related to migration. The cell viability assay which was carried out by MTT revealed that DHF is not cytotoxic to normal HaCaT cells and HCT116 cells were more sensitive to DHF, while SW480 shows more sensitivity towards 5FU compared to HCT116. Cell proliferation by MTT assay revealed that inhibition in cell proliferation in both the cell lines HCT116 and SW480 cell on treatment with DHF was observed. HCT116 cells were more sensitive to DHF compared to SW480, while SW480 cells were more sensitive to 5FU compared to HCT116. HCT116 showed more sensitivity to kaempferol compared to SW480.Whereas, the cell death analysis of SW480 and HCT116 by PI and PI-Annexin using FACS revealed that there is no significant cell death in both the cell lines on treatment with DHF and kaempferol. The above results signified that DHF does not kill HCT116 and SW480 cells, rather inhibited their proliferation. The migration assay revealed that significant suppression of migration in HCT116 and SW480 was observed in presence of DHF. DHF altered the expression of specific proteins E-cadherin, N-cadherin and CXCR4 playing pivotal role in the EMT pathway related to migration.

Therefore, the present thesis work contributes a valuable perspective towards comprehending the inherent chemical characteristics, solubility dynamics, and stability attributes, all of which hold pivotal implications in the realm of efficacious drug carrier platforms tailored for precise and targeted drug delivery strategies. Moreover, the study delves

into the biological effects inherent to DHF, with the primary objective of unraveling its potential as a promising candidate within the domain of drug molecules.

Future Prospects

The primary objective of this research was to enhance our understanding of the chemical properties of the compound DHF, with the goal of preserving its health benefits by preventing degradation due to environmental factors. Through this study, valuable insights into DHF solubility and stability were gained. These findings pave the way for future investigations aimed at developing functional food products containing bioactive compounds, as well as exploring the therapeutic potential of DHF.

One significant discovery in this study was DHF's ability to effectively inhibit the amyloid fibrillation of HEWL. Our results indicate that DHF can influence the aggregation process, redirecting the protein fibrillation pathway towards the formation of amorphous aggregates. This observation sheds light on the mechanisms through which DHF inhibits amyloid fibrillation and offers valuable guidelines for identifying novel inhibitors.

Additionally, our research revealed that DHF treatment led to the inhibition of proliferation and reduced wound healing in HCT116 and SW480 cancer cells. Notably, DHF did not exhibit cytotoxic effects on normal HaCaT cells. While it was found to be non-cytotoxic against cancer cells, DHF demonstrated cytostatic properties by impeding the migration of cancer cells HCT116 and SW480. This ability to hinder cell migration is crucial in the context of metastatic tumours. Consequently, further investigations should delve into the underlying signaling mechanisms and therapeutic efficacy of DHF in *in vivo* mouse models. These findings offer promising prospects for developing interventions targeting cancer metastasis.

References

References

Afshar-Khamseh, R., Javeri, A., Taha, M. F. (2021). MiR-146a suppresses the expression of CXCR4 and alters survival, proliferation and migration rate in colorectal cancer cells. *Tissue and Cell*, *73*, 101654.

Agati, G., Biricolti, S., Guidi, L., Ferrini, F., Fini, A., Tattini, M. (2011). The biosynthesis of flavonoids is enhanced similarly by UV radiation and root zone salinity in *L. vulgare* leaves. *Journal of Plant Physiology*, *168*(3), 204–212.

Ahmad, B., Borana, M. S., Chaudhary, A. P. (2017). Understanding curcumin-induced modulation of protein aggregation. *International Journal of Biological Macromolecules*, *100*, 89–96.

Ahmad, Z., Shah, A., Siddiq, M., Kraatz, H.-B. (2014). Polymeric micelles as drug delivery vehicles. *Rsc Advances*, *4*(33), 17028–17038.

Ahmed, A. M. A., Sharmen, F., Mannan, A., Rahman, M. A. (2015). Phytochemical, analgesic, antibacterial, and cytotoxic effects of *Alpinia nigra* (Gaertn.) Burtt leaf extract. *Journal of Traditional and Complementary Medicine*, *5*(4), 248–252.

Ahmed, E., Arshad, M., Khan, M. Z., Amjad, M. S., Sadaf, H. M., Riaz, I., Sabir, S., Ahmad, N. (2017). Secondary metabolites and their multidimensional prospective in plant life. *Journal of Pharmacognosy and Phytochemistry*, *6*(2), 205–214.

Ahsan, N., Mishra, S., Jain, M. K., Surolia, A., Gupta, S. (2015). Curcumin Pyrazole and its derivative (N-(3-Nitrophenylpyrazole) Curcumin inhibit aggregation, disrupt fibrils and modulate toxicity of Wild type and Mutant α-Synuclein. *Scientific Reports*, *5*(1), 9862.

Allard, P.-M., Bisson, J., Azzollini, A., Pauli, G. F., Cordell, G. A., Wolfender, J.-L. (2018). Pharmacognosy in the digital era: shifting to contextualized metabolomics. *Current Opinion in Biotechnology*, *54*, 57–64.

Amrati, F. E.-Z., Bourhia, M., Slighoua, M., Salamatullah, A. M., Alzahrani, A., Ullah, R., Bari, A., Bousta, D. (2021). Traditional medicinal knowledge of plants used for cancer treatment by communities of mountainous areas of Fez-Meknes-Morocco. *Saudi Pharmaceutical Journal*, *29*(10), 1185–1204.

An, W. F., Tolliday, N. (2010). Cell-based assays for high-throughput screening. *Molecular Biotechnology*, *45*, 180–186.

Androutsopoulos, V. P., Mahale, S., Arroo, R. R. J., Potter, G. (2009). Anticancer effects of the flavonoid diosmetin on cell cycle progression and proliferation of MDA-MB 468 breast cancer cells due to CYP1 activation. *Oncology Reports*, *21*(6), 1525–1528.

Ansari, M. Z., Kumar, A., Ahari, D., Priyadarshi, A., Lolla, P., Bhandari, R., Swaminathan, R. (2018). Protein charge transfer absorption spectra: an intrinsic probe to monitor structural and oligomeric transitions in proteins. *Biophysical Journal*, *114*(3), 586a.

Apter, B., Lapshina, N., Lapsker, I., Handelman, A., Accardo, A., Diaferia, C., Morelli, G., Rosenman, G. (2021). Fold-Sensitive Visible Fluorescence in β-Sheet Peptide Structures. *Advanced Optical Materials*, *9*(23), 2002247.

Aqil, F., Munagala, R., Jeyabalan, J., Vadhanam, M. V. (2013). Bioavailability of phytochemicals and its enhancement by drug delivery systems. *Cancer Letters*, *334*(1), 133–141.

Arisan, E. D., Ergül, Z., Bozdağ, G., Rencüzoğulları, Ö., Çoker-Gürkan, A., Obakan-Yerlikaya, P., Coşkun, D., Palavan-Ünsal, N. (2018). Diclofenac induced apoptosis via altering PI3K/Akt/MAPK signaling axis in HCT 116 more efficiently compared toSW480 colon cancer cells. *Molecular Biology Reports*, *45*(6), 2175–2184.

Ashraf, M. A. (2020). Phytochemicals as potential anticancer drugs: time to ponder nature's bounty. *BioMed Research International*, *2020*.

Atanasov, A. G., Zotchev, S. B., Dirsch, V. M., Supuran, C. T. (2021). Natural products in drug discovery: Advances and opportunities. *Nature Reviews Drug Discovery*, *20*(3), 200–216.

Bansal, S. S., Goel, M., Aqil, F., Vadhanam, M. V, Gupta, R. C. (2011). Advanced drug delivery systems of curcumin for cancer chemoprevention. *Cancer Prevention Research*, *4*(8), 1158–1171.

Baruah, D., Goswami, M., Yadav, R. N. S., Yadav, A., Das, A. M. (2018). Biogenic synthesis of gold nanoparticles and their application in photocatalytic degradation of toxic dyes. *Journal of Photochemistry and Photobiology B: Biology*, *186*, 51–58.

Bassi, P., Kaur, G. (2010). pH modulation: a mechanism to obtain pH-independent drug release. *Expert Opinion on Drug Delivery*, *7*(7), 845–857.

Basu, M., Hassan, P. A., Shelar, S. B. (2023). Modulation of Surfactant Self-Assembly in Deep Eutectic Solvents and its relevance to Drug Delivery-A Review. *Journal of Molecular*

Liquids, 121301.

Benowitz, S. (1996). As war on cancer hits 25-year mark, scientists see progress, challenges. *Scientist*, *10*(24), 1.

Berli, F. J., Moreno, D., Piccoli, P., Hespanhol-Viana, L., Silva, M. F., Bressan-Smith, R., Cavagnaro, J. B., Bottini, R. (2010). Abscisic acid is involved in the response of grape (*Vitis vinifera* L.) cv. Malbec leaf tissues to ultraviolet-B radiation by enhancing ultraviolet-absorbing compounds, antioxidant enzymes and membrane sterols. *Plant, Cell and Environment*, *33*(1), 1–10.

Betts, J. W., Sharili, A. S., Phee, L. M., Wareham, D. W. (2015). *In vitro* activity of epigallocatechin gallate and quercetin alone and in combination versus clinical isolates of methicillin-resistant *Staphylococcus aureus*. *Journal of Natural Products*, *78*(8), 2145–2148.

Bhatt, K. C., Malav, P. K., Ahlawat, S. P. (2018). 'Jumin' a traditional beverage of Nocte tribe in Arunachal Pradesh: an ethnobotanical survey. *Genetic Resources and Crop Evolution*, *65*(2), 671–677.

Bhattacharya, A., Bhowmik, S., Singh, A. K., Kodgire, P., Das, A. K., Mukherjee, T. K. (2017). Direct evidence of intrinsic blue fluorescence from oligomeric interfaces of human serum albumin. *Langmuir*, *33*(40), 10606–10615.

Bhunia, D., Mondal, A. K. (2012). Systematic analysis (morphology, anatomy and palynology) of an aquatic medicinal plant water mimosa (*Neptunia oleracea* Lour.) in Eastern India. *International Journal Life Sciences Biotechnology and Pharma Research*, *1*(2), 290–319.

Biasutto, L., Mattarei, A., Sassi, N., Azzolini, M., Romio, M., Paradisi, C., Zoratti, M. (2014). Improving the efficacy of plant polyphenols. *Anti-Cancer Agents in Medicinal Chemistry (Formerly Current Medicinal Chemistry-Anti-Cancer Agents)*, *14*(10), 1332–1342.

Bisht, S., Feldmann, G., Soni, S., Ravi, R., Karikar, C., Maitra, A., Maitra, A. (2007). Polymeric nanoparticle-encapsulated curcumin. *Journal of Nanobiotechnology*, *5*(1), 1–18.

Borana, M. S., Mishra, P., Pissurlenkar, R. R. S., Hosur, R. V, Ahmad, B. (2014). Curcumin and kaempferol prevent lysozyme fibril formation by modulating aggregation kinetic parameters. *Biochimica et Biophysica Acta (BBA)-Proteins and Proteomics*, *1844*(3),

670–680.

Bourgaud, F., Gravot, A., Milesi, S., Gontier, E. (2001). Production of plant secondary metabolites: a historical perspective. *Plant Science*, *161*(5), 839–851.

Bradford, M. M. (1976). A rapid and sensitive method for the quantitation of microgram quantities of protein utilizing the principle of protein-dye binding. *Analytical Biochemistry*, *72*(1–2), 248–254.

Bu, X.-L., Rao, P. P. N., Wang, Y.-J. (2016). Anti-amyloid aggregation activity of natural compounds: implications for Alzheimer's drug discovery. *Molecular Neurobiology*, *53*, 3565–3575.

Budisan, L., Gulei, D., Jurj, A., Braicu, C., Zanoaga, O., Cojocneanu, R., Pop, L., Raduly, L., Barbat, A., Moldovan, A. (2019). Inhibitory effect of CAPE and kaempferol in colon cancer cell lines—possible implications in new therapeutic strategies. *International Journal of Molecular Sciences*, *20*(5), 1199.

Cádiz-Gurrea, M. de la L., Fernández-Arroyo, S., Segura-Carretero, A. (2014). Pine bark and green tea concentrated extracts: antioxidant activity and comprehensive characterization of bioactive compounds by HPLC–ESI-QTOF-MS. *International Journal of Molecular Sciences*, *15*(11), 20382–20402.

Callcott, E. (2019). The potential of coloured-rice derived polyphenols in alleviating obesity-related oxidative stress and inflammation.

Campbell, P. I. (1983). Toxicity of some charged lipids used in liposome preparations. *Cytobios*, *37*(145), 21–26.

Cantor, C. R., Schimmel, P. R. (1980). Techniques for the study of biological structure and function.

Chakrabartty, I., Vijayasekhar, A., Rangan, L. (2021). Therapeutic potential of labdane diterpene isolated from *Alpinia nigra*: detailed hemato-compatibility and antimicrobial studies. *Natural Product Research*, *35*(6), 1000–1004.

Challa, R., Ahuja, A., Ali, J., Khar, R. K. (2005). Cyclodextrins in drug delivery: an updated review. *Aaps Pharmscitech*, *6*, E329–E357.

Chan, F. T. S., Schierle, G. S. K., Kumita, J. R., Bertoncini, C. W., Dobson, C. M., Kaminski,

C. F. (2013). Protein amyloids develop an intrinsic fluorescence signature during aggregation. *Analyst*, *138*(7), 2156–2162.

Chandu, V. P., Arunachalam, A., Jeganath, S., Yamini, K., Tharangini, K., Chaitanya, G. (2012). Niosomes: a novel drug delivery system. *International Journal of Novel Trends in Pharmaceutical Sciences*, *2*(1), 25–31.

Chang, C., Li, J., Su, Y., Gu, L., Yang, Y., Zhai, J. (2022). Protein particle-based vehicles for encapsulation and delivery of nutrients: Fabrication, digestion, and release properties. *Food Hydrocolloids*, *123*, 106963.

Chareonkla, A., Pohmakotr, M., Reutrakul, V., Yoosook, C., Kasisit, J., Napaswad, C., Tuchinda, P. (2011). A new diarylheptanoid from the rhizomes of Zingiber mekongense. *Fitoterapia*, *82*(4), 534–538.

Chat, O. A., Najar, M. H., Mir, M. A., Rather, G. M., Dar, A. A. (2011). Effects of surfactant micelles on solubilization and DPPH radical scavenging activity of Rutin. *Journal of Colloid and Interface Science*, *355*(1), 140–149.

Chen, X., Wu, Y., Gu, J., Liang, P., Shen, M., Xi, J., Qin, J. (2020). Anti-invasive effect and pharmacological mechanism of genistein against colorectal cancer. *Biofactors*, *46*(4), 620–628.

Chiti, F., Dobson, C. M. (2006). Protein misfolding, functional amyloid, and human disease. *Annu. Rev. Biochem.*, *75*, 333–366.

Christoff, M., Toscano, V. G., Baader, W. J. (1996). Influence of methoxy substitution on flavonoid photophysics: a steady state and laser flash photolysis study. *Journal of Photochemistry and Photobiology A: Chemistry*, *101*(1), 11–20.

Chung, H. S., Chang, L. C., Lee, S. K., Shamon, L. A., Van Breemen, R. B., Mehta, R. G., Farnsworth, N. R., Pezzuto, J. M., Kinghorn, A. D. (1999). Flavonoid constituents of Chorizanthe diffusa with potential cancer chemopreventive activity. *Journal of Agricultural and Food Chemistry*, *47*(1), 36–41.

Chuwa, A. H., Sone, K., Oda, K., Tanikawa, M., Kukita, A., Kojima, M., Oki, S., Fukuda, T., Takeuchi, M., Miyasaka, A. (2018). Kaempferol, a natural dietary flavonoid, suppresses 17β-estradiol-induced survivin expression and causes apoptotic cell death in endometrial cancer. *Oncology Letters*, *16*(5), 6195–6201.

Coppock, R. W., Dziwenka, M. (2016). Green Tea Extract. In *Nutraceuticals: Efficacy, Safety and Toxicity* (pp. 633–652).

Cordero-Herrera, I., Martín, M. A., Bravo, L., Goya, L., Ramos, S. (2013). Epicatechin gallate induces cell death via p53 activation and stimulation of p38 and JNK in human colon cancer SW480 cells. *Nutrition and Cancer*, *65*(5), 718–728.

Cornard, J. P., Merlin, J. C., Boudet, A. C., Vrielynck, L. (1997). Structural study of quercetin by vibrational and electronic spectroscopies combined with semiempirical calculations. *Biospectroscopy*, *3*(3), 183–193.

Corson, T. W., Crews, C. M. (2007). Molecular understanding and modern application of traditional medicines: triumphs and trials. *Cell*, *130*(5), 769–774.

Cragg, G. M., Newman, D. J. (2005). Plants as a source of anti-cancer agents. In *Journal of Ethnopharmacology* (Vol. 100, Issues 1–2, pp. 72–79).

Csokay, B., Prajda, N., Weber, G., Olah, E. (1997). Molecular mechanisms in the antiproliferative action of quercetin. *Life Sciences*, *60*(24), 2157–2163.

Čudina, O., Brborić, J., Janković, I., Karljiković-Rajić, K., Vladimirov, S. (2008). Study of valsartan interaction with micelles as a model system for biomembranes. *Colloids and Surfaces B: Biointerfaces*, *65*(1), 80–84.

Cuevas, A., Saavedra, N., Salazar, L. A., Abdalla, D. S. P. (2013). Modulation of immune function by polyphenols: possible contribution of epigenetic factors. *Nutrients*, *5*(7), 2314–2332.

D'Amelia, V., Aversano, R., Chiaiese, P., Carputo, D. (2018). The antioxidant properties of plant flavonoids: their exploitation by molecular plant breeding. *Phytochemistry Reviews*, *17*, 611–625.

D'Arcy, M. S. (2022). A review of biologically active flavonoids as inducers of autophagy and apoptosis in neoplastic cells and as cytoprotective agents in non-neoplastic cells. *Cell Biology International*, *46*(8), 1179–1195.

Danishefsky, S. (2010). On the potential of natural products in the discovery of pharma leads: a case for reassessment. *Natural Product Reports*, *27*(8), 1114–1116.

Das, B. N., Qais, N. (2012). Antibacterial and cytotoxic activities of the rhizome extract of

Alpinia nigra. *Pharmacie Globale*, *3*(3), 1.

Dearden, J. C., Forbes, W. F. (1959). Light absorption studies: Part XIV. The ultraviolet absorption spectra of phenols. *Canadian Journal of Chemistry*, *37*(8), 1294–1304.

Delin, W., Larsen, K. (2000). Zingiberaceae. *Flora of China*, *24*(1), 322–377.

Dhouafli, Z., Cuanalo-Contreras, K., Hayouni, E. A., Mays, C. E., Soto, C., Moreno-Gonzalez, I. (2018). Inhibition of protein misfolding and aggregation by natural phenolic compounds. *Cellular and Molecular Life Sciences*, *75*, 3521–3538.

Dou, J., Wang, Z., Ma, L., Peng, B., Mao, K., Li, C., Su, M., Zhou, C., Peng, G. (2018). Baicalein and baicalin inhibit colon cancer using two distinct fashions of apoptosis and senescence. *Oncotarget*, *9*(28), 20089.

Dukel, M. (2023). Combination of naringenin and epicatechin sensitizes colon carcinoma cells to anoikis via regulation of the epithelial–mesenchymal transition (EMT). *Molecular and Cellular Toxicology*, *19*(1), 187–203.

Duval, R., Duplais, C. (2017). Fluorescent natural products as probes and tracers in biology. *Natural Product Reports*, *34*(2), 161–193.

Duyckaerts, C., Delatour, B., Potier, M.-C. (2009). Classification and basic pathology of Alzheimer disease. *Acta Neuropathologica*, *118*, 5–36.

Eccles, S. A., Box, C., Court, W. (2005). Cell migration/invasion assays and their application in cancer drug discovery. *Biotechnology Annual Review*, *11*, 391–421.

Esra'a, I. K., Ismail, W. W., Mhaidat, N. M., Alqudah, M. A. (2021). Effect of metformin on irinotecan-induced cell cycle arrest in colorectal cancer cell lines HCT116 and SW480. *International Journal of Health Sciences*, *15*(5), 34.

Eugster, P. J., Guillarme, D., Rudaz, S., Veuthey, J.-L., Carrupt, P.-A., Wolfender, J.-L. (2011). Ultra high pressure liquid chromatography for crude plant extract profiling. *Journal of AOAC International*, *94*(1), 51–70.

Finkelstein, A. V, Badretdin, A. J., Galzitskaya, O. V, Ivankov, D. N., Bogatyreva, N. S., Garbuzynskiy, S. O. (2017). There and back again: Two views on the protein folding puzzle. *Physics of Life Reviews*, *21*, 56–71.

Folch, J., Ettcheto, M., Petrov, D., Abad, S., Pedrós, I., Marin, M., Olloquequi, J., Camins, A.

(2018). Review of the advances in treatment for Alzheimer disease: strategies for combating β-amyloid protein. *Neurología (English Edition)*, *33*(1), 47–58.

Franken, N. A. P., Rodermond, H. M., Stap, J., Haveman, J., Van Bree, C. (2006). Clonogenic assay of cells *in vitro*. *Nature Protocols*, *1*(5), 2315–2319.

GF, P. (1991). The quest for commercial production of chemicals from plant cell culture. *Plant Cell and Tissue Culture in Liquid Systems*, 1–10.

Ghosh, S., Banerjee, S., Sil, P. C. (2015). The beneficial role of curcumin on inflammation, diabetes and neurodegenerative disease: A recent update. *Food and Chemical Toxicology*, *83*, 111–124.

Ghosh, S., Ozek, T., Tabanca, N., Ali, A., ur Rehman, J., Khan, I. A., Rangan, L. (2014). Chemical composition and bioactivity studies of *Alpinia nigra* essential oils. *Industrial Crops and Products*, *53*, 111–119.

Ghosh, S., Padilla-González, G. F., Rangan, L. (2013). *Alpinia nigra* seeds: a potential source of free radical scavenger and antibacterial agent. *Industrial Crops and Products*, *49*, 348–356.

Ghosh, S., Pandey, N. K., Dasgupta, S. (2013). (−)-Epicatechin gallate prevents alkali-salt mediated fibrillogenesis of hen egg white lysozyme. *International Journal of Biological Macromolecules*, *54*, 90–98.

Ghosh, S., Rangan, L. (2014). Molecular docking and inhibition studies of α-amylase activity by labdane diterpenes from *Alpinia nigra* seeds. *Medicinal Chemistry Research*, *23*(11), 4836–4852.

Ghosh, S., Singh, R. K., Kumar Dubey, V., Rangan, L. (2017). Antileishmanial activity of labdane diterpenes isolated from *Alpinia nigra* seeds. *Letters in Drug Design and Discovery*, *14*(1), 119–124.

Gierschner, J., Duroux, J.-L., Trouillas, P. (2012). UV/Visible spectra of natural polyphenols: A time-dependent density functional theory study. *Food Chemistry*, *131*(1), 79–89.

Ginwala, R., Bhavsar, R., Chigbu, D. G. I., Jain, P., Khan, Z. K. (2019). Potential role of flavonoids in treating chronic inflammatory diseases with a special focus on the anti-inflammatory activity of apigenin. *Antioxidants*, *8*(2), 35.

Goïta, A. A., Guenot, D. (2022). Colorectal Cancer: The Contribution of CXCL12 and Its Receptors CXCR4 and CXCR7. *Cancers*, *14*(7).

Gong, J., Chen, M., Zheng, Y., Wang, S., Wang, Y. (2012). Polymeric micelles drug delivery system in oncology. *Journal of Controlled Release*, *159*(3), 312–323.

Grabovac, V., Bernkop-Schnürch, A. (2007). Development and *in vitro* evaluation of surface modified poly (lactide-co-glycolide) nanoparticles with chitosan-4-thiobutylamidine. *Drug Development and Industrial Pharmacy*, *33*(7), 767–774.

Gregoriadis, G. (1990). Immunological adjuvants: a role for liposomes. *Immunology Today*, *11*, 89–97.

Griesbach, R. J., Austin, S. (2005). Comparison of the Munsell and Royal Horticultural Society's color charts in describing flower color. *Taxon*, *54*(3), 771–773.

Grisanti, L., Pinotsi, D., Gebauer, R., Schierle, G. S. K., Hassanali, A. A. (2017). A computational study on how structure influences the optical properties in model crystal structures of amyloid fibrils. *Physical Chemistry Chemical Physics*, *19*(5), 4030–4040.

Grisanti, L., Sapunar, M., Hassanali, A., Došlić, N. (2020). Toward understanding optical properties of amyloids: a reaction path and nonadiabatic dynamics study. *Journal of the American Chemical Society*, *142*(42), 18042–18049.

Gu, Y., Yu, J., Ding, C., Zhou, Y., Yang, J., Yu, W., Zhang, X., Huang, H. (2021). Flavonoid GL-V9 suppresses invasion and migration of human colorectal cancer cells by inhibiting PI3K/Akt and MMP-2/9 signaling. *Journal of Cancer*, *12*(15), 4542.

Guliyeva, A. J., Gasymov, O. K. (2020). ANS fluorescence: Potential to discriminate hydrophobic sites of proteins in solid states. *Biochemistry and Biophysics Reports*, *24*, 100843.

Gupta, M. K., Senthilkumar, S., Chiranjivi, A. K., Banik, K., Girisa, S., Kunnumakkara, A. B., Dubey, V. K., Rangan, L. (2021). Antioxidant, anti-tyrosinase and anti-inflammatory activities of 3, 5-dihydroxy-4′, 7-dimethoxyflavone isolated from the leaves of *Alpinia nigra*. *Phytomedicine Plus*, *1*(3), 100097.

Gupta, S. S. (1994). Prospects and perspectives of natural plants products in medicine. In *Indian Journal of Pharmacology* (Vol. 26).

Guptasarma, P. (2008). Solution-state characteristics of the ultraviolet A-induced visible fluorescence from proteins. *Archives of Biochemistry and Biophysics*, *478*(2), 127–129.

Haleagrahara, N., Siew, C. J., Ponnusamy, K. (2013). Effect of quercetin and desferrioxamine on 6-hydroxydopamine (6-OHDA) induced neurotoxicity in striatum of rats. *The Journal of Toxicological Sciences*, *38*(1), 25–33.

Han, D.-H., Tachibana, H., Yamada, K. (2001). Inhibition of environmental estrogen-induced proliferation of human breast carcinoma MCF-7 cells by flavonoids. *In Vitro Cellular and Developmental Biology-Animal*, *37*, 275–282.

He, J., Wang, Y., Chang, A. K., Xu, L., Wang, N., Chong, X., Li, H., Zhang, B., Jones, G. W., and Song, Y. (2014). Myricetin prevents fibrillogenesis of hen egg white lysozyme. *Journal of Agricultural and Food Chemistry*, *62*(39), 9442–9449.

Hetz, C., and Soto, C. (2003). Protein misfolding and disease: the case of prion disorders. *Cellular and Molecular Life Sciences CMLS*, *60*, 133–143.

Hoffman, F. A. (2015). Botanicals as "new" drugs: US development. *Epilepsy and Behavior*, *52*, 338–343.

Hooshyar, H., Sadeghi, R. (2015). Influence of sodium salts on the micellization and interfacial behavior of cationic surfactant dodecyltrimethylammonium bromide in aqueous solution. *Journal of Chemical and Engineering Data*, *60*(4), 983–992.

Höppener, J. W. M., Ahrén, B., Lips, C. J. M. (2000). Islet amyloid and type 2 diabetes mellitus. *New England Journal of Medicine*, *343*(6), 411–419.

Hsiang, t., Yusoff, M. M. (2012). Chemical and biological studies of *Zingiber phillipseae* rhizomes extract. *International Journal of Pharma and Bio Sciences*, *3*, 631–637.

Hu, B., Liu, X., Zhang, C., Zeng, X. (2017). Food macromolecule based nanodelivery systems for enhancing the bioavailability of polyphenols. *Journal of Food and Drug Analysis*, *25*(1), 3–15.

Huang, C.-C., Hung, C.-H., Hung, T.-W., Lin, Y.-C., Wang, C.-J., Kao, S.-H. (2019). Dietary delphinidin inhibits human colorectal cancer metastasis associating with upregulation of miR-204-3p and suppression of the integrin/FAK axis. *Scientific Reports*, *9*(1), 18954.

Huang, T. H. J., Yang, D.-S., Fraser, P. E., Chakrabartty, A. (2000). Alternate aggregation

pathways of the Alzheimer β-amyloid peptide: an *in vitro* model of preamyloid. *Journal of Biological Chemistry*, *275*(46), 36436–36440.

Huang, W.-W., Tsai, S.-C., Peng, S.-F., Lin, M.-W., Chiang, J.-H., Chiu, Y.-J., Fushiya, S., Tseng, M. T., Yang, J.-S. (2013). Kaempferol induces autophagy through AMPK and AKT signaling molecules and causes G2/M arrest via downregulation of CDK1/cyclin B in SK-HEP-1 human hepatic cancer cells. *International Journal of Oncology*, *42*(6), 2069–2077.

Huang, W.-Y., Cai, Y.-Z., Zhang, Y. (2009). Natural phenolic compounds from medicinal herbs and dietary plants: potential use for cancer prevention. *Nutrition and Cancer*, *62*(1), 1–20.

Hubert, J., Nuzillard, J.-M., Renault, J.-H. (2017). Dereplication strategies in natural product research: How many tools and methodologies behind the same concept? *Phytochemistry Reviews*, *16*, 55–95.

Islam, A. M. T., Chowdhury, M. A. U., Uddin, M. E., Islam, M. R., Sharmen, F., Parvin, M. S., Islam, M. E. (2016). Protective effect of *Alpina nigra* leaves extract in mouse liver injury induced by carbon tetrachloride. *Journal of Scientific Research*, *8*(3), 381–386.

Italia, J. L., Bhatt, D. K., Bhardwaj, V., Tikoo, K., Kumar, M. N. V. R. (2007). PLGA nanoparticles for oral delivery of cyclosporine: Nephrotoxicity and pharmacokinetic studies in comparison to Sandimmune Neoral®. *Journal of Controlled Release*, *119*(2), 197–206.

Jani, N. A., Ibrahim, N., Hashim, S. E., Sirat, H. M. (2015). Antimicrobial and antioxidant activities of Hornstedtia Leonurus Retz. extracts. *Journal of Science and Technology*, *7*(2).

Janyapanich, P., Kotipan, C., Teerachawalwong, K., Watana, S., Nuntharatanapon, N. (2019). Antioxidant, antityrosinase activity and toxicity of *Alpinia nigra* extracts. *Key Engineering Materials*, *819*, 111–117.

Jaramillo, S., Lopez, S., Varela, L. M., Rodriguez-Arcos, R., Jimenez, A., Abia, R., Guillen, R., Muriana, F. J. G. (2010). The flavonol isorhamnetin exhibits cytotoxic effects on human colon cancer cells. *Journal of Agricultural and Food Chemistry*, *58*(20), 10869–10875.

Jie, X.-X., Zhang, X.-Y., Xu, C.-J. (2017). Epithelial-to-mesenchymal transition, circulating tumor cells and cancer metastasis: Mechanisms and clinical applications. *Oncotarget*, *8*(46), 81558.

Jong, K. H., Azar, Y. T., Grisanti, L., Stephens, A. D., Jones, S. T. E., Credgington, D., Schierle, G. S. K., Hassanali, A. (2019). Low energy optical excitations as an indicator of structural changes initiated at the termini of amyloid proteins. *Physical Chemistry Chemical Physics*, *21*(43), 23931–23942.

Jurasekova, Z., Domingo, C., García-Ramos, J. V., Sánchez-Cortés, S. (2014). Effect of pH on the chemical modification of quercetin and structurally related flavonoids characterized by optical (UV-visible and Raman) spectroscopy. *Physical Chemistry Chemical Physics*, *16*(25), 12802–12811.

Kabir, M. S. H., Uddin, M. M. N., Hosen, S. M. Z. (2016). Investigation on hypoglycemic effects of ethanol extract of *Alpinia nigra* (Gaertn.) in animal model. *Journal of Intercultural Ethnopharmacology*, *5*(2), 131–136.

Kalluri, R., Weinberg, R. A. (2009). The basics of epithelial-mesenchymal transition. *The Journal of Clinical Investigation*, *119*(6), 1420–1428.

Kanjilal, P. B., Kotoky, R., Couladis, M. (2010). Essential Oil composition of leaf and rhizome oil of *Alpinia nigra* (Gaertner) BL Burtt. from Northeast India. *Journal of Essential Oil Research*, *22*(4), 358–359.

Kataoka, K., Harada, A., Nagasaki, Y. (2012). Block copolymer micelles for drug delivery: design, characterization and biological significance. *Advanced Drug Delivery Reviews*, *64*, 37–48.

Kaur, M., Velmurugan, B., Tyagi, A., Agarwal, C., Singh, R. P., Agarwal, R. (2010). Silibinin suppresses growth of human colorectal carcinoma SW480 cells in culture and xenograft through down-regulation of β-catenin-dependent signaling. *Neoplasia*, *12*(5), 415–424.

Kelm, M. A., Nair, M. G., Strasburg, G. M., DeWitt, D. L. (2000). Antioxidant and cyclooxygenase inhibitory phenolic compounds from Ocimum sanctum Linn. *Phytomedicine*, *7*(1), 7–13.

Khajuria, A. K., Manhas, R. K., Kumar, H., Bisht, N. S. (2021). Ethnobotanical study of traditionally used medicinal plants of Pauri district of Uttarakhand, India. *Journal of*

Ethnopharmacology, *276*, 114204.

Khan, A. N., Hassan, M. N., Khan, R. H. (2019). Gallic acid: A naturally occurring bifunctional inhibitor of amyloid and metal induced aggregation with possible implication in metal-based therapy. *Journal of Molecular Liquids*, *285*, 27–37.

Khan, J. A., Kainthan, R. K., Ganguli, M., Kizhakkedathu, J. N., Singh, Y., Maiti, S. (2006). Water soluble nanoparticles from PEG-based cationic hyperbranched polymer and RNA that protect RNA from enzymatic degradation. *Biomacromolecules*, *7*(5), 1386–1388.

Khan, M. S. S., Salam, M. A., Haque, R. S. M. A., Abdul Majid, A. M. S., Abdul Majid, A. S. Bin, Asif, M., Basheer, M. K. A., Tabana, Y. M. (2016). Synthesis, cytotoxicity, and long-term single dose anti-cancer pharmacological evaluation of dimethyltin (IV) complex of N (4)-methylthiosemicarbazone (having ONS donor ligand). *Cogent Biology*, *2*(1), 1154282.

Konar, M., Bag, S., Roy, P., Dasgupta, S. (2017). Gallic acid induced dose dependent inhibition of lysozyme fibrillation. *International Journal of Biological Macromolecules*, *103*, 1224–1231. https://doi.org/10.1016/j.ijbiomac.2017.05.158

Kozłowska, A., Szostak-Węgierek, D. (2022). Targeting cardiovascular diseases by flavonols: An update. *Nutrients*, *14*(7), 1439.

Kumar, B. R. (2017). Application of HPLC and ESI-MS techniques in the analysis of phenolic acids and flavonoids from green leafy vegetables (GLVs). *Journal of Pharmaceutical Analysis*, *7*(6), 349–364.

Kumar, K. M. P., Asish, G. R., Sabu, M., Balachandran, I. (2013). Significance of gingers (Zingiberaceae) in Indian system of medicine-Ayurveda: An overview. *Ancient Science of Life*, *32*(4), 253.

Kumar, S., Pandey, A. K. (2013). Chemistry and biological activities of flavonoids: an overview. *The Scientific World Journal*, *2013*.

Kumar, S., Sharma, P., Arora, K., Raje, M., Guptasarma, P. (2014). Calcium binding to beta-2-microglobulin at physiological pH drives the occurrence of conformational changes which cause the protein to precipitate into amorphous forms that subsequently transform into amyloid aggregates. *PLoS One*, *9*(4), e95725.

Kusano, M., Tohge, T., Fukushima, A., Kobayashi, M., Hayashi, N., Otsuki, H., Kondou, Y.,

Goto, H., Kawashima, M., Matsuda, F. (2011). Metabolomics reveals comprehensive reprogramming involving two independent metabolic responses of *Arabidopsis* to UV-B light. *The Plant Journal*, *67*(2), 354–369.

Kwaśniewska, D., Kiewlicz, J. (2022). Study of interaction between cationic surfactant (CTAB) and ascorbic acid/ascorbic acids derivatives by tensiometric and spectroscopic methods. *Journal of Molecular Liquids*, *354*, 118917.

Kwon, G. S., Okano, T. (1996). Polymeric micelles as new drug carriers. *Advanced Drug Delivery Reviews*, *21*(2), 107–116.

Lazar, T. (2003). Taiz, L. and Zeiger, E. Plant physiology. 3rd edn. *Oxford University Press*.

Lee, Y. K., Yuk, D. Y., Lee, J. W., Lee, S. Y., Ha, T. Y., Oh, K. W., Yun, Y. P., Hong, J. T. (2009). (−)-Epigallocatechin-3-gallate prevents lipopolysaccharide-induced elevation of beta-amyloid generation and memory deficiency. *Brain Research*, *1250*, 164–174.

Levine III, H. (1993). Thioflavine T interaction with synthetic Alzheimer's disease β-amyloid peptides: Detection of amyloid aggregation in solution. *Protein Science*, *2*(3), 404–410.

Lewandowska, U., Szewczyk, K., Hrabec, E., Janecka, A., Gorlach, S. (2013). Overview of metabolism and bioavailability enhancement of polyphenols. *Journal of Agricultural and Food Chemistry*, *61*(50), 12183–12199.

Li, K., He, W., Lin, N., Wang, X., Fan, Q.-X. (2010). Downregulation of N-cadherin expression inhibits invasiveness, arrests cell cycle and induces cell apoptosis in esophageal squamous cell carcinoma. *Cancer Investigation*, *28*(5), 479–486.

Lipinski, C. A. (2001). Avoiding investment in doomed drugs. *Curr Drug Discov*, *1*, 17–19.

Liu, K., Gao, H., Wang, Q., Wang, L., Zhang, B., Han, Z., Chen, X., Han, M., Gao, M. (2018). Retracted: Hispidulin suppresses cell growth and metastasis by targeting PIM 1 through JAK 2/STAT 3 signaling in colorectal cancer. *Cancer Science*, *109*(5), 1369–1381.

Liu, S., You, L., Zhao, Y., Chang, X. (2018). Wild *Lonicera caerulea* berry polyphenol extract reduces cholesterol accumulation and enhances antioxidant capacity *in vitro* and *in vivo*. *Food Research International*, *107*, 73–83.

Liu, W., Feng, Y., Yu, S., Fan, Z., Li, X., Li, J., Yin, H. (2021). The flavonoid biosynthesis network in plants. *International Journal of Molecular Sciences*, *22*(23), 12824.

Liu, W., Guo, R. (2006). Interaction between flavonoid, quercetin and surfactant aggregates with different charges. *Journal of Colloid and Interface Science*, *302*(2), 625–632.

Liu, X., Wu, X. (2015). Fluorescence enhancement of fisetin by silver nanoparticles with cetyltrimethyl ammonium bromide micelles. *RSC Advances*, *5*(10), 7433–7439.

Magalingam, K. B., Radhakrishnan, A., Haleagrahara, N. (2013). Rutin, a bioflavonoid antioxidant protects rat pheochromocytoma (PC-12) cells against 6-hydroxydopamine (6-OHDA)-induced neurotoxicity. *International Journal of Molecular Medicine*, *32*(1), 235–240.

Mahler, H.-C., Friess, W., Grauschopf, U., Kiese, S. (2009). Protein aggregation: pathways, induction factors and analysis. *Journal of Pharmaceutical Sciences*, *98*(9), 2909–2934.

Marchesi, F., Monti, P., Leone, B. E., Zerbi, A., Vecchi, A., Piemonti, L., Mantovani, A., Allavena, P. (2004). Increased survival, proliferation, and migration in metastatic human pancreatic tumor cells expressing functional CXCR4. *Cancer Research*, *64*(22), 8420–8427.

Markovic, S., Tosovic, J. (2015). Application of time-dependent density functional and natural bond orbital theories to the UV–vis absorption spectra of some phenolic compounds. *The Journal of Physical Chemistry A*, *119*(35), 9352–9362.

Metodiewa, D., Jaiswal, A. K., Cenas, N., Dickancaité, E., Segura-Aguilar, J. (1999). Quercetin may act as a cytotoxic prooxidant after its metabolic activation to semiquinone and quinoidal product. *Free Radical Biology and Medicine*, *26*(1–2), 107–116.

Mignet, N., Seguin, J., Romano, M. R., Brullé, L., Touil, Y. S., Scherman, D., Bessodes, M., Chabot, G. G. (2012). Development of a liposomal formulation of the natural flavonoid fisetin. *International Journal of Pharmaceutics*, *423*(1), 69–76.

Mishra, B., Patel, B. B., Tiwari, S. (2010). Colloidal nanocarriers: a review on formulation technology, types and applications toward targeted drug delivery. *Nanomedicine: Nanotechnology, Biology and Medicine*, *6*(1), 9–24.

Miura, Y. H., Tomita, I., Watanabe, T., Hirayama, T., Fukui, S. (1998). Active oxygens generation by flavonoids. *Biological and Pharmaceutical Bulletin*, *21*(2), 93–96.

Moffat, J. G., Vincent, F., Lee, J. A., Eder, J., Prunotto, M. (2017). Opportunities and challenges in phenotypic drug discovery: an industry perspective. *Nature Reviews Drug*

Discovery, *16*(8), 531–543.

Mogavero, A., Maiorana, M. V., Zanutto, S., Varinelli, L., Bozzi, F., Belfiore, A., Volpi, C. C., Gloghini, A., Pierotti, M. A., Gariboldi, M. (2017). Metformin transiently inhibits colorectal cancer cell proliferation as a result of either AMPK activation or increased ROS production. *Scientific Reports*, *7*(1), 15992.

Mojr, V., Herzig, V., Buděšínský, M., Cibulka, R., Kraus, T. (2010). Flavin–cyclodextrin conjugates as catalysts of enantioselective sulfoxidations with hydrogen peroxide in aqueous media. *Chemical Communications*, *46*(40), 7599–7601.

Mondal, S., Ghosh, S., Moulik, S. P. (2016). Stability of curcumin in different solvent and solution media: UV–visible and steady-state fluorescence spectral study. *Journal of Photochemistry and Photobiology B: Biology*, *158*, 212–218.

Morales, R., Moreno-Gonzalez, I., Soto, C. (2013). Cross-seeding of misfolded proteins: implications for etiology and pathogenesis of protein misfolding diseases. *PLoS Pathogens*, *9*(9), e1003537.

Moreno-Gonzalez, I., Soto, C. (2011). Misfolded protein aggregates: mechanisms, structures and potential for disease transmission. *Seminars in Cell and Developmental Biology*, *22*(5), 482–487.

Moroi, Y. (1992). Micelles: theoretical and applied aspects. *Springer Science and Business Media.*

Mukherjee, A., Morales-Scheihing, D., Butler, P. C., and Soto, C. (2015). Type 2 diabetes as a protein misfolding disease. *Trends in Molecular Medicine*, *21*(7), 439–449.

Murkovic, M. (2016). Phenolic Compounds: Occurrence, Classes, and Analysis. U: Encyclopedia of Food and Health. Cabarello, B., Finglas, PM, Toldrá, F., ured.), *Academic Press, Cambridge.*

National Center for Biotechnology Information (2023). PubChem Compound Summary for CID 5378832, 3,7-Dihydroxy-3',4'-dimethoxyflavone. Retrieved October 29, 2023 from https://pubchem.ncbi.nlm.nih.gov/compound/3_7-Dihydroxy-3_4_-dimethoxyflavone.

Nelson, V. K., Sahoo, N. K., Sahu, M., Sudhan, H. H., Pullaiah, C. P., Muralikrishna, K. S. (2020). *In vitro* anticancer activity of *Eclipta alba* whole plant extract on colon cancer cell HCT-116. *BMC Complementary Medicine and Therapies*, *20*, 1–8.

Ng, K. R., Lyu, X., Mark, R., Chen, W. N. (2019). Antimicrobial and antioxidant activities of phenolic metabolites from flavonoid-producing yeast: Potential as natural food preservatives. *Food Chemistry*, *270*, 123–129.

Ngoungoure, V. L. N., Schluesener, J., Moundipa, P. F., Schluesener, H. (2015). Natural polyphenols binding to amyloid: A broad class of compounds to treat different human amyloid diseases. *Molecular Nutrition and Food Research*, *59*(1), 8–20.

Noratto, G., Porter, W., Byrne, D., Cisneros-Zevallos, L. (2009). Identifying peach and plum polyphenols with chemopreventive potential against estrogen-independent breast cancer cells. *Journal of Agricultural and Food Chemistry*, *57*(12), 5219–5226.

Oerlemans, C., Bult, W., Bos, M., Storm, G., Nijsen, J. F. W., Hennink, W. E. (2010). Polymeric micelles in anticancer therapy: targeting, imaging and triggered release. *Pharmaceutical Research*, *27*, 2569–2589.

Ono, K., Hasegawa, K., Naiki, H., Yamada, M. (2004). Anti-amyloidogenic activity of tannic acid and its activity to destabilize Alzheimer's β-amyloid fibrils *in vitro*. *Biochimica et Biophysica Acta (BBA)-Molecular Basis of Disease*, *1690*(3), 193–202.

Panche, A. N., Diwan, A. D., Chandra, S. R. (2016). Flavonoids: an overview. *Journal of Nutritional Science*, *5*, e47.

Panizzi, L., Caponi, C., Catalano, S., Cioni, P. L., Morelli, I. (2002). *In vitro* antimicrobial activity of extracts and isolated constituents of *Rubus ulmifolius*. *Journal of Ethnopharmacology*, *79*(2), 165–168.

Panyam, J., Labhasetwar, V. (2003). Biodegradable nanoparticles for drug and gene delivery to cells and tissue. *Advanced Drug Delivery Reviews*, *55*(3), 329–347.

Paul, A., Sharma, B., Mondal, T., Thalluri, K., Paul, S., Mandal, B. (2016). Amyloid β derived switch-peptides as a tool for investigation of early events of aggregation: A combined experimental and theoretical approach. *MedChemComm*, *7*(2), 311–316.

Paul, B., Sen, C. K., Saha, M. R. (2015). Cytotoxic effect of *Alpinia nigra* crude extracts obtained from its rhizomes. *International Journal of Pharmacognosy*, *2*(1), 49–54.

Pavia, D. L., Lampman, G. M., Kriz, G. S., Vyvyan, J. A. (2014). Introduction to spectroscopy. *Cengage learning.*

Perni, M., Galvagnion, C., Maltsev, A., Meisl, G., Müller, M. B. D., Challa, P. K., Kirkegaard, J. B., Flagmeier, P., Cohen, S. I. A., Cascella, R. (2017). A natural product inhibits the initiation of α-synuclein aggregation and suppresses its toxicity. *Proceedings of the National Academy of Sciences*, *114*(6), E1009–E1017.

Pešić, M. B., Milinčić, D. D., Kostić, A. Ž., Stanisavljević, N. S., Vukotić, G. N., Kojić, M. O., Gašić, U. M., Barać, M. B., Stanojević, S. P., Popović, D. A. (2019). *In vitro* digestion of meat-and cereal-based food matrix enriched with grape extracts: How are polyphenol composition, bioaccessibility and antioxidant activity affected? *Food Chemistry*, *284*, 28–44.

Petrides, P. E., Bock, S., Bovens, J., Hofmann, R., Jakse, G. (1990). Modulation of pro-epidermal growth factor, pro-transforming growth factor α and epidermal growth factor receptor gene expression in human renal carcinomas. *Cancer Research*, *50*(13), 3934–3939.

Poklar Ulrih, N. (2017). Analytical techniques for the study of polyphenol–protein interactions. *Critical Reviews in Food Science and Nutrition*, *57*(10), 2144–2161.

Porat, Y., Abramowitz, A., Gazit, E. (2006). Inhibition of amyloid fibril formation by polyphenols: structural similarity and aromatic interactions as a common inhibition mechanism. *Chemical Biology and Drug Design*, *67*(1), 27–37.

Portugal, S. G. M., Montero-Cabrera, L. A., Diaz, L. A., Brinn, I. M. (2006). Excited state acidity of bifunctional compounds: 9. Excited state intramolecular proton transfer in 3, 5-dihydroxy-7, 4′-dimethoxyflavone and 3, 5-dihydroxy-7, 4′-dimethoxyflavanone: spectral and fluorescence decay results. *Journal of Photochemistry and Photobiology A: Chemistry*, *181*(2–3), 370–377.

Pouget, C., Lauthier, F., Simon, A., Fagnere, C., Basly, J.-P., Delage, C., Chulia, A.-J. (2001). Flavonoids: structural requirements for antiproliferative activity on breast cancer cells. *Bioorganic and Medicinal Chemistry Letters*, *11*(24), 3095–3097.

Prasad, S., Mandal, I., Singh, S., Paul, A., Mandal, B., Venkatramani, R., Swaminathan, R. (2017). Near UV-Visible electronic absorption originating from charged amino acids in a monomeric protein. *Chemical Science*, *8*(8), 5416–5433.

Psotova, J., Svobodova, A., Kolarova, H., Walterova, D. (2006). Photoprotective properties of

Prunella vulgaris and rosmarinic acid on human keratinocytes. *Journal of Photochemistry and Photobiology B: Biology*, *84*(3), 167–174.

Puglia, C., Lauro, M. R., Tirendi, G. G., Fassari, G. E., Carbone, C., Bonina, F., Puglisi, G. (2017). Modern drug delivery strategies applied to natural active compounds. *Expert Opinion on Drug Delivery*, *14*(6), 755–768.

Pye, C. R., Bertin, M. J., Lokey, R. S., Gerwick, W. H., Linington, R. G. (2017). Reply to Skinnider and Magarvey: Rates of novel natural product discovery remain high. *Proceedings of the National Academy of Sciences*, *114*(31), E6273–E6273.

Qiao, C., Han, Q., Song, J., Wang, Z., Xu, L., Xu, H. (2007). HPLC determination of two bioactive flavone glycosides and GC-MS analysis of volatile oil constituents in *Alpinia nigra*.*2*(3), 85–91.

Rahmatullah, M., Rahman, M. A., Hossan, M. S., Taufiq-Ur-Rahman, M., Jahan, R., Mollik, M. A. H. (2010). A pharmacological and phytochemical evaluation of medicinal plants used by the harbang clan of the tripura tribal community of Mirsharai area, Chittagong district, Bangladesh. *The Journal Of Alternative And Complementary Medicine*, *16*(7), 769–785.

Rajan, R., Ahmed, S., Sharma, N., Kumar, N., Debas, A., Matsumura, K. (2021). Review of the current state of protein aggregation inhibition from a materials chemistry perspective: Special focus on polymeric materials. *Materials Advances*, *2*(4), 1139–1176.

Rajapaksha, R., Wickramarachchi, W. J., Hansini, K. (2017). Evaluation of the Antifungal Activity of the Extracts of the Rhizome of *Alpinia Nigra*. *Int. J. Adv. Agric. Environ. Eng*, *4*, 86–88.

Ravi, V. K., Swain, T., Chandra, N., Swaminathan, R. (2014). On the characterization of intermediates in the isodesmic aggregation pathway of hen lysozyme at alkaline pH. *PloS One*, *9*(1), e87256.

Reis, C. P., Neufeld, R. J., Ribeiro, A. J., Veiga, F. (2006). Nanoencapsulation I. Methods for preparation of drug-loaded polymeric nanoparticles. *Nanomedicine: Nanotechnology, Biology and Medicine*, *2*(1), 8–21.

Remya, C., Dileep, K. V, Tintu, I., Variyar, E. J., Sadasivan, C. (2014). Flavanone glycosides as acetylcholinesterase inhibitors: computational and experimental evidence. *Indian*

Journal of Pharmaceutical Sciences, *76*(6), 567.

Riccardi, C., Nicoletti, I. (2006). Analysis of apoptosis by propidium iodide staining and flow cytometry. *Nature Protocols*, *1*(3), 1458–1461.

Ringman, J. M., Frautschy, S. A., Cole, G. M., Masterman, D. L., Cummings, J. L. (2005). A potential role of the curry spice curcumin in Alzheimer's disease. *Current Alzheimer Research*, *2*(2), 131–136.

Roghani, M., Niknam, A., Jalali-Nadoushan, M.-R., Kiasalari, Z., Khalili, M., Baluchnejadmojarad, T. (2010). Oral pelargonidin exerts dose-dependent neuroprotection in 6-hydroxydopamine rat model of hemi-parkinsonism. *Brain Research Bulletin*, *82*(5–6), 279–283.

Romar, G. A., Kupper, T. S., Divito, S. J. (2016). Research techniques made simple: techniques to assess cell proliferation. *Journal of Investigative Dermatology*, *136*(1), e1–e7.

Rosenheck, K., Doty, P. (1961). The far ultraviolet absorption spectra of polypeptide and protein solutions and their dependence on conformation. *Proceedings of the National Academy of Sciences*, *47*(11), 1775–1785.

Ross, C. A., Tabrizi, S. J. (2011). Huntington's disease: from molecular pathogenesis to clinical treatment. *The Lancet Neurology*, *10*(1), 83–98.

Roy, A., Khan, A., Ahmad, I., Alghamdi, S., Rajab, B. S., Babalghith, A. O., Alshahrani, M. Y., Islam, S., Islam, M. R. (2022). Flavonoids a bioactive compound from medicinal plants and its therapeutic applications. *BioMed Research International*, *2022*.

Roy, B., Swargiary, A. (2009). Anthelmintic efficacy of ethanolic shoot extract of *Alpinia nigra* on tegumental enzymes of Fasciolopsis buski, a giant intestinal parasite. *Journal of Parasitic Diseases*, *33*, 48–53.

Ryan, K. G., Swinny, E. E., Markham, K. R., Winefield, C. (2002). Flavonoid gene expression and UV photoprotection in transgenic and mutant Petunia leaves. *Phytochemistry*, *59*(1), 23–32.

Sachdeva, A. K., Kuhad, A., Chopra, K. (2014). Naringin ameliorates memory deficits in experimental paradigm of Alzheimer's disease by attenuating mitochondrial dysfunction. *Pharmacology Biochemistry and Behavior*, *127*, 101–110.

Saha, U., De, R., Das, B. (2023). Interactions between Loaded Drugs and Surfactant Molecules in Micellar Drug Delivery Systems: A Critical Review. *Journal of Molecular Liquids*, 121906.

Sahoo, S., Ghosh, G., Das, D., Nayak, S. (2013). Phytochemical investigation and *In vitro* antioxidant activity of an indigenous medicinal plant *Alpinia nigra* B.L. Burtt. *Asian Pacific Journal of Tropical Biomedicine*, *3*(11), 871–876.

Sahoo, S., Kar, B., Dash, S., Ray, M., Acharya, K. G., Singh, S., Nayak, S. (2018). Anticancerous and immunomodulatory activities of *Alpinia nigra* (Gaertn.) Burtt. *Journal of Essential Oil Bearing Plants*, *21*(4), 869–875.

Sahu, A. K., Mishra, A. K. (2022). Photophysical Behavior of Plant Flavonols Galangin, Kaempferol, Quercetin, and Myricetin in Homogeneous Media and the DMPC Model Membrane: Unveiling the Influence of the B-Ring Hydroxylation of Flavonols. *The Journal of Physical Chemistry B*, *126*(15), 2863–2875.

Samii, A., Nutt, J. G., Ransom, B. R. (2004). Parkinson's disease. *Lancet [Internet]. 2004; 363 (9423): 1783–93*.

Santos, P. L., Araujo, A. A. S., Quintans, J. S. S., Oliveira, M. G. B., Brito, R. G., Serafini, M. R., Menezes, P. P., Santos, M. R. V., Alves, P. B., De Lucca Junior, W., Blank, A. F., La Rocca, V., Almeida, R. N., Quintans, L. J. (2015). Preparation, Characterization, and Pharmacological Activity of *Cymbopogon winterianus* Jowitt ex Bor (Poaceae) Leaf Essential Oil of β-Cyclodextrin Inclusion Complexes. *Evidence-Based Complementary and Alternative Medicine*, *2015*.

Saraf, A., Sharma, S., Sachar, S. (2018). Insights into the interactions of sulfamethoxazole with organized assemblies of ionic and nonionic surfactants. *Langmuir*, *34*(48), 14624–14632.

Schluep, T., Hwang, J., Hildebrandt, I. J., Czernin, J., Choi, C. H. J., Alabi, C. A., Mack, B. C., Davis, M. E. (2009). Pharmacokinetics and tumor dynamics of the nanoparticle IT- 101 from PET imaging and tumor histological measurements. *Proceedings of the National Academy of Sciences*, *106*(27), 11394–11399.

Sekijima, Y. (2015). Transthyretin (ATTR) amyloidosis: clinical spectrum, molecular pathogenesis and disease-modifying treatments. *Journal of Neurology, Neurosurgery and Psychiatry*, *86*(9), 1036–1043.

Selvam, S., Mishra, A. K. (2011). Multiple prototropism of fisetin in sodium cholate and related bile salt media. *Photochemical and Photobiological Sciences*, *10*, 66–75.

Sengupta, B., Banerjee, A., Sengupta, P. K. (2004). Investigations on the binding and antioxidant properties of the plant flavonoid fisetin in model biomembranes. *FEBSLetters*, *570*(1–3), 77–81.

Senthilkumar, S., Singh, R., Rangan, L., Swaminathan, R. (2023). Enhanced electronic absorption and solubility of Mammeigin in aqueous micelles and protein aggregate solutions compared to water. *Journal of Molecular Liquids*, *386*, 122510.

Seo, H. W., No, H., Cheon, H. J., Kim, J.-K. (2020). Sappanchalcone, a flavonoid isolated from *Caesalpinia sappan* L., induces caspase-dependent and AIF-dependent apoptosis in human colon cancer cells. *Chemico-Biological Interactions*, *327*, 109185.

Serrano-Andrés, L., Fülscher, M. P. (2001). Charge transfer transitions in neutral and ionic polypeptides: A theoretical study. *The Journal of Physical Chemistry B*, *105*(38), 9323–9330.

Sgarbossa, A. (2012). Natural biomolecules and protein aggregation: emerging strategies against amyloidogenesis. *International Journal of Molecular Sciences*, *13*(12), 17121–17137.

Shaban, S. M., Kang, J., Kim, D.-H. (2020). Surfactants: Recent advances and their applications. *Composites Communications*, *22*, 100537.

Shah, P., Jha, S. K., Bhattarai, A. (2021). Spectrophotometric study of the sodium dodecyl sulfate in the presence of methylene blue in the methanol–water mixed solvent system. *Journal of Molecular Liquids*, *340*, 117200.

Sharma, A., Sharma, U. S. (1997). Liposomes in drug delivery: progress and limitations. *International Journal of Pharmaceutics*, *154*(2), 123–140.

Sharmen, F., Mannan, A., Rahman, M. M., Chowdhury, M. A. U., Uddin, M. E., Abu Ahmed, A. M. (2014). Investigation of *in vivo* neuropharmacological effect of *Alpinia nigra* leaf extract. *Asian Pacific Journal of Tropical Biomedicine*, *4*(2), 137–142.

Shi, Y.-Q., Fukai, T., Sakagami, H., Chang, W.-J., Yang, P.-Q., Wang, F.-P., Nomura, T. (2001). Cytotoxic flavonoids with isoprenoid groups from *Morus mongolica*. *Journal of Natural Products*, *64*(2), 181–188.

Shi, Y., Inoue, H., Wu, J. C., Yamanaka, S. (2017). Induced pluripotent stem cell technology: a decade of progress. *Nature Reviews Drug Discovery*, *16*(2), 115–130.

Shukla, A., Mukherjee, S., Sharma, S., Agrawal, V., Kishan, K. V. R., Guptasarma, P. (2004). A novel UV laser-induced visible blue radiation from protein crystals and aggregates: scattering artifacts or fluorescence transitions of peptide electrons delocalized through hydrogen bonding? *Archives of Biochemistry and Biophysics*, *428*(2), 144–153.

Siddiqui, I. A., Adhami, V. M., Bharali, D. J., Hafeez, B. B., Asim, M., Khwaja, S. I., Ahmad, N., Cui, H., Mousa, S. A., Mukhtar, H. (2009). Introducing nanochemoprevention as a novel approach for cancer control: proof of principle with green tea polyphenol epigallocatechin-3-gallate. *Cancer Research*, *69*(5), 1712–1716.

Singh, P., Wangoo, N., Sharma, R. K. (2020). Phenylalanine dimer assembly structure as the basic building block of an amyloid like photoluminescent nanofibril network. *Soft Matter*, *16*(17), 4105–4109.

Stavrianidi, A. (2020). A classification of liquid chromatography mass spectrometry techniques for evaluation of chemical composition and quality control of traditional medicines. *Journal of Chromatography A*, *1609*, 460501.

Stracke, R., Favory, J., Gruber, H., Bartelniewoehner, L., Bartels, S., Binkert, M., Funk, M., Weisshaar, B., Ulm, R. (2010). The Arabidopsis bZIP transcription factor HY5 regulates expression of the PFG1/MYB12 gene in response to light and ultraviolet-B radiation. *Plant, Cell and Environment*, *33*(1), 88–103.

Su, X.-Z., Miller, L. H. (2015). The discovery of artemisinin and the Nobel Prize in Physiology or Medicine. *Springer*.

Sudsai, T., Leajae, S., Dangmanee, N., Chatgat, W., Chaniad, P., Tewtrakul, S. (2017). Antibacterial and anti-HIV-1 integrase properties of isolated compounds from *Boesenbergia kingii*. *Songklanakarin Journal of Science and Technology*, *39*(1), 131–135.

Sudsai, T., Wattanapiromsakul, C., Tewtrakul, S. (2016). Wound healing property of isolated compounds from *Boesenbergia kingii* rhizomes. *Journal of Ethnopharmacology*, *184*, 42–48.

Suhail, M., Janakiraman, A. K., Khan, A., Naeem, A., Badshah, S. F. (2019). Surfactants and their role in pharmaceutical product development: an overview. *J. Pharm. Pharm*, *6*, 72–

82.

Sulfikkarali, N., Krishnakumar, N., Manoharan, S., Nirmal, R. M. (2013). Chemopreventive efficacy of naringenin-loaded nanoparticles in 7, 12-dimethylbenz (a) anthracene induced experimental oral carcinogenesis. *Pathology and Oncology Research*, *19*, 287–296.

Tajammal, A., Siddiqa, A., Irfan, A., Azam, M., Hafeez, H., Munawar, M. A., Basra, M. A. R. (2022). Antioxidant, molecular docking and computational investigation of new flavonoids. *Journal of Molecular Structure*, *1254*, 132189.

Takahashi, A., Matsumoto, H., Nagayama, K., Kitano, M., Hirose, S., Tanaka, H., Mori, E., Yamakawa, N., Yasumoto, J.-I., Yuki, K., Ohnishi, K., Ohnishi, T. (2004). Evidence for the Involvement of Double-Strand Breaks in Heat-Induced Cell Killing. *In cancer research* (Vol. 64).

Talat, R., Fayyaz, S., Ali, S., Khalid, N., Haider, A., Shah, A., Ullah, F. (2019). Designing of new cationic surfactant based micellar systems as drug carriers: an investigation into the drug cell membrane interactions. *Journal of Dispersion Science and Technology*, *40*(7), 958–968.

Talele, P., Choudhary, S., Kishore, N. (2016). Understanding thermodynamics of drug partitioning in micelles and delivery to proteins: Studies with naproxen, diclofenac sodium, tetradecyltrimethylammonium bromide, and bovine serum albumin. *The Journal of Chemical Thermodynamics*, *92*, 182–190.

Tapas, A. R., Sakarkar, D. M., Kakde, R. B. (2008). Flavonoids as Nutraceuticals: A Review. In *Tropical Journal of Pharmaceutical Research* (Vol. 7, Issue 3).

Tardy, B. L., Richardson, J. J., Guo, J., Lehtonen, J., Ago, M., Rojas, O. J. (2018). Lignin nano- and microparticles as template for nanostructured materials: Formation of hollow metal-phenolic capsules. *Green Chemistry*, *20*(6), 1335–1344.

Taylor, J. P., Brown Jr, R. H., Cleveland, D. W. (2016). Decoding ALS: from genes to mechanism. *Nature*, *539*(7628), 197–206.

Teekaraman, D., Elayapillai, S. P., Viswanathan, M. P., Jagadeesan, A. (2019). Quercetin inhibits human metastatic ovarian cancer cell growth and modulates components of the intrinsic apoptotic pathway in PA-1 cell line. *Chemico-Biological Interactions*, *300*, 91–100.

Teng, Y., Morrison, M. E., Munk, P., Webber, S. E., Procházka, K. (1998). Release kinetics studies of aromatic molecules into water from block polymer micelles. *Macromolecules*, *31*(11), 3578–3587.

Thompson, D. O. (1997). Cyclodextrins—enabling excipients: their present and future use in pharmaceuticals. *Critical Reviews™ in Therapeutic Drug Carrier Systems*, *14*(1).

Tiwari, S., Mall, C., Prakash Solanki, P. (2018). Surfactant and its applications: A review. *Int. J. Eng. Res. Appl*, *8*(9), 61–66.

Tošović, J., Marković, S. (2017). Reproduction and interpretation of the UV-vis spectra of some flavonoids. *Chemical Papers*, *71*(3), 543–552.

Trinh, N.-T., Nguyen, T. M. N., Yook, J.-I., Ahn, S.-G., Kim, S.-A. (2022). Quercetin and quercitrin from *Agrimonia pilosa* Ledeb inhibit the migration and invasion of colon cancer cells through the JNK signaling pathway. *Pharmaceuticals*, *15*(3), 364.

Tungmunnithum, D., Thongboonyou, A., Pholboon, A., Yangsabai, A. (2018). Flavonoids and other phenolic compounds from medicinal plants for pharmaceutical and medical aspects: An overview. *Medicines*, *5*(3), 93.

Tushar, Basak, S., Sarma, G. C., Rangan, L. (2010). Ethnomedical uses of Zingiberaceous plants of Northeast India. *Journal of Ethnopharmacology*, *132*(1), 286–296.

Tyedmers, J., Mogk, A., Bukau, B. (2010). Cellular strategies for controlling protein aggregation. *Nature Reviews Molecular Cell Biology*, *11*(11), 777–788.

Unnikrishnan, R., Dev, S. A., Jayaraj, R. (2020). Pitfalls and promises of raw drug identification techniques in the ayurvedic industry: an overview. *3 Biotech*, *10*, 1–10.

Valeur, B., Berberan-Santos, M. N. (2012). *Molecular fluorescence: principles and applications*. John Wiley and Sons.

Van, H. T., Thang, T. D., Luu, T. N., Doan, V. D. (2021). An overview of the chemical composition and biological activities of essential oils from *Alpinia* genus (Zingiberaceae). *RSC Advances*, *11*(60), 37767–37783.

Van Rooijen, N., van Nieuwmegen, R. (1980). Liposomes in immunology: multilamellar phosphatidylcholine liposomes as a simple, biodegradable and harmless adjuvant without any immunogenic activity of its own. *Immunological Communications*, *9*(3), 243–256.

Ved, D. K., Goraya, G. S. (2007). Demand and supply of medicinal plants in India. *NMPB, New Delhi and FRLHT, Bangalore, India*, *18*(85), 210–252.

Vetri, V., Canale, C., Relini, A., Librizzi, F., Militello, V., Gliozzi, A., Leone, M. (2007). Amyloid fibrils formation and amorphous aggregation in concanavalin A. *Biophysical Chemistry*, *125*(1), 184–190.

Vijaya, K., Ananthan, S., Nalini, R. (1995). Antibacterial effect of theaflavin, polyphenon 60 (*Camellia sinensis*) and *Euphorbia hirta* on *Shigella* spp.—a cell culture study. *Journal of Ethnopharmacology*, *49*(2), 115–118.

Virgone-Carlotta, A., Lemasson, M., Mertani, H. C., Diaz, J.-J., Monnier, S., Dehoux, T., Delanoë-Ayari, H., Rivière, C., Rieu, J.-P. (2017). In-depth phenotypic characterization of multicellular tumor spheroids: Effects of 5-Fluorouracil. *PLoS One*, *12*(11), e0188100.

Vu, T., Datta, P. K. (2017). Regulation of EMT in colorectal cancer: A culprit in metastasis. *Cancers*, *9*(12), 1–22.

Wang, H., Joseph, J. A. (1999). Quantifying cellular oxidative stress by dichlorofluorescein assay using microplate reader. *Free Radical Biology and Medicine*, *27*(5–6), 612–616.

Westermark, G. T., Fändrich, M., Westermark, P. (2015). AA amyloidosis: pathogenesis and targeted therapy. *Annual Review of Pathology: Mechanisms of Disease*, *10*, 321–344.

White, T. C., Findley, K., Dawson, T. L., Scheynius, A., Boekhout, T., Cuomo, C. A., Xu, J., Saunders, C. W. (2014). Fungi on the skin: dermatophytes and Malassezia. *Cold Spring Harbor Perspectives in Medicine*, *4*(8), a019802.

Wolfe, L. S., Calabrese, M. F., Nath, A., Blaho, D. V, Miranker, A. D., Xiong, Y. (2010). Protein-induced photophysical changes to the amyloid indicator dye thioflavin T. *Proceedings of the National Academy of Sciences*, *107*(39), 16863–16868.

Woo, Y.-J., Jang, K. L. (2012). All-trans retinoic acid activates E-cadherin expression via promoter hypomethylation in the human colon carcinoma HCT116 cells. *Biochemical and Biophysical Research Communications*, *425*(4), 944–949.

Wu, S., Liu, B., Zhang, Q., Liu, J., Zhou, W., Wang, C., Li, M., Bao, S., Zhu, R. (2013). Dihydromyricetin reduced bcl-2 expression via p53 in human hepatoma HepG2 cells. *PLoS ONE*, *8*(11).

Xiao, J., Kai, G., Yamamoto, K., Chen, X. (2013). Advance in dietary polyphenols as α-glucosidases inhibitors: a review on structure-activity relationship aspect. *Critical Reviews in Food Science and Nutrition*, *53*(8), 818–836.

Yang, M., Li, W.-Y., Xie, J., Wang, Z.-L., Wen, Y.-L., Zhao, C.-C., Tao, L., Li, L.-F., Tian, Y., Sheng, J. (2021). Astragalin inhibits the proliferation and migration of human colon cancer HCT116 cells by regulating the NF-κB signaling pathway. *Frontiers in Pharmacology*, *12*, 639256.

Yang, W., Perillo, W., Liou, D., Marambaud, P., Wang, P. (2012). AMPK inhibitor compound C suppresses cell proliferation by induction of apoptosis and autophagy in human colorectal cancer cells. *Journal of Surgical Oncology*, *106*(6), 680–688.

Yao, Y., Rao, C., Zheng, G., Wang, S. (2019). Luteolin suppresses colorectal cancer cell metastasis via regulation of the miR-384/pleiotrophin axis. *Oncology Reports*, *42*(1), 131–141.

Yin, F., Liu, J., Ji, X., Wang, Y., Zidichouski, J., Zhang, J. (2011). Silibinin: A novel inhibitor of Aβ aggregation. *Neurochemistry International*, *58*(3), 399–403.

Ying, H., Liu, J., Du, Q. (2014). Analysis and determination of oestrogen-active compounds in fructus amomi by the combination of high-speed counter-current chromatography and high performance liquid chromatography. *Journal of Chromatography B*, *958*, 36–42.

Yokoyama, M., Okano, T., Sakurai, Y., Ekimoto, H., Shibazaki, C., Kataoka, K. (1991). Toxicity and antitumor activity against solid tumors of micelle-forming polymeric anticancer drug and its extremely long circulation in blood. *Cancer Research*, *51*(12), 3229–3236.

Yu, X., He, G. R., Sun, L., Lan, X., Shi, L. L., Xuan, Z. H., Du, G. H. (2012). Assessment of the treatment effect of baicalein on a model of Parkinsonian tremor and elucidation of the mechanism. *Life Sciences*, *91*(1–2), 5–13.

Zeng, Z., Jiang, J. (2010). Analysis of the adverse reactions induced by natural product-derived drugs. *British Journal of Pharmacology*, *159*(7), 1374–1391.

Zhang, H., Jiao, Y., Shi, C., Song, X., Chang, Y., Ren, Y., Shi, X. (2018). Berbamine suppresses cell viability and induces apoptosis in colorectal cancer via activating p53-dependent apoptotic signaling pathway. *Cytotechnology*, *70*, 321–329.

Zhang, R., Zeng, Q., Deng, Y., Zhang, M., Wei, Z., Zhang, Y., Tang, X. (2013). Phenolic profiles and antioxidant activity of litchi pulp of different cultivars cultivated in Southern China. *Food Chemistry*, *136*(3–4), 1169–1176.

Zhang, Y., Su, R., Yuan, H., Zhou, H., Jiangfang, Y., Liu, X., Luo, J. (2023). Widely Targeted Volatilomics and Metabolomics Analysis Reveal the Metabolic Composition and Diversity of Zingiberaceae Plants. *Metabolites*, *13*(6), 700.

Zhao, L., Wang, J.-L., Liu, R., Li, X.-X., Li, J.-F., Zhang, L. (2013). Neuroprotective, anti-amyloidogenic and neurotrophic effects of apigenin in an Alzheimer's disease mouse model. *Molecules*, *18*(8), 9949–9965.

Zheng, Y. Z., Deng, G., Liang, Q., Chen, D. F., Guo, R., Lai, R. C. (2017). Antioxidant activity of quercetin and its glucosides from propolis: A theoretical study. *Scientific Reports*, *7*(1), 1–11.

Zhu, M., Rajamani, S., Kaylor, J., Han, S., Zhou, F., Fink, A. L. (2004). The flavonoid baicalein inhibits fibrillation of α-synuclein and disaggregates existing fibrils. *Journal of Biological Chemistry*, *279*(26), 26846–26857.

Ziemert, N., Alanjary, M., Weber, T. (2016). The evolution of genome mining in microbes–a review. *Natural Product Reports*, *33*(8), 988–1005.

Zou, Q.-Y., Wu, H.-F., Tang, Y.-L., Chen, D.-Z. (2016). A new labdane diterpene from the rhizomes of *Alpinia officinarum*. *Natural Product Research*, *30*(1), 1–6.

Conference Publications:

1. **H. Boro**, L. Rangan, R. Swaminathan, "Effect of pH and SDS micelles on the solubility and structural properties of the flavonoid 3,5-dihydroxy-7,4'- dimethoxyflavone isolated from *Alpinia nigra*" (2021), International Conference on Biotechnology for Sustainable Agriculture, Environment and Health, April 04-08 (2021), Jaipur, India.

2. **H. Boro**, M. Hegde, R. Swaminathan, A. B. Kunnumakkara, L. Rangan, "Role of flavonoid 3,5-dihydroxy-7,4'- dimethoxyflavone in inhibiting cell proliferation and migration in colon cancer cells" (2022), International Conference on Biotechnology for Sustainable Bioresources and Bioeconomy (BSBB-2022), December 7-11 (2022), Indian Institute of Technology Guwahati.

Patent:

1. S.Sanjana, S. Shreekant, M.K. Gupta, **H. Boro**, R. Swaminathan, L. Rangan, "Device for evaporation and recovery of organic solvents using simple labwares", Published patent (Patent No.416769). NewGen project grant.

Conferences/ Workshops Attended:

Heeramoni Boro

1. International Conference on Biotechnology for Sustainable Bioresources and Bioeconomy (BSBB-2022) held during December 7-11,2022 at Indian Institute of Technology Guwahati.
2. International Conference on Biotechnology for Sustainable Agriculture, Environment and Health (BSAEH-2021) held during April 04-08, 2021 at Jaipur, India.
3. 20th Indo-US Flow Cytometry Symposium cum Workshop on Applications of Flow Cytometry in Biotechnology (2019) held during 13-16 March, 2019 at Indian Institute of Technology Guwahati.
4. DBT Program Support Project sponsored Hands on Workshop on "Gene Expression and Function Analysis for Crop Improvement" (2018) held during 16-20 March, 2018 at Indian Institute of Technology Guwahati.
5. International Symposium on Plant Biotechnology for Crop Improvement (2017), held during 20-21 january, 2017 Indian Institute of Technology Guwahati.

6. Indo-Japan Workshop on “Translational Agriculture- Avenues for International Cooperation” (2017) held 0n 29th March, 2017 at Indian Institute of Technology Guwahati.

7. National Symposium on Pulses for Nutritional security and agricultural Sustainability (2017) held during 2-4 December, 2017 at ICAR-IIPR, Kanpur.